# Loughborough University

# Bio-Imaging and Serum Analysis of Zinc and Other Trace Elements in a Study of Age -Related Diseases Using Inductively Coupled Plasma - Mass Spectrometry

Tharwat Nabil Abduljabbar

**A Doctoral Thesis**

Submitted in partial fulfilment of the requirements for the award of Doctor of Philosophy of Loughborough University

May 2018

# Abstract

Trace elements participate in numerous biological processes and understanding their activity is essential in monitoring various diseases. Zinc has long been recognized as a fundamental component of various tissues, being highly concentrated in the retina and an essential structural component of many proteins. It plays a crucial role in many biological activities including homeostasis, immune function, oxidative stress, and aging disorders. During aging, the systemic metabolism of iron, zinc and copper changes, and this disruption in metal homeostasis appears to be associated with age-related disorders such as Alzheimer's disease (AD) and Age related macular degeneration (AMD). As understanding the role of these metals is critical in finding the underlying causes for such diseases, and providing proper diagnosis and treatments, the distribution of these crucial elements in AD and AMD has been investigated.

A rapid, accurate technique using sector field inductively coupled plasma mass spectrometry (SF-ICP-MS) was developed for the preparation and analysis of small volume (30 µl) biological samples. Analytical performance was evaluated using Serum UTAK certified reference material and the method was applied to Zn, Cu and Fe determination in 81 human serum samples from AD and AMD patients. No significant difference was found in Zn and Cu levels between AD and AMD patients, whereas Fe in AMD patients was slightly higher than AD patients. The results showed a decrease in serum Zn and Fe, and a notable increase in serum Cu in both AD and AMD patients compared to healthy controls. Elemental bio-imaging using laser ablation inductively coupled plasma mass spectrometry (LA-ICP-MS) was successfully employed for Zn imaging in 12 rat retina sections given either a conventional or a Zn-containing diet. A new data processing method, involving fitting Gaussian peaks to individual LA-ICP-MS line scans, was established. The RPE/retina peak area ratio was used to evaluate the differences in Zn content between supplemented and non-supplemented rats. In general, the difference between the three differentially fed rat groups was not statistically significant for the relatively small group of twelve rats investigated here. Thickness of Zn bands was also found to vary between controls and supplemented rats. This technique has the potential to support biologists in recognising possible new biomarkers for disease, related to specific trace elements.

# Acknowledgements

First and foremost, I would like to express my full and deepest gratitude to Almighty God, who guided and aided me all the way through my life and in my research.

I would like to express my deepest gratitude and thanks to my beloved Parents for the sacrifices they both made in their lives for me and for their endless love, care, unconditional support and selflessness. I consider myself the luckiest child to the best parents. Words cannot express how grateful I am. I owe a huge debt of gratitude and massive thanks to my lovely sisters and brothers for surrounding me with love, encouragement and support. Immeasurable appreciation and deepest gratitude for help and support is extended to "Amro" whom in one way or another has contributed in making this study possible. All the love goes to my daughter who brought happiness, smiles to my heart, making every day cheerful and for giving my life new perspectives.

My most sincere thanks and deep gratitude goes to my supervisors Prof. Barry Sharp and Dr. Helen Reid for their patience, time, enormous support, continuous help, encouragement and contribution for developing my research and guidance they have provided all the way through my PhD. My sincere thanks must also be extended to Dr. Jim Reynolds who became my official supervisor after both of my supervisors had retired. Every special gratitude and thanks must go to the genius programmer Dr. Peter Reid who created tools which saved me a huge amount of time during my data analysis and he never hesitated to offer his help whenever I had IT issues. I am mostly grateful to the internal examinar Prof. Paul Thomas, for his guidance, wisdom and useful advice. I would also like to thank Dr. Imre Lengyel (Institute of Ophthalmology, University College London) for providing samples for my research and for the helpful meetings for Zn work. My sincere thanks must be extended to Neda Barzegar-Befroei and Po-jung Pao in the same institution for preparing serum and retinal samples. My sincerest gratitude to all fellows in the Centre for Analytical Science at Loughborough University. A special thanks and appreciation to Amy Managh for her valuable advice, discussions and help especially in repairing various instrumentation issues despite her busy schedule. I would also like to thank my colleagues in the research group: Sarah Taylor, Aref Zayed, David Douglas, Taghreed Fagieh, Razi Haider and Pareen Patel, Grant Craig and Claire Camp for their help, expertise and much-valued friendship.

# Table of Contents

# List of Tables

# List of Figures

# Glossary of Terms

| | |
|---|---|
| AAS | Atomic absorption spectrometry |
| AAAS | American Association for the Advancement of Science |
| AMD | Age related macular degeneration |
| ANOVA | Analysis of Variance |
| AREDS | The Age-Related Eye Disease Study |
| Aß | Amyloid beta |
| BM | Bruch's membrane |
| CFH | Complement factor H |
| CNS | The central nervous system |
| CNV | Choroidal neovascularisation |
| CPS | Counts per second |
| CRMs | Certified reference materials |
| CSF | Cerebrospinal fluid |
| DHA | Docosahexanoic acid |
| DNA | Deoxyribonucleic acid |
| EPA | Eicosapentaenoic acid |
| ESA | Electrostatic analyser |
| FC | Flow cytometry |
| FWHM | Full width half maximum |
| GC | Ganglion cell layer |
| i.d | Internal Diameter |
| ICP–MS | Inductively coupled plasma–mass spectrometry |
| INL | Inner nuclear layer |
| IPL | Inner plexiform layer |
| IS | Inner segment |
| LA-ICP-MS | Laser ablation – inductively coupled plasma – mass spectrometry |
| LOD | Limit of Detection Limit |

| | |
|---|---|
| LOQ | Limit of Quantification |
| MCI | Mild cognitive impairment |
| MF | Metal free |
| MT | Metallothionein |
| NAA | Neutron activation analysis |
| Nd:YAG | Neodymium-doped yttrium aluminium garnet |
| NHANES | National Health and Nutrition Examination Survey |
| NIST | National Institute of Standards and Technology Nephrogenic |
| ONL | Outer nuclear layer |
| OPL | Outer plexiform layer |
| OS | Outer segment |
| PDT | Photodynamic therapy |
| PIXE | Proton induced X-ray emission spectrometry |
| RF | Radio frequency |
| RNA | Ribonucleic acid |
| ROS | Reactive oxygen species |
| RPE | Retinal pigment epithelium |
| RSD | Relative standard deviation |
| SEM | Secondary electron multiplier |
| SFA | Saturated fatty acid |
| SF-ICP-MS | Sector-field inductively coupled plasma mass spectrometry |
| SP | Senile plaques |
| STDV | Standard deviation |
| Sub-RPEds | Subretinal pigment epithelial deposits |
| SXRF | Synchrotron X-ray fluorescence |
| TMAH | Tetramethyl ammonium hydroxide |
| VEGF | Vascular endothelial growth factor medication |
| XFM | X- ray fluorescence microscopy |

# 1 Introduction

## 1.1 Introduction to aim, objectives and hypothesis

It is known that metal ions, mainly trace elements, are a vital component of life. Certainly, the homeostasis of metal ions including iron (Fe), copper (Cu) and zinc (Zn), is vital for many biological activities. Understanding their activities is essential in monitoring various diseases. Elemental concentration in serum/plasma has been the most frequently used biomarker of Zn and other trace element status. Serum Zn, Cu and Fe were selected as possible markers for monitoring and early detection of AD and AMD. Both AMD and AD are multi-factorial diseases influenced by age, gender and combinations of environmental and genetic risk factors. The most common characteristic in both diseases is the occurrence of amyloid ß (Aß) deposits in the brain of AD patients and in the drusen of AMD patients. Patients with advanced AMD have been found to be at an increased risk of developing AD. Therefore, parallel studies on the pathogenesis of the two diseases have led to a putative association between the two conditions. Zinc has long been recognized as a fundamental component of various tissues and cells, being highly concentrated in the eye, especially in the retina and RPE cell complex. Zinc has significant functions in retinal cell metabolism and specific retinal processes. The systemic metabolism of Zn, Cu and Fe changes during aging, and this disruption in metal homeostasis appears to be associated with age-related disorders. The most commonly used approach to restore Zn homeostasis disrupted in AMD patients is oral supplementation. Understanding the role of these metals is critical in finding the underlying causes for such diseases, and providing proper diagnosis and treatments.

In general, the focus of the research group is concerned with the discovery of elemental bio-markers in relation to specific disease states. The overall aim of this study is to understand the Zn biology associated with AMD. Since it is well known that there is a link between AD and AMD, and other trace elements play a crucial role in neurodegenerative and age-related diseases, the work has been expanded to include consideration of AD.

Several experimental approaches have been successfully employed to study metal ions such as Zn, Cu and Fe in biology, an area known as metallomics. Therefore, this work

will focus on developing a metallomics approach to studying Zn biology and the relation of Zn in a progressive age-related disease. However, understanding the specific biological functions of metals, and the explanation of their biological path is still challenging and a motivation for further analytical developments.

In the following section the hypothesis, aim and objectives of the study will be presented. The chapters in this thesis were not carried out in chronological order. Although the initial plan was to look at Zn in serum, tissues and cells, some experiments were started before others according to the availability of the instruments and the arrival of the samples. At other times, simultaneous experiments were carried out in parallel during the same period. All samples have been received from Dr. Imre Lengyel and his students (Institute of Ophthalmology, University College London).

### 1.1.1 Hypothesis of the study

*Primary Hypothesis:*

- Is a higher or lower level of Zn in the circulation and/or eye tissues/cells associated with an increased incidence of AMD?

- Is there a significant difference between Zn levels in the blood stream and /or eye tissue of AMD patients and controls?

*Secondary Hypothesis (I):*

- Is there a correlation between Zn, Cu, Fe levels in AD and AMD serum samples?

- Do increased and/or decreased levels of Zn, Cu & Fe contribute in these diseases?

*Secondary Hypothesis (II):*

- Does Zn supplementation affect either the amount or the distribution of Zn in the retina and RPE in rats?

- Do changes in the level of Cu influence Zn levels?

*Secondary Hypothesis (III):*

- Does variation in Zn concentration have an effect on embedded human RPE cells?

- Does Zn concentration vary in different cell compartments?

## 1.1.2 Aim and objectives

**The overall goal of the present study is to establish the role of zinc and other elements in some age related diseases by monitoring Zn in various biological materials:**

**Serum**

*Chemical mixture-simple dilution*

**ICP-MS**

- To develop a readily adaptable method to determine trace elements in a very small amount of serum (30µL).

- To determine and compare the distribution level of Zn, Cu &Fe in serum of 43 AD patients and 38 AMD patients.

**Chapter 2**

**Tissue**

**LA-ICP-MS**

- To image the distribution of Zn across the retina and RPE in 12 sections of aged rats that had received a conventional or supplemented diet, to investigate if there is Zn enrichments in the aging retina of the rat. Zn supplementation levels were approximately equivalent to those given to human AMD patients in AREDS 1 study to examine how this treatment affects the condition.

- To employ a novel data processing approach to examine the relative differences in Zn accumulation between these retinal compartments.

**Chapter 3**

**Cell**

**LA-ICP-MS**

- To test if Zn level has an effect on embedded human RPE cells cultured on Millicell membrane and treated with 0-125µM Zn during the culture process.

**Chapter 4**

- This work will be carried on in the future to compare the effect of Zn levels on different types of cultured, embedded RPE cells.

**ICP-MS**

- To measure Zn concentration in different cell compartments (the cytosol, cell membrane, nuclear fraction and cytoskeletal).

**Chapter 5**

- Future work would include an online cleaning system to remove the high levels of Zn found in the cell partitioning buffers.

4

## 1.2   Introduction to trace elements in human health

Trace elements are naturally occurring components that are distinguished from noble gases, major and minor elements in the periodic table.[1] Major elements such as H, O, C and N comprise around 96% of total human body, while minor elements e.g. Na, K, Ca, Mg, P, S and Cl make up 3.8% of in the human body. There are 73 naturally occurring trace elements present in the body and 18 of them are classified to be essential trace elements such as Li, V, Cr, Mn, Fe, Co, Ni, Cu, Zn, W, Mo, Si, Se, F, I, As, Br and Sn.[1] Nevertheless, other metals (frequently heavy metals) are known to be potentially toxic. The presence of some elements might have adverse effects on living systems by being toxic, mutagenic or carcinogenic.[2] For instance, these elements have been included in the context of carcino- (As, Cr, Pt), immuno- (Au, Co, Cr, Ni, Pt), embryo-/terato- (Hg), spermio- (Cd, Pb, Tl), and  nephro- (Cd, U) or neurotoxicity (Al, Hg, Mn).[3]

### 1.2.1   Importance and functions of trace elements

Trace elements are important in various significant biological functions in the human body. They are needed for several metabolic and physiological processes and the amount required per day ranges between 50 µg and 18 mg.[4] Metals play a crucial role in the functions of enzymes, co-factors, catalysis, mitochondria, neurotransmission, structural stability, oxygen transportation, and cellular signalling. In addition, the stability of the metals is believed to be essential for functioning of the central nervous system (CNS) and regulating and participating in many cellular mechanisms.[5,6] Numerous proteins include metal atoms as part of their structure. It has been estimated that around 33% of all proteins are bound with a cofactor metal ion such as Cu, Fe, An, Se or Mo for carrying our their physiological function.[7]

The activity of a wide range of biomolecules, in particular proteins, is controlled by metal ions, where they are responsible for both catalytic and structural functions. Nevertheless, excess and insufficient level of both non- essential and essential metals could be either toxic or resulting in metabolic failure.[4]

Absorption, excretion and tissue retention are controlled by homeostasis mechanisms of essential elements. The performances of essential functions require safe and sufficient supply of essential trace elements. Although various elements are believed to be essential

for human health, many others are known to be toxic. When the essential elements appear in an organism in excessive quantities and exceed the range of adequate exposure, the elements will become toxic. In contrast, insufficient intake could damage cellular as well as physiological function and most probably lead to different types of diseases. Figure 1.1 explains the relation between a biological function and the dietary intake concentration of a trace element. The diagram is generally applicable to most essential trace elements although each element has its individual precise curve, which varies from others.[1,4]
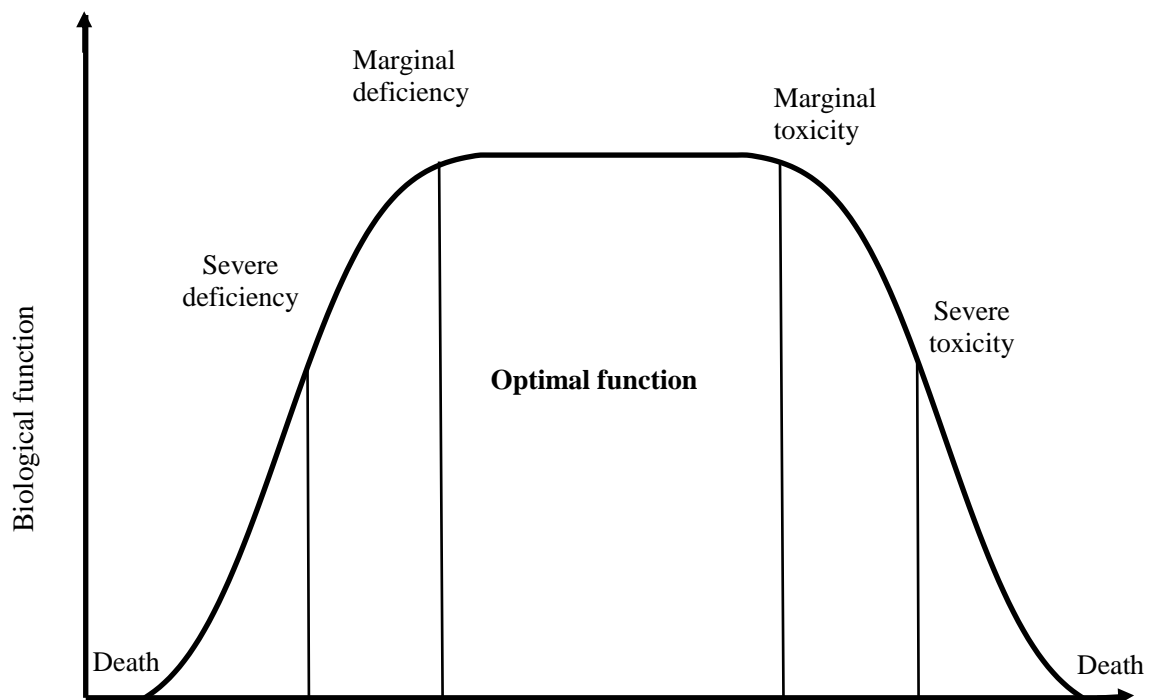


**Figure 1.1** Dose-response curve for essential trace elements. Modified from Mertz, 1981 and reproduced with permission from American Association for the Advancement of Science (AAAS).[4]

## 1.2.2 Deficiency and toxicity

Inadequate nutrition could cause deficiency of trace elements. Iron deficiency is world's most common nutritional illness.[8] Moreover, deficiencies can initiate from genetic or inherited disorders with trace element metabolism implicated in the pathogenesis. An example of such neurological disorder is Menkes disease and Wilsons disease. Both

diseases are genetic disorder caused by Cu deficiency where Cu transport is interrupted and is lethal in early childhood. Also, acrodermatitis enteropathica is an uncommon genetic autosomal recessive disorder, characterized by reduction in Zn absorption which results in its deficiency.[9,10] It has been reported that Zn deficiency adversely affects macrophages, phagocytosis and produces toxic effects on the functions and the growth of the T and B cells.[11]

On the other hand, if excessive amounts are ingested the essential elements can also be toxic. For instance, Mn is an essential trace element; however, it is evident that overexposure and inhalation of dust or fumes in the work environment can cause psychotic behaviour that resembles Parkinson symptoms, known as manganism.[12,13] Trace elements' deficiency and toxicity depend on a number of other factors including: gender, age, chemical form, interaction with other elements, dietary source and nutritional state.[14]

According to a study of nutrient intake (institutionalized, with a mean Mini-Mental State Examination,MMSE), it has been reported that patients with severe AD consumed less Zn than controls owing to poor Zn intake.[15,16] Therefore, if the normal diet of these elderly patients is Zn deficient, adequate supplementation is required to maintain good health.[17] Total Zn intake requirement per day is around 2.2 mg for an adult if the bioavailability is 100%, and various national health institutions reported the dietary reference value for men estimated between (9.4-15 mg/day) and for women (7- 12 mg/day).[18,19]

Elevated Cu level in AD patients could be explained by the increase of ceruloplasmin. Ceruloplasmin is synthesized in the liver and the majority excreted by bile and the rest eliminated by urine. Thus, elevated Cu level could be an indicator of the liver's failure to clear Cu in the elderly and therefore, it is important to perform clinical studies of liver function in AD patients to investigate the reason for the high Cu level.[20] On the other hand, Cu deficiency in tissues does more harm to the antioxidant enzyme system and immune system, and decreases hemoglobin level, thus raising oxidative stress and inflammatory response.[11] Deficiency in some vitamins and micronutrients that play an important role in antioxidant and metabolism (such as Vitamins B1, B2, B6, B12, C, and folate), have been linked with cognition impairment in old people.[21] As Cu and Fe could be a dietary risk factor, Loef and Walach[22] revealed an association between high Cu, Fe and saturated fatty acid (SFA) intake and cognitive decline. Accordingly, old people who

are not at risk of anaemia should avoid diet rich in Cu, Fe together with SFA (0.9 mg/day could be sufficient according to World Health Organization (WHO) recommendation).[23] Interestingly, Mediterranean-type diets have been attributed to decreasing the rate of AD.[24] Hence, in this study, the focus will be primarily on Zn and other trace elements such as Cu and Fe.

### 1.2.3   Zinc (Zn)

Zinc is a metallic transition ubiquitous trace element, and is the second most abundant bio-metal in the human body following Fe. It is an essential trace element in human body and crucial for the biology of living organisms. It can be found in large quantities in body's tissues and organs such as bone, muscle, liver, teeth and skin. [25] Around 95% of total body Zn is bound to intracellular proteins and cell membrane. [26] The mean concentration of Zn in human plasma is approximately 15 µmol $L^{-1}$ (100 µg $dL^{-1}$). [27] However, this small pool is very mobile and key to Zn homeostasis. Serum Zn is bound to albumin (75–80%), α-2 macroglobulin (30%) and transferrin and ceruloplasmin (10%). [28,29]

It is well known that Zn is required for over 300 enzymes as a catalyst, regulatory ions or structural component.[25] Unlike Fe and some biometals, the free divalent cationic form ($Zn^{2+}$) does not produce oxidation-reduction reactions under physiological condition and thus it is relatively non-toxic.[28] Although it is only required in small amounts, Zn is vital for a vast number of fundamental biological functions.[30] Zinc plays a vital role in gene and protein expression, enzyme catalysis, lipid metabolism and several cellular processes, such as protein synthesis, signalling pathway, cell division, DNA replication and transcription.[31,30] In addition, Zn protects intracellular components from oxidative stress caused by inflammation, infection and toxins. For instance, Zn indirectly acts as an antioxidant and it is involved in stabilization of cell membrane structure, contribution of super oxide dismutase (SOD) component and maintenance of metallothionein (MT) concentration in tissues and cell membrane.[32] Albumin is the main protein of human blood plasma  and acts as the major transport protein for Zn in plasma. It can be adversely affected by chemical stresses such as oxidative stress occurring in the ageing degenerative diseases including Alzheimer's disease.[33] Zinc can cross the blood brain barrier, thus it plays a crucial role in maintaining normal brain function[34]. Most of brain

Zn is bound to MTs, while free Zn only corresponds to 10% which exist in neurons.[34] The depletion of free Zn from neurons could cause cognitive abnormalities[34,28] and associated with diseases such as Alzheimer's disease.[35] Accordingly, one of the disease modifying approaches in the treatment of Alzheimer's disease aims to prevent Zn dyshomeostasis.[35]

The main source of Zn intake is food, such as fish, shellfish, egg, red meat, dairy products and nuts; and a small portion from drinking water.[28] Another source of food that contains high levels of phytates including seeds, nuts, legumes, cereals and soya based products are less available for absorption as these foods chelate dietary Zn and Fe, making them less bioavailable. The adults Recommended Dietary Allowance (RDA) of Zn is 8 to 15mg/day, however, doses that exceed 25 mg can cause anemia and Cu deficiency.[36] Significant deficiency of zinc can cause oxidative stress and which in turn damage proteins, lipids and DNA.[37,38] Zinc deficiency could cause some diseases, such as malaria, lower respiratory tract infection and diarrhoea.[39] In contrast, excess level of Zn could lead to Zn toxicity that could cause some symptoms like nausea, vomiting and diarrhea.[40]

### 1.2.4   Copper (Cu)

Like Zn, Cu is an essential trace element and found in all tissues and organs of the human body. Copper plays an essential role as a cofactor in multiple cellular processes including respiration, connective tissue formation and Fe metabolism.[41] Copper containing enzymes are widely distributed in the body such as super oxide dismutase [SOD] and ceruloplasmin.[40] Both Zn and Cu bind to metallothionein (MT), a main regulator of storage and transport of these metals.[42] They work as a catalyst in redox reactions, transport oxygen and protect the cell against oxidative damage.[43] Liver is the main site for Cu storage and homeostasis. It is also found in other organs such as heart, brain, intestine and stomach.[44] In plasma, Cu is mainly bound to ceruloplasmin (95%), while a small portion is bound to plasma albumin and amino acids.[45,46] The free Cu in blood could be harmful to the cell because it is a potent oxidant which could produce reactive oxygen species (ROS) in cells and disrupt homeostasis which may result in toxicity.[25]  High concentrations of Cu and Fe are related to many diseases, such as cancer, cardiovascular, Alzheimer's and Parkinson's diseases and long-term disruption of Cu homeostasis can cause genetic disorders.[47,48] However, a high Cu intake does not necessarily result in Cu

overload due to strong Cu regulation if the exposure of Cu is kept within the homeostatic range.[49] It is also known that an imbalance between Cu and Zn could be an indication of vascular complications, infection and other disease. [50] Therefore, a proportionate intake of Zn and Cu should be maintained.[51]

### 1.2.5 Iron (Fe)

One of the most significant trace elements is iron that plays different biological roles in the human body, such as enzyme activities, electron transport, oxygen transport and DNA synthesis.[25] In addition, Fe is crucial for energy metabolism, electron transport chain, and oxygen transport. Fe has potential for the development of free radicals and is required for ROS generation.[11] It is clear that Fe-related oxidative damage is closely connected with several diseases. The two active forms of Fe are redox forms which are Ferric [$Fe^{3+}$] and ferrous [$Fe^{2+}$] ions.[52] Ferritin is a protein that stores Fe inside the human cell. The ferritin plasma level could be a useful indicator for stored Fe.[53] Iron plays an essential role in tissue oxygenation since it is considered to be an integral part of haemoglobin which works as an oxygen carrier in red blood cells.[52] In addition, Fe plays an important role in neurotransmission since it is included in lipid and cholesterol biosynthesis which are components of neurons. It is clear that Fe has a good relation to brain activity due to high oxygenation and myelin levels in the brain.[52] It is also reported that Fe overload could lead to neurodegenerative disease.[54]

### 1.2.6 Zinc, copper and iron interaction

Zinc, copper and iron participate in several biological activities. They affect each other's homeostasis as some of them are sharing the same transporters and binding proteins including metallothionein (MT). These connections are well recognised for Cu and Zn, which compete for MT binding.[55,23] It has been indicated that Cu-Zn- MTs in AD brains show a decrease in Cu bound to isoforms of MT (MT-1 and MT-3).[56] In addition, Fe mainly, but also Zn and Cu, are shared by another transport mechanism which is divalent metal transporter 1 (DMT1).[55,57]

Zn is mainly bound to Albumin, but also to transferrin (10%).[29] As transferrin is the main transporter of Fe, excessive Fe can decrease Zn absorption, and vice versa. Moreover, alterations in ceruloplasmin (the major Cu carrier) and transferrin levels may result in

abnormal metabolism of both Fe and Cu. Besides the role of ceruloplasmin as a transport protein, it also functions as an enzyme, catalysing the oxidation of Fe. The Cu concentration was found to be notably higher in Fe deficiency (anaemia) in comparsion to control.[58] Zinc, copper and iron are potentially interfering with each other with regard to metabolism, distribution and absorption, and in regulating the cellular response and health effects. Copper is known to react with a selection of nutrients, including Fe and Zn. Excessive amounts of Fe supplementation (more than 25 mg) might decrease Zn absorption. On the other hand, extreme absorption of Zn may suppress Cu and Fe absorption. To illustrate, high Zn intakes (150–450 mg per day) have been linked with low Cu status, changed Fe function and other chronic effects.[58] Therefore, changes in nutritional habits may affect the homeostasis of macro- and micronutrients and this challenging factor would need to be analysed systematically with reliable techniques. [55,58] However, another study suggested that high dietary Zn may not interfere with the levels of Cu in human tissue or plasma.[58]

The alteration of Fe concentration in the brain can cause a dysregulation of the other trace element and thus changed homeostasis. Iron also has been reported to disturb Cu and Ca homeostasis.[59] Moreover, pathophysiological circumstances such as inflammation have an influence on the homeostasis of Zn, Cu and Fe in parallel. These examples obviously indicate the importance of analysing and evaluating several trace elements in parallel.[55] Zn as well as Cu perform as an intracellular scavenger of the reactive oxygen species (ROS) and performs an important function in bone mineralization.[11] Using trace element ratio instead of single trace element as markers for the elemental status could be potentially useful. It was recently observed that Cu/Zn ratio was positively associated with markers of age and general inflammation, mainly those associated with neurodegenerative disorders.[55] Another study reported the link between blood Cu/Zn ratio with age, gender, and disease.[60] Therefore, the ratios might help as aging markers, which should be further tested in other population groups.

## 1.3 Introduction to metallomics

### 1.3.1 Definitions of terms

The term metallome is relatively new, and was first introduced in 2001 by R. J. P Williams, who refers to it as a distribution of free metal ions in biological materials. Subsequently, the term metallomics has been suggested as the study of metallome.[61] This study focuses on interactions and functional connections of metal ions and other metal species with genes, proteins, metabolites, and other biomolecules in biological systems.[62] In general, the terms "metallome" and "metallomics" have been used in different contexts, the former expression is described from a chemical viewpoint as the full complement of metals and metalloid species present in cell or tissue type and analysis therefore referred to as metallomics.[61] From a biochemical perspective, the main area of interest is to examine pathophysiological mechanisms of diseases by identifying how the metals are bound with biomolecules (metalloproteins or metalloenzymes), and studying the mechanisms of enzymatic and biochemical reactions.[63] One of the most significant areas of research is investigation of the structural and functional roles of metal ions linked with proteins, which is usually stated as metalloproteomics.[64] Although metallomics has been recognized as being in its primary phase, compared with genomics and proteomics, metallomics has already obtained a vast quantity of information which will be useful in the rapid development of metalloproteomics.[65]

### 1.3.2 Importance of metallomics

Metallomics and metalloproteomics have been given considerable attention in the last few years. The expansion of these areas of interest into biochemistry and biomedical study has produced a new research area.[66] In addition, the identification of metal cofactors in a protein, which is called qualitative metallomics, may lead to better understanding of protein function and accordingly many biological processes. As a result, the role of vital and toxic metals in health and disease are more likely to be observed. Added to this, a wide-range of novel metal drugs, remedies could be discovered.[63,67] Common examples of metalloproteins are ferritin and metallothioneins. Metallothioneins (MTs) are a family of cysteine-rich, low molecular weight proteins that bind to transition metals. MTs play a crucial role in homeostasis and controlling intracellular metals where they link easily with essential trace metals such as Zn and Cu. They also provide resistance against the

toxicity of heavy metals in cells, e.g. Cd and Hg. MTs are considered biomarkers for intracellular Zn ions, hence it is recommended not only to quantify MT in a biological matrix, but also to detect Zn or other important metals binding with MTs.[68,69] The homeostasis of metal ions is important in central nervous system. On the other hand, metal dyshomeostasis and accumulation of Cu, Zn and Fe in the human brain has been connected to the pathogenesis of many neurodegenerative diseases, such as Alzheimer's and Parkinson's disease.[47,70] In such diseases, the interaction of Cu or Zn with target proteins is altered. Also, ferritin metabolism is altered and Fe ions were found to increase oxidative stress.[70] As can be seen from Figure 1.2 the majority of a biological system comprises an expansive range of structures, distributed in simple (free ions) or complex form (genomics, proteomics, metabolomics and metallomics or metalloprotein), either strongly or weakly bound.[61,62] [61]
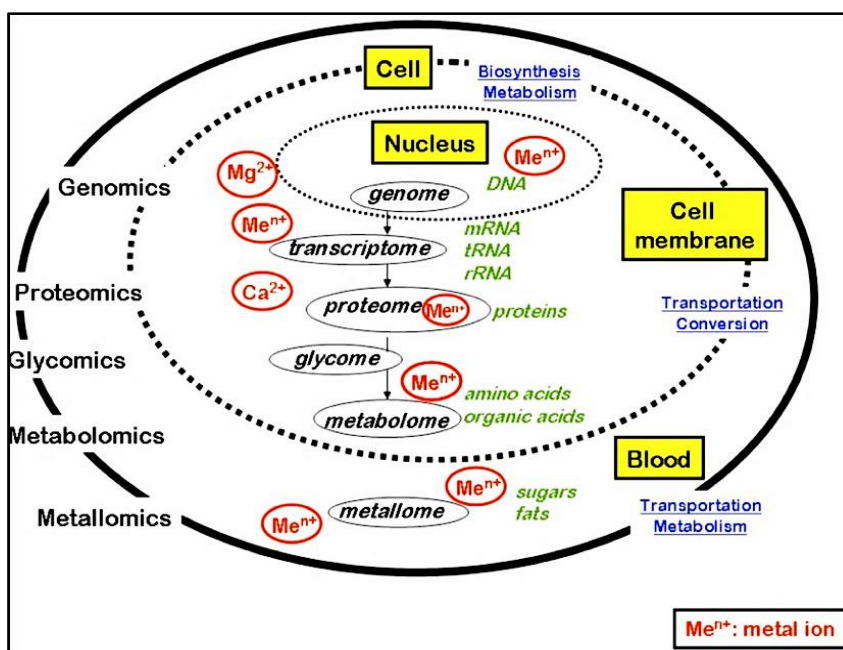


**Figure 1.2** Diagrammatic model of the biological system, showing the correlation amongst genomics, proteomics, metabolomics and metallomics. Reproduced from Lobinski et al., 2010, with permission from De Gruyter.[61]

Many factors may affect metal ions in biological systems. One factor is that the total concentration (quantitative metallomics) of intracellular metals that exists in the cytosolic pool is in the micromolar to picomolar concentration range.[71,3] Trace elements have been implicated in the pathogenesis of various neurodegenerative disorders. The concept of a disturbance of metallostasis or loss of metal homeostasis, has recently been demonstrated as a crucial factor in the pathway leading to Aß toxicity and Alzheimer's disease (AD).[72]

## 1.4 Introduction to some important diseases of ageing

### 1.4.1 Alzheimer's disease

Alzheimer's disease (AD) is the most common cause of dementia that occurs most frequently in elderly people. It is a progressive neurodegenerative disorder, gradually damaging the regions of the brain, leading to memory loss, impaired speech, difficulties in learning and orientation, and other cognitive abilities.[73,20] AD affects over 27 million people worldwide[74] and the likelihood of developing AD is forecast to double every 5 years after the age of 65.[75] AD affects 3–15% of people aged less than 75 years, however this percentage increased up to 30-40% for people aged 85 years and older.[76,77]

#### 1.4.1.1 Signs, diagnosis and stages

The significant pathological hallmark of AD disease is characterized by the formation of extracellular amyloid beta peptide/ protein (Aβ) deposition and neurofibrillary tangle (NFT) within neuron and thus decreased synaptic density and loss of neurons in the cognitive centres of the brain.[78,18,79] Tau protein is the main component of NFTs.[79] A vast Aβ production produces Aβ aggregation and finally leads to senile plaques formation. Neurofibrillary tangles (NFT) are accumulation of abnormal hyper-phosphorylated protein tau, which performs a role in intracellular transport. The existence and distribution of Aβ and NFT in the brain is utilized for AD diagnosis and determines the stage of this disease.[75,80] (see Figure 1.3). In addition, metal ions including $Zn^{2+}$, $Cu^{2+}$, $Fe^{2+}$ which play a role in the etiology of this disease, participate in oxidation and free radical production as represented in Figure 1.4. Early stage detection of AD is of much interest to the researcher, as that may help to clarify the mechanisms of AD and to improve AD patient's quality life.[81] Mild cognitive impairment (MCI) is usually considered a preclinical stage of AD with acquired deficiency in multiple cognitive functions. Patients with MCI show increased risk of developing AD and about 20% of 65 years old people may have MCI.[73,82] It has been indicated that 10-15 % of MCI cases convert to dementia annually.[83] Accordingly, comparative studies between MCI and AD patients in order to track the progression of neurodegeneration as well as understanding the pathogenesis of disease to detect potential biomarkers for early diagnosis is important.[82] Eventually, severe cognitive decline known as dementia has an adverse

impact on daily living activity of patients. Dementia in AD gradually worsens and in the late stage patients rely completely on others in their basic living activities.
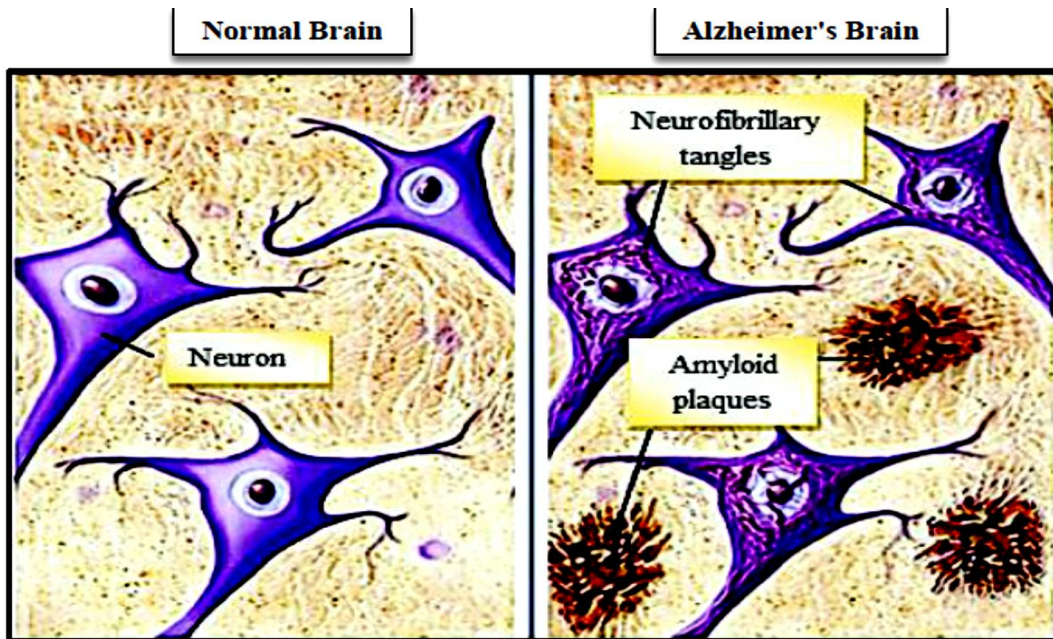


**Figure 1.3** Normal Vs. Alzheimer's disease brain. Reproduced with permission from Bright Focus Foundation programme, 2017.[84]
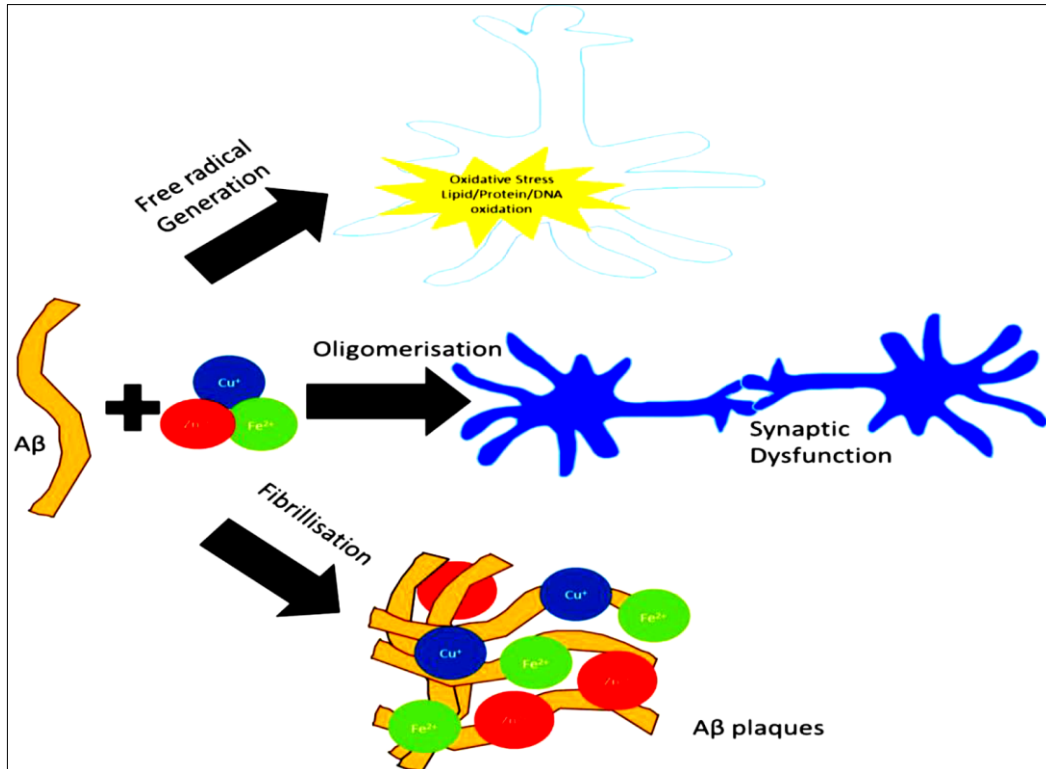


**Figure 1.4** Contribution of metal dyshomeostasis in AD disease. Reproduced with permission from N. Braidy et.al, 2014.[74]

## 1.4.1.2 Risk factors

Despite extensive research, the cause of Alzheimer's disease is still unclear and that is the main barrier for treating and/or preventing AD. However, multiple factors could play a vital role in AD degeneration.[85,86] Age is the most influential risk factor of AD, and with predominance of an aging population in the world the risk factor of AD increases remarkably. Aging and AD are recognized by damaging of blood brain barrier function, gradual and progressive decline in cognitive function and shortages in memory and other mental capacities.[87, 88] The number of nerve cells in the brain are reduced with growing age, and production of free radicals and markers of oxidative stress increase in neuronal cells.[88]

Numerous studies have suggested the contribution of different cellular processes including oxidative stress in the pathogenesis of AD.[80,82,87, 72,70] Oxidative stress and inflammatory response induced by Aβ deposition results in further formation of Aβ fibrils and neurofibrillary tangles which causes oxidative damage to the cells and its function. Therefore, the availability of nutrients in the neuron drops and the process of inflammation is stimulated. This leads to neurotransmitter deficiency and overall death of neural cells and failure in their function, as a whole contributes to Alzheimer's disease progression.[80,87]

Micronutrient deficiency (especially those linked to antioxidant and amino acid metabolism mechanisms) such as vitamins B1, B2, B6, B12, C, and folate, have been correlated with MCI in old age.[23,21] Cholesterol and high fat intake (e.g., saturated fatty acids) enhances the formation of Aβ in the animal model brain and elevate oxidative stress, thus they were associated with the increase risk factor of AD. In addition, some evidence has indicated the strong relationship between AD and cardiovascular diseases.[80,23,21, 89] Overall, a number of risk factors including chronic oxidative stress, age, Aβ production, neurofibrillary tangles accumulation, inflammation, abnormal accumulation and distribution of different metals and other genetic components, play a significant role in the development of AD. Other risk factors have been identified to evaluate AD risk, such as: female gender, positive family history, hypertension, coronary vessel disease and increased body mass index.[23] Medication for AD does not cure the disease but only offers modest benefits. Therefore, effective strategies to delay or prevent AD are needed.[23]

### 1.4.1.3　The role of metals in relation to Alzheimer's disease

While metal ions play an important role in biology, disruption of metal homeostasis is a key element in the pathway leading to Aβ toxicity and AD. Consequently, that will result in neuronal dysfunction, neurotransmitter deficits, and eventually, neuron death.[90] Redox metals in the brain play various essential roles for maintenance of cellular function. However, the impaired regulation of redox reaction at a molecular level of metals such as copper (Cu), zinc (Zn) and iron (Fe) is identified in Alzheimer's disease (AD) due to development of cytotoxic reactive oxygen species (ROS) which lead to neuronal damage.[74] In addition, the β- plaques isolated from AD affected brain tissue were observed to contain sequestered biometals, which could implicate those metals as potential pathological cofactors in AD.[52] Alzheimer's disease disrupts the brain metallostasis, causing redistribution of metals into inappropriate compartments, in particular Fe, which is the most excessively available transition metal in the brain. There are tightly organized mechanisms in order to control Fe in the brain. However, dysregulation, Fe overload and Fe deficits are harmful to the brain.[91] Therefore, targeting the transition metals such as Zn, Cu, and Fe that have an impact on molecular mechanisms of disease could be an alternative approach to treat this disease.[79,90]

In old age nutritional deficiency is common, this further decrease in AD Zn levels could in turn affect levels of the ion in brain tissue and entrap Zn within the plaque leading to exaggeration of amyloid pathology. Copper and zinc is highly developed within AD plaques (1055μM) compared to normal age- matched neuropil (350 μM).[92] The continual development of specialized tools and a rising interest of the role of metal ions in normal biological functions and diseases will deliver much needed insight into potentially a wide range of disorders.[5]

### 1.4.2　Age related macular degeneration

Age related macular degeneration (AMD) is an inflammatory, chronic eye disease, attacking the macula and causing severe and irreversible vision loss in elderly people.[93,94] As can be seen from Figure 1.5 (A) the macula is a small spot located near the central part of the retina, and it is the light-sensitive tissue at the back of the eye that provides the clearest, most distinct vision. In general, the damage done to the macula develops over time, gradually decreases the quality of the central vision, often referred to as

macular degeneration.[95,96] Due to this progressive deterioration of central vision, the quality of life and the ability to perform some daily activities such as reading, driving and recognising faces will probably be affected.[97,98] Early AMD affects about a quarter of people above the age of 65 years[99], while the prevalence of advanced AMD increases severely with age, and is estimated to be doubled by 2020 in North America and Europe.[97] In the UK, vision loss that is caused by AMD accounts for approximately 42% between the age of 65–74 years, nearly two-third of those aged between 75-84 years, and around 75% over the age of 85.[99]

### 1.4.2.1   Types and stages of AMD

The two vision threatening types of AMD are dry form, also known as non-exudative or geographic atrophy, and wet form, also known as exudative or neovascular. The vast majority of AMD patients are attacked by geographic atrophy form, whereas the exudative AMD is less common and appears only between 10-20% in AMD patients. Although both forms are responsible for reducing the vision loss, advanced AMD (neovascular form) is the most severe form and accounts for 90% of legal blindness.[93,97,98] The early sign of dysfunction of retinal pigment epithelium (RPE) and retina are characterised clinically by the presence of pigmentary changes in the RPE and accumulation of yellow deposits called drusen.[100] Drusen are located between the RPE and the inner choroidal layer in the Bruch's membrane (BM).[97,99,101] It has been identified that vitronectin, an abundant glycoprotein found in serum and extracellular matrix, can be considered as the main component of drusen.[100] In the early stage multiple small or intermediate drusen deposits (63μm-125 μm) will appear and the progression risk of AMD in this stage is low (between 0.4%-0.3%) over a period of 5 -10 years (Figure 1.5, B).[98,99] However, if extensive drusen (>125 μm) are present in both eyes, the risk might increase up to 47.3%, and this stage is usually considered as intermediate age related macular degeneration.[98,99] In the advanced period of dry AMD, the RPE degenerates slowly and may lead to complete atrophy to the photoreceptors and choriocapillaris layer of the choroid (Figure 1.5, C). [94,97] During the late stage of wet AMD, the damage to the macula occurs rapidly as the growth of abnormal blood vessels, called choroidal neovascularisation (CNV), could cause bleeding and formation of scar tissue into sub-retinal space[97,98,99] (Figure 1.5, D). A detailed diagram showing the stages and types of AMD pathology within the layers of the eye are illustrated in Figure 1.6.
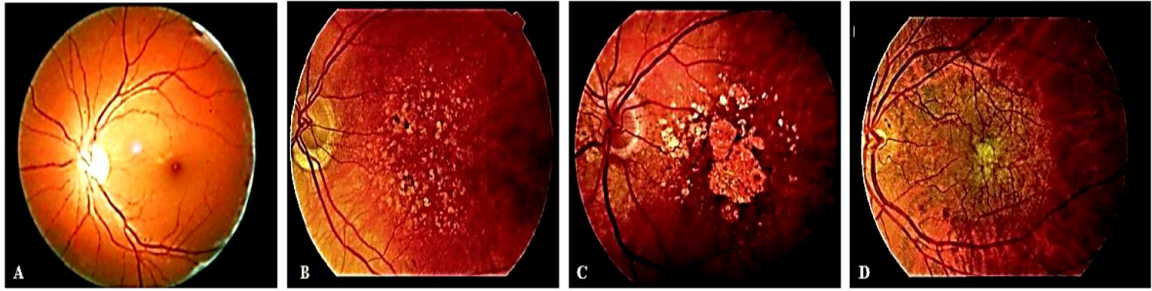
**Figure 1.5** (A) The macula is a small component of the eye found in the central area of the retina (healthy eye), (B) Macula of early AMD with numerous small and intermediate soft drusen, (C) Macula of advanced dry AMD with geographic atrophy, (D) Macula of Advanced wet AMD with a choroidal neovascular membrane with sub retinal haemorrhage. (A) My eye, Vision Express, 2015. (B-D) Reproduced from Chakravarthy et al., 2010, with permission from BMJ Publishing Group Ltd.[93,98]
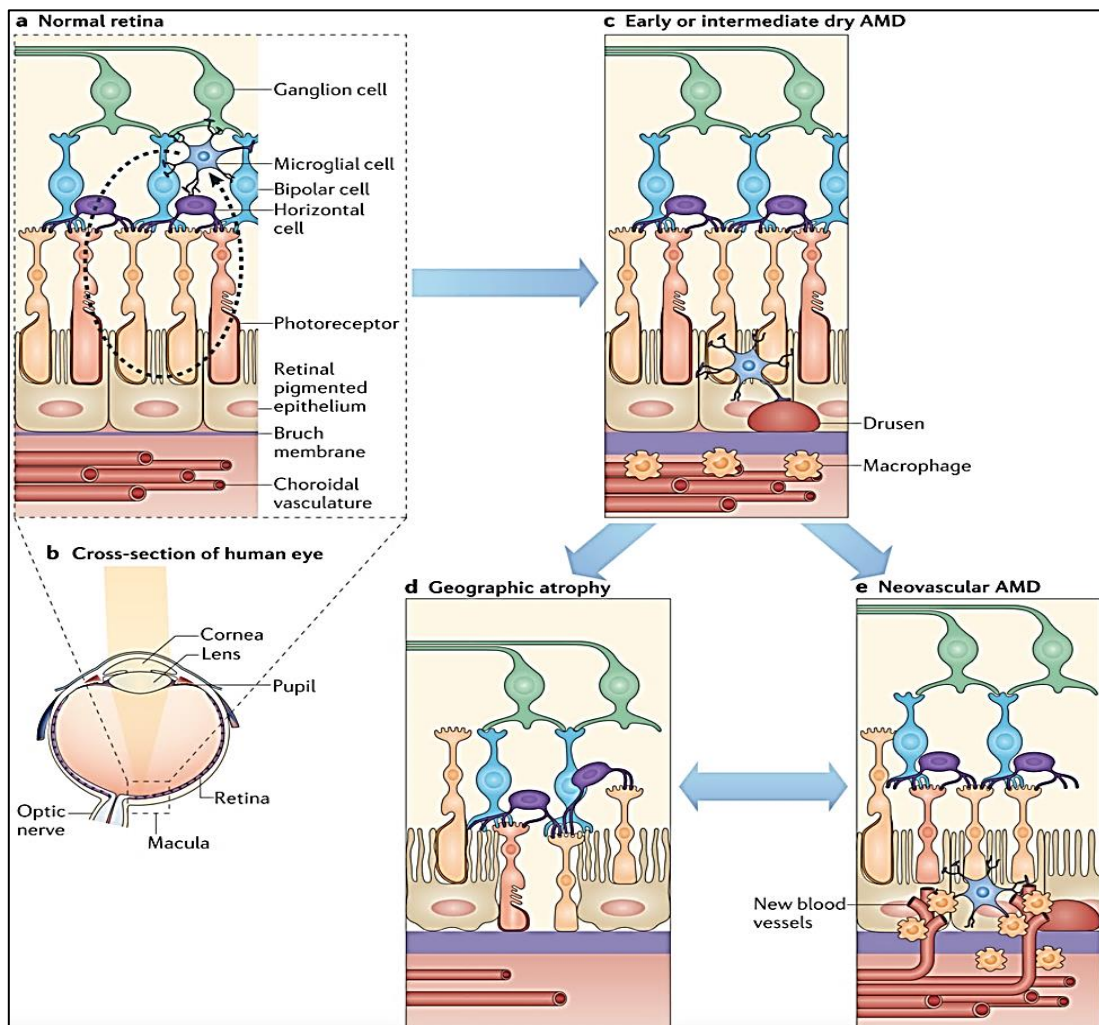


**Figure 1.6** AMD Pathophysiology. This diagram highlights: the several layers of the normal retina (a); a cross-section of the human eye (b); and the stages/types of AMD (c), (d), (e). Reproduced from Ambati et al., 2103, with permission from Springer Nature publications.[102]

### 1.4.2.2 Suggested treatments and pathology mechanism

Several potential options have emerged as a treatment for exudative age related macular degeneration, including laser photocoagulation, photodynamic therapy (PDT), surgical intervention, and anti-angiogenic drugs (such as anti-vascular endothelial growth factor medication VEGF).[93,97,103] The development of anti-VEGF agents, in particular, has provided an indication to stop the progression of wet AMD and also improve the visual acuity.[97] However, no effective treatment has been proven for geographic atrophy or restoring visual loss in AMD patients.[94,104,105] Therefore, the attention has focused on attempts to stop the progression of the disease by inhibiting the damage that leads to this condition.[104]

As the retina and retinal pigment epithelium contain high level of oxygen and polyunsaturated fatty acid as well as the chronic exposure to light, both of which are strong sources of free radicals, thus the accumulative results of oxidative stress play a principal role in initiating macular degeneration.[95,98,106,107] As a consequence of oxidative damage, biochemical and structural changes could occur that produce inflammation and angiogenesis (development of new blood vessels), especially in genetically predisposed patients.[97,99] Hence, an antioxidant balance that can be obtained from diets, Zn or vitamin supplementations can possibly maintain a healthy retina and the factors which result in stimulating oxidative stress should be avoided.

### 1.4.2.3 Risk factors

It is clear that there are several factors - genetic as well as environmental - which may contribute to the process of AMD.

### 1.4.2.3.1 Age

The incidence of many diseases increases significantly with age. AMD develops as people grow older and that is considered one of the most important and strongest risk factor.[99,108] With age, Bruch's membrane (which is located between the retinal pigment epithelium (RPE) and choroid) grows to be thick, as a result of accumulation of deposits. Therefore, the formation of lipid and protein deposits in the central and peripheral retina probably plays a main role in AMD development.[109]

#### 1.4.2.3.2  Gender and ethnicity

The prevalence of neovascular AMD in women over 75 years has been shown to increase two-fold compared to men of the same age.[110] However, another study has suggested that the effect of gender on AMD development was not statistically significant.[111]

AMD is commonly found in white people than people with colored skin.[112,113] Although some studies such as the National Health and Nutrition Examination Survey III (NHANES III)[114] have shown that drusen appeared in same rate in white and colored individuals. These studies also demonstrate an increased prevalence of advanced AMD in white people compared with others.[99] It is proposed that increased level of melanin may increase the possibility of the free-radical scavenging of the retinal pigmented epithelium and Bruch's membrane, hence reducing the risk of advanced age-related macular degeneration.[99]

#### 1.4.2.3.3  Genetics

Increasing evidence has been reported to show that the variation in some genes is strongly associated with several diseases. Genetic investigations have indicated that the gene coding for Factor H, a major regulatory glycoprotein in the complement-mediated immune system, was the first important gene to be involved in the pathogenesis of AMD.[115,116] Moreover, Tyr402His variant and several noncoding variants in the complement factor H (CFH) gene were found to increase the risk of advanced AMD over sevenfold.[117,118] As mentioned earlier, an early sign of AMD is the formation of subretinal pigment epithelial deposits (sRPEds) which can be focal (drusen) or diffuse (basal linear and laminar). These deposits contain more than 140 combined proteins including factor H and other components which are secreted by various cell types including the RPE.[119,120] Both factor H and the accumulation of high concentration of Zn in the external retina are considered risk factors for AMD. However, their contribution in the progression of AMD is still ambiguous.[121,122] Under oxidative stress through light exposure, the secretion of Zn from the Zn-rich RPE cells is raised. As Zn has been found in sRPEds and Bruch's membrane in AMD, it is suggested that the pathological release of Zn from surrounding tissues such as the RPE–choroid complex may be implicated in formation of deposits.[109,119] Zn binds more strongly with the His402 allotype than the Tyr402 allotype. Patients with the His402 allotype will be at higher risk of AMD since this form of

complement factor H is more likely to cause large oligomer formation. Added to this, increased deposit formation has recently been linked with the His402 polymorphs in patients.[121]

### 1.4.2.3.4  Smoking

Smoking is related to a number of eye diseases, such as nuclear cataract and thyroid eye disease.[123] Numerous case-control studies,[124,125] population-based studies[126] (e.g. the Beaver Dam Eye Study and the Blue Mountains Eye Study[127]), studies of both physicians[128] and nurses[129] have strongly confirmed that smoking is the strongest environmental risk factor associated with AMD. This factor is the only preventable one as there is a direct relation between AMD development and the number of cigarettes smoked[124,108]. It is also evident that current smokers had a significant four-fold increased risk of advanced AMD compared to non-smokers, and there was a threefold higher risk of geographic atrophy in past smokers.[127] Moreover, cigarette smoking appears to have toxic effects on the retina[130] and often great adverse consequences in people with low High-density lipoprotein (HDL) cholesterol level, and low fish consumption.[127]

### 1.4.2.3.5  Exposure to sunlight

Chemical and light stimulated oxidative damage to the photoreceptors and thus the function of RPE is adversely affected.[131] The retina is mainly prone to oxidative stress owing to its high consumption of oxygen and its continual exposure to intense light.[106,107,131] The Beaver Dam Study and others suggested that the exposure to high level of sunlight, in particular the UV light, may cause ocular damage and therefore increase the risk of developing AMD.[132]

### 1.4.2.3.6  Dietary fat

Several studies [133,125] identified a link between AMD progression and diets with high level of fat, although some types of fatty acid may be protective.[131,125,134] The Beaver Dam study confirmed that the risk of early AMD increased by 80% among patients with the highest intake of saturated fat and cholesterol.[107,135]

#### 1.4.2.3.7  Unsaturated fatty acid

Omega-3 long-chain polyunsaturated fatty acids, in particular, docosahexanoic acid (DHA) and eicosapentaenoic acid (EPA), and monounsaturated fatty acids[134] play a vital role in AMD prevention.[131] DHA is a key fatty acid as it is found in high concentrations in the retinal tissue.[136] It has an effect on retinal cell signaling mechanisms and the photoreceptor membrane works by changing thickness, fluidity, permeability, lipid phase properties and the activation of membrane- bound proteins.[131]

Regular consumption of DHA and EPA was attributed to decrease the risk of advanced AMD by 38%.[131] In addition, the Mountains Eye Study revealed that fish intake three times a week could reduce the risk of both early and late AMD.[137,138] The effects of DHA and EPA supplementation on AMD development has been tested in the Age-Related Eye Disease Study AREDS II.[131]

#### 1.4.2.3.8  Cardiovascular disease

AMD is assumed to share common risk factors with cardiovascular diseases such as dietary fat, smoking [130], high cholesterol level and hypertension. [127] On the other hand, raised concentration of HDL cholesterol, which is normally assumed to be cardioprotective is often associated with reducing AMD risk.[139] Some studies indicated a direct correlation between AMD and hypertension[140] and increased level of cholesterol in the serum[141] and diet.

Drusen is also postulated to share several molecular components with atherosclerosis plaques, such as lipids, vitronectin, apolipoprotein E, calcium, and complement constituents.[100]  One study presented data suggesting a strong association between advanced AMD and both carotid artery atherosclerosis[142] and cardiovascular deaths.[143]

#### 1.4.2.4  The relation between age related macular degeneration and mortality

A study based on large population indicated the relation between visual impairment (visual acuity less than 20/40) and increased mortality. According to AREDS, 91% of participants who had worse than 20/40 visual acuity at baseline in one eye were recognised in AMD category 4.[143] A hypothesis analyzed the reason for mortality and proposed that nuclear cataract and AMD category 4 may be linked with the main cause

of death which is cancer and diseases of the circulatory system, respectively.[139] Furthermore, vision loss could affect mortality directly, if it leads to accidents, for example, fatal fall, automobile accident or depression that in turn are reported to increase mortality.[143]

### 1.4.2.5   The role of antioxidant supplementations and dietary intake in AMD

Observational studies which evaluated the effect of dietary antioxidants on the risk of age-related macular degeneration have been investigated, with inconsistent results. A recent European Union study carried out by cross-sectional population had proposed a two-fold increase in the risk of advanced AMD due to intense exposure to sunlight combined with low concentration of antioxidants in their serum.[98,144] Therefore, the antioxidant nutrients are assumed to be protective through their role as antioxidant, these include lutein, zeaxanthin, β-carotene, vitamins C, E, B and Zn.[131]  A major National Eye Institute study and the Age-Related Eye Disease Study (AREDS) showed that supplements of antioxidant vitamins C (500mg), E (400 IU), beta-carotene(15 mg), zinc oxide (80 mg), and copper (as cupric oxide 2 mg) decreased the risk of developing advanced AMD by 25%, and the risk reduction for those taking antioxidants alone or Zn alone account for 17% and 21%, respectively.[107,145] By contrast, other studies found no certain effect of antioxidant supplementation on patients with early nonexudative AMD or active exudative.[93,104,108] Additionally, three randomised controlled trials found that vitamin E or β- carotene supplements failed to have a beneficial effect on AMD.[108]

### 1.4.2.6   The role of zinc in AMD

### 1.4.2.6.1   The positive role of zinc in the pathogenesis of AMD

Zinc is involved in numerous biological processes including stabilisation of cell membranes, RNA/DNA metabolism, regulation of gene expression, protien synthesis, supporting immune function, cell growth, and motivation of the activity of numerous enzymes in the body.[134,146,147] These significant properties of Zn may have therapeutic benefits in a range of diseases in humans. Zn has been successfully used as a treatment for two fatal genetic diseases, acrodermatities enteropathica and Wilson's disease. Zn supplementation can also treat acute diarrhea in children, chronic hepatitis C, common cold and several bacterial infections in the elderly.[134]

The human retina is rich in Zn, hence it is essential for retinal cell survival, visual cycle and the controlling of antioxidant enzymes.[119] Zinc supplementation decreases oxidative stress, decreases the generation of inflammatory cytokines[134], and elevates its concentration in the plasma. This in turn enhances the immune system and provides superior protection in AMD[2]. Based on the large Age-Related Eye Disease Study (AREDS), a strong association was found between Zn supplements intake and preventing the progression of AMD.[95,119,134,148]

The recommended dietary allowance for Zn is 12–15 mg/day in the USA and 8–9.5 mg/day in the UK. A recent large-scale study observed that a healthy balanced diet providing the necessary Zn and vitamins is associated with a 35% reduction in the risk of AMD[95] and are much better than supplementation (AREDS).[94,145] Yet, for people who are already suffering from Zn deficiency due to malnutrition, Zn supplementation would be strongly recommended.[94]

A wide variety of sources contain Zn e.g. red meat, oysters, beans, nuts, shellfish, whole grains, cereals and seeds.[147] However, the bioavailability of Zn is affected by other components. Non-digestible plants, including phytate and some dietary fibers bind with Zn to form insoluble complexes, thereby Zn absorption is inhibited. Another factor that influences the bioavailability of Zn supplements is the formulation. Zinc oxide, which is commonly used in supplements for AMD, has very low bioavailability, whereas Zn salt, e.g. zinc acetate has relatively high bioavailability.[101,147] As a result, that may cause Zn deficiency which is characterised by several symptoms, for example, growth retardation, cognitive impairment, immune dysfunction, eye and skin lesions, and the generation of inflammatory cytokines.[134]

### 1.4.2.6.2 The negative role of zinc in the pathogenesis of AMD

It is postulated that the formation of lipid and protein deposits in the focal or peripheral retina may be a major factor in the progression of AMD.[109] As Zn is highly concentrated in the eye, particularly in the RPE/choroid complex where the sub-RPE deposits are formed, it is argued that the accumulation of Zn binding proteins and other components may play a role in formation of sub-RPE deposits and therefore in development of AMD. Moreover, Zn binding proteins may precipitate accidentally in Bruch's membrane in the late stages of AMD.[101] Studies that have shown the effect of Zn supplements on

decreasing the development of AMD yielded conflicting results.[94] Lengyel and Peto (2008) proposed that no clear link was found between antioxidants, Zn supplements and reduced risk of AMD.[94,101] In addition, another systematic review supported the lack of benefits of supplementation in primary prevention of AMD.[104]

In 2001, the Age-Related Eye Disease Study (AREDS) established a supplement containing high doses of vitamins C and E, betacarotene, and the minerals Zn and Zu (called AREDS formulation). The American Academy of Ophthalmology recommends using the AREDS formulation as it can slow the progression to advanced AMD. However, it appears from some literature that there are adverse effects of high doses of Zn supplementation.[94,101,106,107] Added to this, there have been concerns that the high dose of Zn in AREDS can lead to Cu deficiency and other side effects as well as increasing the risk of lung cancer in smokers with high dose of beta-carotene.[94,106,107] Therefore, in 2006 AREDS2 was launched and improved AREDS formulation by reducing the Zn dose, removing beta-carotene and adding some other nutrients. The study also examined how different combinations of the supplements performed. While waiting for the availability of AREDS2 results, the AREDS formulation remains the treatment of choice for patients with intermediate AMD and advanced AMD in one eye.[149,40]

## 1.5  Introduction to analytical techniques

### 1.5.1  Sector field inductively coupled plasma-mass spectrometry

Inductively coupled plasma mass spectrometry (ICP-MS) is powerful, reliable and commonly used for trace element analysis due to its ability to identify and quantify most elements in the periodic table in numerous matrices.[150,151] This highly sensitive analytical technique is used for isotope ratio measurements and fast simultaneous multi-elemental analysis at low volume consumption. In addition, ICP-MS offers a wide linear range, reduced interferences and very low detection limits down to ppt level.[152,153] Moreover, the capability of coupling ICP-MS with other sampling methods including solution sample nebulisation, laser ablation[154] and chromatographic[155] and other separation techniques[156,157] make this technique a versatile tool of exceptional quality. Thus, ICP-MS is considered an ideal method for Zn, Cu and Fe determination in biological samples. The basic instrumentation of ICP-MS will be discussed briefly in the following section. The following section briefly discussed basic instrumentation of ICP-MS.

### 1.5.1.1  Instrumentation

The Instrument will be briefly described in this section, and the five major parts of SF-ICP-MS, as used in the research presented in this Thesis, are as following:

- Sample introduction system
- The plasma (ionisation)
- The interface
- The mass analyser
- The detector

A schematic diagram of an ICP-MS instrument is shown in Figure 1.7.
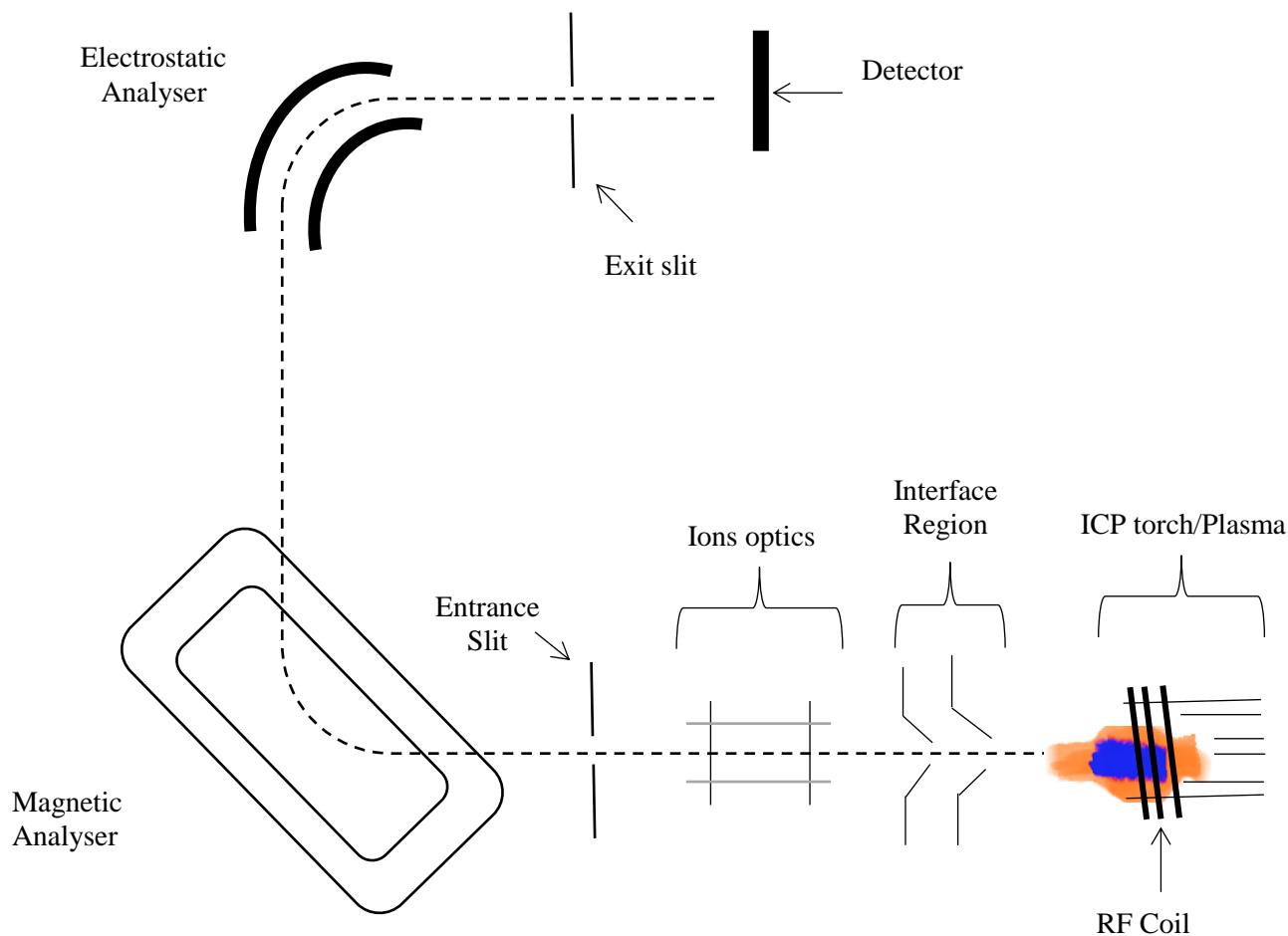
**Figure 1.7** Schematic diagram of the reverse Nier-Johnson magnetic sector field ICP-MS instrument.

### 1.5.1.2 Solution-based sample introduction

Although many different sample introduction systems are combined with ICP-MS, the most common ICP-MS work is performed on liquid samples by using an analytical nebulizer. While each method may be primarily different, they have the similar aim of sweeping the sample of interest into the ICP torch in an aerosol form for analysis. The introduction of solid samples into the ICP via laser ablation (LA) will be covered in section 1.5.2. The solution nebulisation system consists of a peristaltic pump and a nebuliser which converts a flowing liquid into a stream of aerosol droplets. The produced aerosols tend to cover a wide particle size distribution (approximately $0.1 - 25$ μm[158]) and thus the function of the spray chamber is to separate large droplets from small ones. Only the small droplets, (typically those <10 μm in diameter[153]) are swept by a flow of argon gas to the sample injector and then ionised by the plasma, whilst the large droplets

fall out via gravity and exit by a drain tube to waste. While a typical flow rate of the nebuliser is around 1 ml min$^{-1}$, micro-flow nebulisation with uptake rates of between 20-600 μL min$^{-1}$ are significantly useful especially in biological and clinical fields, where only limited amounts of sample may be available.[152,159]

### 1.5.1.3 The plasma – formation and ion generation

In the ICP-MS, the ionisation source is represented by the plasma and is an electrically conducting gaseous mixture, formed by using inert gas (typically Argon) that flows continuously throughout the quartz torch. RF generator, radio frequency (RF) coil, a torch and argon gas are the main requirements for plasma generation. The ICP torch consists of three concentric tubes: sample injector, middle and outer tube as illustrated in Figure 1.8. The central tube is the injector, transferring the sample aerosol into the plasma. The two middle and outer tubes transport the gas flows which both produce and cool the plasma in the torch. The top end of the torch is surrounded by a Cu induction coil, which provides a high radio-frequency (RF) electric current of around 27-50 MHz.[160] While the RF generator supplies RF power to the coil, a magnetic field is generated. A flow of argon gas is introduced between the two outermost tubes of the torch and a high voltage spark is applied for a short time to introduce free electrons into the gas stream. These released electrons are accelerated in the magnetic field and collide with other argon atoms causing further ionisation.[152] As long as the magnetic field is maintained by the RF, ions and electrons will continue to collide. The typical temperature of the plasma in the ICP-MS ranges between 6000-8000 K and it is maintained at normal atmospheric pressure. Under these conditions, the sample passes through the central channel of the plasma, where it is de-solvated, atomised and ionised, and these newly formed ions then travel to the mass spectrometer via the vacuum interface region. Most elements in the plasma have an ionisation efficiency of about 100%, which makes the ICP-MS an efficient and versatile tool capable of detecting most elements in the periodic table.[152,160]
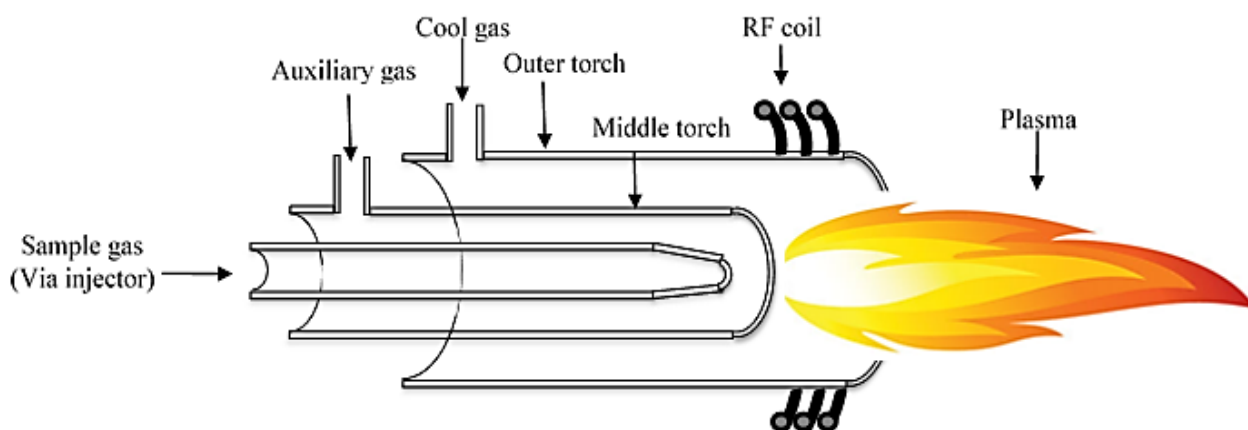
**Figure 1.8** Cut-through schematic of an inductively coupled plasma torch.

The interface is the region between vacuum and plasma. While the ICP plasma operates at atmospheric pressure (760 Torr) and the mass analyser as well as detector operates at high vacuum ($10^{-6}$ Torr), an interface region is necessary.[153] The function of the interface is to direct the produced ions from the atmospheric pressure plasma and reduce the pressure so the ions can be extracted in the higher vacuum region, where the ion focussing lenses, mass analyser and detectors are situated. This interface consists of two high thermal conductivity metal cones; the most popular are made of nickel or platinum. The first cone that is positioned at the end of the plasma is called the sampler cone with an orifice of approximately 0.8-1.2 mm. The second one sits behind the sampler cone and has a marginally smaller orifice diameter (0.4 - 0.8 mm) that is referred to as the skimmer cone[153] (see Figure 1.9). A mechanical roughing pump reduces the pressure between the two cones to 1-2 Torr, creating a region of intermediate pressure between the 2 regions. When the sample passes through this orifice, the gas flow speed increases and exceeds the speed of sound where supersonic ion expansion occurs between the sampler and skimmer cone owing to the sudden drop in pressure and thus particle density. This results in a shock wave formation behind the sampler cone, comprising a region known as the zone of silence.

After the ion beam passes through the interface region, a series of electrostatic ion optics lenses are used to focus and accelerate the ions before they enter the mass analyser. In addition, the ion optics prevent photons, or neutral species from entering the mass analyser and detector as it could cause signal instability and thus high backgrounds.[153,160]
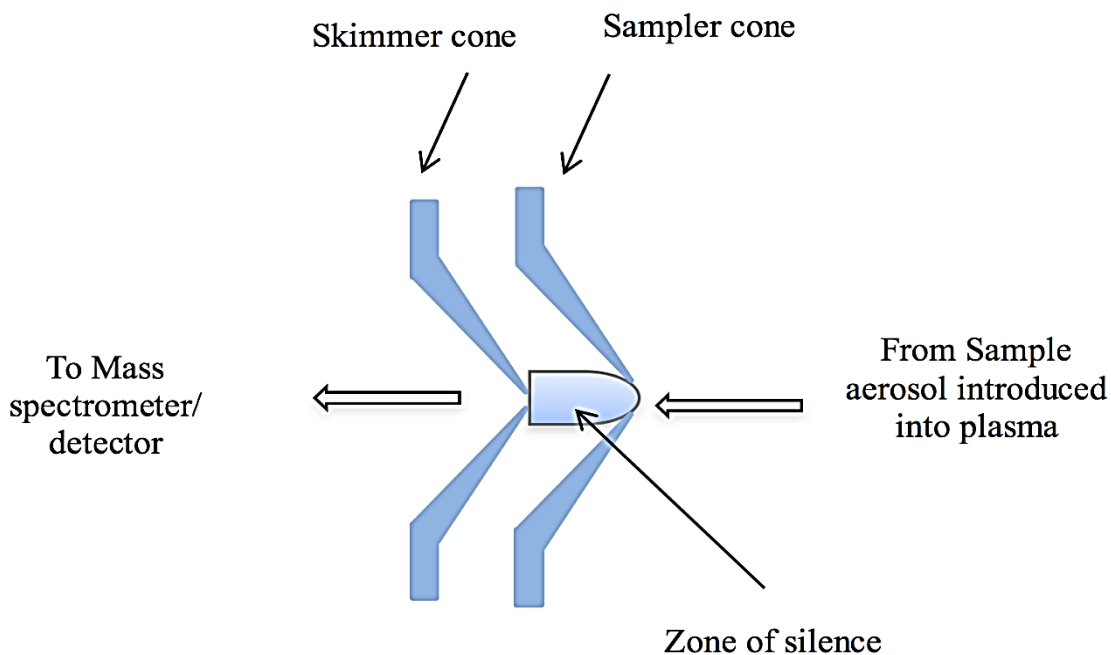
**Figure 1.9** Schematic drawing of the cone interface region.

### 1.5.1.4   Mass analyser

The mass spectrometer consists of a mass analyser and detector that detect as well as separate the ions based on mass to charge ratio. Mainly three types of mass analysers are used in ICP-MS; magnetic sector, time of flight and quadrapole. The quadrupole mass analyser is possibly the most commonly used due to its speed, stability and low cost. However, it can only be operated in a low-resolution mode and requires a collision reaction cell to eliminate polyatomic interferences. Whereas, a magnetic sector provides the best sensitivity as it has the ability to separate most polymeric interferences by operating at high resolution in the region of 10,000. As a high resolution sector field mass spectrometer was the main instrument used in the project, further discussion will be confined to this type.[160]

In magnetic sector instruments two designs are use, the reverse Nier-Johnson design and forward (or standard). The ICP-MS configuration used in this work is a Thermo Element 2 XR with a reverse Nier-Johnson geometry, with the magnetic analyser placed prior to the electrostatic analyser (ESA). The initially circular ion beam becomes rectangular as the ions are focused and pass through a slit into the magnetic sector of the instrument. The slit can be used to control the resolution by adjusting the width of the slit, and thus the ion beam dispersion. Two slits are used to control the resolution, recognized as the

31

entrance and exit slits. The entrance slit is located between the ion optics and the mass analyser, whereas the exit slit is located between the electrostatic analyser and the detector. Resolution is defined in the equation below, where R is the resolution, m is the mass of the analyte of interest and Δm is the peak width of the mass at 5% peak height.

$$R = \frac{m}{\Delta m}$$

The three resolution settings of the instrument are; low resolution (R~300), medium resolution (R~4000) and high resolution (R~10000). Although high resolution allows for greater separation of peaks as the slit width is narrow, the number of ions transmitted is reduced, and thus the sensitivity is dropped as low as 1-2% of the counts seen for low resolution.[151,152,161]

The double focusing principle for both designs (forward or reverse) consist of two analysers, a traditional electromagnetic and an electrostatic analyser (ESA). The magnetic field, which is dispersive with regards to momentum (and therefore ion mass), separates ions of different masses then focuses all the ions with diverging angles of motion from the entrance slit. Inside a curved magnetic field of a given strength, ions of different mass travel on different trajectory dependening on their mass to charge ratio. When the magnetic field is held constant, the ions of varying m/z can be focused onto an intermediate slit,varying the acceleration voltage, and hence the velocity of the ions, thus stopping the transmission of any ions of higher or lower m/z than the desired analyte. The ions exiting the magnetic sector have different kinetic energy, depending on the formation position in the plasma. Thus, this energy dispersion leads to peak broadening and loss of resolution. To overcome this, a second mass analyser, an electrostatic analyser (ESA), is employed after the magnetic sector. The ESA, which is dispersive only with respect to ion energy, then focuses all the ions onto the exit slit, where the detector is located.[162] The ESA consists of two curved plates, which have opposing voltages applied to them. The inner plate has a negative charge which attracts the positively charged ions, whilst the positively charged outer plate repels them, thus focussing and deflecting the ions. When the energy dispersion of the magnet and the ESA are equal in magnitude but opposite in direction, by using a combination of the magnetic and electrostatic sectors, the ion beam allows for the focussing of ions based on the m/z ratio. Their combined usage is referred to as double focussing.[152]

There are two main scan modes used with double-focusing mass spectrometers, magnetic scan (B Scan) and electric scan (E Scan).[161] E Scan is the default mode used by the Element XR. In this mode, the magnetic field moves initially to the start mass and is then kept constant whereas the acceleration voltage and corresponding ESA voltage are both changed together. This enables rapid scanning; however, the maximum range for E-scan is limited (30% of the start mass). B Scan is the opposite, the accelerating voltage and the electrostatic sector (ESA) voltages are kept constant and the magnetic field is varied. Although B Scan mode is much slower compared to E scan, it is not limited in range. Consequently, it is preferred for the analysis of large, continuous mass ranges, as is required for mass calibration.[161]

### 1.5.1.5   The Detector

After the ion beam passes through the exit slit, it enters the detector and is converted to electrical signals. The Element XR contain two types of detectors; a Secondary Electron Multiplier (SEM) and Faraday Cup. SEM, the most common detector, consists of a series of 19 metal dynodes. The ion beam is directed towards a conventional dynode before entering the SEM, resulting in an electron is ejected from it. When the electron hits the first dynode surface, one or more electrons are released. The influence of the first dynode generates secondary electrons, which hit the second electrode, producing more electrons, and so on along the length of the detector. Consequently, the number of electrons grows and the original signal is amplified. This results in a very high pulse of electrons being produced from the final dynode which is converted into an electrical signal and communicated to the computer in units of counts per second (cps). The SEM detector can operate in two modes of counting depending on the signal intensity. In counting mode, both sections of the SEM detector are switched on. This mode is useful for trace analysis where signal is expected to be less than $5 \times 10^6$ cps. Whereas, the analogue mode can be used for higher count rates, allowing for detection between $5 \times 10^6$ and $1 \times 10^7$ cps. [161] In this mode, the second section of the SEM is switched off to protect the dynode from exposure to the huge signals, and thus extend the lifetime of the SEM. If higher signal intensity is required, the dynamic range of the instrument could be further increased by the use of a Faraday cup.[152]

### 1.5.2   Laser ablation

Laser ablation (LA) is frequently used as a direct sample introduction for solid samples with ICP-MS. LA-ICP-MS has experienced a series of improvements since its first introduction by Gray in 1985.[163] However the general principle and various components of a typical laser ablation system have not changed.[160] This powerful technique is capable of reliable and rapid analysis to obtain information on the spatial distribution of trace and ultra-trace elements in many different types of solid samples.[164,165,166,167,168] Although geological applications typically cover around 30-50% of all LA-ICP-MS papers[154], the attention to biological applications[169,170,171,172,173] in the last few years has significantly increased. The basic instrumentation of laser ablation will be discussed briefly in the following section.

During the ablation process, a laser pulse is directed onto the sample using a high-power, short-pulsed laser focused onto the sample surface by mirrors and lenses. The aerosol plumes that contain atoms, ions, and particles are formed and released from the laser ablation crater. These particles then are transported to the ICP by a stream of carrier gas, where it is vaporized, atomized, and ionized and subsequently analysed in the mass spectrometer.[174]

#### 1.5.2.1   Instrumentation

A typical LA sampling system involves; a laser beam, a series of optical devices, a viewing system, an ablation cell, and a transport connection between LA and ICP-MS. Figure 1.10 shows a schematic of a typical laser ablation setup.[175]

#### 1.5.2.2   Types of laser source

Many types of laser sources have been successfully used for laser ablation, including Ruby, excimer and neodymium-doped yttrium–aluminium–garnet (Nd:YAG). The most commonly used of these is Nd:YAG due to its ease of use, reliability, low cost and robustness.[175] It comprises of a rod containing a single yttrium aluminium garnet (YAG) solid crystal fixed with neodymium ions. The use of UV lasers has become more widespread than IR.  The fundamental wavelength of this laser is 1064 nm, which is poorly absorbed by several matrices. Thus, harmonic generation is necessary to allow Nd:YAG laser to operate at shorter wave length, such as 266nm, and 213nm.[160] A

Nd:YAG functioning at 193nm has recently been introduced and is commercially available.
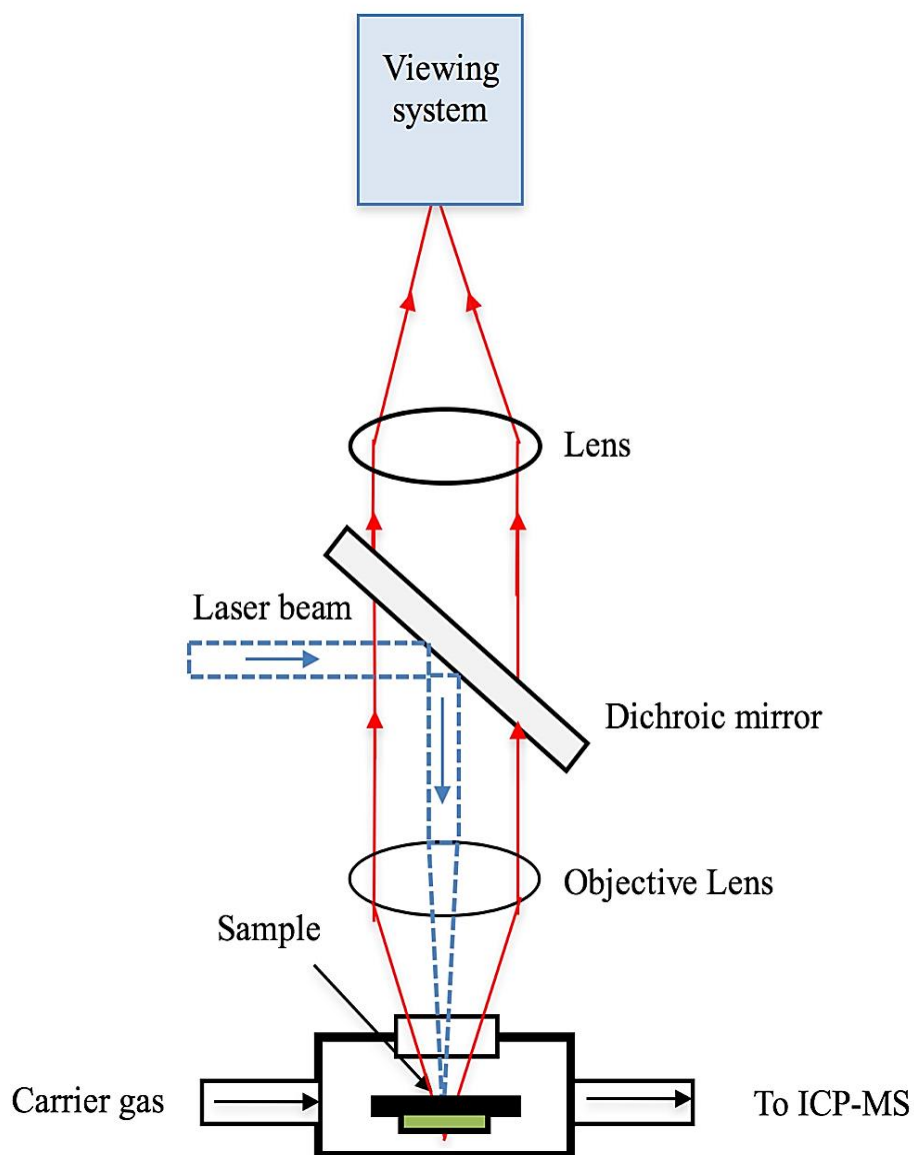


**Figure 1.10** Schematic of a laser ablation system.

Overall, shorter wavelengths provide better ablation features for sample introduction to ICP-MS and better signal intensity.[176] The absorbance features of the sample matrix are the key factor in choosing the appropriate wavelength, as this affects the ablation production. For example, Becker suggests that 266 nm is sufficient to ablate completely soft biological tissues as it is easy to ablate.[177] The most common laser pulse duration

available in economical systems of LA-ICP-MS in early work is nanosecond. However, there is now a developing trend towards the use of shorter pulse width depending on the analytical measurement, such as pico- and femto-second. Russo et al.[178] reported that picosecond laser pulses could give improved accuracy and enhanced ablation efficiency compared to nanosecond laser pulses. In addition, the improvement of femtosecond over nanosecond explains the significance of laser pulse duration and related effects on the ablation process.[179]

### 1.5.2.3   Laser focusing

In order to direct and focus the laser beam onto the sample, a series of mirrors or prisms and objective lens are required. These mirrors that have insulator optical coating on a highly polished surface and high transmission for other wavelengths are proven to be robust and long lasting. The shape and the size of the ablation crater are often adjustable. Normally the ablation craters are either conical or cylindrical in shape and few µm in diameter. Some advanced laser systems allow the use of spot sizes down to 1 micron or below.[154,175]

### 1.5.2.4   The ablation cell

The sample is located inside a laser ablation cell while ablation takes places. A variety of different ablation cells have been designed and developed for LA-ICP-MS. Each ablation chamber consists of a few basic components: a sample holder, ports for carrier gas entry and exit, fused silica window to allow the laser beam to pass through. Most ablation cells are mounted on an adjustable platform usually under computer control, to allow sample positioning in different directions, hence the target is easily and precisely selected. The cell is connected to the ICP via plastic tubing and the ablated materials typically transported to the ICP through this tube. Tubing is usually over a metre in length and about 3-4 mm internal diameter. While the laser is firing in continuous mode, the stage is moved in a specific pattern; generally parallel lines to create images. When the ablated materials reach the mass spectrometer, the acquired spectra can be transformed into two-dimensional colour maps and signal intensity displayed as a function of the image dimensions.[174]

### 1.5.2.5 Carrier gas

During the ablation process, the generated materials are swept to the ICP via a carrier gas that flows continuously through the cell to provide an inert atmosphere for ablation. A careful selection of carrier gas is required as it plays an important role in particle size distribution and production. Argon (Ar) carrier gas was traditionally used for initial LA experiments. Nevertheless, many users have replaced the use of Ar gas with Helium (He) gas owing to improved ablation and transport properties. Horn and Günther compared different carrier gases and their influence on the size distribution and thus transport efficiency. They concluded that utilizing He as a carrier gas during ablation produces smaller particles distributions than in argon, and therefore transported to the ICP with better efficiency which leads to sensitivity improvement. The physical properties of the He carrier gas such as lower density, higher thermal conductivity and higher ionization energy, contributed to the change in particle size distribution to smaller particles.[174,180]

# 2 Trace Determination of Zn, Cu and Fe in Human Serum Samples from Age Related Macular Degeneration and Alzheimer Patients using ICP-MS

## 2.1 Introduction

The liquid fraction of the whole blood after the removal of cells (white, red) and platelets is termed as plasma, which constitutes 55% of the total blood volume.[181] Serum is obtained from blood plasma after separating the main blood clotting protein (fibrinogen) that mainly consists of water that has a high concentration of proteins, hormones, inorganic salt and variety of minerals.[181,25] According to their biochemical importance and ease of accessibility, serum and other biological samples including blood, plasma and urine have been selected by many clinical and analytical researchers.[182] Minerals play a key role in supporting many biological functions, hence biomonitoring of trace elements in human biological fluids would provide essential information on the nutritional studies and the health of individuals.[183] The concentration level of all minerals is maintained constantly through the homeostasis process in order to avoid the increase or decrease of the nutrients which cause either toxicity or deficiency. As there are many illnesses associated with an excess or shortage of the minerals, understanding the interaction of minerals in the body represents a comprehensive vision of diagnosis, screening and treatment of illnesses.[183,184,185]

The essential trace elements, Fe, Zn, and Cu play crucial role in retinal structure, and pathology. They are principally involved in numerous retinal functions for instance, retinal cell metabolism, the visual cycle, photo transduction, and the process of neurotransmission.[186] Several experimental studies have indicated that the alteration of Zn, Cu and Fe homeostasis and inflammation in the retina may lead to retinal dysfunction and therefore initiate the age related macular degeneration (AMD) abnormality.[187,188,189]

As noted in section 1.4.2, AMD is a chronic eye disease, which mainly attacks the macula thus causing severe and irreversible vision loss in elderly people.[94] The main focus in this study is on one of the AMD types which causes damaging of blood vessels that grow

underneath the retina, known as Choroidal Neovascularisation (CNV). CNV can lead to the leakage of blood and accumulation of serum in the eye leading to irreversible vision loss in a short period of time.[190] In their 2016 paper, Gwairi et al.[190] noted that there is a link between AMD and serum lipids levels.

Accumulation of Fe in the retina and the changes occurring during homeostasis mechanism is an indication of aging and believed to contribute to retinal degeneration such as AMD disease.[186] Hahn et al.[191] have revealed that, Fe levels rise with aging in the mammalian retina and this increase is higher in women in comparison with men. The level of Fe and Cu seems to respond slowly with the change in the plasma level, whereas, the pool of Zn in the retina exchanges quickly with plasma.[186] In the body, Fe is mainly bound with ferritin in serum and it is a reflection of Fe stores. Various authors have reported that, when the ferritin level in serum increases, Cu level increases in the blood, whereas Zn concentration decreases in the plasma or serum.[186,192,193]

Alterations in serum/plasma trace elements have been reported in patients with neurodegenerative and other diseases.[194,195] Essential and toxic metal ions have been found to influence neuron degeneration. Dysfunctional homeostasis of some elements and their relevant enzymes have led to the formation of amyloid beta (Aß) plaques which are implicated in Alzheimer's disease pathogenesis.[196,79] It is evident that accumulation of Aβ and tau proteins in both amyloid plaques and neuronal tangles are associated with neurodegenerative process in the brain of Alzheimer's patients. The defective antioxidant defence could also result in oxidative damage in AD patients.[196] Zinc, copper, and iron appear to participate in the interaction of the major protein constituent of AD.[197] Of these metals, Zn in particular is found at a high level in senile plaques (SP)[78] in AD patients and, therefore accelerates the oligomer aggregation of amyloid beta peptide together with a number of metallothioneins and metalloproteases.[70,78,198] Due to the lack of understanding of the exact role of the element in the etiology and the pathogenesis of the disease[82] several studies have been undertaken to measure the metal concentration in brain tissues[199], serum[82,15,200,201,72] and cerebrospinal fluid.[202,5] As serum can be taken from a large number of patients in different AD stages hence the focus in this study will be in serum. According to the meta-analysis by Ventriglia 2015[202], six studies have investigated the level of Zn in the serum of AD patients by using ICP-MS, whilst others found AAS sufficiently sensitive for the Zn levels (~1 ppm) in the serum. Various conflicting studies have shown different results regarding the serum Zn level in AD

patients. Some studies showed an increase in Zn level in the serum of AD patients.[201] Other studies[81,83,203,204,205] observed no significant differences in serum Zn between AD and healthy control. On the other hand, in 2015 Ventriglia et al.[202] reported in the meta-analysis that AD patients had a significant decrease in serum Zn level in comparison with healthy controls.[196,15,72,17] A possible reason for decreasing serum Zn level in AD patients might be the accumulation of Zn in the brain as amyloid plaques trap Zn and deplete it in other body compartments.[15]

Zn deficiency and variation in AD patients could be related to the interaction with Cu metabolism.[202] Another cause of reduction of serum Zn in AD patients is due to dietary Zn deficiency. In contrast to whole blood, serum/plasma level of minerals reflects short-term changes and may be influenced by present dietary intake.[195] Moreover, Several factors such as age and gender could affect AD, and Rembach et al. 2014 [72] found that serum Zn concentration dropped around 0.4% per year with age but they did not indicate a correlation between serum Zn and gender. Conversely, a recent meta-analysis did not observe a significant difference in serum Zn level between AD patients and healthy controls according to age.[202] Bjorksten et al. found serum Zn levels in men aged under 60 years higher than women.[206,207] Wang et al. added in his meta-analysis that differences in serum Zn concentration related to different gender ratio, whereas differences in Fe level appeared to be due to the difference in mean age.[208]

Both Cu and Fe demonstrate considerable increases in serum levels with age.[85] Copper absorption was greater in women (71%) than in men (64%) aged 20-59 years, but became constant in men and women aged 60-83 years.[209] It appears that there is no significant difference in Fe serum level between AD patient and healthy control, however, case-control and autopsy studies reported an elevated level of Fe in the brain in AD patients.[22] Most of the study's results revealed serum Cu concentration to be significantly higher in AD patients in comparison with controls[208,20,210,211] but remaining unchanged in the brain and CSF.[22] In circulation, Cu is strongly bound to the main Cu transporter protein ceruloplasmin and is a marker of plasma Cu level and inflammation.[209] Therefore, Agarwal et al.[20] measured serum ceruloplasmin level to find out if there is a positive relation between Cu and ceruloplasmin. They found a significant increase in serum ceruloplasmin in both genders of AD patients as compared to healthy individuals as control. Variation in Zn, Cu and Fe concentrations are affected by different factors such as age, gender, hormonal state, diet, the length of fast, time of day and geographic

area.[206,85] Squitti et al.[23] recognized other factors that could estimate AD risks like family history, physical activity, body mass index, systolic blood pressure and total cholestrol level. Therefore, the investigation should occur on a bigger scale in different populations and should take the age, gender, and other factors into account.

Several analytical methods have been used in the past to measure trace and ultra-trace elements in serum. Flame or graphite furnace atomic absorption spectrometry (FAAS/GFAAS)[212,213,214,215] neutron activation analysis (NAA)[212,216] and proton induced X-ray emission spectrometry (PIXE)[182] were generally the main techniques used for this application. In the last decades, a powerful alternative technique ICP-MS has been extensively used for multi-element determination in human serum samples.[183,83,213,217,218,219,220,221,222,223,224] It is the most popular, efficient, robust and suitable methodology for this requirement because it is fast, highly sensitive, flexible and easy to use, with a low detection limit and wide linear dynamic range, and is capable of simultaneously quantifying multiple elements in a short time precisely and accurately.[221,220,225]

## 2.1.1   Aim of the work

The comparison of serum analysis in AMD and AD patients and its possible correlation is not reported to date. Therefore, the main purpose of the present work is to compare the distribution level of serum Zn, Cu and Fe between age related macular degeneration patients (AMD) (of the Choroidal Neovascularization  (CNV) type), and Alzheimer patients (AD) using SF-ICP-MS. A wider aim was to develop a method suitable for the determination of transition metals, specifically Zn, Cu and Fe, in minimal sample volume (50µL and below), the method to be readily adaptable for automation,  and to run unattended for long periods.  Use of a denaturing reagent mix compatible with the nebuliser keeps the sample introduction system clean and free flowing for long periods. Minimal sample volume consumption during analysis is important to conserve the sample (often available in limited quantitities, as in this work) and offer the possibility of repeat analyses.

## 2.2 Methodology

### 2.2.1 Ethics and sample collection

Ethical approvals (09/H0710/10) and (08/H0805/6) were obtained from health research authority, NRES committee London-Harrow (Ethics applications and approvals are included in the appendix). All the necessary safety precautions were taken before handling the serum samples.

Low concentration of elements in the biological samples and the risk of contamination during sample collection could make this type of evaluation challenging as well as difficult to perform. For example, stainless steel needles are most probably used in the clinics and these needles could be a vast source of contamination. Thus, siliconized needles are recommended to use.[59] A 1.0 mL sample of blood was drawn from both AMD and AD patients into blue capped trace metal free vacutainers (Becton Dickinson, Oxford). The serum was collected by centrifuging the blood at 2500 rpm for 20 min. An aliquot (100 µL) was transferred into a 1 mL clean polypropylene (Eppendorf) tubes and then stored immediately in -80 °C freezer until analysis. All samples were labeled with the disease type, patient's code number and date. A range (81) of human serum samples were obtained from Dr. Imre Lengyel, Institute of Ophthalmology, University College London.

### 2.2.2 Instrumentation and statistical methods

The analysis of the elements of interest (Zn, Cu, Fe) was made within a single sampling with no alteration in instrument operating conditions, in addition to the selection of resolution mode. Due to the range and complexity of the interferences, medium resolution was required (R = 4000) to avoid spectral interferences; specifically, $^{64}Ni$ on $^{64}Zn$, $^{54}Cr$ on $^{54}Fe$ and $^{40}Ar^{16}O$ on $^{56}Fe$ and to ensure the accurate analysis of Zn, Cu, and Fe. The analysis was performed on a sector-field inductively coupled plasma mass spectrometer (SF-ICP-MS) (Thermo Scientific, Element 2 XR, Bremen, Germany). The instrument was fixed with platinum sampler and skimmer cones (ICPMS cones Ltd., Chester, UK), and a sample introduction system equipped with a conical glass concentric nebulizer (Glass Expansion, Victoria, Australia), a Cyclonic spray chamber (Glass Expansion, Victoria, Australia) and a 0.5 mm i.d. probe (Elemental Scientific, Omaha, USA). The sample flow rate was set to provide a flow rate of approximately 400 µL/min. Daily, the

ICP-MS gas flows and torch positions were tuned to optimise conditions, achieving high signal intensity and low oxide ratio. Typical operating parameters and instrument conditions for ICP-MS are summarized in Table 2.1. Data obtained from sample analysis by the mass spectrometry techniques described in this chapter were collected, organised and analysed by using statistical tools in Microsoft Excel 2016. Other software such as Minitab® and Origin 2015 were used for plotting some schematic diagrams.

**Table 2.1** ICP-MS typical operating parameters for $Zn^{66}$, $Cu^{65}$ and $Fe^{57}$

| Parameter | Condition |
| --- | --- |
| Radio frequency (RF) power | 1252 W |
| Cool gas flow rate | 15.50 L/ min |
| Auxiliary gas flow rate | 0.88 L/min |
| Sample gas flow rate | 1.05 L/min |
| Resolution | Medium |
| Torch X position | 4.6 mm |
| Torch Y position | 3.8 mm |
| Torch Z position | -2.5 mm |
| Sampler cone | Pt |
| Skimmer cone | Pt |

### 2.2.3 Reagents and chemicals

Ultra-pure water (18 MΩ) was obtained from a Milli-Q Element system (Millipore, Watford, UK). 10 ppm multi-element solution 2 (MES 2; Ag, Al, As, Ba, Be, Bi, Ca, Cd, Co, Cr, Cs, Cu, Fe, Ga, In, K, Li, Mg, Mn, Na, No, Ni, Pb, Rb, Se, Sr, Ti, V, Zn) was purchased from SPEX Certi prep Ltd (Middlesex, UK) and diluted to 1 ppb. The instrument was calibrated by external single element standards solution (1000 ppm) Zn, Cu and Fe (Qmx Laboratories, Essex, UK). 1000 ppm Gallium was used as internal standard (Qmx Laboratories, Essex, UK). The sample preparation included the following reagents: 70% ultra-pure nitric acid and 25% ultra-pure Ammonia solution purchased from Romil Ltd (Cambridge, UK), Triton X-100 (Sigma-Aldrich, Poole, UK) and Butanol (Fisher Scientific, Loughborough, UK). Two Standard reference materials were used: Seronorm™ trace elements serum, level 1 (6 × 3 mL) (Alere, UK) and serum control-trace elements normal range (5 × 5 mL) (UTAK Laboratories Inc., Valencia,

USA). Accurate weighing of chemicals was performed on a five-figure balance (AND, San Jose, CA, USA) and a vortex mixer (Labnet Intl. Inc., Edison, NJ, USA) was used to ensure the homogeneity of the sample. 100% disposable Bio-clean Pipette tips were purchased from VWR (Lutterworth, UK) and Anachem Ltd, (Luton, UK). 2 ml colorless micro centrifuge tube (Elkay, UK) and 15 and 50 mL polypropylene metal-free tubes with natural HDPE lid (VWR) and Nalgene Teflon™ PFA bottles (Thermo Scientific, USA) were used for sample preparation, storage and ICP-MS analysis tubes.

### 2.2.4 Challenges in sample preparation and contamination control

Sample preparation is one of the most critical steps in the analytical procedure, as it requires special care to reduce the risk of contamination to bare minimum or losses of analytes by either precipitation and/ or volatilization. Contamination is certainly the most common source of error in the determination of trace elements. Zinc is a relatively difficult element to analyse due to its presence in the environment and that could increase the risk of contamination and lead to high background level. The major difficulty is to keep the blank level as low as possible with such ubiquitous elements especially if clean laboratory facilities are unavailable. Hence, careful preparation of blanks, standards and samples are highly important. Some general precautions have been taken into account while preparing and analysing samples for trace elements by ICP-MS, as follows:

- Care was taken to minimise operator contact with samples during their preparation and analysis, and time and number of steps were minimised.

- Disposable powder-free nitrile gloves were worn all the time. Cream and cosmetics were avoided and hair was covered.

- A selection of clean metal-free tubes, PFA bottles and 100% bio clean pipette tips have been used and all sample storage containers were pre-cleaned to remove additional contamination. Also, the pipette tips were rinsed with the same reagent or 2% $HNO_3$ prior to use.

- Every sample and their associated standards were prepared on the same day or at most a day before analysis.

- Deionized water, ultra-pure acids and other high purity reagents were used. This was done by choosing the lower levels of the metal of interest in any reagents.

- Exposure to metallic parts was avoided, and nebulizer, probe and cyclonic spray chamber were washed thoroughly before using the ICP.

- The colorless caps of the ICP analysis tubes were drilled to minimise contact with lab atmosphere and they were soaked in 10 % $HNO_3$ then rinsed with Milli-Q water prior to analysis.

- During the analysis period, every single sample was opened individually and the system was washed thoroughly between each sample with freshly prepared washing solution.

- The samples and standards were isolated from potential contamination source and protected from dust and fibers as much as possible.

### 2.2.5   Method development of sample preparation

The determination of elements in complex matrices by ICP-MS has been challenging, in particular at trace and ultra-trace levels.[226] The matrix composition of serum with high salt and 6-8% protein content is unsuitable for direct analysis by ICP-MS,[214] hence sample treatment before analysis is required. Sample preparation can be divided into two main types, sample dilution or digestion.[227] Some researchers have chosen to dilute samples with 0.5% $HNO_3$[220] or water[185,223] and others used a mixture of sample diluents including ammonium hydroxide and Triton X.[184,224,227] Additionally, different digestion procedures are commonly used in sample preparation.[183,219,228]

Five serum samples and Seronorm were initially diluted 50-100 fold with 0.5% $HNO_3$. However, because of continuous blockage, especially with PFA nebulizer (PFA-ST Elemental Scientific, Omaha, USA), the procedure was changed to the digestion described below.

The general digestion procedure was performed by adding 70% $HNO_3$ to measured volume of Seronorm and heating at 70 °C for 1h, followed by addition of 30% $H_2O_2$ (Sigma-Aldrich, Poole, UK) and heating to the same temperature for a further 4 h. The sample was then evaporated to dryness under a stream of nitrogen by using a TurboVap Concentration Workstation (Biotage, Uppsala, Sweden). Next, the dry sample was reconstituted in 2% $HNO_3$ prior to analysis. During the digestion procedure, the lids of the Eppendorf vials were pierced by using a sterile needle to prevent pressure build up.

In order to avoid using metal needles as it could contaminate the sample, a small pipette tip was inserted into the side of the lid, so it was not fully closed (slightly opened). However, this step increased the signal intensity of Zn in the blank instead of decreasing it, but the blank of the elements Cu and Fe remained the same in both cases. The general procedure applied to Seronorm was modified and summarised in Table 2.2 with different dilution factors, digestion and evaporation methods. Based on previous publications,[83,219,221,220] different dilution factors (20, 30, 40, 60,100 and 1000 fold) were used in the present investigation. Satisfactory results were achieved with dilution factors 60 and 100-fold. However, results using the dilution factors 20, 30 and 40-fold were unsatisfactory as the resulting serum sample volume of 1.0- 3.0 mL was not enough for two replicate measurements, whereas dilution factor of 1000-fold provides serum sample volume of 50 mL but is more diluted than required for precise measurements and close to the detection limit.

Although digestion has the benefit of eliminating protein that reduces instrumentation clogging and matrix effect, however, it could introduce a potential source of contamination.[219]

Microwave-assisted digestion is considered an alternative sample preparation method for serum, as it can be much faster than using conventional heating. However, there are a number of disadvantages which restrict using this method. (i) The digestion vessel should be cleaned before and after the digestion procedure, and the transfer of samples in vessels could introduce potential external contamination. (ii) A closed-vessel during the digestion process can produce high pressure and temperature and that could lead to potential loss of analytes on sample venting and poor sample throughput. (iii) Extra safe handling techniques are needed due to the high pressure and temperature. (iv) Some microwave-assisted digestion systems are limited to batches of 12 vessels, so that makes the analysis for large number (e.g ≥200 samples) of samples impractical. [25]

Several experiments on Seronorm were applied as a test, using the procedures described in Table 2.2

**Table 2.2** Different methods for digestion procedure

| Tests no. | Dilution factor | Digestion procedure | Evaporation | Reconstituted |
|---|---|---|---|---|
| 1 | 20, 30, 40, 60, 100 and 1000-fold | Add 300 µL $HNO_3$ and 100 µL $H_2O_2$ [83,229] | TurboVap, Manual evaporation under a stream of nitrogen through 1ml colorless pipette tips, overnight in the hot block, overnight in the oven. | 2% $HNO_3$, Water |
| 2 | 60, 100-fold | Add 100 µL $HNO_3$ and 100 µL $H_2O_2$ | Overnight in the hot block (70 °C) | 2% $HNO_3$, Water |
| 3 | 60, 100-fold | Add 150 µL $HNO_3$ and 100 µL $H_2O_2$ [219] | Overnight in the hot block (70 °C) | 2% $HNO_3$, Water |
| 4 | 35, 50 and 100-fold | Add 35 µL $H_2O_2$ and 100 µL $HNO_3$ | No evaporation procedure | Water |

The Turbo Vap evaporation procedure was not successful regardless of the dilution factor and the digestion procedure. This may be due to the nozzle that was made of metal and thus the blank reading was higher than the samples. In order to reduce the risk of metal contamination, another method of evaporation was used.[230] The metal nozzle was substituted by 100% pure virgin grade polypropylene pipette tips and the stream of high purity argon gas was directed manually to the samples while they were placed in a hot block (70 °C) to increase the process of evaporation. Due to frequent hovering of hands over the samples to check the level and adjusting the pipette tips inside centrifuge tube in the open lab atmosphere, this procedure was not a good option due to contamination issues. Leaving the sample overnight in the oven at 70°C was not a good choice either. The only option was to evaporate the samples overnight on a hot plate in a closed fume hood at 70 °C. The common drawback of this procedure was mainly related to sample burning due to overnight heating. The samples were over-dried as well as hard such that it was not possible to completely dissolve after reconstitution. Moreover, small bubbles were created possibly due to the high temperature during the overnight heating. Consequently, the bubbles transferred to the probe and the nebulizer during analysis and that caused frequent clogging and inconsistent spraying. As a result, the calibration standards were not in good linearity and, therefore, the results were affected. To tackle these issues, the temperature was reduced from 70 °C to 45 °C, and the probe and

nebulizer were taken apart and washed thoroughly through a standalone pump with the following solutions: 70% methanol, 25% ammonia, 2% $HNO_3$ and deionized water in between each reagent. In addition, the samples were sonicated prior to analysis, and the probe was cut to a very small length (around 20-25 cm). After attempting the previous solutions and repeating the Seronorm samples numerous times with different dilution factors, the results were still unreliable and the overall mean of Seronorm did not match with the certified reference value. In order to check the quantity of sample delivered to the ICP-MS, sample centrifuge tubes were weighed before and after each run and the difference was recorded. The amount of the sample weighed varied, therefore a different PFA nebulizer and spray chamber were tested in order to determine the source of problem. The PFA nebulizer was found to be cross threaded and was sent for refurbishment and a new nebulizer was used. In addition, a final procedure was tested by omitting the evaporation step and hence reducing the acids used for digestion as shown in Table 2.2.

20 samples of AD patients were analysed by using the proposed method with Y and Sc as internal standard. Even though the number of bubbles were significantly reduced by this procedure, still it was not practical to use. The centrifuge tube must be weighed at different stages: including empty tube, after the addition of $H_2O_2$/ $HNO_3$, digestion, addition of internal standard and finally reconstitution with water. Most of the experiments gave good agreement with the certified reference value for Cu and Fe but not for Zn. Some selected examples of the method development results on Seronorm level of Zn, Cu and Fe in different batches with various preparation procedures will be included in the results and discussion (section 2.3.4, Table 2.7). Interestingly, it has been reported by Maekawa et al. [231] that selenium concentration in Seronorm (Trace Elements Serum) level 2 batch was inaccurate, and it could be the same case with Zn in Seronorm. It seems that a combination of reasons contributes to conventional serum digestion being difficult and unreliable. As a result, an alternative sample preparation method was applied.


During method development nebulizers constructed from PFA and glass were used, but the glass nebulizer performed more reliably, therefore it was retained for the subsequent work.

## 2.2.6 Recommended procedure of sample preparation

A direct dilution preparation method, which will be considered for this work, had the advantage of being cheaper, reducing the sample preparation steps which result in consuming less time and introducing less cross-contamination. Yet, the heavy matrix of serum still could create a problem. However, based on different studies, it is evident that alkaline media provide a good alternative to conventional acid digestion for several biological materials, in addition to increasing the performance of some analytical techniques such as ICP-MS.[184,224,227,232]

Serum samples stored at -80 ℃ were thawed at room temperature for approximately 1-2 h. After complete defrosting, samples were vortexed about 10 seconds to ensure complete homogenization. High dilution factors such as 50 or 100 can be used for Cu, Fe and Zn metals because of their high concentration level in serum.[233] 50 µL of serum samples were transferred to 15 mL polypropylene metal-free tubes and diluted 100-fold up to 5 mL. In the second run 30 µL of serum sample samples were diluted 100-fold up to 3 mL. All the samples were kept in capped containers in the fridge until the analysis was performed. The sample diluent was a mixture of Triton X-100, butanol, ammonia and nitric acid[234] as summarised in Table 2.3.

**Table 2.3** Preparation of sample diluents

| Sample diluents* | Butanol (99.92%) mL | Ammonia (25%) mL | Triton X-100™ (1.0%) mL | HNO₃ (0.1%) mL | Total volume mL |
|---|---|---|---|---|---|
| 1% Butanol, 0.5% v/v ammonia, 0.02% v/v Triton X-100, 0.01% v/v HNO₃ | 5 | 10 | 10 | 50 | 500 |

\* Although the blank mixture is referred to as a "diluent", this matrix is also chemically active in terms of denaturing protein and complexing trace metal.

1% Triton X-100 was prepared by part filling 100 mL PFA container with ultra-pure water, adding 1 mL of Triton X-100 and then making up to 100 mL with water. During preparation, every so often a foam in the solution was created, so it was placed in the ultra-sonic bath for about 15 minutes and the container was inverted to make sure the solution mixed thoroughly. Ideally, 1% Triton X-100 was prepared before the day of analysis to ensure complete dissolution, but the rest of the sample diluents were prepared

on the same day of analysis. Triton X-100, a non-ionic surfactant, is used as a diluent in biochemical applications to solubilize proteins, which form a stable mixture with the diluted sample. It has been widely considered for aerosol production and efficient nebulization.[235] Nitric acid was added to ensure that the trace elements were maintained in solution, and to change the effect of the matrix upon analyte sensitivity. However, the acid concentration must be kept to a minimum, in order to avoid protein precipitation and loss of analytes.[233] Butanol was added to match the carbon content of standards and samples and also for ionization efficiency stability[233]. Ammonia solution produces a clear homogeneous solution and keeps the diluted sample stable up to 48 h if stored at 4 °C.[233] It is useful for red cells lysis,[233] preventing precipitation[184] as well as improving the sensitivity of the determination.[185]

The use of external calibration standards is the most common approach for quantitative analysis. The range of calibration standards was produced including blank by diluting 1000 mg L$^{-1}$ single element stock solution of (Zn, Cu, and Fe) to 8 standard concentrations (0, 1, 3, 5, 7, 10, 12, 15, 20 ppb) for each element measured. Blank and external calibration standards were made up in the same diluent as the samples.

### 2.2.7 Standard reference material (SRM)

Reference materials are required and important to support quality control and for validation of the developed analytical procedures. Freeze dried reference serum, normal level, from UTAK laboratory and Seronorm™ trace elements serum level 1, were used to verify the accuracy of procedures that measure the levels of trace elements in serum. To prepare the stock solution of the reference material, the control material was reconstituted by adding exactly 5 mL of deionized water (recommended by manufacturer). It was left for 15 minutes, divided into 5 aliquots and stored in the fridge. The stability of these samples was only 30 days. Then the reference serum material was prepared in exactly the same way as the patient's sample.

### 2.2.8 Internal standards

In ICP-MS, the signal changes caused by variations in sample mixture, nebulisation efficiency and instrument performance lead to errors which can be corrected using an internal standard. Therefore, the purpose of the internal standard is to compensate for

instrumental instability and correction for matrix effects. Ideally, the changes in the signal intensity of the internal standard are directly proportional to those of the analyte. So, any factor affecting the analyte signal will affect the IS signal to the same extent and thus the ratio of the two signals remains constant and less variable than the analyte signal.[236] It has been reported that[237] both mass and ionization potential are important factors for good internal standard choices. On the other hand, Vanhaecke and colleagues [238] have stated that internal standards should be based on similarity in mass only. Considering both factors are important to select proper internal standards, it is also important to assess experimentally the performance of any internal standard before employing it for routine analysis.

The use of gallium (Ga)[220,223] as internal standard has been previously reported for analysis of Zn, Cu, and Fe in serum. Each blank, calibration standards, reference material and serum samples were spiked with Ga to a concentration of 3.0 ng mL$^{-1}$. Calibrations and analyses were carried out with and without internal standard and it was found that the accuracy, as indicated by consistency with the Serum UTAK reference values were equivalent for both procedures. However, precision and limit of detection without using internal standard were superior indicating that the sample matrix did not adversely affect the performance of the sample introduction system. Therefore, the results reported here were obtained without the use of internal standard and that will be discussed in the following section.

## 2.3 Results and discussion

### 2.3.1 Blank level

As mentioned earlier, it is very important to keep the contamination level to a minimum as it may lead to a negative impact on the measured concentration. Hence, in order to assess the contribution of contamination from sample preparation or analysis, three types of blanks were analysed: firstly, the calibration blank used to create the calibration curve alongside the standards; secondly, the procedural blanks analysed randomly in a sequence to monitor any contamination either from the sample diluent or the instrument during analysis; and finally, the rinse blank, namely the sample diluent, deionized water and nitric acid (2%v/v), used to flush the system between each standard and samples. Normally, the washing time varies between 2 to 5 min between samples, but after running the set of standards and the calibration verification standards between every 7-10 samples, the wash time was increased up to 10-15 min. In all experiments, the sequence started and finished with blank to check if the blank remains at similar level. Tests were applied to deionized (DI) water and nitric (2%v/v), acid to check the level of contamination in the tube for analysis. This was done by comparing between the normal falcon tube (NFT) (with blue lid) and the metal free tube (MFT) and an example of the results for DI water are demonstrated in Figure 2.1. Based on the data shown in Figure 2.1, the trend for Zn, Cu and Fe analysis followed the sequence:

DI water-normal falcon tube (NFT) **>** DI water-metal free tube (MFT)

Thus, in the subsequent work, all experiments were carried out by using MF tube.
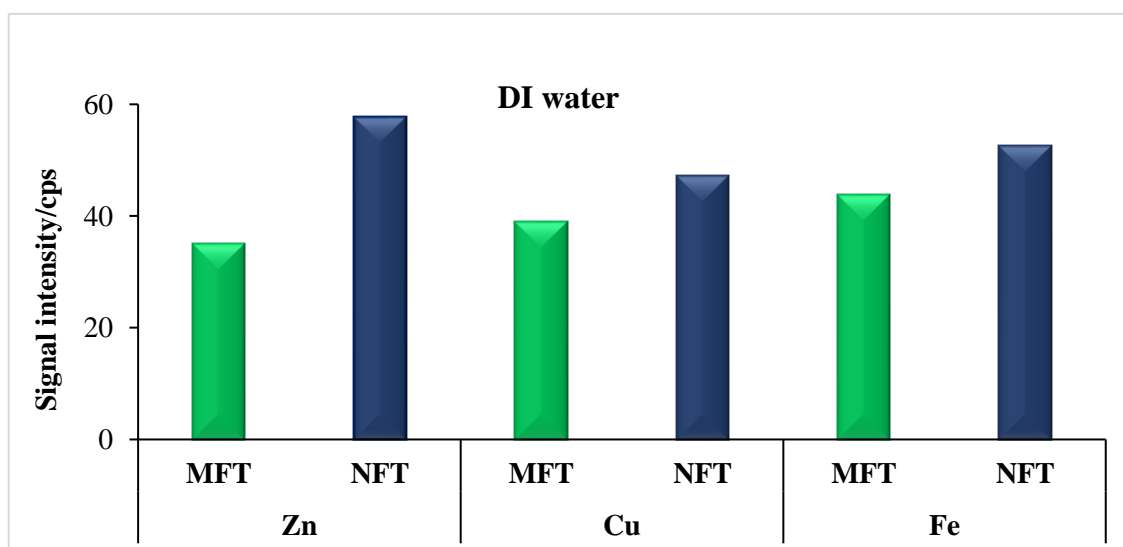


**Figure 2.1** Comparison of $Zn^{66}$, $Cu^{65}$ and $Fe^{57}$ signal recorded for water blank samples in normal Falcon (blue) and metal free tubes (green).

## 2.3.2 Analytical performance

Based on the calibration curve, the concentration of the elements in serum samples were precisely determined. Calibration curves were established by using eight different concentration points including zero. The plots showed a good linear relationship between signal intensity (cps) and concentration (ppb). The calibrations obtained for the target analytes ($Zn^{66}$, $Cu^{65}$ and $Fe^{57}$) are presented in Figure 2.2. The corresponding regression equations of the linear plots for the three analytes in all experiments are given in the appendix 2. The correlation coefficient ($R^2$) value ranged between 0.9972 and 0.9999 for all calibration curves. The limits of detection ranged from 0.20-0.83 µg $L^{-1}$, 0.08-0.66 µg $L^{-1}$ and 0.18-0.93 µg $L^{-1}$ and the limits of quantification ranged from 0.65-2.75 µg $L^{-1}$, 0.28-2.20 µg $L^{-1}$ and and 0.59-3.11 µg $L^{-1}$ for Zn, Cu and Fe, respectively. The limit of detection was taken to be three times the standard error of the calibration graph divided by the gradient applied to a plot of the calibration standards from 0-10ppb, the most common approach to calculate LOD and LOQ as stated in the equations below: [239]

$$\text{Limit of Detection Limit (LOD)} = \frac{3sy/x}{m} \tag{2.1}$$

$$\text{Limit of Quantification (LOQ)} = \frac{10\ sy/x}{m} \tag{2.2}$$

Where sy/x= Standard Error of the calibration curve and m=Slope of the linear plot.

In the calibration graphs, sometimes one (or possibly two) standard measurement appears to differ unexpectedly from the others. Thus, Grubbs' test and Dixon's test were used to exclude the outliers in all measurements of all three elements by using the following equations:[239]

$$\text{Grubb's test, G calc} = \frac{|suspect\ value - X|}{S} \tag{2.3}$$

$$\text{Dixon's test, D calc} = \frac{|suspect\ value - nearest\ value|}{largest\ value - smallest\ value} \tag{2.4}$$

Where, $\overline{X}$ and S are the mean and the standard deviation, respectively.
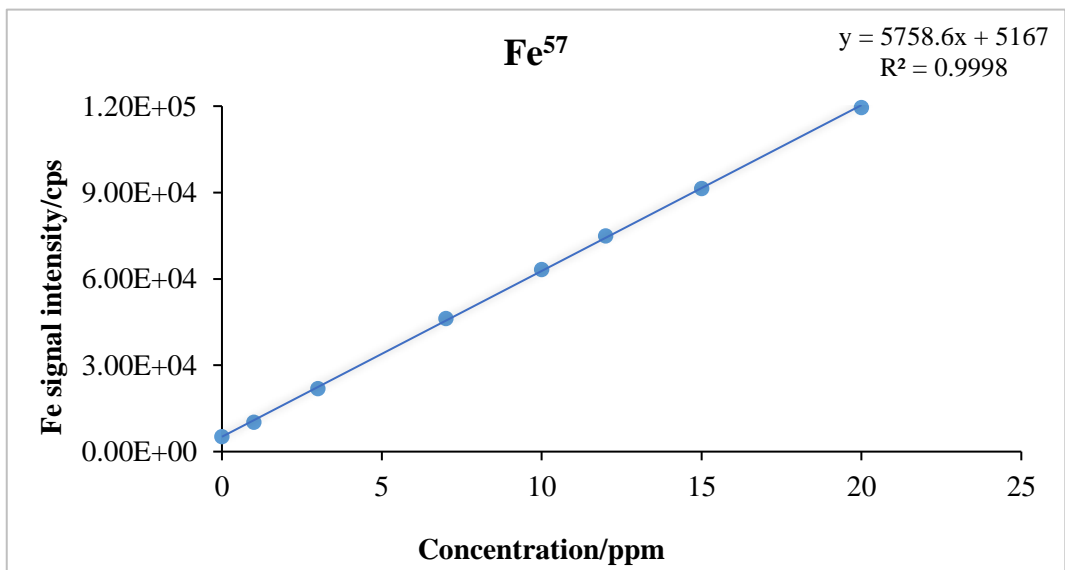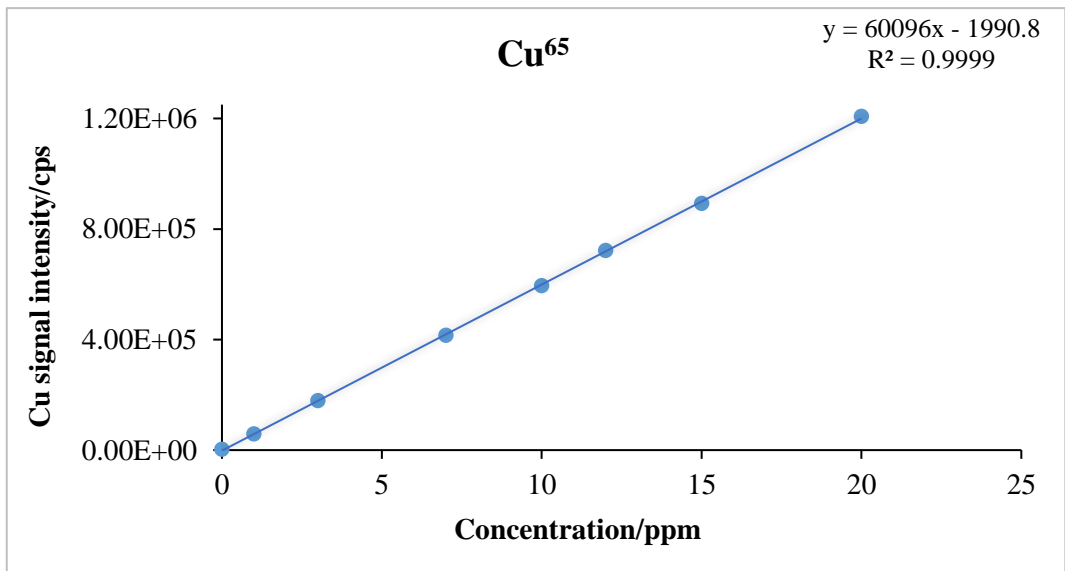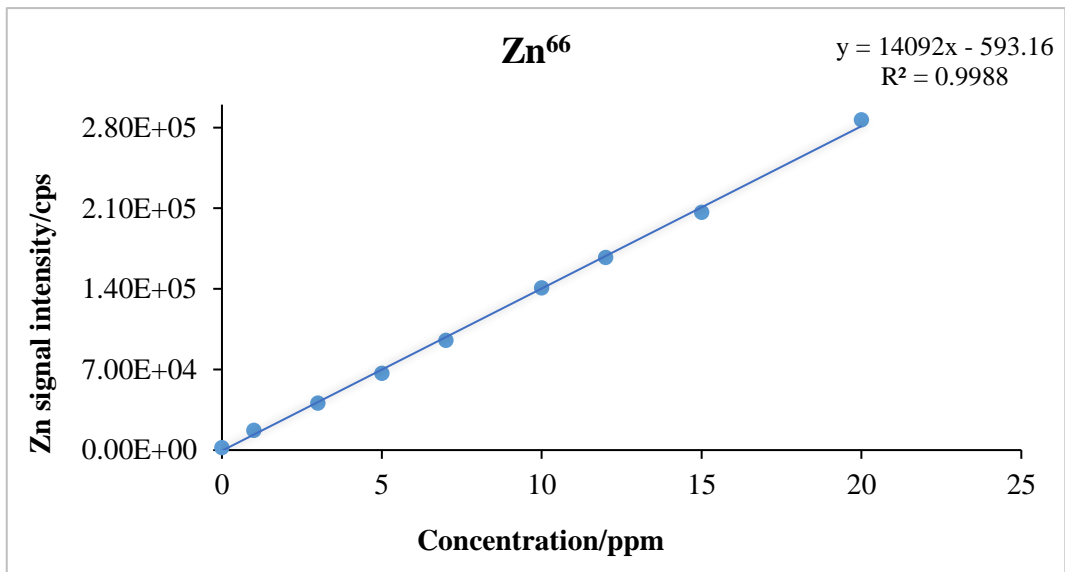
**Figure 2.2** Calibration graph used to calculate Zn, Cu and Fe concentrations in serum samples

A comparison between the analytical features of the proposed methods for Zn, Cu and Fe determination and many published articles based on ICP-MS are summarized in Table 2.4,[184,83,219,221,220,217,218] Table 2.5[219,221,220,217,218] and Table 2.6[219,221,220,217] respectively. Based on the values for LOD and LOQ (Tables 2.4-2.6) and the linear dynamic range (LDR), it can be concluded that some of the methods outlined in Tables 2.4-2.6 exhibited high LOD and serious matrix interferences, whilst the low LOD reported for others may well be due to the different calculation methods used. Overall the proposed method compares favourably with other reported methods in terms of simplicity, speed, sensitivity, specificity and sample volume. Moreover, to our knowledge there are no studies reporting the successful analysis of as little as 50 µL of blood serum or plasma using ICP-MS.

Calibrations and analyses were carried out and calculated with and without internal standard. It was found that the trends of the results and accuracy, as indicated by consistency with the Serum UTAK reference values was equivalent for both procedures. However, the precision and limit of detection without using internal standard were superior as the propagation of error from division by the internal standard signal is eliminated. Furthermore, there is a considerable economy in reagent use and time if samples and standards do not have to be spiked with the internal standard. Therefore, the results reported here were obtained without the use of internal standard. The achievement of good accuracy without the use of internal standard is an indication that the sample matrix was not significantly affecting the sample introduction system because it was providing identical signals for equivalent analyte concentrations in both the samples and standards. A case can still be made for the use of an internal standard as on days when there was unexpected instrumental drift, the internal standard compensated for the drift and provided accurate answers. The choice of approach will depend on how frequently drift problems occur set against the overhead of using the internal standard. Added to this, in order to monitor the instrumental drift, one of the standards with known metal concentrations (10ppb) was analysed every 7-10 samples and the standards were recalculated relative to 10ppb. No significant differences were noticed before and after recalculation of the standards as demonstrated in Figure 2.3.

**Table 2.4** Comparison of the proposed method with other reported methods for Zn determination*

| Techniques | Samples | Linear D range, (µg L$^{-1}$) | LOD (µg L$^{-1}$) | LOQ (µg L$^{-1}$) | Matrix and Remarks | Ref. |
|---|---|---|---|---|---|---|
| HR-ICP-MS | Serum | 0-20 | 0.20 [a] | 0.65 | **30.0** µL serum volume, simple dilution with 1% butanol, 0.5% v/v ammonia, 0.02% v/v TritonX-100, 0.01% v/v HNO$_3$, 100-fold | Present work |
| HR-ICP-MS | Plasma | 0–100 | 0.14 [b] | 0.45 | **100 µL** sample volume, simple dilution with 0.5% HNO$_3$ 20-fold, | 220 |
| HR-ICP-MS | Serum | 0–100 | 0.20 [c] | 0.66 | **100µL** sample volume, digestion 300 µL of OPTIMA HNO$_3$ and 100 µL on hot plate, 100-fold dilution | 83 |
| Q-ICP-MS | Blood, plasma, urine, hair | ND | 0.63 | 2.1 | **400 µL** sample volume, diluted with purified water, acid, triton X100 and butanol. | 218 |
| HR-ICP-MS & Q-ICP-MS | Plasma, Serum | 10-150 | 8.6 | 28.38 | **150 µL** serum volume, digestion with nitric acid and hydrogen peroxide placed in express hot block digester, 100-fold dilution | 219 |
| Q-ICP-MS system | Serum | 0-20 | 0.03 [d] | 0.099 | The serum samples where diluted with 10% acetic acid and 0.1% Triton X-100, 10-fold | 217 |
| Q-ICP-MS | Serum | 1-25 | 0.321 | 1.06 | **2.0 mL** serum volume, 1/10 dilution with a solution of EDTA and NH$_4$OH | 221 |
| Q-ICP-MS | Whole blood, plasma | ND | 0.14 [e] 1.6 [f] | 0.46 [a] 5.3 [b] | **0.2 or 0.5 mL** of human whole blood and serum samples were subjected to alkali dilution (ammonia solution) or acid digestion (nitric acid), 1:25 fold. | 184 |
| Q-ICP-MS | Blood | 5–48.33 | 1.5 | 5 | **2.0 mL** of prepared solution of 65% conc. HNO$_3$/H$_2$O$_2$ (2:1 v/v) was thoroughly ingested by microwave assisted acid digestion into a flask containing 0.5 mL blood. | 240 |
| Q-ICP-MS | Serum | ND | 0.408 | 1.23 | **150 µL** of the serum samples were diluted (1:10) using the diluent solution: 5% 1-butanol, 0.05% EDTA, 0.05% triton X-100 and 0.25% ammonium hydroxide. | 241 |

* The values of LOD in the table were based on different calculation method; ND= not detected.

[a] The LOD in the present work were calculated as three times the standard error of the calibration graph divided by the gradient.

[b] The LOD was calculated as 10 SD above the value for 0.5% HNO$_3$ plus the dilution factor (20 Fold).

[c,d] The LOD was calculated as 3 times the standard deviation of the analytical signal from the blank solution.

[e] The LOD of acid digestion; [f] LOD of Alkali dilution; LOD were calculated in both methods as three times the standard deviation of the element concentration in the calibration blank.

**Table 2.5** Comparison of the proposed method with other reported methods for Cu determination*

| Techniques | Samples | Linear range, (µg L$^{-1}$) | LOD (µg L$^{-1}$) | LOQ (µg L$^{-1}$) | Matrix and Remarks | Ref. |
|---|---|---|---|---|---|---|
| HR-ICP-MS | Serum | 0-20 | 0.08 [a] | 0.28 | **30.0 µL** serum volume, simple dilution with 1%butanol, 0.5% v/v ammonia, 0.02% v/v TritonX-100, 0.01% v/v HNO$_3$, 100-fold | Present work |
| HR-ICP-MS | Plasma | 0–100 | 0.15 | 0.48 | **100 µL** sample volume, simple dilution with 0.5%HNO$_3$ 20-fold | [220] |
| Q-ICP-MS | Whole blood, plasma, urine and hair | ND | 0.14 | 0.47 | **400 µL** sample volume, diluted with purified water, acid, triton X100 and butanol. | [218] |
| HR-ICP-MS & Q-ICP-MS | Plasma/ serum | 10-150 | 0.32 | 1.056 | **150 µL** serum volume, digestion with nitri0c acid and hydrogen peroxide placed in express hot block digester, 100-fold dilution | [219] |
| Q-ICP-MS | Serum | 0-20 | ND | ND | The serum samples where diluted with 10% acetic acid and 0.1% Triton X-100, 10 fold | [217] |
| Q-ICP-MS | Serum | 1-25 | 0.077 | 0.25 | **2.0 mL** serum volume, 1/10 dilution with a solution of EDTA and NH4OH | [221] |
| Q-ICP-MS | Whole blood, plasma | ND | 0.02 [b] 0.22 [c] | 0.07[a] 0.73[b] | **0.2 or 0.5 mL** of human whole blood and serum samples were subjected to alkali dilution (ammonia solution) or acid digestion (nitric acid), 1:25 fold. | [184] |
| Q-ICP-MS | Blood | 1–50 | 0.303 | 1.0 | **2.0 mL** of prepared solution of 65% conc. HNO$_3$/H$_2$O$_2$ (2:1 v/v) was thoroughly ingested by microwave assisted acid digestion into a flask containing 0.5 mL blood. | [240] |
| Q-ICP-MS | Serum | ND | 0.0029 [d] | 0.0088 | **150 µL** of the serum samples were diluted (1:10) using the diluent solution: 5% 1-butanol, 0.05% EDTA, 0.05% triton X-100 and 0.25% ammonium hydroxide. | [241] |

* The values of LOD in the table were based on different calculation method; ND= not detected.

[a] The LOD in the present work were calculated as three times the standard error of the calibration graph divided by the gradient.

[b] The LOD of acid digestion; [c] LOD of Alkali dilution; LOD were calculated in both methods as three times the standard deviation of the element concentration in the calibration blank.

[d] The LODs and LOQs were determined according to the recommendation of the International Conference on Harmonization (ICH) guidelines.

**Table 2.6** Comparison of the proposed method with other reported methods for Fe determination*

| Techniques | Samples | Linear range, (µg L$^{-1}$) | LOD (µg L$^{-1}$) | LOQ (µg L$^{-1}$) | Matrix and Remarks | Ref. |
|---|---|---|---|---|---|---|
| HR-ICP-MS | Serum | 0.0-20 | 0.18 [a] | 0.59 | **30.0 µL** serum volume, simple dilution with 1%butanol, 0.5% v/v ammonia, 0.02% v/v TritonX-100, 0.01% v/v HNO$_3$, 100-fold | Present work |
| HR-ICP-MS | Plasma | 0.0–100 | 0.08 [b] | 0.25 | **100 µL** sample volume, simple dilution with 0.5%HNO$_3$ 20-fold | [220] |
| HR-ICP-MS & Q-ICP-MS | Plasma/ serum | 10-150 | 8.6 | 28.38 | **150 µL** serum volume, digestion with nitri0c acid and hydrogen peroxide placed in express hot block digester, 100-fold dilution | [219] |
| Q-ICP-MS | Serum | 0.0-20 | 0.69 | 2.28 | The serum samples where diluted with 10% acetic acid and 0.1% Triton X-100, 10 fold | [217] |
| Q-ICP-MS | Serum | 1-25 | 0.002 | 0.0066 | **2.0 mL** serum volume, 1/10 dilution with a solution of EDTA and NH4OH | [221] |
| Q- ICP-MS | Whole blood, plasma | ND | 0.42 [c] 0.50 [d] | 1.39 [a] 1.65 [b] | **0.2 or 0.5 mL** of human whole blood and serum samples were subjected to alkali dilution (ammonia solution) or acid digestion (nitric acid), 1:25 fold. | [184] |
| Q-ICP-MS | Blood | 2.00–40.50 | 0.606 | 2.0 | **2.0 mL** of prepared solution of 65% conc. HNO$_3$/H$_2$O$_2$ (2:1 v/v) was thoroughly ingested by microwave assisted acid digestion into a flask containing 0.5 mL blood. | [240] |
| Q-ICP-MS | Serum | ND | 0.0246 [e] | 0.0745 | **150 µL** of the serum samples were diluted (1:10) using the diluent solution: 5% 1-butanol, 0.05% EDTA, 0.05% triton X-100 and 0.25% ammonium hydroxide. | [241] |

* The values of LOD in the table were based on different calculation method; ND= not detected.

[a] The LOD in the present work were calculated as three times the standard error of the calibration graph divided by the gradient.

[b] The LOD was calculated as 10 SD above the value for 0.5% HNO$_3$ solution plus the dilution factor (20 Fold).

[c] LOD of acid digestion; [d] LOD of Alkali dilution; LOD were calculated in both methods as three times the standard deviation of the element concentration in the calibration blank.

[e] The LODs and LOQs were determined according to the recommendation of the International Conference on Harmonization (ICH) guidelines.
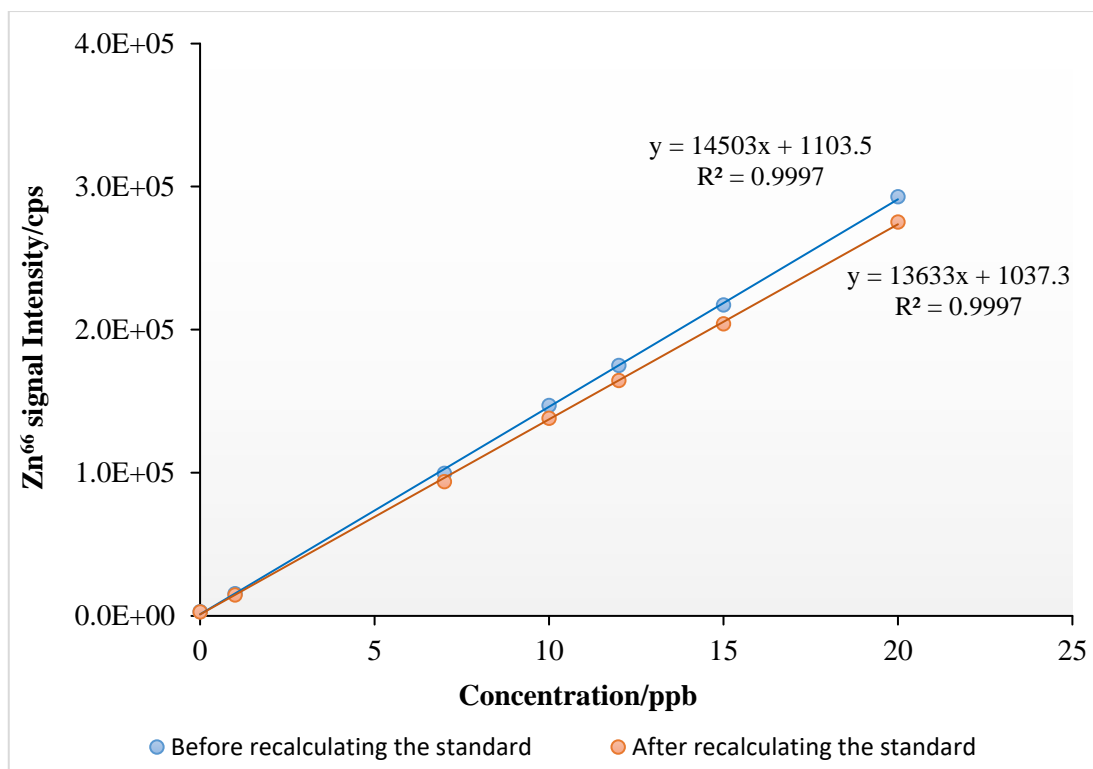
**Figure 2.3** Calibration plots before and after recalculating the standard.

### 2.3.3  Instrumental interferences

There are two major types of interferences which should be taken into consideration. Firstly, there are interferences between elemental ions sharing the same mass, such as $Zn^{64}$ and $Ni^{64}$. Another important interference is polyatomic interferences generated by a combination of two or more isotopes from atmospheric and/or plasma gases. The most common species comprise $Ar_2^+$, $ArO^+$, $O_2^+$, and $N_2^+$. A clear illustration of this type is the interferences between $Fe^+$ and $ArO^+$ at m/z 56. As can be seen from Figure 2.4 the interference can be separated in ICP-SFMS with medium and high resolution. In all human serum samples, different isotopes were used for each element with a medium resolution setting ($M/\Delta M = 4000$). The results for Zn ($Zn^{66}$, $Zn^{64}$), Cu ($Cu^{63}$, $Cu^{65}$) and Fe ($Fe^{54}$, $Fe^{57}$) were approximately the same as the natural isotopic ratio of around 1.78, 2.30, 2.82, respectively. Thus, in the subsequent work, the following isotopes $Zn^{66}$, $Cu^{65}$, $Fe^{57}$ were selected.
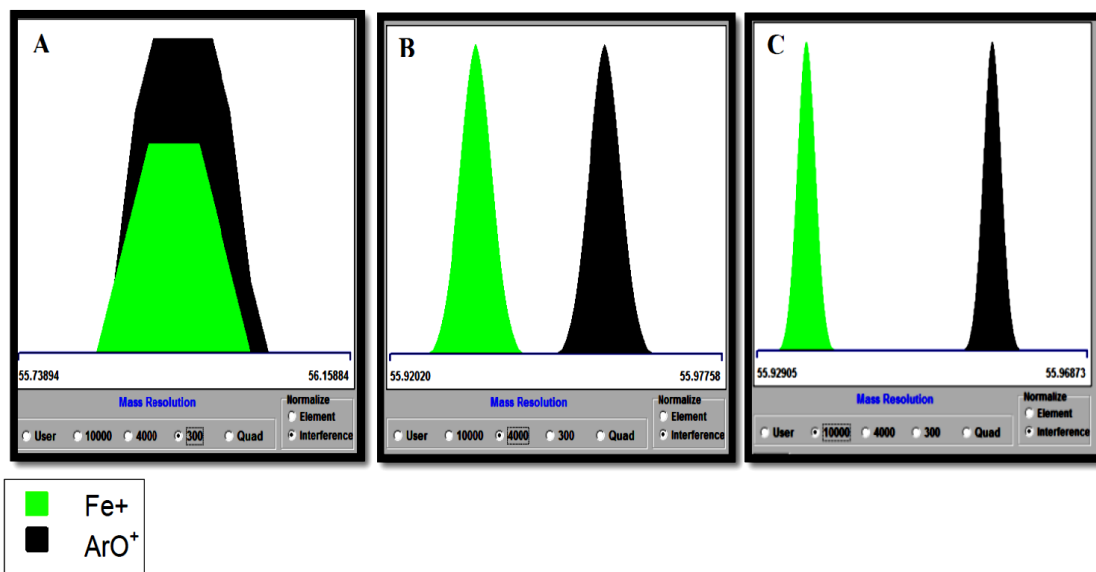
**Figure 2.4** Interference on $Fe^+$ by $ArO^+$ at m/z 56, demonstrated in Low (A), Medium (B) and high (C) resolution. Figure generated using ELEMENT.exe (Finnigan MAT, Thermo manufacturer).

### 2.3.4   Data of certified reference materials (CRMs)

In order to verify measurement accuracy at low concentration, the analysis of certified reference materials is necessary. Two reference materials have been used before, after and throughout the analysis. The concentrations of Zn, Cu and Fe in batch 4 of Seronorm[TM] Trace Elements level 1 (LOT 0903106) and Serum UTAK were found to be in good agreement with the certified values. However, Serum UTAK reference material was more reliable and gave more stable results.

Over 40 days of tests over a one-year period, 4 batches of Seronorm were analysed with different preparation procedures as discussed in Table 2.2. The certified concentration ranges of Seronorm CRMs for Zn, Cu and Fe are 1.596-1.880 mg/L, 1.523- 1.859 mg/L and 1.23- 1.55 mg/L, respectively. In batches 1 and 2, Zn and Cu level in samples with dilution procedure were constantly lower than the expected reference value in contrast to Fe which was higher. Nevertheless, in batch 3, Zn and Fe level were higher than reference value but Cu almost matched the certified values. Some examples of the results for measured Seronorm in batch 1-4 are shown in Table 2.7.

**Table 2.7** Selected examples of Seronorm levels (mg L$^{-1}$) of Zn, Cu and Fe in different batches with various preparation procedures*

| Batch no. | Seronorm preparation descriptions (dilution or digestion) | Dilution factor | Zn | Cu | Fe |
|---|---|---|---|---|---|
| 1 | 0.5% HNO$_3$ | 100 X | 0.95 | 1.04 | ND |
| | | 100 X | 1.07 | 0.94 | ND |
| 2 | 0.5% HNO$_3$ | 100 X | **1.65** | **1.68** | **1.44** |
| | | 50 X | **1.63** | **1.63** | ND |
| | | 40 X | 1.28 | 1.47 | 2.21 |
| | | 20 X | 1.16 | 1.40 | 1.74 |
| | DI water | 100 X | 0.76 | 0.66 | ND |
| | | 20 X | 0.65 | 0.65 | ND |
| | 1.5%HNO$_3$+1.5%TMAH | 100 X | 1.58 | **1.69** | **1.10** |
| | | 50 X | 1.37 | 1.46 | **1.00** |
| | Seronorm digested and evaporated in Oven, reconstituted with 2%HNO$_3$ | 40 X | 2.49 | ND | ND |
| | Seronorm digested and evaporated in hot block, reconstituted with 2%HNO$_3$ | 40 X | **1.81** | ND | ND |
| | Seronorm digested and evaporated in hot block, reconstituted with 2%HNO$_3$ | 100 X | 2.49 | **1.77** | **1.55** |
| 3 | Seronorm digested but not evaporated_ centrifuge lid loosely closed by small pipette tip | 50 X | 2.82 | **1.79** | 1.85 |
| | Seronorm digested but not evaporated_ centrifuge lid pierced with metal needle | 30 X | **1.61** | **1.79** | 1.85 |
| 4 | Dilution with (1% Butanol, 0.5% v/v ammonia, 0.02% v/v TritonX-100, 0.01% v/v HNO$_3$). | 100 X | **1.67** | **1.70** | **1.44** |
| | | | **1.77** | **1.78** | 1.38 |
| | | | 1.55 | 1.90 | **1.24** |

* The concentrations in bold are the ones that matched with Seronorm reference value.

Maekawa et al. [231] has reported that selenium concentration in Seronorm™ Trace Elements Serum (Level 2) may be in error noticeably in some batches. Over a 12-month period, the external reference materials were analysed extensively and the results confirmed a constant increase in selenium concentrations. Therefore, in the subsequent work, all experiments were carried out by using Serum UTAK reference material. The concentration average of found value, standard deviation (STDV), relative standard deviation (RSD) and acceptable range CRMs are summarized in Table 2.8.

**Table 2.8** The concentration of reference (UTAK) and found value (mg $L^{-1}$)

|  | **Zn** | **Cu** | **Fe** |
|---|---|---|---|
| **Reference value range** | 0.50-0.83 | 0.87-1.45 | 0.47-0.79 |
| **N** | 20 | 21 | 23 |
| **found value** | 0.68 | 1.16 | 0.60 |
| **STDV** | 0.05 | 0.16 | 0.06 |
| **RSD %** | 8.03 | 13.52 | 10.75 |

### 2.3.5   Analysis of serum samples

The study by Lu and colleagues[184] has aimed to compare between alkali dilution and acid digestion methods in metal analysis by ICP-MS, and it suggested that alkali dilution is suitable for Zn and Cu serum/ blood analysis, while acid digestion was preferred for Fe. Another study [221] has tested four different pre-treatments on serum (1%$HNO_3$, 0.5%$HNO_3$, 0.05% EDTA+ 1% $NH_4OH$, and EDTA + 1% $NH_4OH$+ 2% 1-butanol). The data indicated the best treatment for serum samples as the solution of EDTA and $NH_4OH$. In addition, it has been suggested by Bocca et al.[242] that simple dilutions are mainly selected for serum analysis, whereas blood samples may be digested. In the present study, 81 serum samples were collected from AMD and AD patients. Samples were analysed in four batches of about 20 samples within 4 days where duplicate preparations were made for serum, if sufficient sample was available. Single runs were performed for 20 out of 81 serum samples because of the small sample volume available. In the 1/100 (V/V) dilution, no clogging during nebulization and no particles were found in the injector tube throughout the run of serum analyses. This behaviour is most likely attributed to the use

of a glass nebulizer, short sample probe (80cm capillary, 0.5mm ID) and the low sample aspiration rate of 400µL/min. Higher dilution factors raise the limits of detection, but lower dilution factors increase the risk of particle deposits as reported earlier[224]. ICP-MS data for the analysed samples for Zn, Cu and Fe level for all samples in serum are summarized in the Tables demonstrated below.

### 2.3.5.1 Quantification of zinc, copper and iron level in serum of AD patients

Burnet[243] was the first author to associate Zn deficiency with dementia, and since this work, several studies have discussed the crucial role of Zn in pathogenesis of AD. Many studies have correlated the changes in Zn to elevated brain levels. These studies are contradictory and the exact reasons for increased level of Zn in the brain in AD are still unclear. Haines and his co-workers[244] have revealed no substantial differences between AD and control serum Zn, while Jeandel et al.[245] have reported a significant decrease in the level of Zn and other nutrients in AD serum. On the other hand, Rulon et al.[201] and Gonzales et al.[204] have reported significant boosts of Zn levels in AD serum. Serum Zn seemed to be one of the risk factors associated with the development of AD.

The measured Zn, Cu and Fe concentrations of 43 serum samples from AD patients are presented in Table 2.9, Table 2.10 and Table 2.11. The results revealed that the ICP-MS technique was able to measure directly the tested elements in 50 microliter serum samples in a (1:100v/v) dilution with Triton-X-100, butanol, ammonia and $HNO_3$. The data have revealed that, sample number 17 was the lowest while sample number 49 was the highest Zn concentration in the AD patients tested. The highest Cu level was in samples numbered 308 & 21, whereas the lowest Cu content is sample number 42. Sample number 44 shows the highest Fe concentration, however sample 200 is by far the lowest. Sample number 80 was excluded from further data analysis as the concentration was higher than 20ppb and thus outside the range of the calibration standards (Table 2.11).

Several statistical tests including correlation, regression, $t$-tests, and analysis of variance, are based on the assumption that the data used are drawn from a normal population. However, with large sample sizes (> 30 or 40), the disruption of the normality assumption should not cause major problems. [246] A simple way of seeing whether a set of data is consistent with the assumption of normality is to plot a cumulative frequency curve. The percentage of cumulative frequency is calculated by using the formula below: [239]

**% cumulative frequency** = 100 * cumulative frequency/ (n + 1)            **(2.5)**

Where n is the total number of measurements.

The cumulative frequency curve for the three elements in serum of AD patients yields an S-shape as can be seen in Figure 2.5, which means the data come from a normal population.

Additionally, Zn, Cu and Fe concentrations measured in AD patients' serum were tested for normality of distribution using the Kolmogorov–Smirnov (K-S) test. The original data where transformed into a standard normal variable (z), by using the equation below:[239]

$$\text{Standard normal variable, } Z = \frac{\chi - \mu}{\sigma}$$            (2.6)

Where, $\chi$ is the mesured value, $\mu$ is the mean and $\sigma$ is the standard deviation.

The distribution of Zn, Cu and Fe in AD patients was normal according to the Kolmogorov-Smirnov tests. The full calculations of K-S test, normal cumulative distribution and the normal probability plot obtained by using Minitab software of Zn, Cu and Fe distribution in AD patients are are summarized in Appendix 2.

The one-way analysis of variance (ANOVA) is used to determine whether there are any statistically significant differences between the means of more than two independent groups.[239] Thus, one-way ANOVA test was applied to compare Zn, Cu and Fe variation in AD patients, showing that the concentrations of these elements were significantly different as the F critical is smaller than the F calculated (P <0.0001). The results obtained from this test at 5% significance level are shown in Table 2.12 for comparison between Zn, Cu and Fe in the AD samples.The results illustrate that the total average of serum Zn in general is noticeably lower than Cu and Fe. Copper shows the highest level in comparison to Zn and Fe, in the case of AD.

**Table 2.9** Total concentration (mg L$^{-1}$) of Zn in serum of AD patients*

| Samples number | Zn ± STDV | Samples number | Zn ± STDV |
|---|---|---|---|
| 17 | 0.58 ± 0.05 | 52 | 0.74 ± 0.07 |
| 18 | 0.74 ± 0.07 | 57 | 0.75 ± 0.07 |
| 21 | 0.99 ± 0.09 | 58 | 0.66 ± 0.06 |
| 22 | 0.78 ± 0.07 | 64 | 0.79 ± 0.07 |
| 25 | 0.73 ± 0.07 | 67 | 0.62 ± 0.06 |
| 26 | 0.83 ± 0.08 | 72 | 0.9 ± 0.08 |
| 27 | 0.84 ± 0.08 | 76 | 0.71 ± 0.07 |
| 28 | 0.76 ± 0.07 | 77 | 0.72 ± 0.07 |
| 33 | 0.99 ± 0.09 | 78 | 0.59 ± 0.06 |
| 34 | 0.61 ± 0.06 | 80 | 0.68 ± 0.06 |
| 35 | 0.98 ± 0.09 | 200 | 0.93 ± 0.09 |
| 36 | 0.79 ± 0.07 | 201 | 0.93 ± 0.09 |
| 37 | 0.61 ± 0.06 | 301 | 0.69 ± 0.06 |
| 38 | 0.64 ± 0.06 | 302 | 0.81 ± 0.08 |
| 40 | 0.86 ± 0.08 | 303 | 0.83 ± 0.08 |
| 41 | 0.95 ± 0.09 | 304 | 0.61 ± 0.06 |
| 42 | 0.80 ± 0.08 | 305 | 0.68 ± 0.06 |
| 43 | 0.69 ± 0.06 | 306 | 0.77 ± 0.07 |
| 44 | 0.69 ± 0.06 | 307 | 0.66 ± 0.06 |
| 49 | 0.93 ± 0.09 | 308 | 0.92 ± 0.09 |
| 50 | 0.80 ± 0.08 | 309 | 1.07 ± 0.10 |
| 51 | 0.70 ± 0.07 | | |

* The quoted STDV values were calculating by multiplying the measured values by the RSD of 20 replicates of Serum UTAK reference materal divided by 100.

**Table 2.10** The total concentration (mg L$^{-1}$) of Cu in serum of AD patients*

| Samples number | Cu ± STDV | Samples number | Cu ± STDV |
|---|---|---|---|
| 17 | 1.50 ± 0.20 | 52 | 1.23 ± 0.17 |
| 18 | 1.29 ± 0.17 | 57 | 1.70 ± 0.23 |
| 21 | 1.83 ± 0.25 | 58 | 1.03 ± 0.14 |
| 22 | 1.20 ± 0.16 | 64 | 1.32 ± 0.18 |
| 25 | 1.04 ± 0.14 | 67 | 1.24 ± 0.17 |
| 26 | 1.15 ± 0.15 | 72 | 1.09 ± 0.15 |
| 27 | 1.31 ± 0.18 | 76 | 1.02 ± 0.14 |
| 28 | 1.17 ± 0.16 | 77 | 0.79 ± 0.11 |
| 33 | 1.35 ± 0.18 | 78 | 1.1 ± 0.15 |
| 34 | 1.24 ± 0.17 | 80 | 0.98 ± 0.13 |
| 35 | 1.35 ± 0.18 | 200 | 1.29 ± 0.17 |
| 36 | 1.06 ± 0.14 | 201 | 1.19 ± 0.16 |
| 37 | 1.13 ± 0.15 | 301 | 0.81 ± 0.11 |
| 38 | 0.94 ± 0.13 | 302 | 0.98 ± 0.13 |
| 40 | 1.33 ± 0.18 | 303 | 1.19 ± 0.16 |
| 41 | 1.42 ± 0.19 | 304 | 1.32 ± 0.18 |
| 42 | 0.77 ± 0.10 | 305 | 0.85 ± 0.11 |
| 43 | 1.08 ± 0.15 | 306 | 1.25 ± 0.17 |
| 44 | 1.20 ± 0.16 | 307 | 0.95 ± 0.13 |
| 49 | 1.54 ± 0.21 | 308 | 1.53 ± 0.21 |
| 50 | 0.95 ± 0.13 | 309 | 0.87 ± 0.12 |
| 51 | 1.11 ± 0.15 | | |

* The quoted STDV values were calculating by multiplying the measured values by the RSD of 21 replicates of Serum UTAK reference materal divided by 100.

**Table 2.11** The total concentration (mg L$^{-1}$) of Fe in serum of AD patients*

| Samples number | Fe± STDV | Samples number | Fe± STDV |
|---|---|---|---|
| 17 | 0.69 ± 0.07 | 52 | 1.22 ± 0.13 |
| 18 | 1.23 ± 0.13 | 57 | 0.95 ± 0.1 |
| 21 | 1.19 ± 0.13 | 58 | 1.43 ± 0.15 |
| 22 | 2.05 ± 0.22 | 64 | 1.16 ± 0.12 |
| 25 | 1.40 ± 0.15 | 67 | 0.76 ± 0.08 |
| 26 | 1.87 ± 0.2 | 72 | 1.24 ± 0.13 |
| 27 | 0.96 ± 0.1 | 76 | 0.88 ± 0.09 |
| 28 | 0.81 ± 0.09 | 77 | 0.56 ± 0.06 |
| 33 | 2.29 ± 0.25 | 78 | 0.51 ± 0.06 |
| 34 | 0.96 ± 0.10 | 80** | 2.78 ± 0.30 |
| 35 | 1.95 ± 0.21 | 200 | 1.66 ± 0.18 |
| 36 | 1.09 ± 0.12 | 201 | 1.06 ± 0.11 |
| 37 | 1.24 ± 0.13 | 301 | 0.56 ± 0.06 |
| 38 | 0.92 ± 0.10 | 302 | 1.41 ± 0.15 |
| 40 | 0.89 ± 0.10 | 303 | 1.06 ± 0.11 |
| 41 | 1.76 ± 0.19 | 304 | 0.80 ± 0.09 |
| 42 | 1.70 ± 0.18 | 305 | 0.86±0.09 |
| 43 | 0.66 ± 0.07 | 306 | 0.95 ± 0.10 |
| 44 | 0.53 ± 0.06 | 307 | 0.77 ± 0.08 |
| 49 | 1.02 ± 0.11 | 308 | 0.52 ± 0.06 |
| 50 | 1.29 ± 0.14 | 309 | 1.35 ± 0.15 |
| 51 | 0.81 ± 0.09 |  |  |

* The quoted STDV values were calculating by multiplying the measured values by the RSD of 23 replicates of Serum UTAK reference materal divided by 100.
** Sample number 80 of Fe was above the calculated linear dynamic range (20ppb) in the diluted samples.
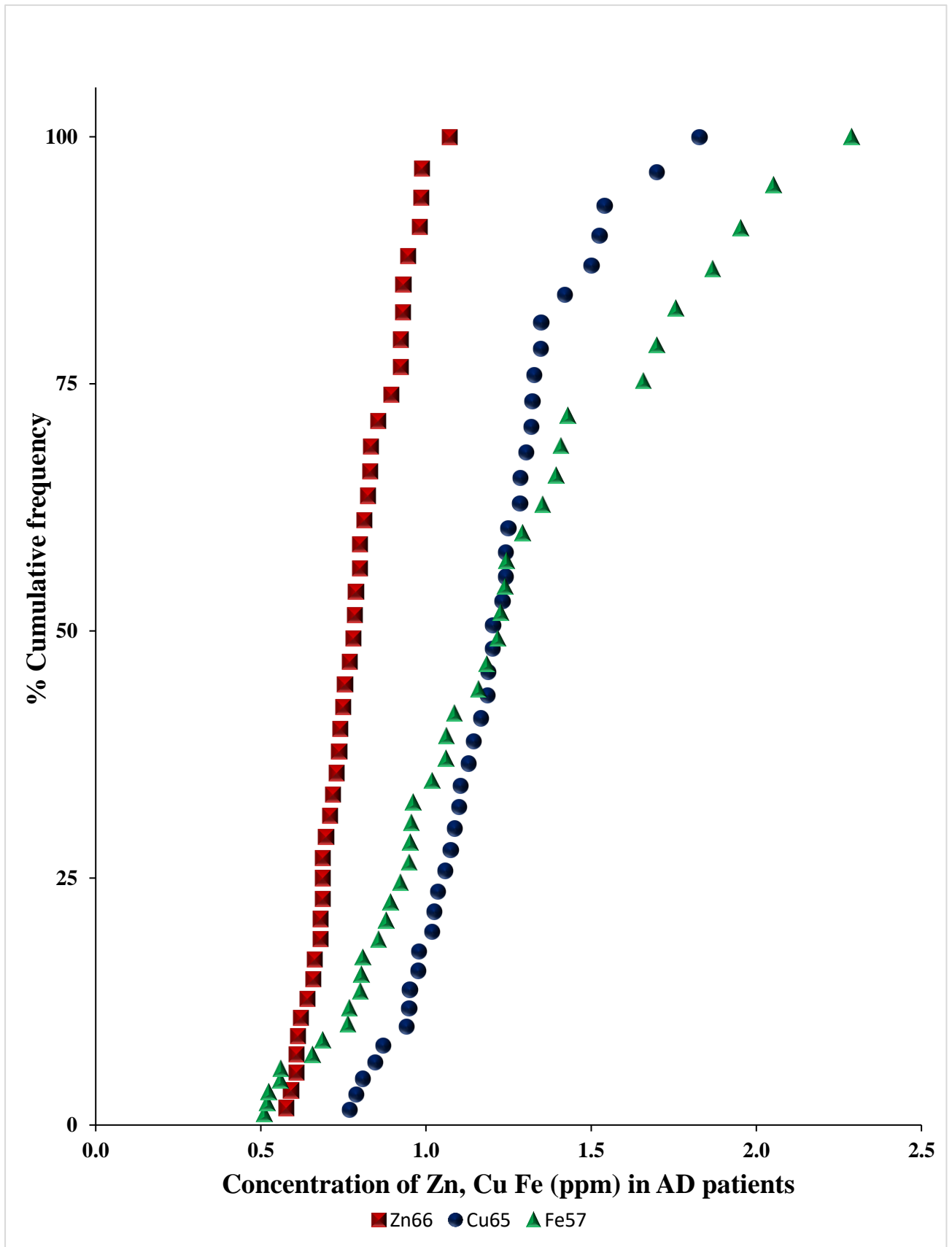
**Figure 2.5** The cumulative frequency curve for the measurements of serum Zn, Cu and Fe in AD patients.

**Table 2.12** ANOVA: One-factor with (n = 43) of serum Zn, Cu and Fe detected from AD patients.

SUMMARY

| Groups | Count | Sum | Average | Variance |
|---|---|---|---|---|
| $Zn^{66}$-AD | 43 | 33.35 | 0.78 | 0.02 |
| $Cu^{65}$-AD | 43 | 50.68 | 1.18 | 0.05 |
| $Fe^{57}$-AD | 42 | 47.03 | 1.12 | 0.19 |

ANOVA

| Source of Variation | SS | df | MS | F | P-value | F crit |
|---|---|---|---|---|---|---|
| Between Groups | 4.07 | 2.00 | 2.03 | 23.36 | 2.41E-09 | 3.07 |
| Within Groups | 10.89 | 125.00 | 0.09 | | | |
| Total | 14.96 | 127.00 | | | | |

### 2.3.5.2  Quantification of zinc, copper and iron level in serum of AMD patients

In the present investigation, sera of 38 AMD patients were analysed for Zn, Cu, and Fe by ICP-MS. The results are shown in Table 2.13, Table 2.14 and Table 2.15. ICP-MS was able to measure directly the selected elements in 50 microliter serum samples in a 1:100 (v/v) dilution with sample diluent as mentioned in section 2.3.5.1. The concentrations of Zn are usually lower than Cu and Fe. The data revealed that, sample number 51 was the lowest while sample number 39 was the highest Zn concentration in the AMD patients tested. The highest Cu level was in sample number 21, whereas the lowest Cu content is sample number 53. Sample number 23 shows the highest Fe concentration, however sample 43 is by far the lowest. Sample numbers 51, 57 and 58 were excluded from further data analysis as the concentration of the diluted serum was higher than 20ppb and thus outside the range of the calibration standards (Table 2.15).

The cumulative frequency curve for the three elements in AMD patients' serum produces an S-shape as can be seen in Figure 2.6 indicating that the data come from a normal population. In addition, Kolmogorov–Smirnov (K-S) method was applied to test for normality. The distribution of Zn, Cu and Fe in AMD patients was normal according to the Kolmogorov-Smirnov tests. The full calculations of K-S test, normal cumulative distribution and the normal probability plot obtained by using Minitab software of Zn, Cu and Fe distribution in AMD patients are summarized in Appendix 2.

**Table 2.13** The total concentration (mg L$^{-1}$) of Zn in serum of AMD patients*

| Samples number | Zn ± STDV | Samples number | Zn ± STDV |
|---|---|---|---|
| 21 | 0.87 ± 0.08 | 42 | 0.62 ± 0.06 |
| 23 | 0.7 ± 0.07 | 43 | 0.85 ± 0.08 |
| 24 | 0.71 ± 0.07 | 44 | 0.59 ± 0.06 |
| 25 | 0.63 ± 0.06 | 45 | 0.68 ± 0.06 |
| 26 | 0.65 ± 0.06 | 46 | 0.75 ± 0.07 |
| 27 | 0.71 ± 0.07 | 48 | 0.98 ± 0.09 |
| 28 | 0.86 ± 0.08 | 49 | 0.57 ± 0.05 |
| 29 | 0.69 ± 0.06 | 51 | 0.52 ± 0.05 |
| 30 | 0.66 ± 0.06 | 52 | 0.74 ± 0.07 |
| 31 | 0.85 ± 0.08 | 53 | 0.56 ± 0.05 |
| 32 | 0.84 ± 0.08 | 55 | 0.65 ± 0.06 |
| 33 | 0.95 ± 0.09 | 56 | 0.72 ± 0.07 |
| 34 | 1.02 ± 0.10 | 57 | 0.78 ± 0.07 |
| 35 | 1.04 ± 0.10 | 58 | 0.86 ± 0.08 |
| 36 | 1.26 ± 0.12 | 59 | 0.88 ± 0.08 |
| 37 | 1.19 ± 0.11 | 60 | 0.66 ± 0.06 |
| 38 | 0.62 ± 0.06 | 61 | 0.73 ± 0.07 |
| 39 | 1.33 ± 0.12 | 62 | 0.57 ± 0.05 |
| 41 | 1.32 ± 0.12 | 63 | 0.77 ± 0.07 |

* The quoted STDV values were calculating by multiplying the measured values by the RSD of 20 replicates of Serum UTAK reference materal divided by 100.

**Table 2.14** The total concentration (mg L$^{-1}$) of Cu in serum of AMD serum patients*

| Samples number | Cu ± STDV | Samples number | Cu ± STDV |
|---|---|---|---|
| 21 | 1.92 ± 0.25 | 42 | 1.22 ± 0.16 |
| 23 | 1.41 ± 0.18 | 43 | 1.04 ± 0.13 |
| 24 | 1.02 ± 0.13 | 44 | 1.61 ± 0.21 |
| 25 | 0.87 ± 0.11 | 45 | 1.37 ± 0.18 |
| 26 | 0.93 ± 0.12 | 46 | 1.49 ± 0.19 |
| 27 | 1.07 ± 0.14 | 48 | 0.98 ± 0.13 |
| 28 | 0.83 ± 0.11 | 49 | 1.21 ± 0.16 |
| 29 | 1.42 ± 0.18 | 51 | 1.09 ± 0.14 |
| 30 | 0.77 ± 0.1 | 52 | 1.15 ± 0.15 |
| 31 | 1.03 ± 0.13 | 53 | 0.85 ± 0.11 |
| 32 | 1.33 ± 0.17 | 55 | 1.01 ± 0.13 |
| 33 | 1.16 ± 0.15 | 56 | 1.20 ± 0.15 |
| 34 | 1.48 ± 0.19 | 57 | 0.98 ± 0.13 |
| 35 | 0.91 ± 0.12 | 58 | 0.95 ± 0.12 |
| 36 | 1.31 ± 0.17 | 59 | 1.07 ± 0.14 |
| 37 | 1.15 ± 0.15 | 60 | 1.01 ± 0.13 |
| 38 | 0.99 ± 0.13 | 61 | 1.16 ± 0.15 |
| 39 | 1.34 ± 0.17 | 62 | 1.14 ± 0.15 |
| 41 | 0.92 ± 0.12 | 63 | 0.98 ± 0.13 |

* The quoted STDV values were calculating by multiplying the measured values by the RSD of 21 replicates of Serum UTAK reference materal divided by 100.

**Table 2.15** The total concentration (mg L$^{-1}$) of Fe in serum of AMD serum patients*

| Samples number | Fe ppm ± STDV | Samples number | Fe ppm ± STDV |
|---|---|---|---|
| 21 | 1.29 ± 0.14 | 42 | 1.30 ± 0.14 |
| 23 | 2.06 ± 0.22 | 43 | 0.51 ± 0.05 |
| 24 | 1.26 ± 0.14 | 44 | 1.26 ± 0.13 |
| 25 | 1.06 ± 0.11 | 45 | 1.68 ± 0.18 |
| 26 | 1.18 ± 0.13 | 46 | 1.63 ± 0.17 |
| 27 | 1.88 ± 0.20 | 48 | 1.11 ± 0.12 |
| 28 | 0.99 ± 0.11 | 49 | 1.08 ± 0.12 |
| 29 | 1.31 ± 0.14 | 51** | 3.22 ± 0.35 |
| 30 | 0.96 ± 0.10 | 52 | 1.60 ± 0.17 |
| 31 | 0.87 ± 0.09 | 53 | 1.72 ± 0.18 |
| 32 | 2.20 ± 0.24 | 55 | 1.32 ± 0.14 |
| 33 | 1.83 ± 0.20 | 56 | 1.25 ± 0.13 |
| 34 | 0.63 ± 0.07 | 57** | 3.43 ± 0.37 |
| 35 | 1.52 ± 0.16 | 58** | 3.17 ± 0.34 |
| 36 | 1.03 ± 0.11 | 59 | 0.74 ± 0.08 |
| 37 | 0.84 ± 0.09 | 60 | 2.41 ± 0.26 |
| 38 | 1.24 ± 0.13 | 61 | 1.64 ± 0.18 |
| 39 | 1.68 ± 0.18 | 62 | 1.13 ± 0.12 |
| 41 | 1.59 ± 0.17 | 63 | 0.68 ± 0.07 |

* The quoted STDV values were calculating by multiplying the measured values by the RSD of 23 replicates of Serum UTAK reference materal divided by 100.

** Samples number 51,57 and 58 of Fe were found higher than calculated linear dynamic range (20ppb) in the diluted samples.
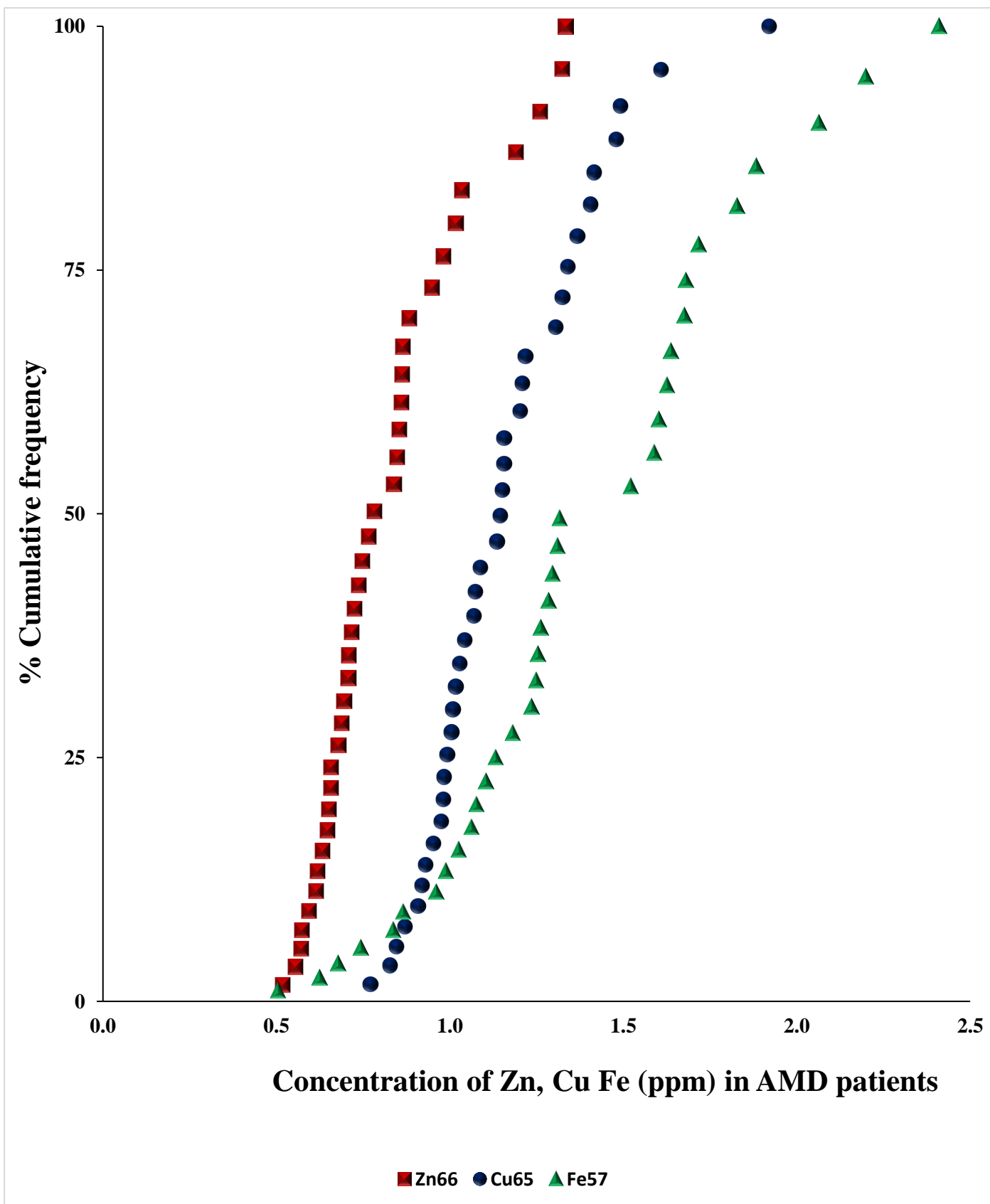
**Figure 2.6** The cumulative frequency curve for the measurements of serum Zn, Cu and Fe in AMD patients.

One-way ANOVA test was applied to compare Zn, Cu and Fe variation in AMD patients, showing that the concentrations of these elements were significantly different as the F critical is smaller than the F calculated (P <0.0001). The results obtained from this test at 5% significance level are shown in Table 2.16 for comparision between Zn, Cu and Fe in AMD patients.The results illustrate that the total average of serum Zn in general is noticeably lower than Cu and Fe. Iron shows the highest level in comparison to Zn and Cu, in the case of AMD.

**Table 2.16** ANOVA: One-factor with  (n = 38) of serum Zn, Cu and Fe detected from AMD patients.

SUMMARY

| Groups | Count | Sum | Average | Variance | | |
|---|---|---|---|---|---|---|
| $Zn^{66}$-AMD | 38 | 30.38 | 0.80 | 0.04 | | |
| $Cu^{65}$-AMD | 38 | 43.37 | 1.14 | 0.06 | | |
| $Fe^{57}$-AMD | 35 | 46.46 | 1.33 | 0.20 | | |

ANOVA

| Source of Variation | SS | df | MS | F | P-value | F crit |
|---|---|---|---|---|---|---|
| **Between Groups** | 5.27 | 2.00 | 2.64 | **26.91** | **3.29E-10** | **3.08** |
| **Within Groups** | 10.58 | 108.00 | 0.10 | | | |
| | | | | | | |
| **Total** | 15.86 | 110.00 | | | | |

## 2.3.5.3  Associations between age-related macular degeneration and Alzheimer disease

Alzheimer disease and age related macular degeneration are chronic diseases associated with aging.[247] Both diseases share similar pathogenesis pathway and environmental risk factors thus some authors named AMD 'Alzheimer disease in the eye'.[248,249] Aging, obesity, unhealthy diet, atherosclerosis, hypertension, and smoking are the common risk factors.[248,77] Although genetic background seems to be different between these diseases, cellular aging pathology have parallel association in the retina and brain tissues. As the growing age of the population has increased and age is the most common risk factor, these two age-related diseases have recently received a great deal of attention from researchers.[249,77]

The retina is similar to other areas of the brain and an integral section of the central nervous system (CNS), it is derived from the neural tube of the CNS. Both brain and the retina have blood-tissue barriers feature. Retinal degeneration affects patients with in Alzheimer's disease.[250] AMD and AD share several pathological features such as inflammation, inreased oxidative stress, vitronectin and amyloid-β accumulation.[248,249] Amongst the common markers of both AMD and AD are extracellular deposits consisting of primarily comparable aggregated proteins in both diseases.[77] In AMD, the yellow deposits that are located between the retinal pigment epithelium and Bruch's membrane (BM) are called drusen. Large and confluent drusen are substantial risk factors for developing choroidal neovascularisation (AMD).[249] On the other hand, in AD, the deposits in the brain are characterised by amyloid-β-containing senile plaques.[248,249] Although Amyloid-β is accumulated in the drusen and in the brain, the phenotype is different between AD and AMD, and the latter is not generally considered an amyloid-deposit disease. [248,249,251,252] In addition, the cells affected by Aß and the area of Aß deposition in the retina or brain are different between AMD and AD.[249] With increasing age, the small amounts of Aß deposit in the normal brain and in the normal retina increases and thus the accumulation of Amyloid-β 42 oligomers cause chronic inflammation and therefore contribute to blood–retinal barrier dysfunction.[248,249,253] In AMD, choroidal blood flow is decreased, similarly, cerebral blood flow is 20% lower in AD patients in comparison with age-matched controls.[248,254,255] Klaver et.al[256] (the Rotterdam study) investigated the incidence of both diseases in 1,438 patients above the age of 75 years and followed up examination for an average of 25.2 months. Patients with advanced AMD showed an increased risk of Alzheimer's disease occurrence. The risk was decreased after adjustments for smoking and atherosclerosis, suggesting a common pathogenesis for neuronal degeneration. This finding was confirmed by other studies[257,258] which observed a raised incidence of cognitive impairment in patients with AMD in the Age-Related Eye Disease Study (AREDS). Hoh Kam et al. (2010)[259] demonstrated that Aß accumulation occurred with aging even in the normal mouse retina and human retina. It has been observed that patients with AD usually have visual and retinal abnormalities such as failure and damage of the central visual pathways, optic nerve and ganglion cell degeneration and reduction of the thickness of the retinal nerve fibre layer.[249] The data suggested that a related pathogenic mechanism may occur between AMD and AD. Therefore, therapeutic approaches that have targeted Aß in AD patients can also be useful and practical to AMD.[249] For example, immunotherapy

targeting amyloid-β has been proven effective in protecting the retinal pigment epithelium.[260,261]

Nutritional antioxidant supplements are effective in delaying both diseases.[248] On the other hand, Keenan et al. reported[262] that the risk of AD following AMD was not raised according to English National Health Service. Future research is required to identify whether AMD and AD patients receive appropriate investigation and treatment.[262]

### 2.3.5.4 Comparison of data from AMD and AD samples

It is important to compare the random errors of the two sets of data, i.e. standard deviations. For each of the three elements analysed an $F$-test was conducted to test if there is significant difference between the two sample variances. For Zn, the calculated $F$-value was higher than the critical $F$-value ($P<0.0001$). Therefore, the null hypothesis of equal variances is rejected and there is significant difference between the two variances at the 5% probability level. However, for Cu and Fe the calculated F values were lower than the critical F values ($P>0.10$), thus, the null hypothesis of equal variances is retained and there is no significant difference between the two variances at the 5% probability level. As a result, an equal variance $t$-test for Cu and Fe (two tailed) and unequal variance $t$-test for Zn (two tailed) was carried out, in order to test differences in the two experimental means. According to the relevant $t$-test, the results of Zn and Cu in the serum showed no significant differences between AD and AMD as the calculated $t$ value is smaller than the critical value at 95% confidence level. ($P>0.10$). However, Fe in AMD patients is slightly higher than AD patients as the calculated t value for Fe between AD and AMD patients in serum is greater than the critical value at 95% confidence level. ($P=0.04$). The measurements of $t$-tests, $F$-tests and their critical and $P$-values are illustrated in Table 2.17 at 5% probability level.

Another simple and fast way of representing data in a plot is the box-and whisker diagram. The plot depicts at a glance the spread and symmetry of the data through their quartiles. This alteration of Zn, Cu and Fe is outlined in the box- and whisker plots represented in Figure 2.7, which show the clear imbalance in the three elements in each group of patients.

**Table 2.17** Descriptive statistics for all analysed elements in both group of patients showing *F*-calc and *t*-calc and *P* scores

| Zn | AMD | AD |
|---|---|---|
| Mean | 0.80 | 0.78 |
| Variance ($S^2$) | 0.04 | 0.02 |
| Observations | 38 | 43 |
| **t Stat** | **0.61** | |
| P(T<=t) two-tail | 0.54 | |
| t Critical two-tail | 2.00 | |
| **F ($S1^2/S2^2$)** | **2.83** | |
| P(F<=f) two-tail | 6.48E-04 | |
| F Critical two-tail | 1.69 | |

| Cu | AMD | AD |
|---|---|---|
| Mean | 1.14 | 1.18 |
| Variance | 0.06 | 0.05 |
| Observations | 38 | 43 |
| **t Stat** | **0.71** | |
| P(T<=t) two-tail | 0.48 | |
| t Critical two-tail | 1.99 | |
| **F ($S1^2/S2^2$)** | **1.05** | |
| P(F<=f) two-tail | 0.43 | |
| F Critical two-tail | 1.69 | |

| Fe | AMD | AD |
|---|---|---|
| Mean | 1.33 | 1.12 |
| Variance | 0.20 | 0.19 |
| Observations | 35 | 42 |
| **t Stat** | **2.05** | |
| P(T<=t) two-tail | 0.04 | |
| t Critical two-tail | 1.99 | |
| **F ($S1^2/S2^2$)** | **1.03** | |
| P(F<=f) two-tail | 0.46 | |
| F Critical two-tail | 1.71 | |
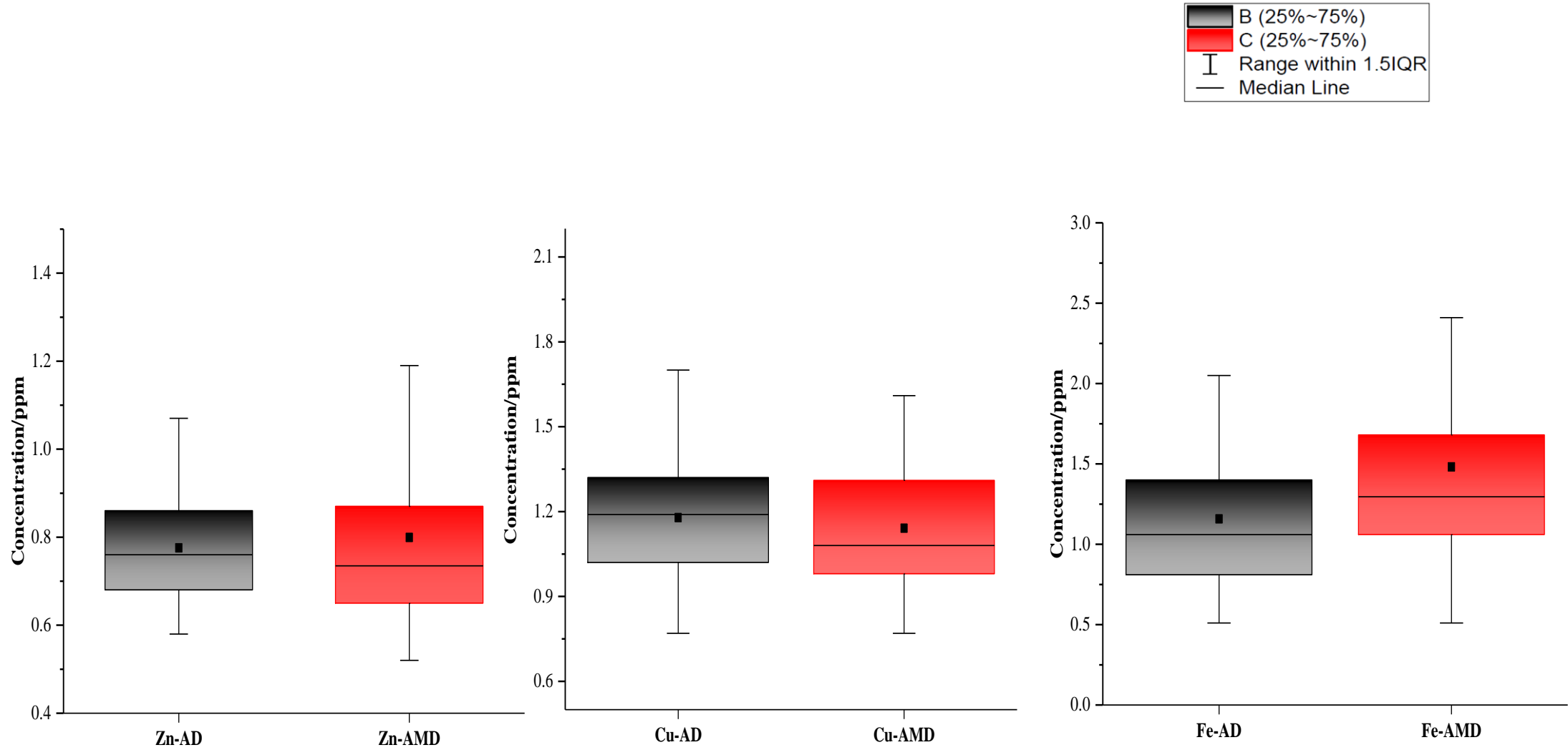
**Figure 2.7 Box-and-whisker plot** showing the different patterns of **AD and AMD concentrations in Zn, Cu and Fe, respectively.** Symbols on each box plot represent: mean value (■), median (line in box), minimum and maximum data values (whiskers), and $75^{th}$ and $25^{th}$ percentile (upper and lower the edge of box).

### 2.3.5.5 Comparison with healthy controls

Some published values for Zn, Cu and Fe concentrations in the serum of healthy control people are given in Table 2.18 and compared with AD and AMD patients' serum levels found in this work. In patients' samples, Zn/Fe concentrations were lower compared to healthy people whereas Cu levels in patients' sera were higher in comparison to healthy people as can be seen in Figure 2.8. This finding supports other reports in the literature.[15,72,202,208,20,210,263]

Rembach et al[72] reported that serum Zn concentration dropped around 0.4% per year with age. A possible reason for decreasing serum Zn level in AD patients might be the accumulation of Zn in the brain as amyloid plaques trap Zn which is then depleted in other body compartments.[15] In addition, Zn deficiency and variation in AD patients could be related to the interaction with Cu metabolism.[202] Ceruloplasmin is the major Cu-carrying protein which accounts for 85-95% of circulating Cu. As inflammation is potentially linked with AD pathogens, and ceruloplasmin levels rise during inflammation response[208], serum levels of ceruloplasmin have been found to be higher in AD compared to healthy controls.[208] This is consistent with the higher Cu levels in AD patients found in this work. Like ceruloplasmin, transferrin and ferritin are the main proteins that regulate the transportation and the storage of Fe in the body and they are significantly decreased in the serum of AD patients compared to controls.[263] Moreover, it was indicated that the alteration of the gene of both proteins is related to AD. According to this evidence, it is sensible to consider that Fe homeostasis might be linked with AD progression.[263] In general, the concentration of serum Zn, Cu and Fe are likely to vary with different ages.[191,207,209] In addition, these elements displayed differential changes with regard to gender and nutritional state.[22] Further studies from different countries are needed to assess the correlation between serum metal levels in healthy people and AD/AMD patients.

To test for significant difference between the observed and known values (apart from that due to random variation), the statistic $t$ is calculated from the equation below:[239]

$$t = \frac{(\bar{X} - \mu)\sqrt{n}}{s} \qquad (2.7)$$

Where $\bar{x}$ = sample mean, $s$ = sample standard deviation and $n$=sample size.

The means of the patients and the known values of the healthy control were compared for all elements using the equation above (2.7) of  $t$-test. Since the observed values of $| t |$ is larger than the critical value, the data sets for all elements were significantly different at $p=0.05$, except that Fe in AMD patients was not significantly different from healthy controls as the $t$-calculated is less than the critical value, thus the null hypothesis is retained and there is no evidence of systematic error.

The possibility of carrying out multi-variate analysis (e.g. PCA, MLR, cluster analysis, etc) on the serum analysis data was considered. However, following discussion with supervisors and the external collaborator, it was concluded that, due to the limited number of samples for which complete patient data were available, there would be insufficient statistical power in any conclusions drawn from multi-variate analysis at this stage and this might jeopardize publication of the work which is primarily concerned with the development of improved analytical methodology.

**Table 2.18** Comparison of the concentration (mg $L^{-1}$ ) of Zn, Cu and Fe serum among AD (n=43) and AMD (n=38) patients with published values of healthy controls (n=1250 )

| Trace elements | N | Age (years) | published Healthy control | Ref. | Present study of AD patients | Present study of AMD patients |
|---|---|---|---|---|---|---|
| Zn | 302 | 65.6 ±12.2 | 1.29 ±0.39 | 264 | 0.78± 0.13 | 0.80± 0.21 |
| Cu | 716 | 69 ± 6.8 | 0.93 ± 0.18 | 265 | 1.18± 0.23 | 1.14± 0.24 |
| Fe | 302 | 65.6±12.2 | 1.47± 0.65 | 264 | 1.12± 0.44 | 1.33± 0.45 |

* All values were expressed as mean ± STDV.
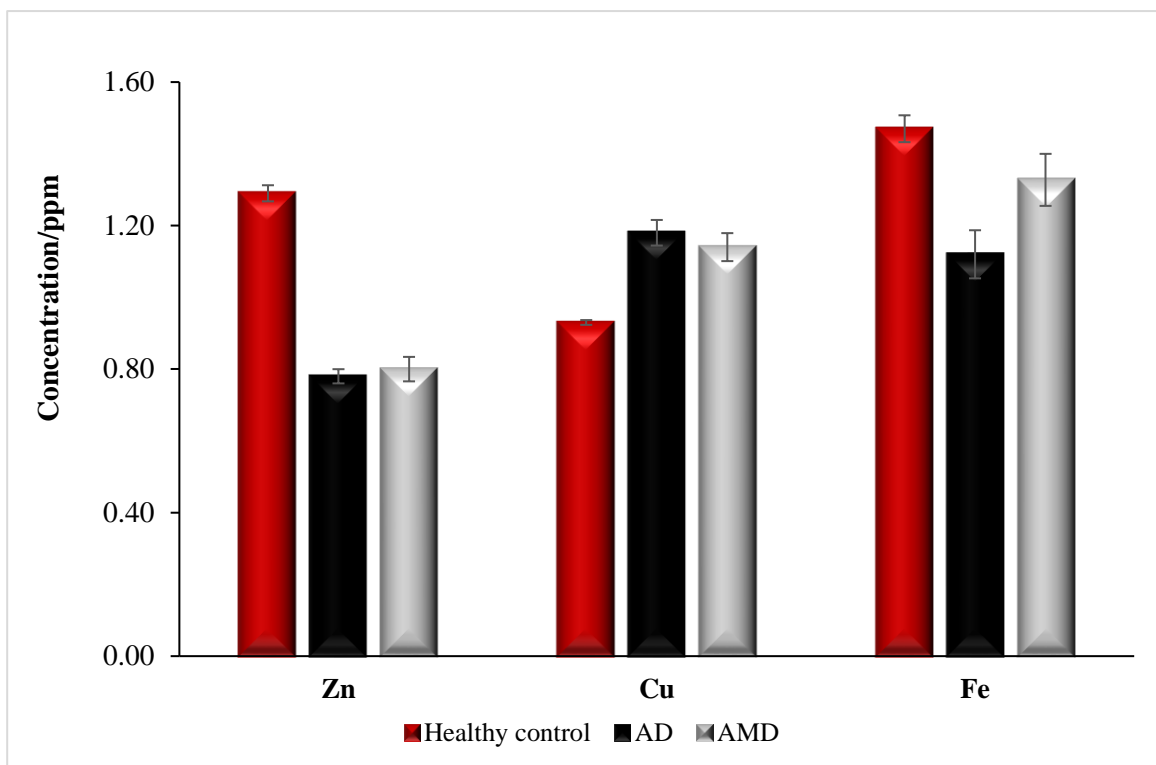
**Figure 2.8** Comparisons between Zn, Cu and Fe concentrations (mg L$^{-1}$) in AD, AMD patients and published healthy controls. Error bars represent the standard error of the mean (STDV/√n), n=43 in AD patients and n=38 in AMD patients. Healthy control data were taken from references 254 and 255.

## 2.4    Conclusion

Simple dilution-based procedures show successful results and provide an alternative to conventional acid digestion for biological materials, since precision, satisfactory accuracy, and instrument performance have been reported in the majority of such studies. In this study, we have demonstrated that high resolution sector field ICPMS is capable of determining Zn, Fe and Cu level in 50 µL or less of AD and AMD serum samples with satisfactory results in terms of LOD and precision. A minimal requirement of sample volume is important to preserve sample and allow researchers to accurately determine trace elements in different biological matrices. Although the term "sample diluent" was used in this procedure and it only requires adding reagents to the samples, in practise it is more than a diluent as this mixture is chemically active in a way that trace elements are stabilized in the solution and samples nebulised properly. Moreover, the preparation procedure used was compared with many other procedures and it was found that this matrix gives stable calibration curves, low blanks and reliable results with standard reference material to enable these trace elements to be determined in small sample volumes. To the best of our knowledge, no other published studies in the literature have used such a low volume of serum sample to quantify Zn, Cu and Fe. Because of the ubiquitous nature of the elements of interest in the environment, an extensive blank testing regime has been carried out, in which different sample vessels were tested, sample preparations were performed under careful protocol and precautions, and the sample introduction system was cleaned out on a regular basis in order to sustain a low and consistent blank, which was successfully achieved as described in the chapter.

The importance of studying age related disease has significantly increased over the last century due to the rise of aging rate of the world population. It is still unclear whether the metal-related abnormalities are a cause or an effect of the retinal degeneration in AMD. Alteration of serum Zn, Cu and Fe levels are involved in the pathogenesis of Alzheimer disease. Parallel studies between AD and AMD have led to a link between the two conditions. Understanding the common mechanisms may provide new insights into AD and AMD pathogenesis and treatment. AMD and AD is a multi-factorial disease influenced by age, gender and combination of environmental and genetic risk factors. The hypothesis involved in measuring trace elements in serum samples is to find out if there is a correlation between the observed levels of these trace elements and the state of the disease in individual patients. In this study, it was indicated that serum Fe levels in AMD patients are slightly higher than

AD patients, whereas serum Zn and Cu were not significantly different between AD and AMD patients. Furthermore, the total average of serum Zn in general is lower than Cu and Fe and this finding is supported by the literature as discussed earlier in the introduction.[85,196,15,72,17] As the set of control samples was not possible to obtain, our AMD and AD patients were compared with published healthy control elsewhere.[208,263] The results show a decrease in Zn and Fe serum level in AD and AMD patients compared to healthy controls[264,263] whereas serum Cu level appears notably increased in AD and AMD patients compared to healthy controls.[265,263] These findings are in line with those recently reported.[263] The comparisons between controls and patients will be more reliable if they were of similar age group and gender. Therefore, the next stage of this research will include phenotypic details such as, gender, age, nutrition and lifestyles of the anonymised participants. Such information would be derived from follow on clinical collaborations as part of a study and that would allow for comprehensive information and reliable comparisons.

There is controversy about measuring bulk serum concentrations for trace elements to study particular pathogenesis of diseases. Although serum Zn is maintained homeostatically, it is still the most commonly accepted biomarker of Zn status.[147] It is possible now to analyse trace metals in single cells which have been done in our group and reported elsewere.[266] Therefore, the work described later in chapter 4 was an attempt to look for Zn inside the cell as intracellular Zn may be a better measure of the biological processes involved.

# 3 Bio-imaging of Zinc in Retina Tissue by Laser Ablation Inductively Coupled Plasma Mass Spectrometry

## 3.1 Introduction

### 3.1.1 Distribution of zinc in the eye

The highest concentration of Zn is found in the eye compared to other tissues, in particular retinal pigment epithelium (RPE) and choroid complex.[267] The order of Zn concentration in ocular tissues as reviewed extensively by Galin was concluded to be as follows: retina and choroid > ciliary body > iris > optic nerve > sclera > cornea > lens. The Zn concentration in the retina and choroid is found to be around 464 ppm and 472 ppm, respectively.[267,268] The structure of the eye is highly organised and complex. Figure 3.1 provides a schematic illustration of the eye in general and the layers of the retina in particular.[269] The choroid is the vascular layer of the eye containing the main supply of blood vessels to the retina and lying between the retina and the sclera. Bruch's membrane (BM) is an elastin- and collagen-rich extracellular matrix which is involved in exchange of oxygen and micronutrients between the choroid and the retinal pigment epithelium (RPE), the RPE is a monolayer of pigmented cells which interacts with photoreceptors in the maintenance of visual cycle and delivers nutrients from the blood to photoreceptors. The retina is a complex transparent tissue consisting of several layers, a healthy retina is vital to clear vision as it receives light that the lens has focused, converts the light into neural signals, and sends these signals on to the brain for visual recognition.[270]

Zinc is undeniably vital for normal functioning of the eye, as it plays a fundamental role in maintaining normal ocular function and retinal physiology. It is involved in several retinal functions including visual cycle and photoreceptor survival, photo transduction, and the process of neurotransmission. Additionally, Zn is thought to influence cell metabolism through a variety of mechanisms and may also function as part of antioxidant defence mechanisms in the retina.[267,186,42]
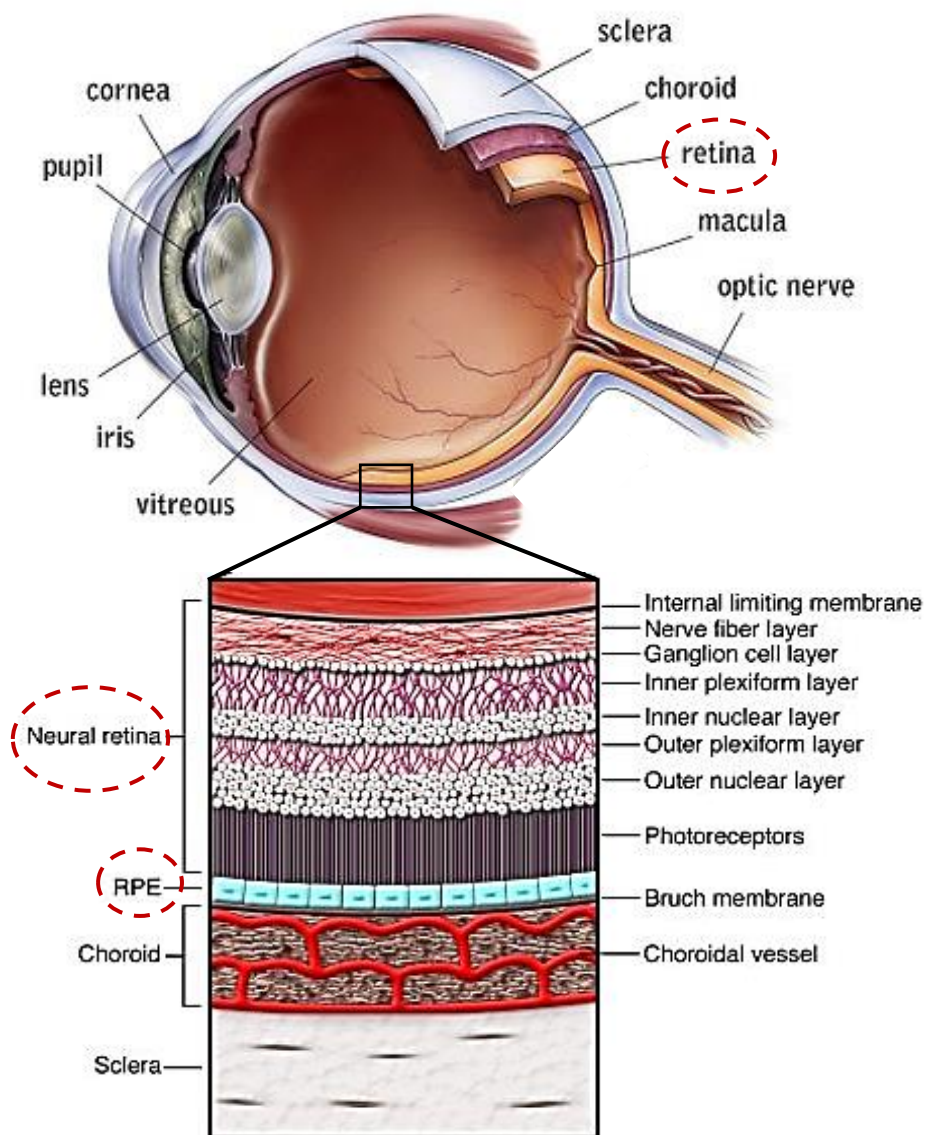
**Figure 3.1** Schematic diagram of the anatomy of the eye. The section of interest (Retina) enlarged to show the anatomical layers. Reproduced from Caspi, 2010, with permission from American Society for Clinical Investigation.[269]

Experimental evidence suggested that Zn may have positive or negative consequences on retinal physiology and pathophysiology of cells, depending on the localisation (extracellular vs. intracellular), concentration and state (bound or free).[186,271] As the level of Zn is high in the retina, a large number of Zn ions are tightly bound to proteins and other molecules to regulate their structure and function in retina. Therefore, exchangeable Zn may be essential for participation in numerous biological processes. Excess levels of "free" or loosely bound metal ions can cause toxic effects.[186] Like any other cells, the

RPE can be damaged by excessively large or excessively small amounts of Zn which can cause retinal cell dysfunction and pathology.[272] Studies have shown *in vitro* [273] and *in vivo* [274] that high quantities of Zn can be harmful and lead to neuronal damage deterioration.[271] However, low doses of Zn given therapeutically could be beneficial in treating some diseases. [271]

The high concentration of Zn in retinal pigment epithelium (RPE) can decrease during Zn deficiency. It causes reduction in: metallothionein concentration, cell/ protein production and activity of catalase in RPE as well as cells becoming more vulnerable to oxidative damage and thus neuronal death.[275,40] Zinc deficiency is associated with night blindness, poor darkness adaptation and macular degeneration. [42,271] Another study found that feeding rats with a Zn-deficient diet increased the accumulation of the aging pigment in the retina.[276] Morphological changes in retinal structures could be a cause of Cu deficiency.[42]

## 3.1.2   Zinc in retinal physiology and related disease

Altered metal homeostasis is frequently implicated in a wide range of disease.[277] As discussed earlier, metal ions are known to play an important role in many age related diseases including AMD and retinal health. In this disease, abnormal regulation of redox active metal ions can provoke oxidative stress by producing cytotoxic reactive oxygen species (ROS).  It also extends to non-redox active metals such as Zn and Ca, which are cytotoxic at high concentrations and often associated with neurodegenerative diseases.[278]

It is well known that, during aging, Zn homeostasis changes and may contribute to specific retinal disorders.[186] Aging has been linked with Zn reduction in human retina and RPE. Age is a major cause of cellular function failure and death. Both cone and rod lose their mediated responses. In addition, cell density declines with age and a decreased cone photoreceptor in pigmented rat was observed.[279] According to a study by Wills et al.[42], the level of Zn decreases in the neuroretina of men, whereas no changes were detected in women. Another study[280] showed the link between metallothionein (MT) and Zn in the retina which was thought to protect the cells from oxidative damage. MT has the property of releasing and binding Zn whereas Zn can stimulate MT production and if the need arises it can also detach itself from MT in case of low level of Zn that may follow rapid degeneration rate of MT. Thus, the study indicated that the elevation and reduction

in MT level in human RPE cells are associated with the elevation and reduction of Zn level.[280]

chronic inflammation and oxidative stress may play significant causative roles, thus Zn reduction in human eyes was suggested to be a sign of age-related macular degeneration (AMD).[281,282,40] A study by Erie et al.[189] found that the concentration of Zn in the retinal pigment epithelium (RPE) and choroid was 24% lower in patients suffering from AMD than in a control group.[186,189]

As a result, imaging metals in biological samples including tissue specimens in human or animal models is a required tool in order to understand the behaviour of metals in age-related diseases and find a treatment or a cure.[278]

### 3.1.3 Application of bio imaging by LA-ICP-MS

Several imaging techniques have been used to study biological specimens and provide spatially resolved data on trace elements.[283] These include scanning electron microscopy (SEM)[284], particle-induced X-ray emission (PIXE)[285], secondary ion mass spectrometry (SIMS)[74], transmission electron microscopy (TEM)[286], synchrotron-radiation XRF[287], synchrotron X-ray fluorescence (SXRF)[186]/ (μSXRF)[288] microscopy, X- ray fluorescence microscopy (XFM)[276,289], laser-induced breakdown spectroscopy (LIBS)[290]. Inductively coupled plasma–mass spectrometry (ICP– MS) has been widely utilized in the life sciences to determine trace elements in various sample types including tissues. The analytical capabilities of ICP–MS are extended through the use of laser ablation (LA) which allows for direct analysis of elements in solid samples.[291]

LA-ICP-MS is among the most versatile and commonly used techniques owing to its low detection limits, multi-element capability, and wide dynamic range.[292,293] Contiguous sampling across thin sections of a tissue sample enables construction of 2D colour maps showing the elemental distribution across the sample. Using the latest technology can achieve high spatial resolution, which makes it an ideal choice to study the small scale features involved in the retinal complex with respect to AMD diseases.[3,294] The applications of such bio-imaging using LA-ICP-MS are well known and have included: imaging of Cu and Zn in liver[173] and kidney[295] sections, the mapping of Cu, Zn, Fe and Mn in sections of brain tissue,[277,296,297,292] the detection of Cu, Zn and Fe in breast cancer tissue[298], quantitative mapping of Mg, Ca, Fe, Zn, Cu, Mn in oral mucosa[293], quantitative

mapping of Al, Ba, La, Sr in teeth[299], quantitative mapping of Gd in articular cartilage[300] and quantitative mapping of Ca, Mg, Zn, Cu, and Pb in patients' blood serum and arterial wall sections (blood vessels).[301] In 2014 Konz *et al.* performed quantitative imaging of cryosectioned human eye lenses, revealing a homogeneous distribution of Zn in the lens.[170] A subsequent study by this group imaged the retina and RPE cells, showing a preferential accumulation of Zn within the RPE compared to the retina and sclera.[302] Hence, LA-ICP-MS represents a useful tool for studying the distribution of metals and their relationship to specific disease states and treatments. However, comparison between small features of similar concentration is difficult, since perceptions of these structures are heavily influenced by the choice of false colour scheme used to display the data.[303]

### 3.1.4   Aim of the study

As discussed earlier, Zn appears to play a crucial role in many cellular metabolic pathways and is found in high concentrations within the retina/choroid complex. Also, it is known that Zn homeostasis at systemic and cellular levels is disrupted in AMD patients. Therefore, restoring normal Zn balance has been suggested to slow the development of the disease. The most commonly used approach to restore Zn homeostasis in humans is oral supplementation. However, clinical trials using Zn supplements have given conflicting outcomes due to the lack of understanding of how Zn levels affect the eye.

**Therefore, this chapter was focused on:**

- Investigation of the role of supplementation on the distribution of Zn across ocular compartments.
- Utilisation of LA-ICP-MS to image the distribution of Zn across the retina and retinal pigment epithelium in aged rats that had received a conventional or supplemented diet with varying amounts of Zn and Zn+ Cu for an extended period.
- Use of a novel data processing approach to examine the relative differences between Zn accumulation in these compartments and evaluation of its potential for use in future retinal imaging experiments.

## 3.2 Methodology

### 3.2.1 LA-ICP-MS

The instrumentation experiments were performed by using laser ablation system (UP-213, Electro Scientific Industries, Cambridgeshire, UK) incorporating a neodymium - doped yttrium-aluminium-garnet (Nd:YAG) laser, coupled with sector-field ICP-MS instrument (Element 2XR, Thermo Scientific, Bremen, Germany). The laser system was fitted with a low volume teardrop shaped cell which has been described elsewhere.[304] The sections are mounted on a suitable and movable support in order to ablate the sample directly. Helium was used as an ablation gas, at flow rate of 0.55 L/min, and Ar was used as a make-up gas introduced through a Y- piece between the cell and the injector, at a flow rate of 0.8 L/min. A certified reference material, NIST 611 glass (National Institute of Standards and Technology, Gaithersburg, USA) is often used for tuning the ICP parameters. The system was tuned on a daily basis before each experiment by ablating NIST 611 multi-element standard at a high repetition rate in a raster pattern to give a smooth signal. The signal generated from NIST 611 ablation was used to tune for optimum $^{238}$U signal intensity, besides maintaining the Th/U ratio to approximately 1 and the ThO/Th ratio lower than 1%.

Tissue sections were ablated by performing a series of adjacent line scans across a section of the slide. Vertical adjacent lines were drawn through each section, covering the maximum y distance of the sample. The number of lines was varied according to the size of the section and consequently the line length and number of lines varied between sections. Optimised operating conditions for the imaging study are given in  Table 3.1. The laser ablation parameters applied for analysis, such as laser energy, repetition rate, spot size and scan speed, will be discussed in the following sections individually according to the type of the section.

**Table 3.1** The ICP-MS measurement parameters

| ICP-MS operating parameters | Value |
|---|---|
| Analyte | $Zn^{66}$* |
| Radio frequency (RF) power W | 1250 |
| Cool gas (L min$^{-1}$) | 15.50 |
| Auxiliary gas flow (L min$^{-1}$) | 0.95 |
| Sample gas flow rate (L min$^{-1}$) | 1.02 |
| Torch X position (mm) | 5.2 |
| Torch Y position (mm) | 3.8 |
| Torch Z position (mm) | -2.10 |
| Resolution | Low |
| Mass window | 10% |
| Integration window | 20% |
| Settling time (s) | 0.001 |
| Sample time (s) | 0.005** |
| Samples per peak | 50 |
| Segment duration (s) | 0.025** |
| Scan type | E-Scan |
| Detection mode | Triple |
| Integration type | Average |

*In some sections $Cu^{63}$ and $Ca^{44}$ were measured.

** Time was changed according to the size of ablating section and number of elements measured.


### 3.2.2 Data treatment

LA-ICP-MS can generate very large amounts of data; more than common spreadsheet software can handle. In addition, comparing data from intra- or inter-laboratory tests is relatively complicated.

Two dimensional images of the samples were created using mainly the software IGOR Pro (version 6.22 A, Wavemetrics, Oregon, USA). Iolite version 2.15 an add-on to IGOR Pro, non-commercial download software package (Melbourne Isotope Group, Melbourne, Australia) was used for data visualisation.

The software extracts data from ICP-MS in the conventional FIN2 format and transforms each data point into a colour coded pixel. Therefore, the colour profile of the resulting image represents the distribution of the corresponding elements across the sampled region. The raw data were also examined using IGOR Pro's in-built Multipeak Fitting package. The data were baseline subtracted and peaks were fitted to the features in each line of data using the optimum fit type for each peak (from a choice of Gaussian, Lorenzian, log normal or exponentially modified Gaussian). The height, peak areas, peak widths at the baseline and full width half maxima for the choroid, retina and RPE were directly exported into Excel for further processing. The peak areas were used to calculate the RPE/retina Zn ratio for each sample, whilst the peak widths were used to determine the thickness of each feature. Although this software is able to process different datasets, regardless of the number of files involved, occasionally it freezes due to the massive number of files.

### 3.2.3   Ethics and sample collection

Ethical approval (08/H0721/12) was obtained from the research ethics and governance committee of Moorfields Eye Hospital. All the necessary safety precautions were taken before handling the samples. Slides for LA-ICP-MS were prepared and obtained from Dr Imre Lengyel's group at Institute of Ophthalmology, University College London, Bath Street, London, UK, EC1V 9EL.

### 3.2.4   Collection and preparation of human sub-RPE sections

Tissues were taken from human donated eye sections, UCL Institute of Ophthalmology and Moorfields Eye Hospital Eye Tissue Repository within 24 hours of death. Patients that had been diagnosed with CNV secondary to AMD were invited to take part in the study initially at the same Hospital. The thickness of the section was 20-30 µm and it was taken from underneath the RPE cell layer, so it includes: drusen, Bruch's membrane (BM) and choroid.

The first initial test was performed on three human sub-RPE sections (D1, D2, and D3) to identify the level of Zn and Cu. The second test was performed on 4 other human retinal sections (D4, D5, D6 and D7) to identify the level of Zn and Ca. The typical operation parameters are summarized in Table 3.2.

**Table 3.2** Laser instrument parameters for human RPE sections D1, D3, D4 and D6

---

### ESI UP-213 laser ablation parameters

---

Repetition frequency:..............................5Hz

Line length: ..........................................475µm

**For section D1:**

Laser energy:.........................................30%

Scan speed:...........................................15µm/s

Spot size:..............................................15µm

Line spacing: ........................................3 µm

Numbers of lines:..................................35 lines

Fluence:................................................3.35 J/cm$^2$

**For section D3:**

Laser energy:.........................................30%

Spot size:..............................................15µm

Scan speed:...........................................15µm/s

Line spacing: ........................................Zero

Numbers of lines:..................................42 lines

Fluence:................................................2.17 J/cm$^2$

**For section D4 & D6:**

Laser energy:.........................................35%

Spot size:..............................................25µm

Scan speed:...........................................25µm/s

Line spacing: ........................................Zero

Numbers of lines:..................................25 lines

Fluence:................................................2.60 J/cm$^2$

---

### 3.2.5   Rat retinal sections preparation

The work described in this section was carried out at the UCL Institute of Ophthalmology under the supervision of Dr Imre Lengyel.

Rodent models replicate many features associated with pathological changes of the outer retina in AMD disease and can provide valuable information which can be transferred to human studies.[40]

10 months old female Long Evans rats received supplemented drinking water for a period of 8 months as follows: 1) normal lab water; 2) +10 mg/L zinc carbonate 3) +10 mg/L zinc carbonate and + 0.25 mg/L copper carbonate.  The Cu was added to avoid the influence of Zn induced Cu deficiency. The bottles were carefully labelled with the type of water (Zn supplemented or lab) and changed every 3 days.

Calculations were based on body weight. The dose of Zn was based upon the approximate supplementation levels equivalent to those given to human AMD patients in the Age-Related Eye Disease Study (AREDS 1) to examine how this treatment affects the condition. The rats were sacrificed at 18 months; the eye was stored in 4% PFA at 4°C for embedding and sectioning. The resin embedded sections were carefully dissected and trimmed into approximately 1 cm x 0.5 cm blocks. Samples were typically cryosectioned to approximately 10 µm thick and mounted on DI water washed microscopic slides (Fisher Scientific, UK) and stored in a cool place. All slides were cut to approximately 1.5 cm by 1.5 cm diameter to enable each slide to fit inside the laser cell chamber prior to analysis. A total of 41 retina sections were analysed; 27 of which were used for method development, two were excluded due to major tears in the section, whilst the remaining 12 were used for the imaging study.

### 3.2.6   Optimisation of initial test of rat retina imaging

The laser camera is not a microscope and limited by the camera's capabilities, so it provides pictures of relatively low resolution. In fact, high resolution pictures are probably needed and initially they were not available. Therefore, each section was marked and observed under the microscope (Swift Instruments International, US) and the microscope camera was used to capture a picture of the whole section of the retina

through the lens of the microscope. Several optimisation experiments were performed on the rat retinal sections which are summarized in the following points:

1- Before any experiment the glass microscopic slides were tested, followed by another attempt using superfrost ultra plus microscopic slide (Thermo Superfrost, Thermo Scientific, UK), plastic/glass cover slip and membrane.

2- Three selected slides were obtained from the UCL Institute of Ophthalmology to perform a preliminary test on the rat tissues. Section number 4.1 is a control slide, 9.3 slide was rat fed with Zn diet and for slide 14.1 the rat was on Zn and Cu diet. Initially, only Zn was measured in all slides. An example of the optimisation of the operation conditions on a small and large section is summarized in Table 3.3.

3- Another 12 slides were obtained from the same block to carry out further tests on the rat retinal tissue. In the slides where the rat was fed on Cu and Zn, both elements were measured. While determining two elements, some of the ICP method was slightly changed as a sample time of 0.002 s was used, which resulted in segment duration of 0.02 s. In this experiment, a bigger section was ablated to improve the laser images visualisation. Table 3.4 and Table 3.5 illustrate the slides description and numbers and general LA operation parameters, respectively.

4- The experimental tests were carried out for an additional 12 slides of a very thin section (less than 5µm) with the parameters of ~5 J cm$^{-2}$ laser fluence, 5 Hz repetition frequency, 55 µm spot size and 55 µm s$^{-1}$ scan speed, and zero spacing between ablated lines. As ablation requires a very long time, in this test the number of lines was decreased to 50 to enable ablation of 4 sections on the same day for more reliable comparison between non-fed and fed rat. In order to avoid signal intensity drop during lengthy analysis, the instrument was tuned before, after and between each section.

5- A brief test was performed and two sections of the retina were scanned. Almost the same previous operating parameters were used; however, the repetition frequency was increased to 10 Hz in order to provide a smooth signal.

**Table 3.3** Example of Laser instrument parameters for rat RPE sections 4.1, 9.3, and 14.1

| ESI UP-213 laser ablation parameters |
|---|
| Repetition frequency: .............................5 Hz |
| |
| **Small section:** |
| Laser energy:..........................................35% |
| Scan speed:.............................................25 µm/s |
| Spot size:................................................25 µm |
| Line spacing: .........................................Zero |
| Numbers of lines:...................................25 lines |
| Fluence:..................................................2.4 J/cm$^2$ |
| Line length ............................................475 µm |
| |
| **Large section:** |
| Laser energy:..........................................30% |
| Spot size:................................................55 µm |
| Scan speed:.............................................55 µm/s |
| Line spacing: .........................................Zero |
| Numbers of lines:...................................80 lines |
| Fluence:..................................................2.63 J/cm$^2$ |
| Line length ............................................1.00 mm |

**Table 3.4** Names and numbers of the rat retina slides

| Slide name | Slide number |
|---|---|
| Control | 2.1 |
| | 3.1 |
| | 4.1 |
| | 5.3 |
| Rat on Zn diet | 6.1 |
| | 7.1 |
| | 9.3 |
| | 10.2 |
| Rat on Zn and Cu diet | 11.3 |
| | 12.3 |
| | 14.1 |
| | 15.1 |

**Table 3.5** Laser instrument parameters for 12 slides of rat RPE sections

| ESI UP-213 laser ablation parameters |
| --- |

Repetition frequency: ..............................5 Hz

**For the 12 slides:**

Laser energy: ..........................................35%

Scan speed: ............................................55 µm/s

Spot size: ................................................55 µm

Line spacing: .........................................Zero

Range of lines: ......................................(70-101) lines

Range of Fluence: .................................(3.60-4.51) J/cm$^2$

Range of line length ..............................(0.866-2.29) mm

### 3.2.7 Recommended setup and final experiment for rat retina imaging

Final experiments were performed on 14 rat retina sections of which two samples were unsuccessful due to some unusual structures in the slides. Low laser energy was chosen in this experiment to prevent the laser from penetrating the glass slide and thus avoiding Zn signal interferences with the sample as discussed earlier. Table 3.6 summarizes the final laser instrument parameters for rat retina sections. Vertical adjacent lines were drawn throughout the section, covering the maximum y distance of the sample. The number of lines were varied according to the size of the section and consequently the line length is different for each section. As the feature of the retina is faded and difficult to focus on, the line was duplicated and refocused after every 10 lines to ensure total coverage of the sample in the x-axis with optimal focusing (see Figure 3.2, A). The spacing between each line was equal to zero as the energy level is low. Neural retina is a tissue with multiple concentric layers, the total thickness is around 192 µm[305], excluding the choroid and sclera, depending on the rat type. Representative cross-section of the neural rat retina and retinal pigment epithelium (RPE) showing normal morphology[305,306,307,308,309,310] and retinal layers with thickness are shown in Figure 3.2 (B).
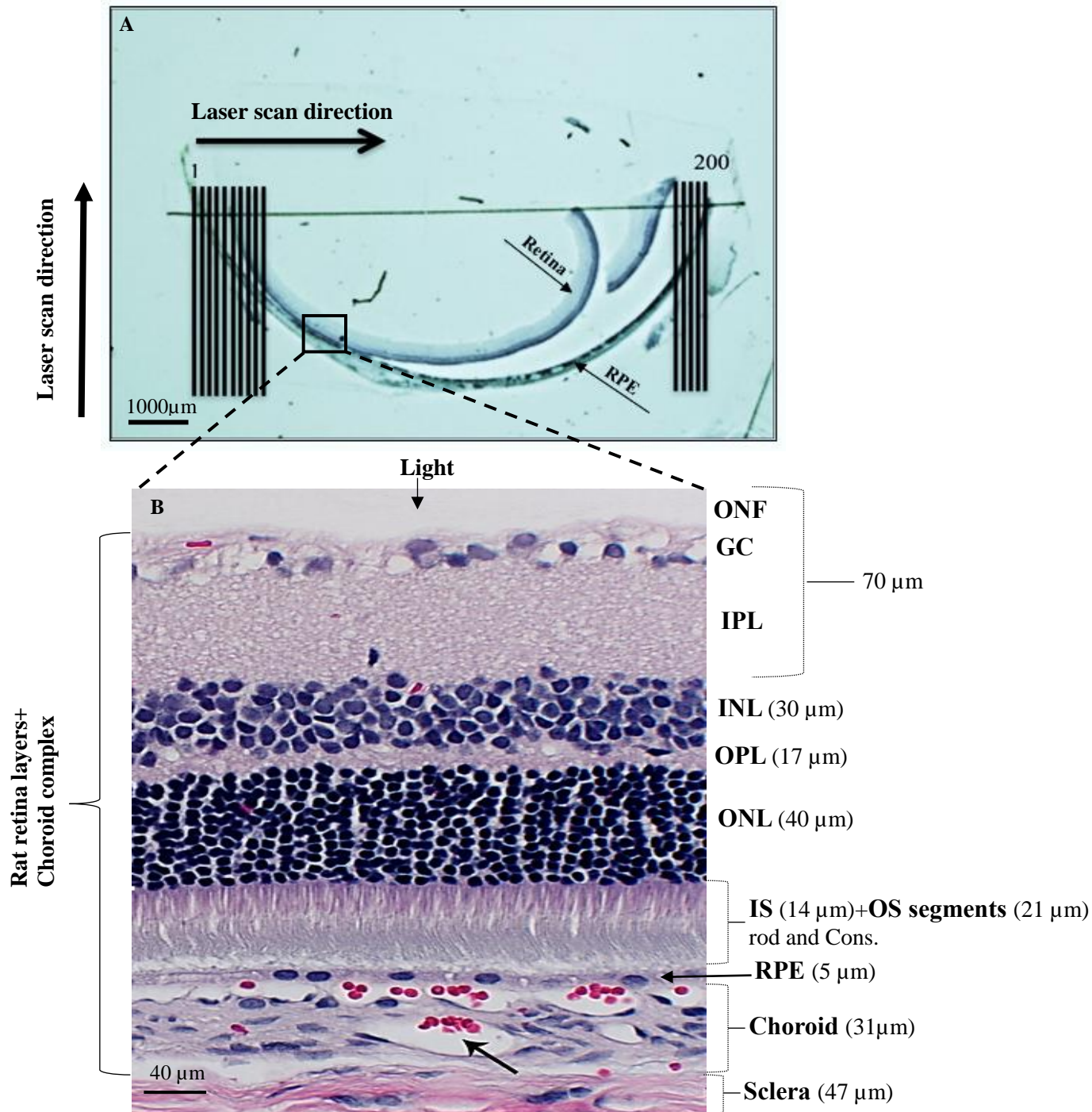
**Figure 3.2 (A)** Schematic representation of the laser scan direction during ablation and the position of RPE and retina in microscopical rat retina section (4×). **(B)** Histological section of normal rat retina (paraffin embedment, hematoxylin stain) showing the thickness of the rat cellular organization layers of the retina/RPE and choroid complex: Bruch's membrane (BM); retinal pigment epithelium (RPE); outer segment (OS); inner segment (IS) outer nuclear layer (ONL); outer plexiform layer (OPL) inner nuclear layer (INL); inner plexiform layer (IPL), ganglion cell layer (GC) and optic nerve fibre (ONF). Arrows (→) indicate blood vessels in the choroid. The micropscopic image **(A)** obtained from Dr Imre Lengyel, UCL Institute of Ophthalmology and Figure **(B)** reproduced with permission from S.J Fliesler et al., 2010, licenced by ©American Society for Biochemistry and Molecular Biology.[311]

**Table 3.6** Typical Laser instrument parameters for 12 rat retina sections and one human retina section

## ESI UP-213 laser ablation parameters

Repetition frequency ...............................10 Hz

Laser energy ..........................................30%

Scan speed.............................................25 µm/s

Spot size ...............................................25 µm

Line spacing ........................................Zero

Range of lines........................................(160-250) lines

Fluence:

6.1 (Zn diet)..........................................1.43 J/cm$^2$

4.1(control)...........................................1.17 J/cm$^2$

12.1(Zn& Cu diet)..................................1.44 J/cm$^2$

10.2 (Zn diet)........................................1.37 J/cm$^2$

5.3 (Control).........................................1.35 J/cm$^2$

11.3 (Zn& Cu diet)................................1.14 J/cm$^2$

3.1 (Control).........................................1.91 J/cm$^2$

9.3 (Zn diet)..........................................1.17 J/cm$^2$

2.1 (Control).........................................1.23 J/cm$^2$

7.1 (Zn diet)..........................................1.20 J/cm$^2$

15.1 (Zn& Cu diet)................................1.61 J/cm$^2$

14.1 (Zn& Cu diet)................................1.17 J/cm$^2$

Human retina ........................................1.26 J/cm$^2$

## 3.3  Results and discussion

### 3.3.1  Blank test and contamination

Zinc is a vital and ubiquitous element present in trace amounts in a large amount of routine lab equipment. Zinc contamination could increase from unpredicted sources; it is important that all parts and equipment used in the experimental analysis are tested for the possible presence of contaminants.[312] Since the glass microscope slides contained background levels of Zn, the laser fluence required careful optimisation to ensure complete ablation through the sections, whilst minimising penetration of the glass slide.

Sample gas was tested alone and the $Zn^{66}$ signal was relatively high. The gaseous interferences involved in the ablation could lead to broadening of the signal generated when the analyte is transported through the tube. It has been reported that using helium as a carrier decreases the peak width, as does minimizing the ablation cell volume and the length and diameter of the transfer tube.[313]

Several blank tests were performed on different microscopic slides to check the level of Zn content in the glass. Two different laser patterns were chosen to scan the blank slide: either applying lines (spot size 15 μm, repetition frequency 5 Hz) or drilling down using 50 shots on the same area, repetition frequency 1 Hz and spot size 15 μm. The laser energy was set up on 60% in both cases. A clean/blank microscopic glass slide was ablated and showed that the slide itself contains unexpectedly high level of Zn due to its presence in nature. Figure 3.3 illustrates the signal intensity of Zn in the ablated glass slide with 60% energy.  Accordingly, to minimise ablation of the glass, the energy has been reduced and tested at 50%, 40%, 30% and 25%.
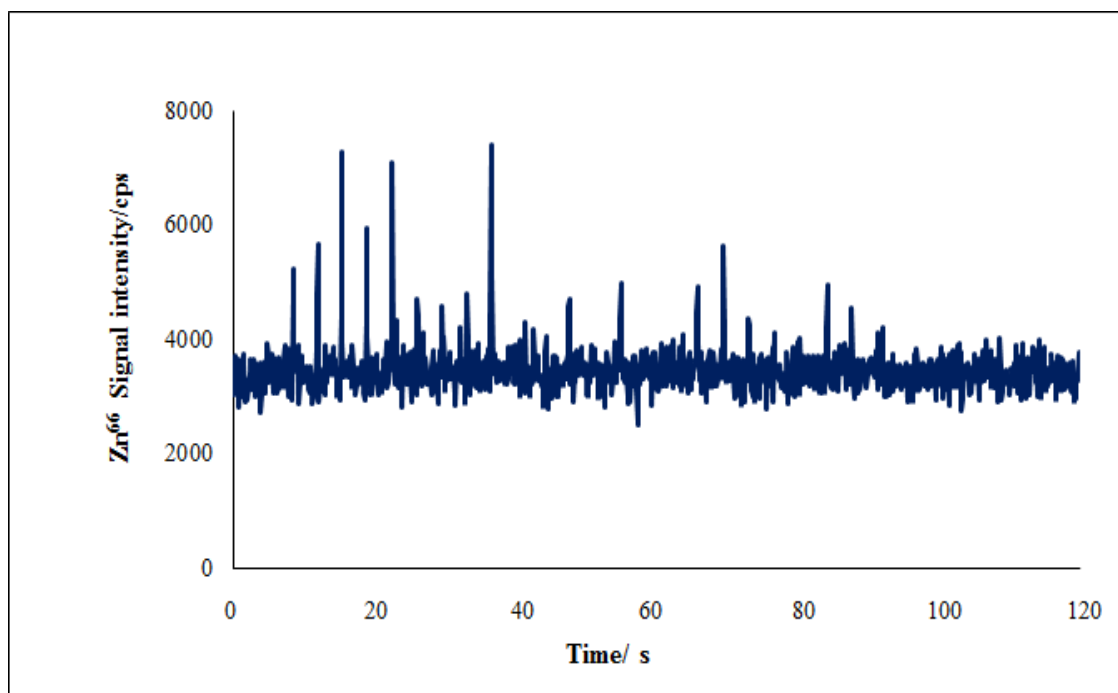
**Figure 3.3** An example of time- resolved peaks showing Zn[66] signal intensity of the blank glass slide at laser energy of 60%.

Attempts were carried out on alternative material slides including: superfrost ultra plus microscopic slide, glass coverslip, plastic sheet slides and Millicell membrane to find an appropriate slide that contained less Zn. It was very difficult to focus on the plastic sheet slide and white membrane. Due to their low thickness, these were fixed to a glass slide using double sided sellotape to prevent them from moving during ablation.

The signal intensity of Zn ranged between 2000-3000 cps for the different ablation energy and that indicated either low background or, more likely, that limited ablation of the slide had occurred due to the focussing issues described above. The glass cover slip produced similar results to a glass microscope slide, whereas, the superfrost ultra plus microscopic slide resulted in by far the highest signal intensity, reaching up to $2\times10^{-6}$ cps. Overall, the signal intensity in all glass slides was decreased by decreasing the laser energy. Besides these slides, PTFE/ Teflon coated microscope slides or Zn free slides were tried but they were costly.

Another solution to minimise ablation of a microscopic glass slide is to mount a coating on the slide to act as a barrier between the sample and the glass. A clear nail polish (Miss Beauty No.1) which is available commercially was used by Craig[314] as it is hardwearing and adheres strongly to most surfaces.  It was noted that Zn is not present in the content

of the nail polish used. In addition, it was postulated that the nail polish layer coating would potentially prevent the laser from ablating through the glass even at full power (Sejal Odedra, MSc research project, Loughborough University, 2015).

The blank results were sent to UCL Institute of Ophthalmology to enable the tissues to be mounted on the most appropriate slide. However, it was agreed to use normal microscopic slide washed by deionized water as long as the Zn signal was differentiated between the resin used to embed the sections and the retina. After cutting the slide, a compressed air duster can be sprayed on the surface of the slide before analysis to remove any dust or contamination.

### 3.3.2    Optimisation of drusen test

Several age-related disorders of the central nervous system are characterized by extracellular protein accumulation and deposition, frequently interfered by metals such as Zn, Ca, Fe and Cu.[315] These metals which become trapped within Bruch's Membrane (BM) affect its structure and function with adverse consequences such as oxidative stress and inflammation.[40] Although Ca, Fe and Cu have been implicated as leading causes of AMD pathology, the concentration and distribution of these metals in sub-RPE deposits was not known.[315] Drusen aggregation appears naturally with age and is able to push into the neural retina after distorting and disrupting through the RPE.[316] The composition of sub-RPE deposits is very complex as they contain abundant amounts of proteins and lipids in addition to unusual and high concentrations of Zn.[317] This is suggested to trigger the oligomerization of proteins with Zn and is directly implicated in the formation and accumulation of drusen and thus likely to be a crucial factor in AMD pathogenesis. In 2014, Lengyel and Flin et al.[315] determined the concentration of Ca, Cu and Fe and compared these with Zn in sub-RPE deposits from an 86-year-old donor eye with diagnosis of early AMD. They found that Zn and Ca regularly existed in all deposits but reached the highest concentration in soft drusen.[315]

Seven human retinal sections obtained from the elderly donor showed deposits in the macula, and the microscopic images were obtained from UCL Institute of Ophthalmology as illustrated in Figure 3.4. Attempts to scan two sections were not successful due to instrumentation issues. Adjacent line scans were performed initially over  a 475 µm × 630 µm area of the slide using LA-ICP-MS to analyse the general distribution of Zn and

Zn/Cu in drusen in a small section of the RPE tissue as shown in Figure 3.5 and Figure 3.6 respectively. These clearly show regions of high Zn intensity, which seem to correlate to features in the microscope image. In addition, a difference in signal intensity between the tissue itself and the blank slide is also shown. Figure 3.6 shows dual analysis of Cu and Zn, however, the image does not appear as high in intensity as Figure 3.5. The reason is that the instrument used for this analysis is not designed to allow simultaneous multi-element detection. Thus, the instrument switched rapidly between measurement of the two different elements (in a few ms), but certainly this switch means less time is spent measuring each element, and this resulted in missing a key feature in the Zn signal, whilst measuring Cu.
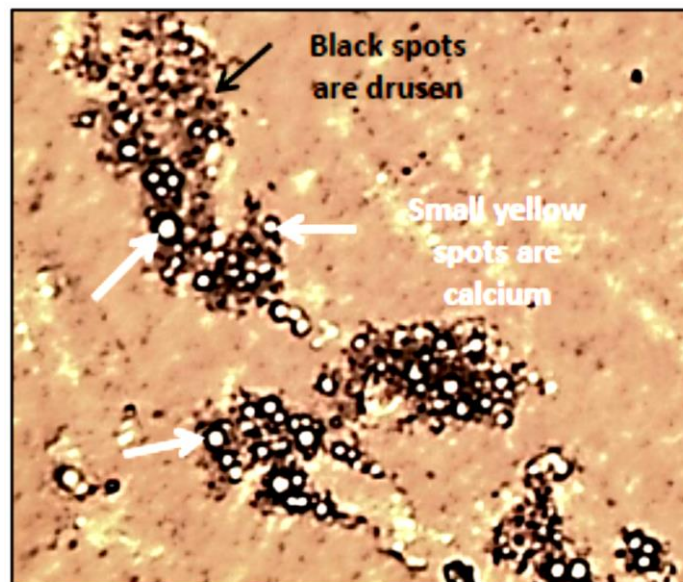


**Figure 3.4** Microscopic image of 40× magnification of human retinal section (obtained from Dr Imre Lengyel, UCL Institute of Ophthalmology). The black deposits are drusen and the small yellow spots inside the drusen are calcium deposits.
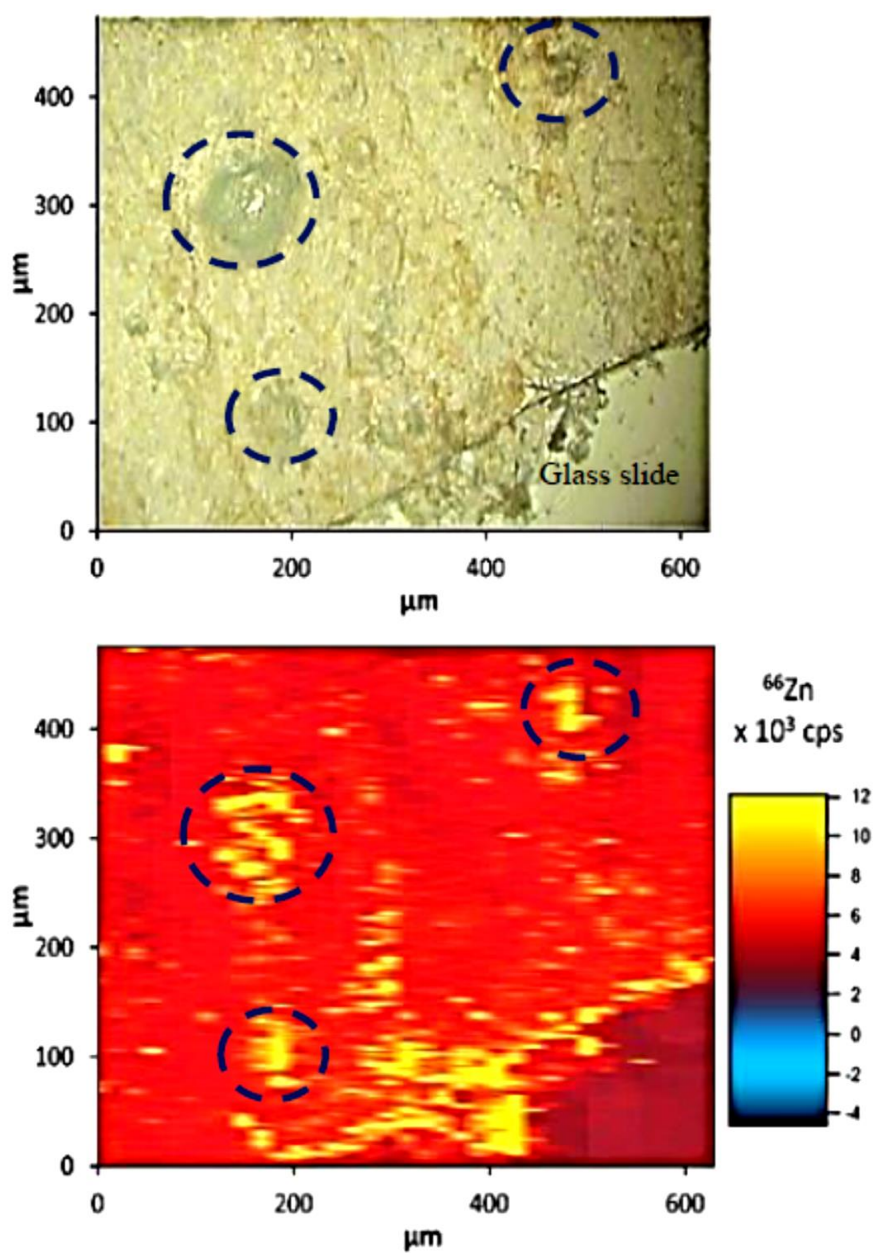
**Figure 3.5** Top: microscopic image of a $475 \times 630$ µm section underside of human retina tissue (D1), obtained using the built-in microscope on the UP-213 laser ablation system. Bottom: LA-ICP-MS image of the same section, showing the distribution of Zn in drusen. Complete laser parameters are given in Table 3.2. The edge of the section seems be contaminated as it contains a high level of Zn.(possibly from the glass cutter used to cut the slide)
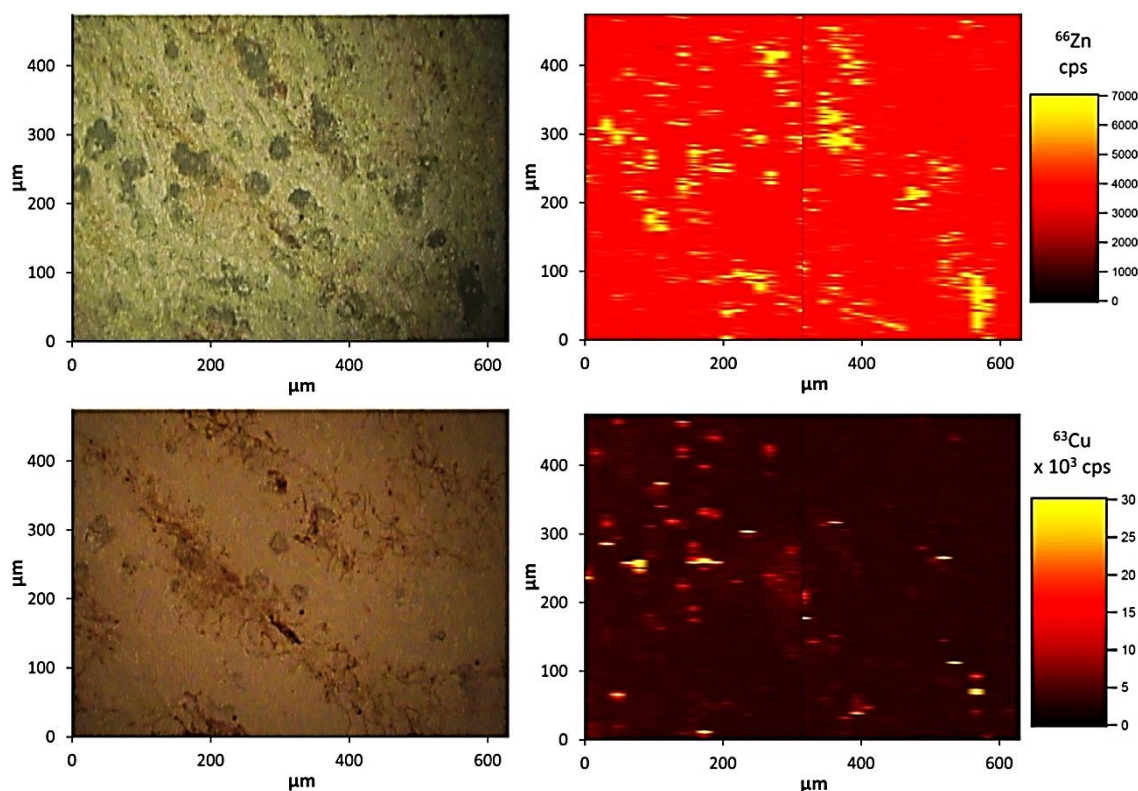
**Figure 3.6** Left: microscopic images of a $475 \times 630$ µm section of underside of human retina tissue (D3) obtained using the built-in microscope on the UP-213 laser ablation system. Right: LA-ICP-MS images of the same section, showing the distribution of Zn (top) and Cu (bottom) in drusen. Complete laser parameters are given in Table 3.2.

As mentioned earlier, Ca is highly enriched in drusen in addition to Zn.[315] It had been expected to find Ca in sub-RPE deposits, as calcification had been reported in relation to aging and AMD[318, 319] and calcium is the most abundant metal in the cornea followed by Zn.[320]

Further tests were performed on the human RPE sections that contain drusen. The following Figures illustrate the distribution of Ca in (Figure 3.7) and Zn in (Figure 3.8) in a small section of the underside of the RPE tissue. As can be seen from section D4, the regions show a high Ca intensity, which seem to correlate to features in the microscope image. 25 lines were not enough for scanning throughout the section to create a good image, and that led to pixelated images. Section D4 is lower in resolution than section D3. Owing to the lack of human retinal sections, the test was directed to rat retinal imaging instead of drusen test as discussed in the sections below. In general, it is important to commence similar studies on isolated sub-RPE deposits from donor eyes of varied ethnic background.
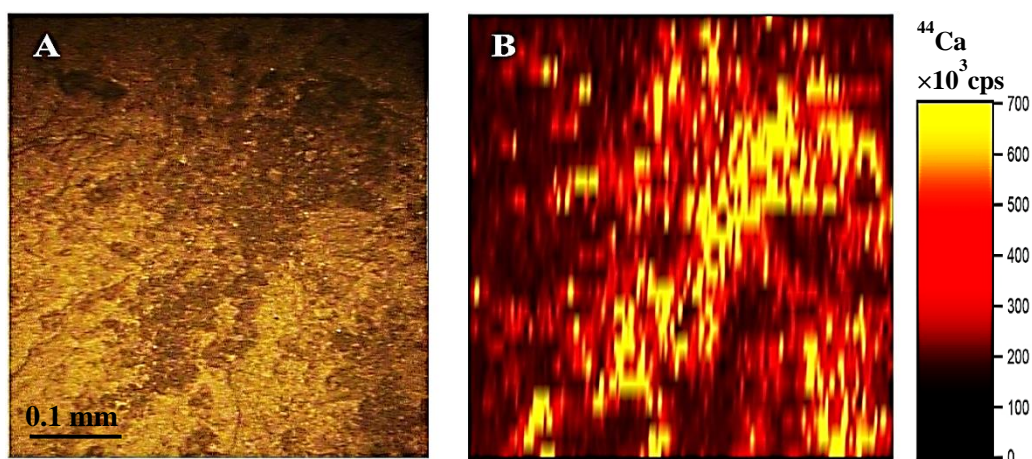
**Figure 3.7** (A) Microscopic image of a 475 × 625µm section of underside of human retina tissue (D4), obtained using the built-in microscope on the UP-213 laser ablation system. (B) LA-ICP-MS image of the same section, showing the distribution of calcium in drusen. Complete laser parameters are given in Table 3.2.
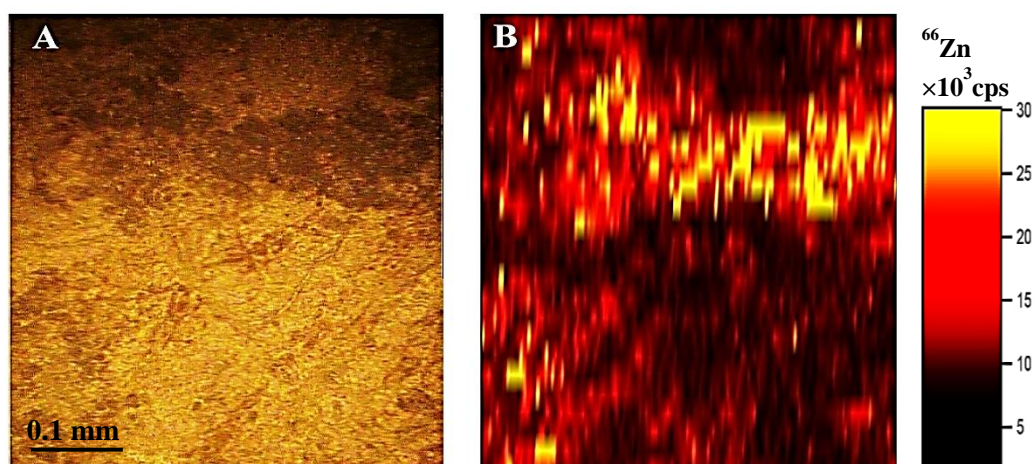


**Figure 3.8** (A) Microscopic image of a 475 × 625µm section of underside of human retina tissue (D6) obtained using the built-in microscope on the UP-213 laser ablation system. (B) LA-ICP-MS images of the same section, showing the distribution of Zn in drusen. Complete laser parameters are given in Table 3.2.

### 3.3.3　Optimisation of small and large rat retina sections

Several tests were carried out on small and large rat retina sections. In the small sections, 25 lines were scanned with 25 µm spot size; however, the section was blurry and did not exhibit clarity and good quality. Furthermore, such small sections are not necessarily representative of the entire tissue.  Therefore, an additional 80 lines were scanned over 4.4 mm × 1.0mm area of the slide. Figure 3.9 and  Figure 3.10 illustrate an example of small and large rat retina imaging (the microscopic images were supplied by UCL Institute of Ophthalmology). In the large imaging section, the contrast between certain sections and the surrounding retina tissue can be observed, and it also appeared clearer than the small one.   As the initial experiments showed promising results, further investigations were carried out on a large scale.
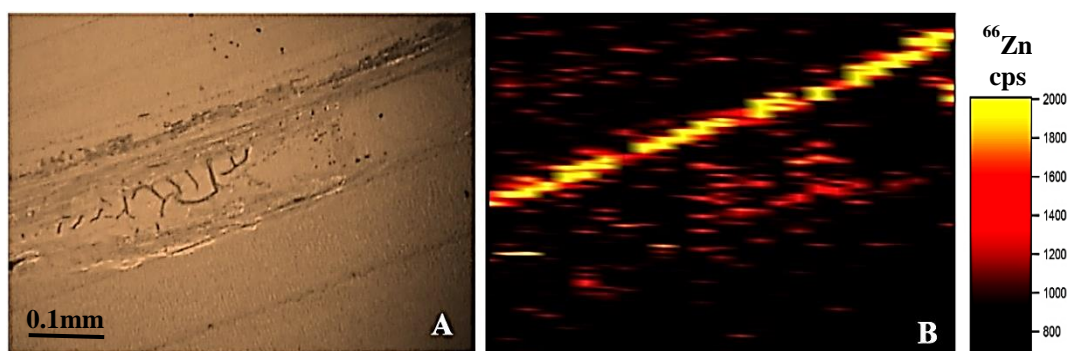


**Figure 3.9** (A) Microscopic image of a $475 \times 625 \mu m$ section of rat retina tissue, obtained using the built- in microscope on the UP-213 laser ablation system. (B) LA-ICP-MS images of the same section, showing the distribution of Zn. The rat was on Zn diet. Complete laser parameters are given in Table 3.3.
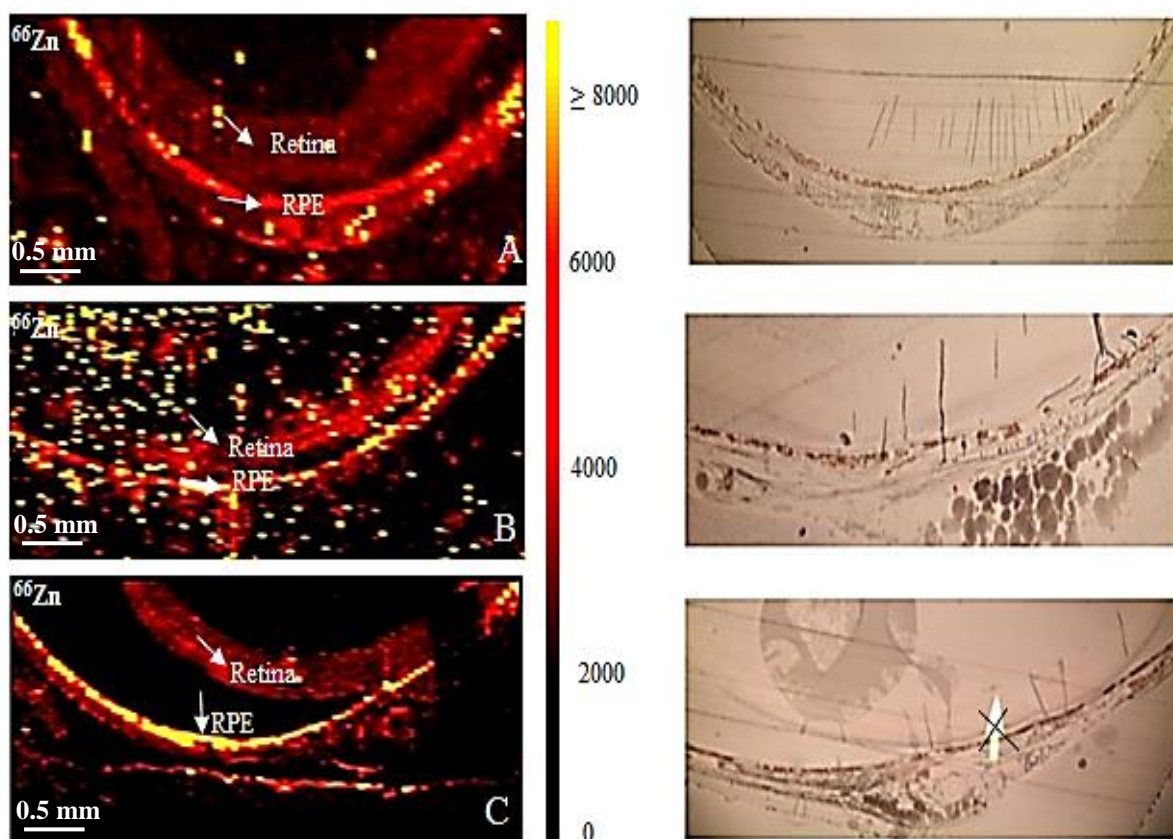
**Figure 3.10** Right: Microscopic image of 5× magnifications of a section of rat retina tissue (obtained from Dr Imre Lengyel, UCL Institute of Ophthalmology). left: LA-ICP-MS image showing the distribution of Zn. (A) Control (B) Rat on Zn diet and (C) Rat on Zn & Cu diet. The yellow spots in images A&B were dust contamination that contain high level of Zn. The colour scale depicts the signal intensity in counts per second (cps). Complete laser parameters are given in Table 3.3.

### 3.3.4 Second optimisation test and data processing

12 slides were scanned in large retina sections and the levels of Zn and Cu were measured. Some of the images were successfully constructed but others showed very low quality. Figure 3.11 shows an example of successful laser image results. The resin did not cover the whole slide, thus the scan ablated the glass slide and both edges gave a high Zn signal. Different issues were encountered during the recording of these images, in particular: a bug in the software which prevented the generation of FIN2 files, the RF generator suddenly switching off after the full scan, some high oxide ratios and difficulty of focusing on such thin and unclear features of the retinal section. As the laser techniques will damage the sample to an extent and some sections did not generate data due to these issues, the comparisons between the sections could not be completed, and ablation of new retinal sections was required.
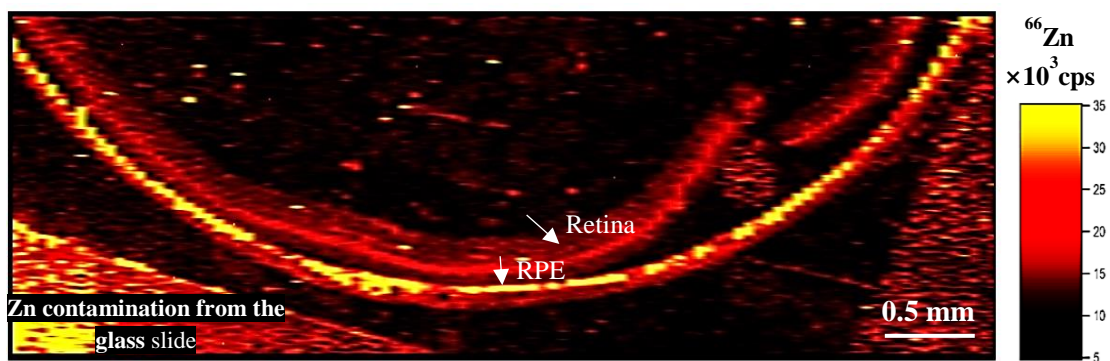
**Figure 3.11** An example of LA-ICP-MS image of a 1.8×5.6 mm section of retina tissue from a rat on a Zn diet (6.1) , showing the distribution of Zn.The colour scale describes the signal intensity in counts per second (cps). Complete laser parameters are given in Table 3.5.

### 3.3.5   Third optimisation test

12 sections were scanned, and in this experiment 4 sections were run on the same day for more reliable comparison between supplemented and non-supplemented rat. As can be seen in Figure 3.12 both Zn and Cu were mapped in control section and Zn & Cu supplemented rat section. In addition, Zn was measured in the section where the rat was on Zn diet and control. The signal intensity of the Cu is very low and can almost be discounted; whereas the Zn signal is higher. The tear-drop shaped ablation cell used for the analysis has previously been reported to produce peak widths of less than a second for a single laser shot.[304] Single detector sector-field instruments, such as the one used in this study, are not ideal for multi-element analysis of such transient signals due to the slow and sequential rate at which they detect each isotope. In other words, whilst the instrument was measuring Zn, data for Cu was not acquired (and vice-versa).

The retinas in some sections were missing, as the series of adjacent line scans were not long enough to cover the detached retina. This is because the feature of the retina was not clear while drawing the lines due to the relatively low resolution image and low resolution of LA camera especially if the retina was detached from the RPE. The system was re-tuned between each section and signal intensities of Th and U were monitored. The signal variation of Th and U between each section ranged between (14%-4%) and (10%-7%), respectively.

The preliminary data processing was to select data from one-line scan per image and represent that in a graph as illustrated in Figure 3.13 (control). The first peak shows the retina and the second shows the RPE. To compare the signal intensity of both peaks between control and test sample would be inaccurate, however, using the relative ratios between retina and RPE enables comparison between different sections. The data were selected from each peak and manually summed. In the control section, the sum of the signal intensity of the retina, resin and RPE are $1.63E^{+05}$, $3.04E^{+05}$ and $3.02E^{+05}$. The ratio of the RPE/Retina is 1.86 and RPE/resin 1.00 and retina/resin 0.54. In the other Zn supplemented rat section, the ratio of the RPE/Retina is 1.16.

Repeating the retina imaging was required for reliable comparison. The present data was based on only one line, which is not representative of the whole section. Therefore, subsequent improvements include the following: Scanning various numbers of lines throughout the section, drawing a long line in a large section to cover the RPE and the retina in the imaging especially if they are detached. Cu showed very low signal and switching swiftly between two elements led to reduction in analysis time and thus signal intensity. Therefore, the focus was switched to Zn alone for the imaging study.

The test was performed on retinal sections with 10 Hz repetition frequency to provide a smooth signal. As fewer lines were scanned, a blurred image was generated. Large ablation section with 10 Hz repetition rate will be used in the final experiment.
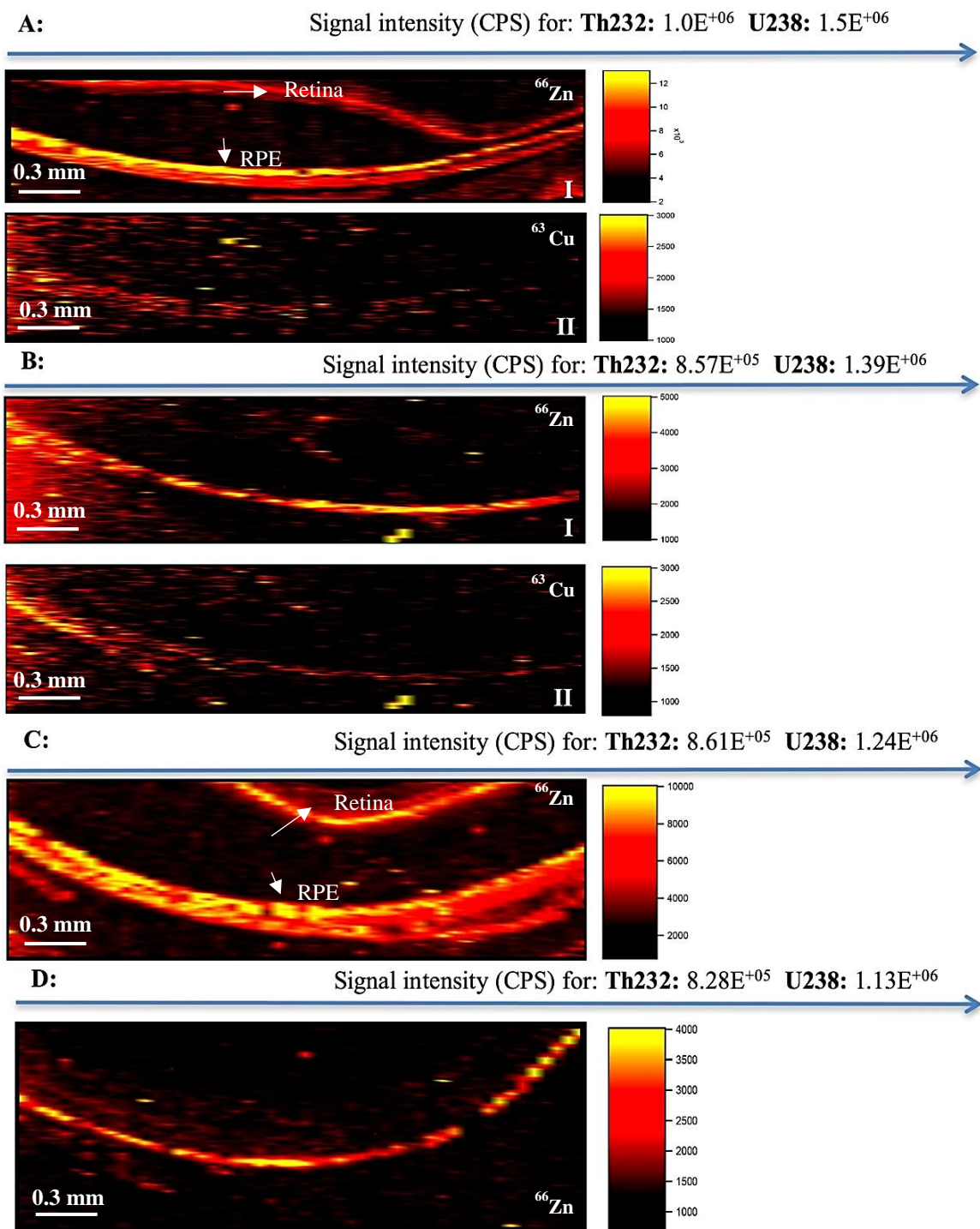
**Figure 3.12** Example of 4 LA-ICP-MS rat retina images recorded on the same day, with the signal intensity of Th & U on NIST glass between each section. **A-** LA-ICP-MS image of a 2.8×0.866 mm section of rat retina tissue, showing the distribution of Zn (I) and Cu (II) in control slide (5.3). **B-** LA-ICP-MS image of a 2.8×1.05 mm section of rat retina tissue, showing the distribution of Zn(I) and Cu (II), the rat was on Zn& Cu diet (14.1). **C-** LA-ICP-MS image of a 2.8× 0.838 mm section of rat retina tissue, showing the distribution of Zn in control slide (5.3). **D-** LA-ICP-MS image of a 2.8×0.895 mm section of rat retina tissue, showing the distribution of Zn. The rat was on Zn diet (10.2). The colour scale depicts the signal intensity in counts per second (cps). Complete laser parameters are summarised in Table 3.5.
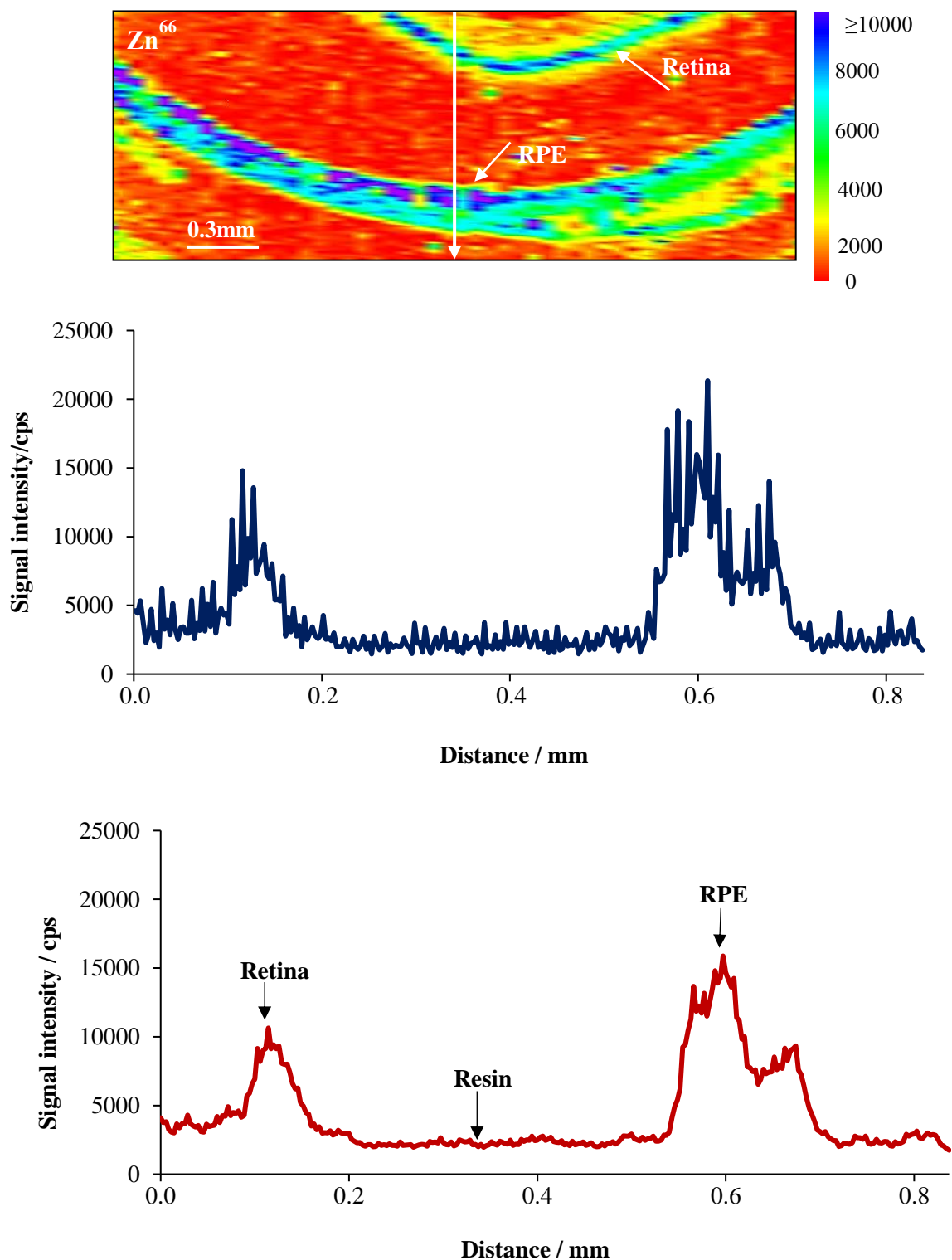
**Figure 3.13** LA-ICP-MS imaging of a section of retina tissue (control sample). Top panel: LA-ICP-MS image of the 2.8 x 0.84 mm section showing the distribution of $Zn^{66}$ (signal intensity, cps). Middle panel: the raw signal intensity for one line of the above image (arrow indicates location and scan direction). Bottom panel: Smoothing of the above data using a 5 point moving average. The colour scale depicts the signal intensity in counts per second (cps).

### 3.3.6 Final and recommended procedure for rat retina sections

It is a challenging task to determine small features in specific areas in the eye that remain biologically relevant but need to be large enough to allow the elements to be detected.

The choice of colour scheme used to provide an accurate representation of the data can have a powerful influence on the apparent structure presented within the data. A colour scheme is a series of colours that are presented in a certain colour space with corresponding values. This can allow each value within the data to be replaced or mapped effectively with its allocated colour for display. A grayscale is the most common, simplest and cheapest colour scheme available for publication. However, the limitation of this is the ability of the human eye to distinguish between colours, which is influenced by brightness of surrounding regions, and that effect is known as simultaneous contrast. Therefore, adding colours is beneficial because it raises the dynamic range of a colour pattern.[303,321] Although Rainbow colour scheme (represented in Figure 3.13 as an example) is by far the most popular and frequently used in scientific visualisation (appearing in 48 of the articles on MS imaging examined by Bunch and colleagues), they could result in a significantly misleading representation of the data.[303] While there is no preferable single colour scheme that should be used, human perception of colours should be taken into consideration and avoiding a large number of objects is also recommended as it may have an adverse impact on data representation.[303] A black-red-yellow colour scheme with 5 colour gradients was applied for this data set. Studies have shown that people intuitively identify red and yellow colours as high values[322], thus this colour scheme presented a clear contrast of high intensity features against the dark, low signal intensity background.

Twelve rat retina sections were successfully imaged to determine and compare the distribution of Zn in the retina and the RPE. High resolution images are extremely important for clear visualization as well as for matching anatomical features. Thus, these were acquired from UCL Institute of Ophthalmology to enable correlation between features in the LA images and the microscopic pictures. An example of 3 different microscopic and LA-ICP-MS images are shown in Figure 3.14 , Figure 3.15 and Figure 3.16 showing the qualitative Zn distribution in control slide (2.1), Rat on Zn diet (7.1) and rat on Zn and Cu diet (15.1), respectively. The remaining images are presented in chapter 8 (appendix 3). The microscopic images are not always identical with the LA-

ICP-MS image as they are two different sections. The purpose of the stained image is to represent the features of the retina clearly and the non-stained sections were ablated to avoid the contamination of Zn during staining. Therefore, a slight difference will be noticed due to the different sectioning. Comparison of the anatomical details in the visible microscopic images of the rat sections with the Zn distribution in the ICP-MS images shows good correlation, illustrating the usefulness of LA-ICP-MS in the characterisation of the metalloprotein distribution within the structure shown.

As can be inferred from the rat retina images (Figure 3.14-3.16 and remaining images in the appendix) there is no specific and consistent pattern that all control and fed rat sections follow. However, preferential accumulation of Zn in the RPE, compared to the retina, was clearly observed for all sections analysed. An apparent narrowing of the Zn distribution in the RPE in the Zn fed rats was observed. The layers of the retina are not very clear because of the reduction of the signal and that will be discussed in the future work.

The laser energy was chosen to be 30% and the ablation was achieved on a large section (exact dimensions are described in Figure 3.14, Figure 3.15 and Figure 3.16). At this energy level, the top of the slide surface effectively has just been skimmed without ablating the glass (slight visible ablation craters seen). This led to a noticeable difference in signal between the samples and the blank areas surrounding the samples. The concern of ablation of a large section is the lengthy acquisition time. Various generations of mass spectrometers especially sector-field instruments were not designed to accomplish short duration signals.[323] For instance, imaging Zn only across a 6×2.5 mm tissue section with a spot size of 25 µm might take up to 8-10 hours. Therefore, only two sections could be run per day. Other researchers have recently developed improvements to increase the speed of the analysis, through design of fast-washout LA instrumentation.[324] To evaluate the instrument drift, 3 lines were scanned on NIST glass before and after each sample. The intra-day response was approximately 10% variation, while the inter-day variation showed around 12%.
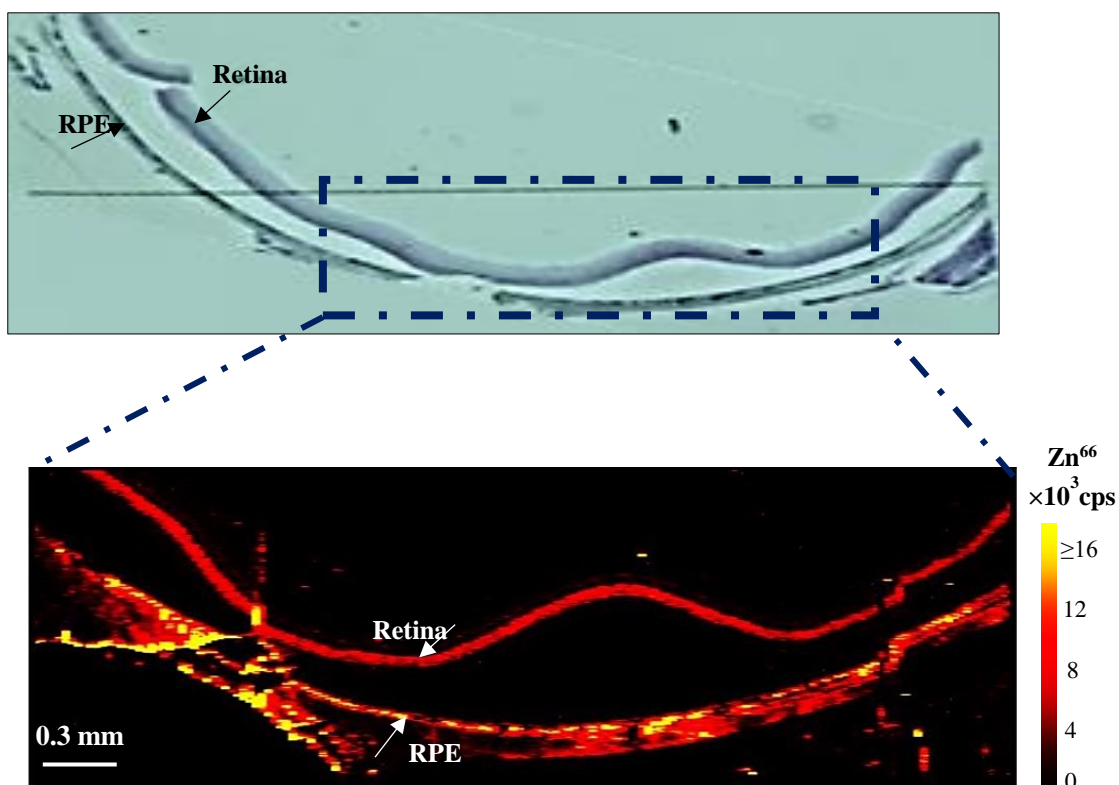
**Figure 3.14** High resolution imaging of a section of rat retina tissue. Top: Microscopic image of a 4.0×1.3 mm section of rat retina tissue (obtained from Dr Imre Lengyel, UCL Institute of Ophthalmology). Bottom: corresponding LA-ICP-MS image showing the distribution of Zn in control slide (2.1). The colour scale depicts the signal intensity in counts per second (cps). Complete laser parameters are given in Table 3.6.
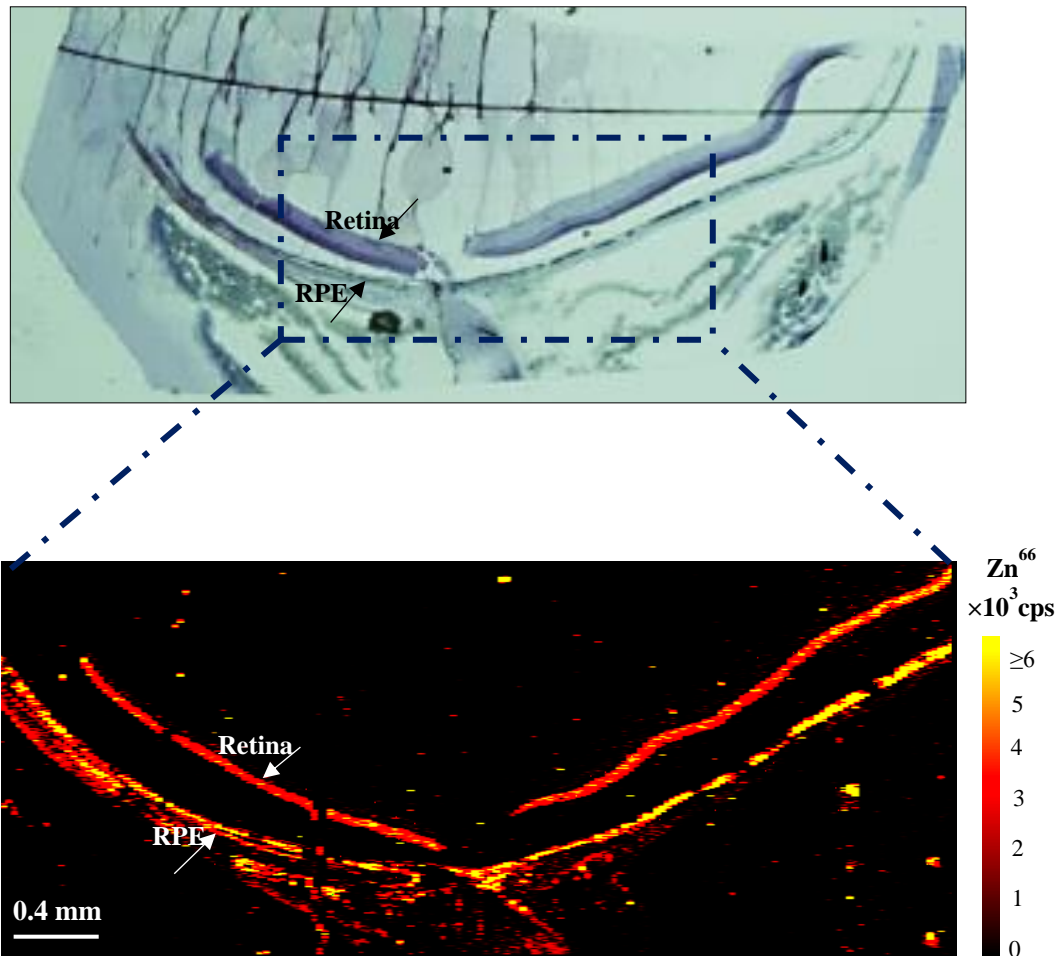
**Figure 3.15** High resolution imaging of a section of rat retina tissue. Top: Microscopic image of a 4.50×1.88 mm section of rat retina tissue, (obtained from Dr Imre Lengyel, UCL Institute of Ophthalmology). Bottom: corresponding LA-ICP-MS image showing the distribution of Zn in rat on Zn diet (slide 7.1). The colour scale depicts the signal intensity in counts per second (cps). Complete laser parameters are given in Table 3.6.
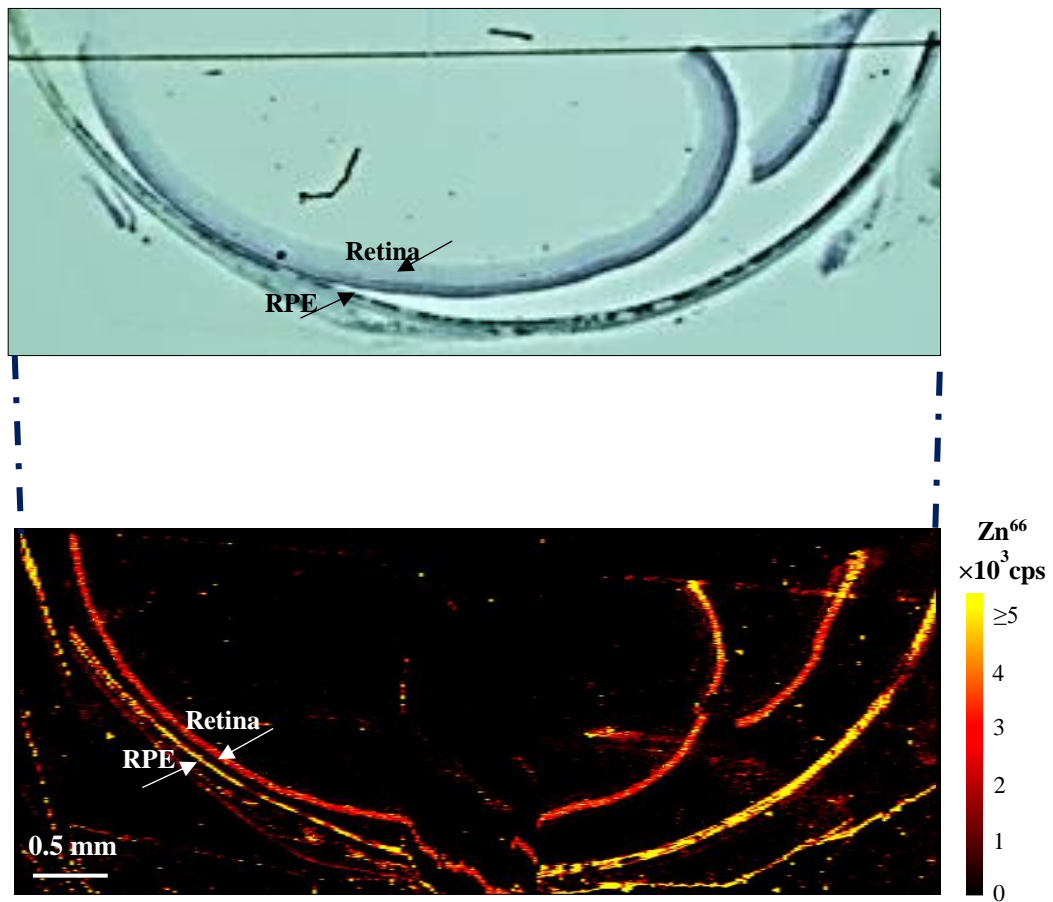
**Figure 3.16** High resolution imaging of a section of rat retina tissue. Top: Microscopic image of a 6.25 ×2.52 mm section of rat retina tissue, (obtained from Dr Imre Lengyel, UCL Institute of Ophthalmology). Bottom: corresponding LA-ICP-MS image showing the distribution of Zn in rat on Zn & Cu diet (slide 14.1). The colour scale depicts the signal intensity in counts per second (cps). Complete laser parameters are given in Table 3.6.

### 3.3.7 Final data processing

As discussed earlier, the aim of the current work was to achieve a reliable comparison between the retina and RPE within each section in order to identify changes in the distribution of Zn between rats receiving supplementation versus those in the control group. In order to compensate for any intra and inter-day variation in instrumental sensitivity, relative ratio of the peak area has been applied instead of absolute signal for reliable comparisons. Twenty ablated lines were randomly selected from each section for data processing. The data files acquired in each experiment represented the signal intensity in (FIN2) format. Initially, the raw data produced from each scanned line was plotted and the areas of RPE and retina were selected manually by selecting visually the start and end of each peak, then calculating the sum of the signals between these points. This time-consuming method was found to introduce variance depending on how the start and end points of each region were manually defined. Subsequently, this method was replaced by a Macro programme, which generated laser images. The corresponding area of RPE/Retina was selected to produce the time plot and calculate the sum. However, this procedure was still not practical, as it produced poor images and was time consuming. Various attempts have been applied on IGOR pro software, by drawing a square manually on each produced peak and then the software generates a report with peak area results. Clearly this procedure was not satisfactory as the results produced may vary depending on how the peak was manually defined. Finally, easy and fast data analysis was performed by using Multi Peak Fitting 2 package in IGOR Pro (Wavemetrics, USA). IGOR Pro's Multipeak Fitting package was employed to enable automated identification of the retina and RPE and to obtain the integrated signal areas for these features. A Gaussian fit was found to be optimal for modelling all the features identified. A typical workflow for processing the recorded data into a suitable format for image operation programs is represented in Figure 3.17 and the key for the Figure described in Table 3.7. Figure 3.18, Figure 3.19 and Figure 3.20 illustrate examples of the fitted data from one-line scan per image and demonstrate how Gaussian peaks can be fitted to the data to obtain the integrated signal areas for the retina and the RPE. The baseline noise was subtracted from all data. The peak area of RPE and retina were selected for individual line and then the relative ratio of RPE/retina was applied for the 20 lines per section.
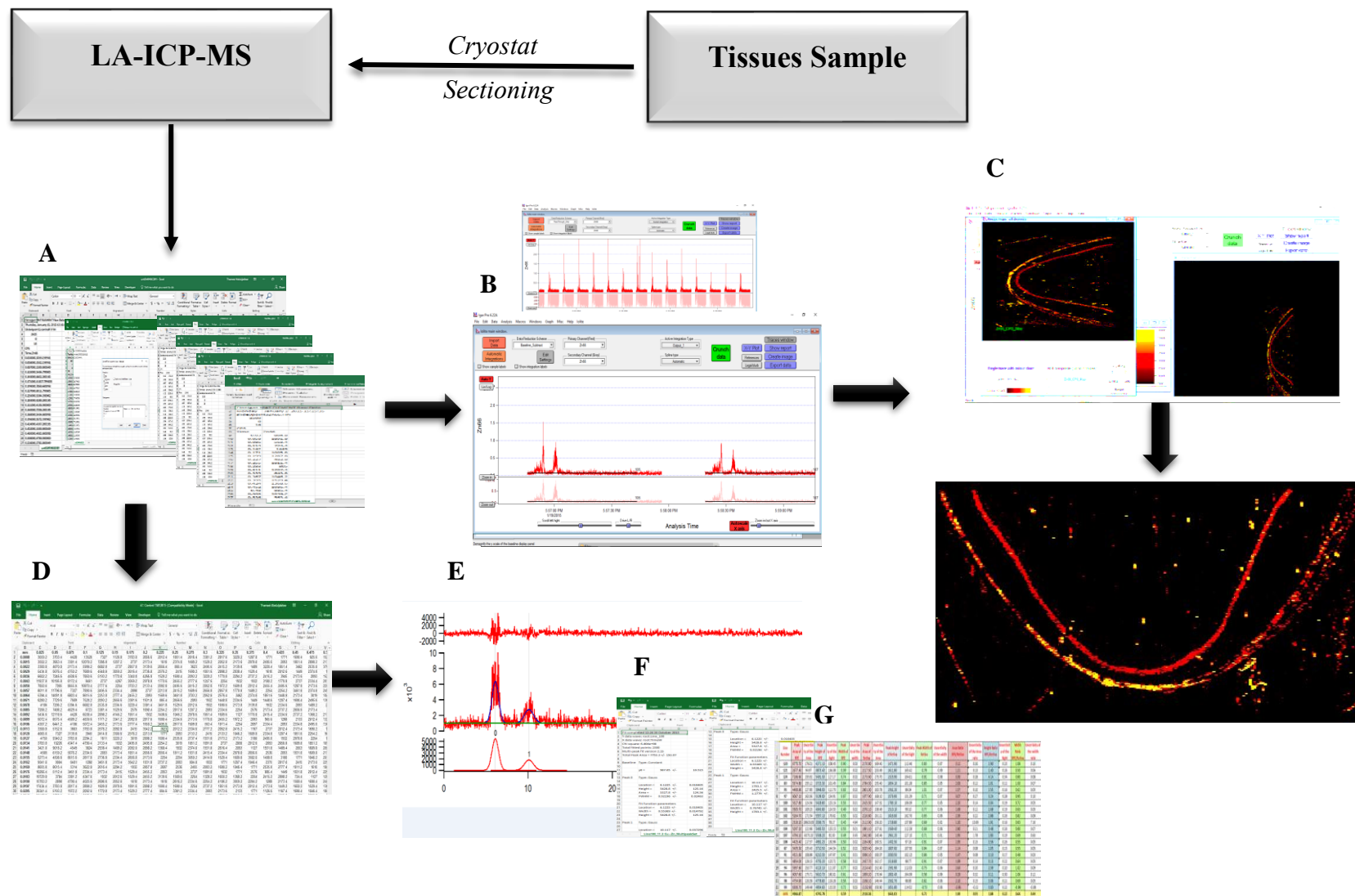
**Figure 3.17** Typical workflow for imaging by LA-ICP-MS and data processing. the key for the Figure described in Table 3.7.

**Table 3.7** Key for Figure 3.17 explaining data processing steps

| | |
|---|---|
| **Images workflow** | |
| **A** | Each single line of ablation produced individual data file (a comma separated value (.csv) file format), containing the signal intensity (CPS) data per unit point of time. |
| **B** | The folders of data of each experiment (eg. 200 lines) were uploaded into IGOR Pro programme and generated 200 time-resolved peaks. |
| **C** | Then the data was processed and the images were created |
| **Gaussian workflow** | |
| **D** | Each data file (A) generated from each line were combined into one Excel sheet, using the app (LA-ICP-MS RDP v0.17, Reid-IT Limited, Loughborough UK) |
| **E** | The combined Excel spread sheet was uploaded into Iolite add-on to calculate Gaussian peak of selected lines |
| **F** | Each Gaussian peak produced spread sheet of the average of the peak area, height and width |
| **G** | All spread sheets for the 20 line/ per experiment were combined for final calculation in one spread sheet using the app (LA-ICP-MS RDP v0.17, Reid-IT Limited, Loughborough UK) |
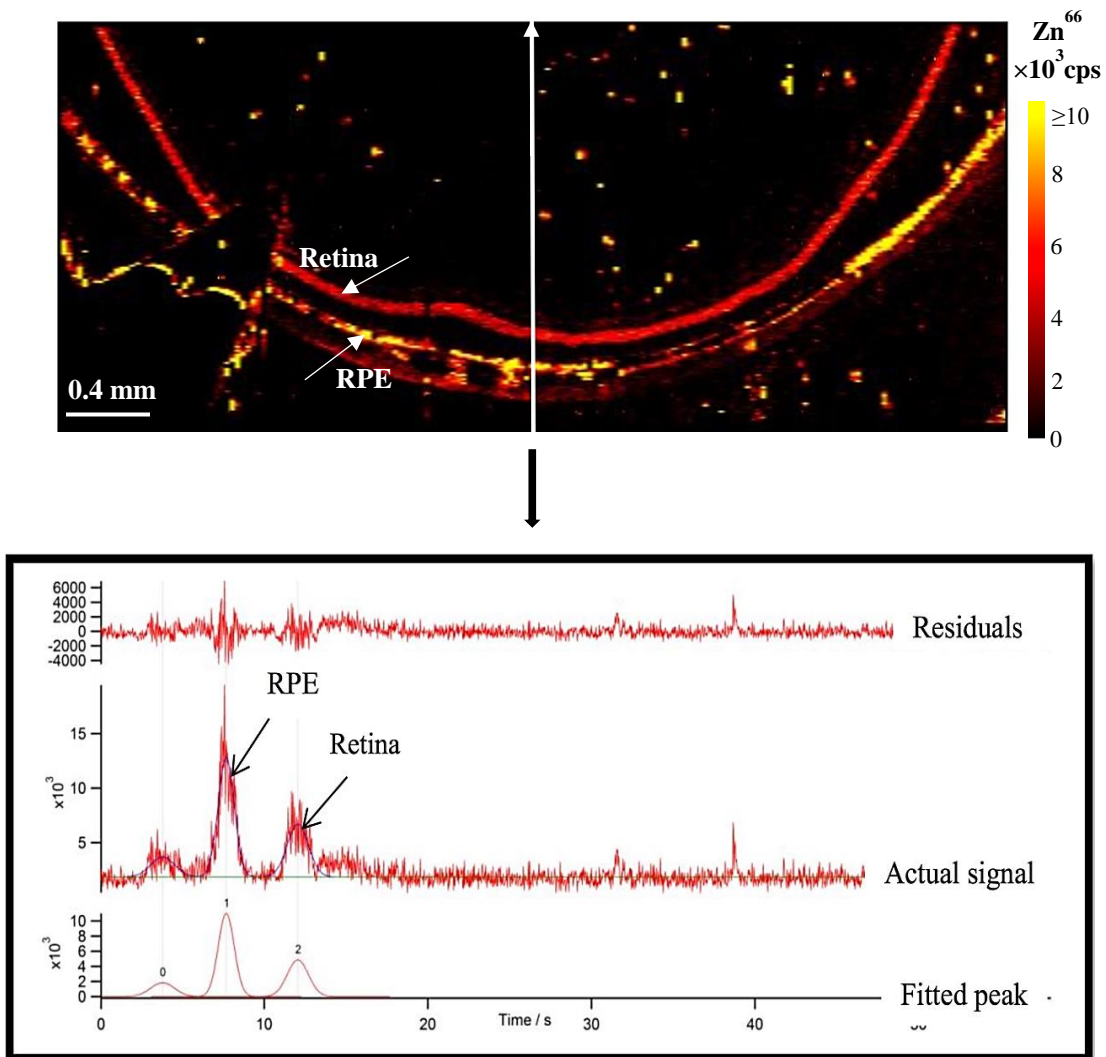
**Figure 3.18** Top**:** LA-ICP-MS image, showing the distribution of $Zn^{66}$ (cps) in a $4.53 \times 1.34$ mm section of rat retina tissue (control-4.1). Bottom: Example data for one ablated line from each image (arrow in the corresponding image indicates the location and scan direction of the line). Gaussian peaks were fitted to the choroid (peak 0) RPE (peak 1) and retina (peak 2). Complete laser parameters are given in Table 3.6.
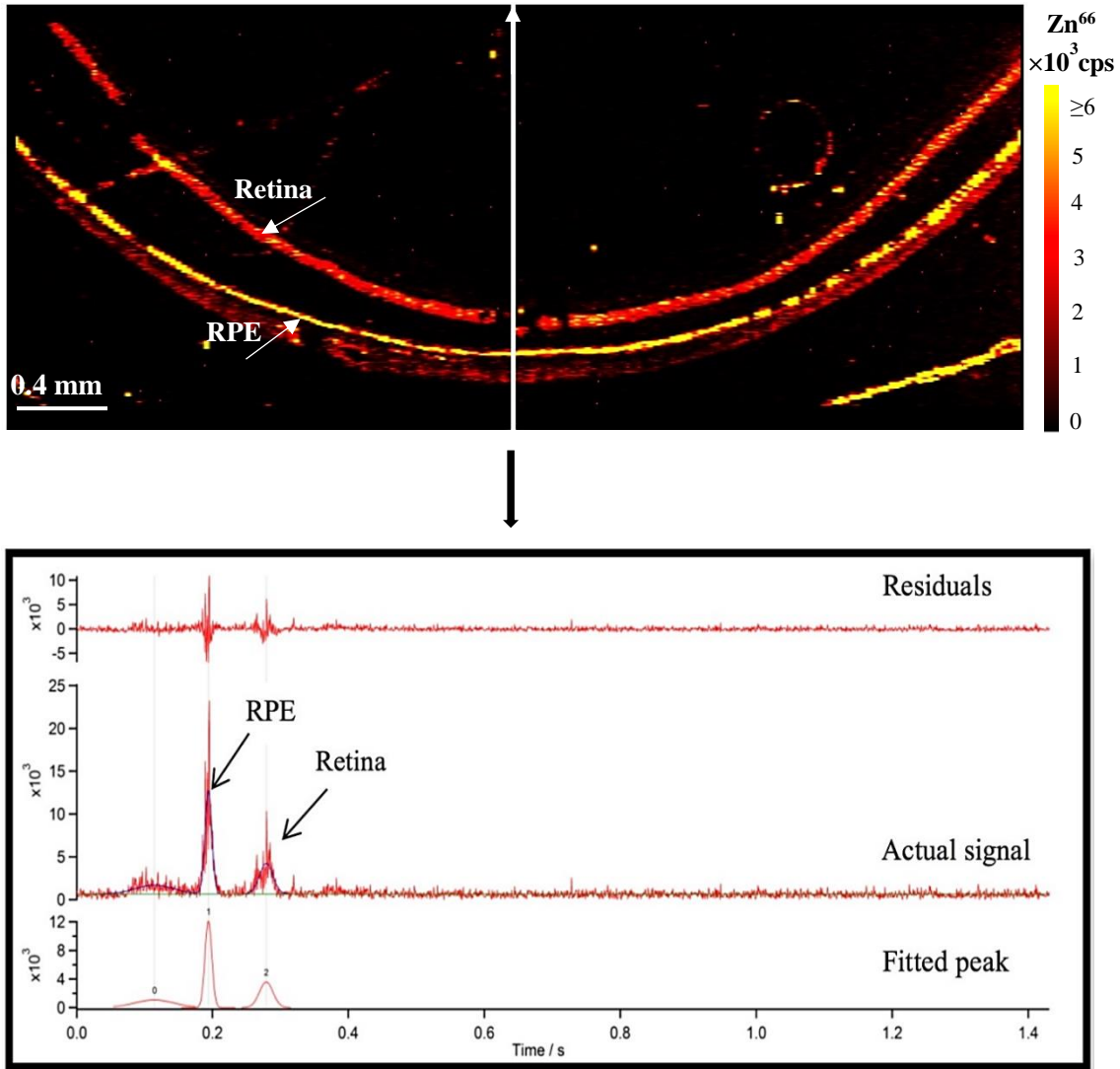
**Figure 3.19** Top: LA-ICP-MS image, showing the distribution of $Zn^{66}$ (cps) in a 4.50×1.41 mm section of rat retina tissue (rat fed with Zn- 9.3). Bottom: Example data for one ablated line from each image (arrow in the corresponding image indicates the location and scan direction of the line). Gaussian peaks were fitted to the choroid (peak 0) RPE (peak 1) and retina (peak 2). Complete laser parameters are given in Table 3.6.
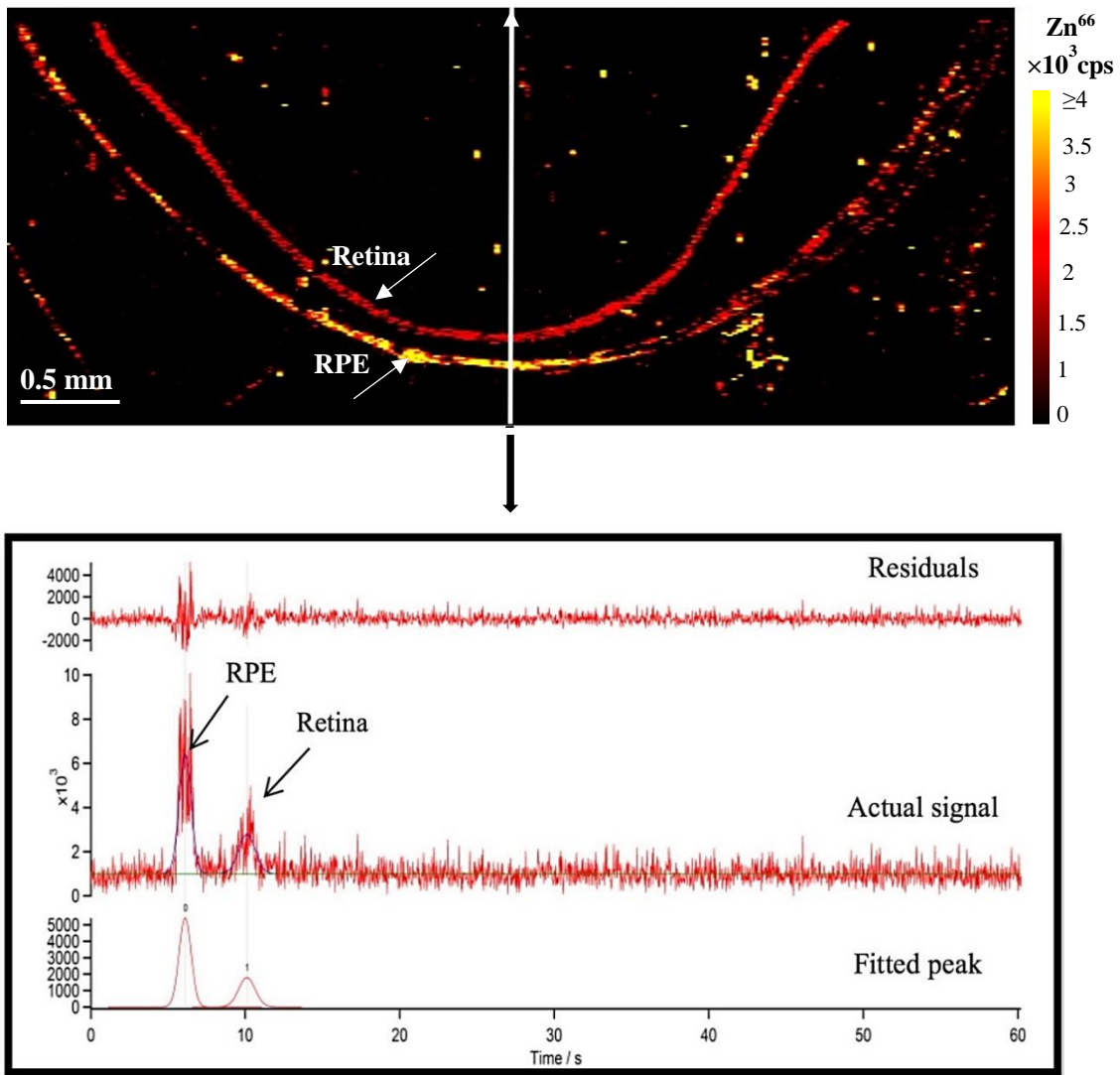
**Figure 3.20** Top: LA-ICP-MS image, showing the distribution of $Zn^{66}$ (cps) in a 5.00×1.39 mm section of rat retina tissue (rat fed with Zn& Cu diet-11.3). Bottom: Example data for one ablated line from each image (arrow in the corresponding image indicates the location and scan direction of the line). Gaussian peaks were fitted to the RPE (peak 0) and retina (peak 1). Complete laser parameters are given in Table 3.6.

The total average of the relative ratio of Zn RPE/retina peaks area and the standard deviation for the 12 rat retina sections are summarized in Table 3.8. Overall, the highest average RPE/retina ratio of 1.91 was observed for the group that received combined Zn and Cu supplementation, compared to an average ratio of 1.51 for rats receiving Zn supplementation alone and 1.52 for the control group (Figure 3.21). However, significant variability was seen between different locations within the same sample (average within sample RSD of 33%) and between the 4 rats analysed in each group (intra-group RSD of 30, 18 and 34 % for the control, Zn and Zn+Cu groups, respectively). Therefore, the difference between the three differentially fed rat groups was not statistically significant for the relatively small group of twelve rats investigated here. The association between the three groups of rats was investigated using a one-way analysis of variance (ANOVA). $P$-values appeared higher than 0.10 (ANOVA, $\alpha=0.05$, $p=0.44$), suggesting that the three groups of rats are not significantly different.

**Table 3.8** The average of the relative ratio of the Zn peak area of RPE and retina*

| Sample description | Sample number | RPE/Retina area ratio | STDV | RSD % |
|---|---|---|---|---|
| **Control** | 5.3 | 0.98 | 0.42 | 42 |
| **Control** | 4.1 | 1.39 | 0.49 | 35 |
| **Control** | 2.1 | 1.65 | 0.66 | 40 |
| **Control** | 3.1 | 2.05 | 0.64 | 30 |
| **Zn fed rat** | 7.1 | 1.30 | 0.41 | 31 |
| **Zn fed rat** | 9.3 | 1.32 | 0.41 | 31 |
| **Zn fed rat** | 10.2 | 1.52 | 0.35 | 23 |
| **Zn fed rat** | 6.1 | 1.90 | 0.61 | 32 |
| **Zn+ Cu fed rat** | 15.1 | 1.08 | 0.22 | 20 |
| **Zn+ Cu fed rat** | 14.1 | 1.75 | 0.84 | 48 |
| **Zn+ Cu fed rat** | 11.3 | 2.20 | 0.71 | 32 |
| **Zn+ Cu fed rat** | 12.1 | 2.60 | 0.9 | 34 |

* The relative ratio of Zn in RPE/retina is expressed as a mean and standard deviation (STDV) of 20 scanned lines
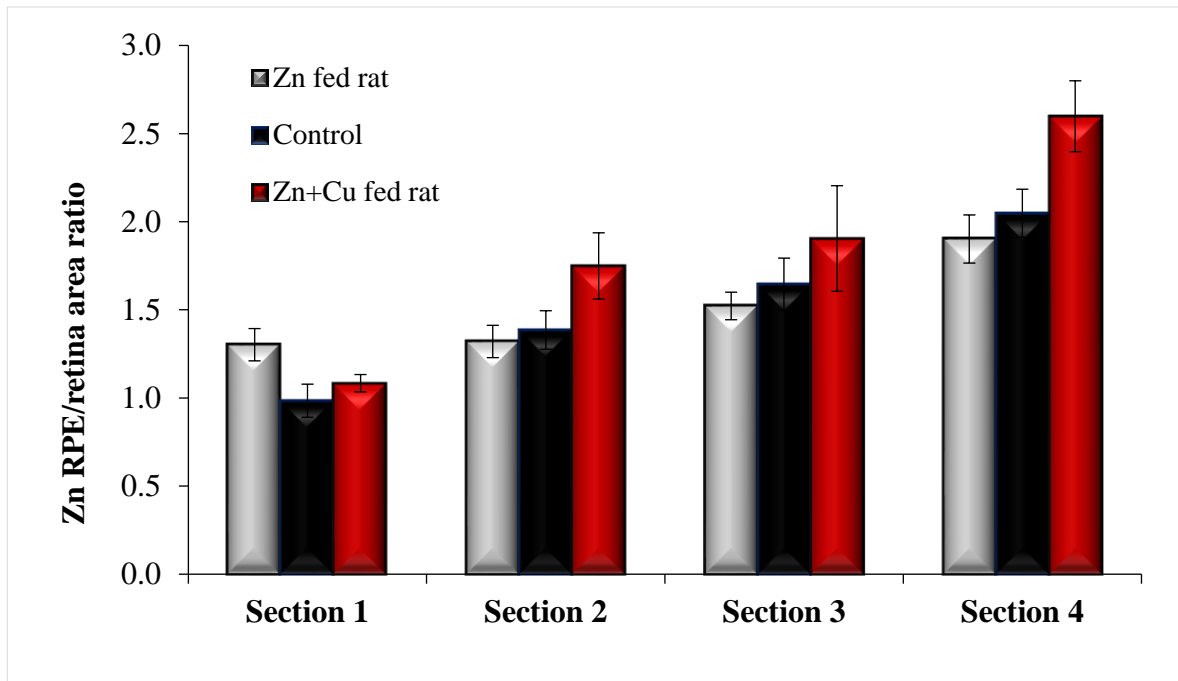
**Figure 3.21** Comparisons between the RPE/retina Zn level in 4 sections of control and Zn fed rat and Zn+ Cu Fed rat. Sections are presented in order of increasing RPE/retina Zn peak area ratio. Error bars represent the standard error of the mean, n=20 scanned lines.

The widths of the fitted peaks were used to compare the thickness of the imaged features. Figure 3.22 shows the variation in the width of the RPE and retina peaks for the three conditions studied. It is clear that retinal peak width is far higher than RPE. The thickness of the retina was approximately equivalent for all samples, but a thinning of the RPE was observed for the supplemented rats. As mentioned earlier, the data set narrowing was seen in the RPE of the Zn fed rat, therefore, the retina and RPE peak width of the control and fed rat were calculated and compared. Based on one-way ANOVA (p<0.001), the control peak width of RPE was found higher than fed rat. These data are in good agreement with earlier reported findings[189] which indicated that Zn supplementation may be linked with a reduced Zn level in the RPE-Choroid complex in AMD patients. Evaluating the thickness of the retina is essential to help in the signs and diagnoses of some ocular and neurological disease.[250,325] Alamouti and Funk reported that both retinal and nerve fibre layer thickness are significantly reduced with age.[326] The reason for this reduction is due to the death of retinal neuronal ganglion cells and the loss of axonal cells in the optic nerve.[325] A recent study in 2017 found that age, ethnicity, and smoking status also play an important role in RPE-BM thickness

variation.[327] Further investigation is needed as this finding has important implications in the understanding of the Zn function within the retina.
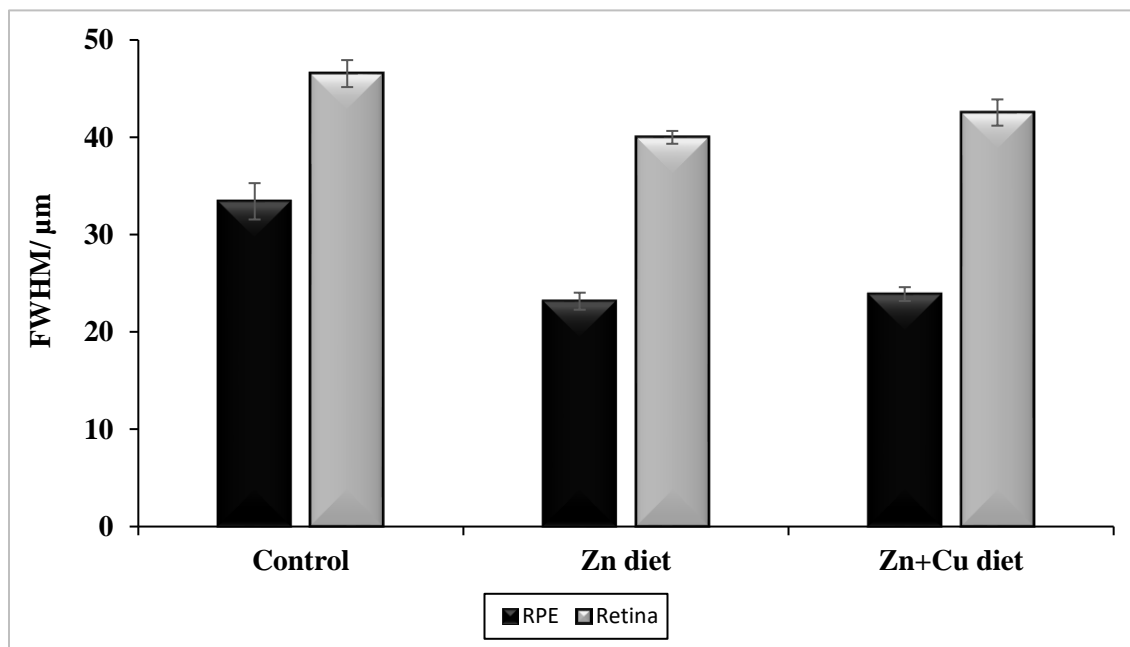


**Figure 3.22** Comparison between the Retina and RPE Zn peak width in control and fed rat. Peak width presents the full width at half maximum (FWHM). Error bars depict the standard error of the mean, n=60 lines.

### 3.3.8 Further application used for imaging

### 3.3.8.1 Rat section

D-Plot is an interface software designed for scientists, engineers, and other technical workers who are interested in creating presentation-quality X-Y plots and/or contour plots of data. D-Plot can also produce a waterfall plot, a 3D bar chart, a simple wireframe mesh and D-Plot graphs can manipulate 2D and 3D data from a variety of sources in many different formats.

The images that were produced before by IGOR Pro software, were applied to another professional imaging application called D-plot. An example of one rat retina section processed by D-plot is represented in Figure 3.23.
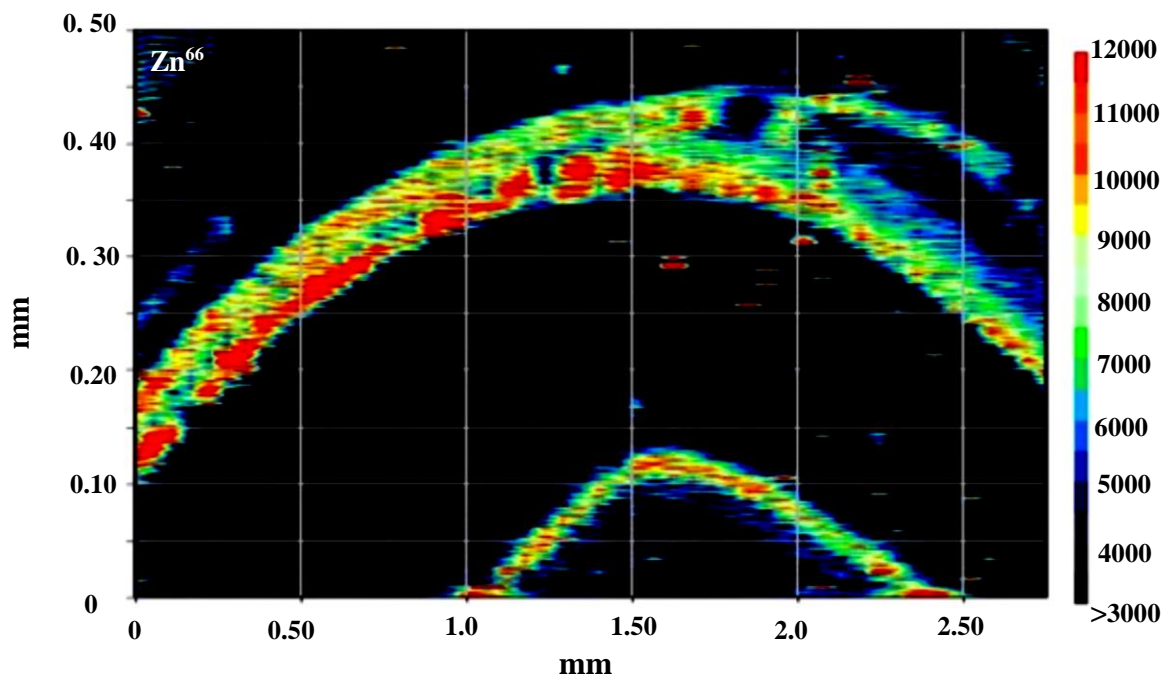
**Figure 3.23** An example of one LA-ICP-MS rat retina section processed by D-Plot imaging programme, showing the distribution of Zn. The colour scale depicts the signal intensity in counts per second (cps). Complete laser parameters are given in Table 3.5.

### 3.3.8.2 Comparisons between human and rat sections and enhanced data processing

The structure of the eye is extremely complex and organized, indicating the high degree of specialty that is necessitated to maintain its function. Representative microscopic section distributed into distinct histological layers of the normal human retina with the thickness [328,329,330,331,327,332,333] are shown in Figure 3.24 using optical coherence tomography (OCT) and spectral- domain optical coherence tomography (SD-OCT) for thickness measurement. The retina is approximately 0.5 mm thick (excluding the choroid). However, the retinal thickness shows greatest variations depending on the position of the retinal structure (central retina, or peripheral retina, foveal floor, foveal rim, nasal, or temporal). In addition, age, ethnicity and smoking status play an important role on RPE-BM complex thickness.[327]

In humans, experimental access to sections of the eye is difficult to achieve, yet one section of human retina has been acquired from UCL Institute of Ophthalmology. Zinc had noticeable distributions in a human retina section and the biologically important Zn plays vital roles in retinal function.
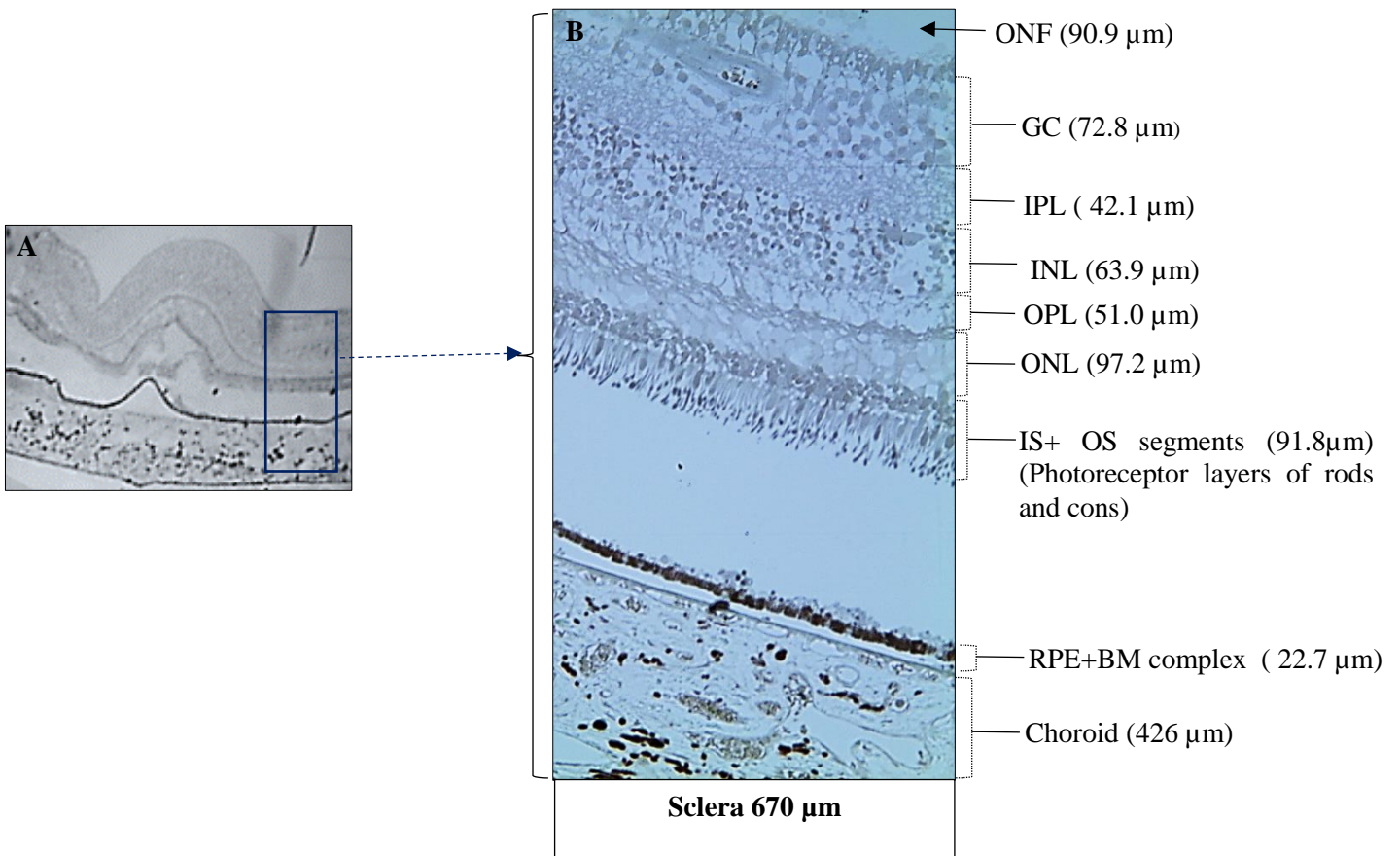
**Figure 3.24** Microscopic images of 5× (A) and 20× (B) magnifications of normal human retina section, showing the thickness of the human cellular organization layers of the retina and choroid complex using optical coherence tomography (OCT) and spectral- domain optical coherence tomography (SD-OCT). The following layers are shown: Bruch's membrane (BM); retinal pigment epithelium (RPE); outer segment (OS); inner segment (IS) outer nuclear layer (ONL); outer plexiform layer (OPL) inner nuclear layer (INL); inner plexiform layer (IPL), ganglion cell layer (GC) and optic nerve fibre (ONF). Both micropscopic images obtained from Dr Imre Lengyel, UCL Institute of Ophthalmology.

The human retina image was generated using a recently developed custom Live Code based application. This new programme was created by Peter Reid in collaboration with Amy Managh (LA-ICP-MS ImageTool v0.33, Reid-IT Limited, Loughborough UK).[334] The technique developed was applied to a specimen taken from a post-mortem section of a human eye and the image is shown in Figure 3.25. The image was acquired using the parameters given in Table 3.6.

This image, generated in 2015, is believed to be the earliest image of the human retina produced using LA-ICP-MS, pre-dating a 2018 paper reporting such imaging.[302] The same data processing technique was used by A. Managh [323] to identify and integrate $^{197}$Au individual peaks obtained from a single Au labelled macrophage[323], however this is the first time that the imaging data processing approach was applied to a retina section. There are a great number of advantages of this programme including automation of image generation, based on user defined image parameters. This represents a substantial time saving since it is computationally more efficient and reproduces the images 10 times faster than IGOR Pro. To illustrate, 200 lines ablated from the human retina section generates 200 FIN2 files and each of these files have 3270 data points, producing an image in less than 1 minute. Whereas IGOR Pro. generates the image in less than 10 minutes. Processing the huge amount of data points in a few minutes would be a considerable saving of time if this tool is used in the future. The retinal layers are not very clear in Figure 3.25 and in order to distingush between each layer a new laser instrument with high resolution is required.

The image (Figure 3.25) was compared with the rat section and it can be seen that the fidelity of the image collected here corresponds to the rat's section shown previously, and as such we can be confident that it is reliable. It is clear the differences between the rat retina and the human retina are due to the lack of the anatomical macula features in rats. The thicknesses of both rat and human retina were measured by calculating the peak width and the data processed from one scanned line selected from the central image. Figure 3.26 shows that the width of the human RPE/retina is far higher than control rat, as would be expected. The human RPE/choroid complex is about 7-8 times wider than Rat RPE/choroid complex, whereas the human retina is 2 times wider than the rat retina. Indeed, the thickness of the RPE-choroid complex in the human retina is much wider than the retina because the RPE-choroid complex is highly enriched with Zn whereas the retinal layers are less concentrated with Zn and with the old laser system it was challenging to distinguish the different retinal layers. Detection is complicated by the small size of the features present in the eye, which necessitates the use of a high-resolution approach for their imaging. Further research with more subjects and highly sensitive techniques may help to clarify these age-related changes and gender-related differences in thickness of the retinal layer.

Gender and age are considered as significant factors that may have an impact on retinal function and structure. [335] As a consequence, the thickness of several retinal layers has been found to differ according to gender and age.[330] Zinc and copper levels in RPE and choroid complex in AMD patients' eyes was decreased by 23% compared to healthy people. The patient donors were subjected to Zn and Cu supplementation, suggesting the important role of metal homeostasis on AMD and in retinal health. However, no difference was found in retinal Zn and Cu levels between AMD patients and healthy subjects. [189] Therefore, while analysing the thickness of the retinal layers, the status of the subject (healthy or patient), age, and gender should be taken into consideration.[330]

Human studies such as AREDS can be expensive and take many years. An accurate animal model can help to understand the developments of novel therapies of AMD. There are several advantages of the non-human animals such as mice, rats, rabbits, rodents, including: low cost, rapid disease progression that allow more efficient studies and easily amenable to genetic manipulation. While there are numerous models which mimic many of the important pathological features of AMD, none of them reproduces all human characteristics. In addition, mice and rats lack an anatomical macula. In spite of all the anatomical differences, several animal models have been created for studies of AMD and the human retina, although developing a model that imitates AMD features has been challenging as the disease involves complex processes involving both genetic and environmental factors.[336] All in all, examination of the effects of Zn supplementation in animal models and Zn status in humans have shown some exciting observations. These highlight the need for further research into the role of Zn in the healthy and pathological aging retina.
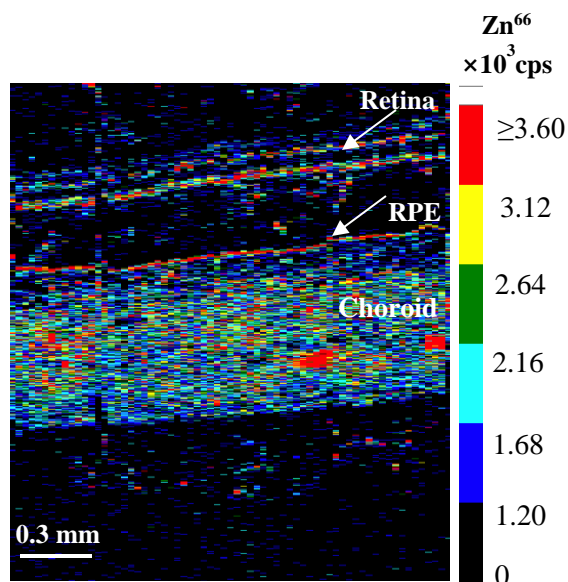
**Figure 3.25** LA-ICP-MS image of a 1.66 ×1.88 mm section of human retina tissue, showing the distribution of Zn. It was processed by LA-ICP-MS ImageTool v.0.31. The colour scale depicts the signal intensity in counts per second (cps) and complete laser parameters are given in Table 3.6.
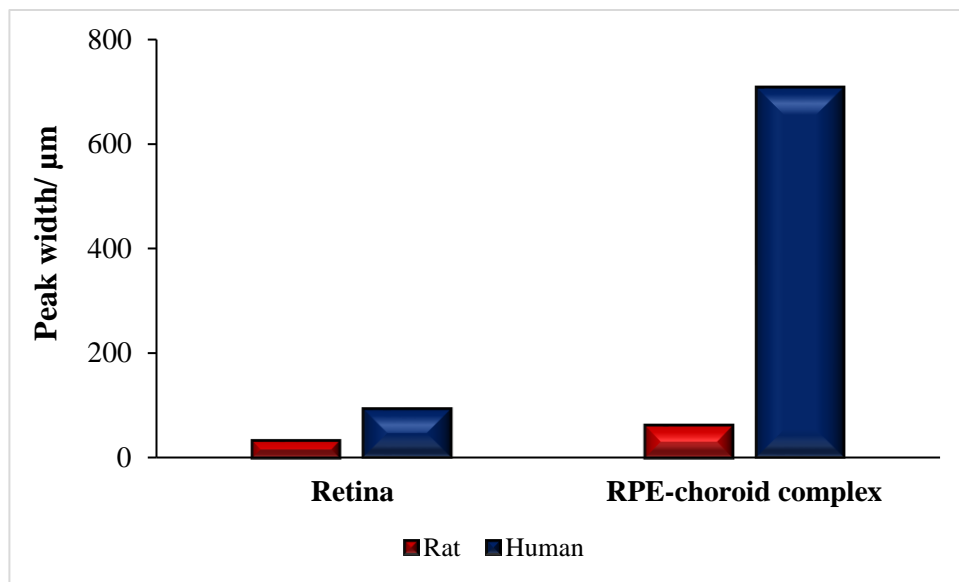


**Figure 3.26** Comparison of the Zn peak width between human and rat retina and RPE-choroid complex.

## 3.4  Conclusion

Zinc appears to play a crucial role in many cellular metabolic pathways and is found in high concentrations within the retina/choroid complexes. It is well known that Zn homeostasis changes during aging, thus contributing to several specific retinal disorders.

The present study was carried out on aged and long term Zn supplemented rats. For the first time, the application LA-ICP-MS was successfully used for mapping the relative concentration of Zn across 12 retina sections of rat given either a conventional or a Zn-supplemented diet. Various ways of data analysis have been considered. Clearly processing the data manually was unsatisfactory, not practical and time consuming because it is subjective and the results generated were inconsistent on different days. Therefore, the need of a way to produce the same result every day is crucial. A novel data processing method was used to evaluate the differences in Zn content in the retina and RPE. For reliable comparisons between supplemented and non-supplemented rats, the relative ratio of the RPE/retina peak areas was used in order to allow for intra and inter day variation of absolute signal. The ocular features were well modelled by a Gaussian function which effectively smoothed the data and facilitated calculating the peak area ratio. An alternative view is that the data should not be smoothed as the individual peaks (spikes) within each peak may represent biological features. Although the relative Zn peak area in the RPE/retina did not vary significantly between the control and Zn fed rat, the distribution of the Zn was concentrated in a much narrower band across the RPE of the fed rat. Whilst a biological explanation of narrowing Zn distribution would be speculative at this stage, it could be argued that according to the Zn concentration increase it could become trapped and precipitate in a narrow  band in the RPE where the plaque starts to form. Retinal thickness variation is an important factor to study as it could be an indication of some ocular disease including AMD.

Although the resolution used in this study is comparable with the highest resolution LA-ICP-MS retinal imaging reported by a recent study[302], spot sizes below 25 µm are needed to determine whether the spikes correspond to biological features or noise. Higher resolution was not possible in this instance due to the sensitivity limitations of the system.  Instrument design plays a fundamental role in improving elemental bio-imaging. In recent years a

number of groups have introduced modifications to increase the speed of the analysis, through design of fast-washout LA instrumentation and implementation of faster data acquisition.[323,324,337,294,338] These innovations are now starting to reach the market. The implementation of these increasingly faster and more efficient laser systems, with potential to reach ~1 µm resolution, will enable detailed imaging at higher sensitivity. Due to the massive amount of data generated (4238 data points per one line scanned), there is also a need for increased automation to speed up the data processing. The new automated programme created by Peter Reid in collaboration with Amy Managh (LA-ICP-MS ImageTool v0.33, Reid-IT Limited, Loughborough UK)[334] is very promising for the future. The data presented here is a small-scale depiction to evaluate the method. A more detailed study, involving a greater number of replicate animals, will be required to fully assess the biological significance of the results presented here. More comprehensive understanding on the influence of Zn supplementation levels and their distribution could be the key for better treatment of AMD.

# 4 Bio-imaging of Zinc in Milli cell membrane by Laser Ablation Inductively Coupled Plasma Mass Spectrometry

## 4.1 Introduction

Bruch's membrane (BM) is a unique thin cellular structure in the eye, located between the retina and choroid. BM partially regulates nutrients, oxygen, fluids and metabolic waste products between the retina and overall circulation. It has been established that the molecular, structural and functional properties of BM depend on age, genetic composition, environmental factors, retinal location and disease condition. The variations occurring in BM with age include increased accumilation of Ca in elastic fibres, increased crosslinkage of collagen fibres and increased income of glycosaminoglycans. In addition, advanced glycation end products (AGEs) and fat accumulate in BM. The age-related changes in BM may affect healthy photoreceptor cells, and lead to progression of diseases such as age-related macular degeneration (AMD).[317] Barzegar Beforoei has reported that morphological examination of ultra-thin sections from the eyes of aged rats following Zn supplementation revealed significant thinning of the Bruch's membrane at the peripheral retina.[40]

Retinal pigment epithelium (RPE) is a continuous monolayer of differentiated and pigmented cells located between the photoreceptor and choroidal circulation. Among the ocular tissues, the highest concentration of Zn is present in the RPE-choroid complex. The principal roles of RPE are carrying of nutrients, ions, and water, absorption of light and defence against photooxidation.[339] As such, RPE plays an important function in the metabolic exchange between the photoreceptor outer segments and blood circulation. Many of the RPE's functions depend on Zn, from pigmentation to enzymes involved in phagocytosis.[270,340] Here we hypothesized that RPE cells in cultures receive insufficient supply of Zn for optimal differentiation, if extra Zn is not added to the culture medium. Thus, extra Zn (125 uM) was added to the apical side (top of the membrane with cells) but not the basal side since RPE phagocytes contain high levels of Zn. Factor H (FH) is genetically associated with age-related macular degeneration (AMD), characterised by the presence of sub-retinal pigment

epithelial (RPE) deposits in which FH and Zn were present. Therefore, the focus of this study is to identify if Zn concentrations across the membrane would show a concentration gradient due to the addition of Zn and/or its secretion from RPE. For example, if more Zn accumulates just beneath the cells, then this would be interesting to explore the effect of the Zn on the protein deposit (FH) formation beneath the cells. An additional aim was to compare varying Zn levels (within and outside the cell) in the culture media (RPE cell culture) using LA-ICP-MS.

## 4.2 Methodology

### 4.2.1 LA-ICP-MS

Several tests were performed for optimizing the operational conditions. The final LA-ICP-MS parameters for this analysis are shown in Table 4.1.

**Table 4.1** Laser instrument parameters for RPE cultured sections

| ESI UP-213 laser ablation parameters | |
| --- | --- |
| Repetition frequency | 10 Hz |
| Laser energy | 40-50% |
| Scan speed | 12-15 µm/s |
| Spot size | 12-15 µm |
| Line spacing | Zero |
| Range numbers of lines | (130-200) lines |
| Range of fluence | (6.66- 7.93) J/cm$^2$ |
| Range of line length | (0.42-1.10) mm |

## 4.2.2 Slide preparation

All slides for LA-ICP-MS were prepared by Po-Jung Poa supervised by Dr. Imre Lengyel at Institute of Ophthalmology, University College London, Bath Street, London, UK, EC1V 9EL. OCT-embedded human RPE cells (Human foetal cells, ScienceCell research laboratories) were cultured on a filter membrane (Millicell PIHA01250, Merck Millpore) and treated with Zn (0-125µM) during culture. Cells will not pass through the membrane as the pore size of the membrane is around 0.45 µm. The Zn form is zinc sulphate. The filter membrane is a semi permable diffusable membrane and it mimicked the Bruch's membrane. The EpiCM culture medium recommended by the cell manufacturer was replaced by Miller medium. This medium was supplemented with 0.5% retinal extract and various concentrations of Zn were applied to the apical chamber after one week of seeding, while the basal chamber contained pure Miller medium. The thickness of sections was about 10-20µm. Four groups of slides were prepared for LA-ICP-MS analysis:

- Section 1: cell cultured with 125µm Zn
- Section 2: Cell cultured without Zn (0 µm)
- Section 3: No cells cultured but with 125µm Zn
- Section 4: No cells cultured but with 0µm Zn (the membrane)

  The membrane (Figure 4.1,A) is made of mixed cellulose ester and it is like a filter paper. It was coated with laminin to help cell attachment and then the cell was placed on the top as illustrated in Figure 4.1, B.
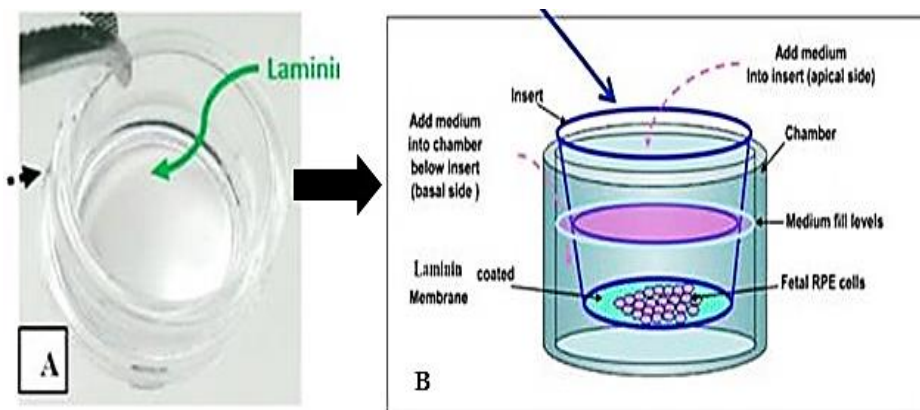


**Figure 4.1** Picture of membrane and explanation of its use in cell culture. Reproduced with permission from Po-Jung Poa, UCL Institute of Ophthalmology,2015.

## 4.3 Results and discussion

A daily supplementation of 80 mg Zn is recommended to AMD patients. Consequently, the effects of Zn on human primary RPE cells were studied by culturing these with µM levels Zn in the medium. Several tests were carried out on 11 sections to map the Zn level in the human RPE cell sections. All tests were applied in the section where cells were cultured and treated with 125µm of Zn. An example of a successful initial testing is shown in Figure 4.2 (section A and B). Cells might have detatched during sectioning, due to the cutting presuure applied to the sample, thus the cells were pushed away from the membrane. Yet, that should not affect the presence of Zn within the membrane, if there is a difference in Zn concentration across the membrane (see Figure 4.2 section B). Instead of doing DAPI-staining on every single section to know the exact locations of attached and detached cells, the sections were re-prepared with careful sectioning as shown in Figure 4.3. The microscopic images (Florescence microscope, Nikon SMZ1500, TRITC) were obtained from Po-Jung, UCL Institute of Ophthalmology.

In conclusion, at this stage the presented images show the principles and early results of mapping RPE human cell culture embedded on filter paper which mimicked the Bruch's membrane. The concept of this study is novel and it has not been applied before. In addition, this study reports for the first time the application of LA-ICP-MS for mapping RPE human cells. It is challenging to detect such a small sized feature around 15-20 µm in diameter for a single RPE cell. It would be powerful to continue this study in the 4 section types to understand the effect of Zn on sub-RPE deposits and RPE cells treated with and without Zn. This work has illustrated the feasibility of using LA-ICP-MS for imaging in such a study and showed a great potential to be progressed in the future which may help us to understand the effectiveness of Zn supplementation on reducing AMD disease progression.
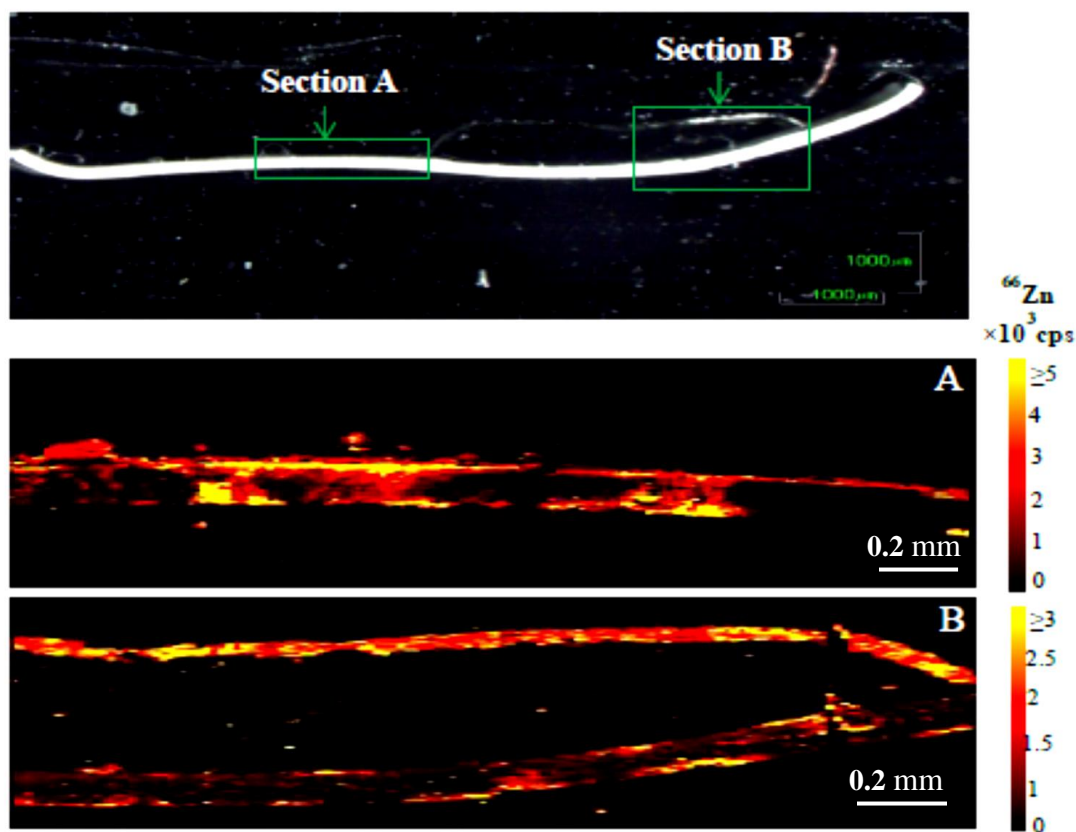
**Figure 4.2** Top: microscopic image of 2.4×0.61mm (A) and 1.95×1.10 mm (B) of human RPE cell section, obtained from Po-Jung Poa (UCL Institute of Ophthalmology). Bottom: LA ICP-MS images of the same section, showing the distribution of Zn in attached and detached cell with the membrane treated with 125µm of Zn. The colour scale depicts the signal intensity in counts per second (cps).
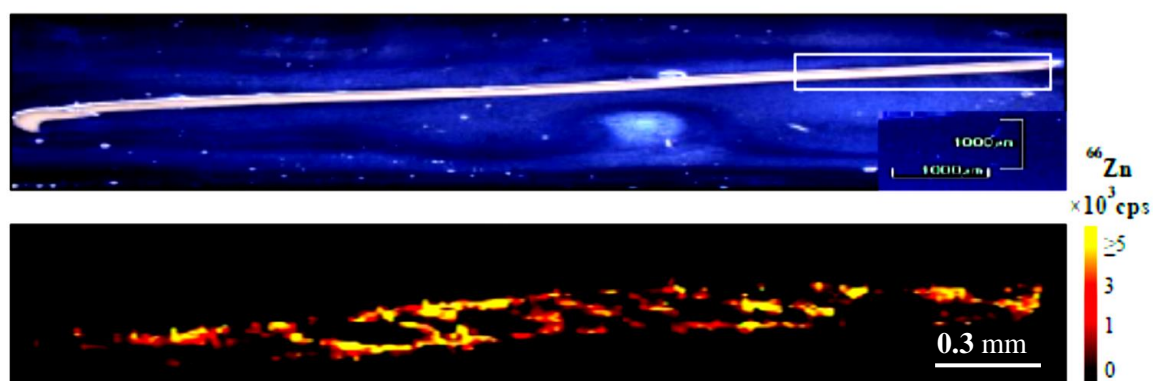


**Figure 4.3** Top: microscopic image of 3.0× 0.42 of human RPE cell section, obtained from Po-Jung Poa (UCL institute of ophthalmology). Bottom: LA ICP-MS images of the same section, showing the distribution of Zn in attached and detached cell with the membrane treated with 125µm of Zn. The colour scale depicts the signal intensity in counts per second (cps).

137

# 5 Quantification of Zn in Buffers in Subcellular Extraction Kit by ICP-MS

## 5.1 Introduction

In order to determine the cell distribution of Zn, a cell partitioning technique has been used. The CalbioChem ProteoExtract® Subcellular Proteome Extraction Kit (obtained from Merck, UK) divides cell components into four functional compartments; the cytosol, cell membrane, nuclear fraction and cytoskeletal sections. Each of these fractions has a particular function within the cell. The cell fractionation kit provides "four fractions with decreased proteome complexity"[341]. When the extraction buffers are added, the cytosolic proteins are released, followed by the membranes and membrane organelles (which are solubilised in Extraction Buffer II), then the nuclear proteins are released, and finally, the cytoskeleton components are solubilised in Extraction buffer IV.[341]

The research group had some experience previously in separating out the protein/DNA from different compartments of cells to study the distribution of platinum from chemotherapy drugs[229], and a further interest arising from that work is to look at the intra-cellular distribution of other metals such as Zn, Cu and Fe. In this work the aim was to measure the distribution of Zn in each compartment of the cell and thus determine where the Zn accumulates. However, it was found that the reagents used in the cell partitioning kit were contaminated with the metal of interest. Therefore, this work was directed towards cleaning up the reagents successfully instead of testing the cell partitioning kit on actual cells. The developed method for cleaning up the reagents ought to be valid in the future research work.

## 5.2 Methodology

The analysis was performed on a sector-field inductively coupled plasma mass spectrometer (SF-ICP-MS) (Thermo Scientific, Element 2 XR, Bremen, Germany). The instrument was fitted with platinum sampler and skimmer cones (ICPMS cones Ltd., Chester, UK), and a sample introduction system equipped with a conical glass concentric nebulizer (Glass

Expansion, Victoria, Australia), and a Cyclonic spray chamber (Glass Expansion, Victoria, Australia). The sample flow rate was set to provide a flow of approximately 400 μL/min. A PFA nebulizer and PFA bottles and MF tubes were used.

A multi-elemental standard solution (10 mg/mL) was diluted 100 fold (0.1 ppm) with 2% $HNO_3$. ProteoExtract® Subcellular Proteome Extraction Kit (obtained from Merck, UK) contained the following: Wash Buffer (100ml), Extraction Buffer I (22ml), Extraction Buffer II (22ml), Extraction Buffer III (11ml) and Extraction Buffer IV (10ml). From the extraction buffers I-IV 40 μL were taken and diluted up to 4mL with deionized water (18 M-Ω, from a Milli-Q water purification system, Millipore Corporation, Bedford).

Several steps and tests were successfully carried out to clean the buffers. Glass wool and Chelex-100 were used for this purpose. For the preparation of Chelex 100, 4 g of Chelex was weighed and 20 ml of water was added. 50 ml each of 2% &10% $HNO_3$ were prepared. In order to test the level of Zn contamination in both glass wool and Chelex-100, the final procedure was performed as follows:

- The glass wool was soaked in 10 % $HNO_3$ for 24 hours.
- The following day, 10% $HNO_3$ was diluted to 2% $HNO_3$ to be analysed to check Zn contamination level.
- Firstly: Glass wool was assembled in 2 pipette tips.
- 3 ml of DI water was poured on the top of one of the pipette tips to rinse the glass wool.
- Then 3 ml of DI water was added and the eluate was collected in a 15 ml MF tube.
- 10 samples of DI water eluate were collected (sample 1 was the earliest eluate and sample 10 was the last eluate).
- The same procedure was performed in the second pipette tip with 2% $HNO_3$.
- Secondly: Glass wool and Chelex were assembled in another 2 pipette tips.
- 10 eluates of $H_2O$ and 2% $HNO_3$ were collected as in the above procedure (Figure 5.1 illustrates the procedure).
- The same pipette tips were used to pass buffer through after cleaning the Chelex and glass wool with DI water and 2% $HNO_3$.

**1- 2% HNO$_3$**
**2- H$_2$O**

Chelex-100

Glass wool

Collecting 20 analyte in tubes after adding H$_2$O and HNO$_3$ then analyse them by ICP-MS
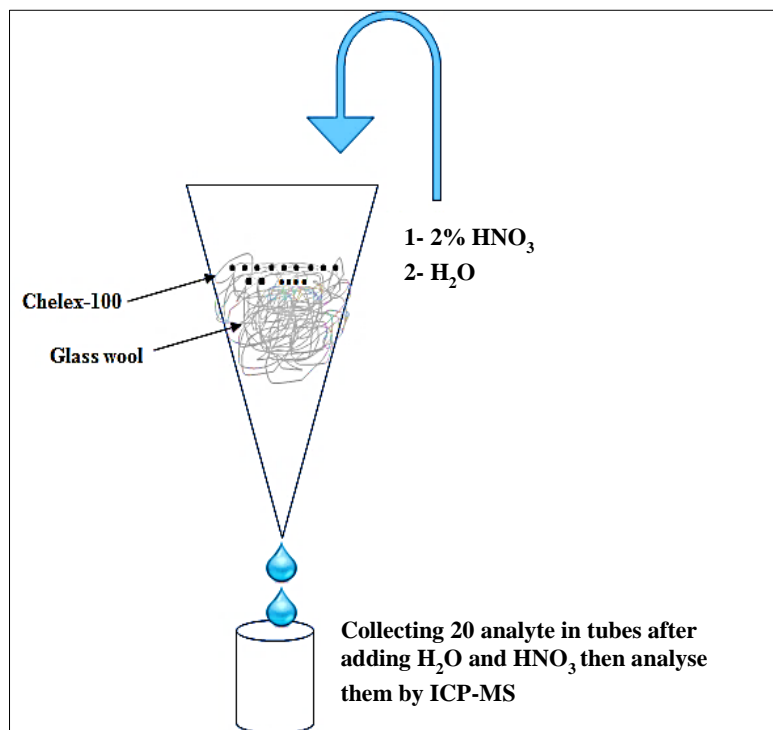
**Figure 5.1** Explanation of the Procedure of cleaning glass wool and Chelex-100.

## 5.3 Results and discussion

A full magnet scan was performed on each of the 4 buffers. The buffer was then analysed specifically for Zn. Table 5.1 shows the Zn signal (cps) of blanks before and after running the 4 buffers. In general, the scanned 4 buffers displayed no significant difference between them, and were found to be much higher when compared with 1 ppb standards ($4.57E^{+04}$). As can bee seen from the table the blanks were affected after running the buffers. Therefore, the cleaning procedure was applied.

20 eluate samples of DI water and 20 eluate samples of 2% HNO$_3$ were collected after cleaning with both glass wool and Chelex and analysed by ICP-MS. The signal intensity of Zn$^{66}$ of the soaked nitric acid is very high as expected ($8.49E^{+06}$ cps). An example of Zn$^{66}$ signal intensity test of the DI water collected after the glass wool and Chelex cleaning is shown in Figure 5.2 and Figure 5.3 showing the reduction of Zn$^{66}$ in buffers 1 and 2 before and after Chelex. Cu signals were similarly reduced after cleaning.

**Table 5.1** An example of one of the run of the buffers to check $Zn^{66}$ level

| Buffers and blanks | $Zn^{66}$ signal intensity |
|---|---|
| Before: DI water | $3.43E^{+03}$ |
| 2%HNO$_3$ | $1.00E^{+04}$ |
| Buffer 1 | $7.25E^{+05}$ |
| Buffer 2 | $8.24E^{+05}$ |
| Buffer 3 | $8.03E^{+05}$ |
| Buffer 4 | $8.21E^{+05}$ |
| After: DI water | $8.33E^{+05}$ |
| 2%HNO$_3$ | $1.97E^{+04}$ |

In conclusion, a deposition of a white residue was noticed on the ICP-MS cones following analysis of the kit reagents. It was thought that this phenomenon may be attributed to the presence of salts, EDTA and mixtures of ionic and non ionic detergents within the cell partitioning buffers. Therefore, this experiment was applied to investigate and reduce the contamination levels in order to enable such cell partitioning kits to be used to measure intra-cellular distribution of ubiquitous elements, particularly Zn. Future work would include the development of an online cleaning system using the above reagents in a flow system to streamline the removal of the high levels of Zn found in the cell partitioning buffers.

 After cleaning the buffers, a cell partitioning experiment could be performed on a RPE cell culture to investigate how the Zn is distributed and in which cell fraction the Zn is most concentrated. Subsequently, the cytosol fraction, for instance, could be separated, detected and quantified by coupling either  online gel electrophoresis (GE) or HPLC to ICP-MS to examine the Zn containing proteins (albumin, α2-macroglobulin and metallothionein), and also for Cu containing ceruloplasmin and Fe containing transferrins. Once the methodology is fully developed, this technique could be applied to blood samples from AMD patients and a healthy control group.
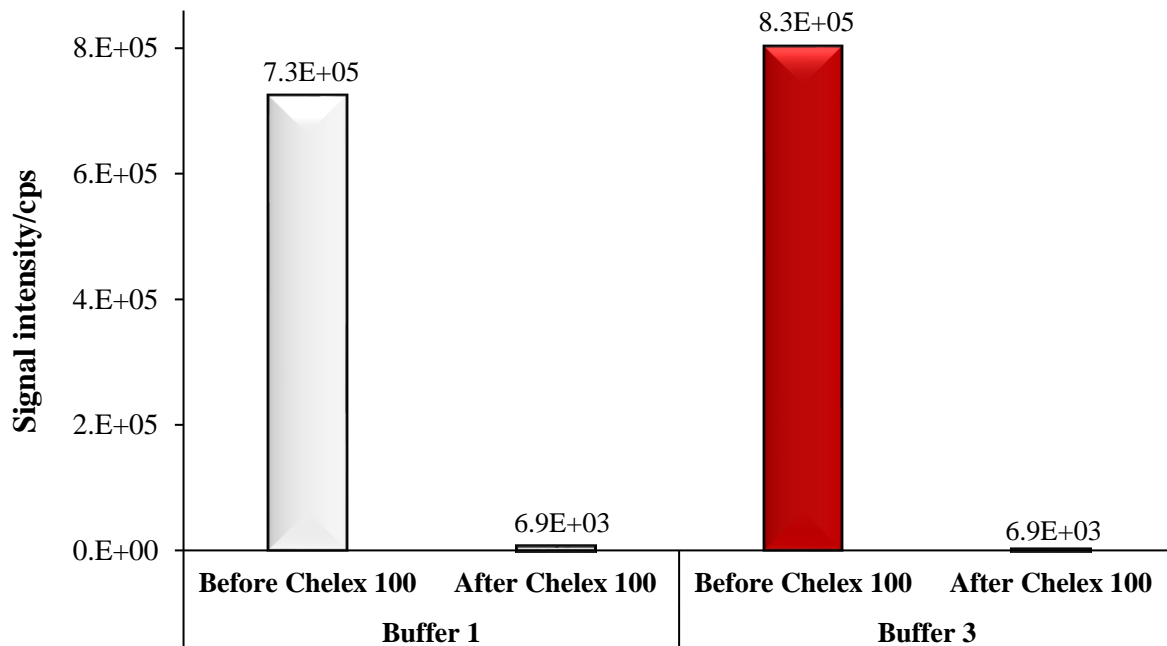
**Figure 5.2** An example $Zn^{66}$ signal intensity test of buffer 1 and buffer 3 before and after chelex cleaning with $HNO_3$.
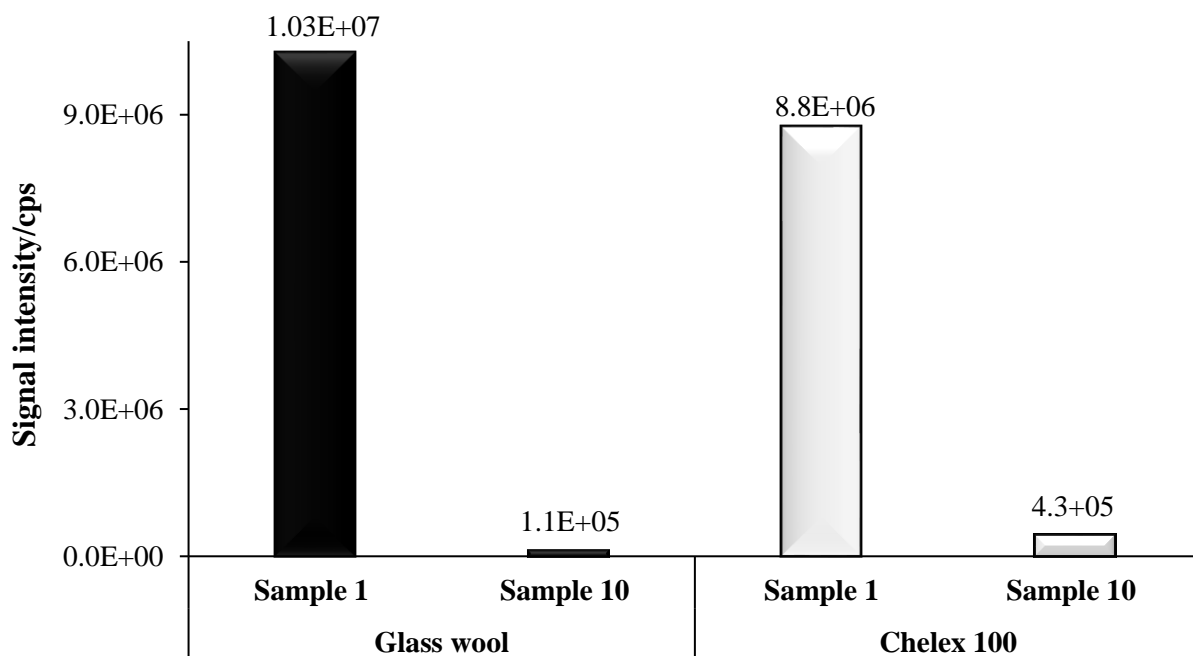


**Figure 5.3** An example $Zn^{66}$ signal intensity test of the DI water collected after the glass wool and chelex cleaning. Sample 1 represents the first eluate collected and the sample 10 represents the tenth eluate collected.

# 6  Conclusion and Suggestion for Future Work

Simple dilution-based sample preparation procedures have enabled successful quantification by ICP-MS of Zn, Cu and Fe in small volumes of serum from AD and AMD patients, providing an alternative to conventional time consuming procedures and being amenable to automation. To the best of our knowledge, no other published studies in the literature have used such a low volume (30 µL) of serum for such an analysis. Due to the ubiquitous nature of the elements of interest in the environment, great care was taken to avoid contamination in the analytical protocol and extensive testing was carried out to validate the procedure. Compared to other procedures,[241,342] the use of ammonia, Triton X-100 and nitric acid in the matrix for serum samples provided stable performance over extended periods and was efficient at keeping the sample introduction system clean and free from clogging. The accuracy of the analytical technique was tested by using reference materials. Serum UTAK was found to be more stable than Seronorm and the analytical results of the former showed very good agreement with the certified value.

The sample preparation procedure ought to be easily automated. Moreover, flow injection technology coupled to ICP-MS possesses advantages including lower sample consumption without affecting the analytical performance, and is simple and fast with higher sample throughput. Recently, the use of advanced functional materials in solid phase extraction (SPE) to remove complex matrices and pre-concentrate target analytes for trace element determination by ICP-MS, has been an active field.[215] The methodology could be extended and coupled to a separation/preconcentration step for other ultra-trace elements.

The importance of studying age related diseases has significantly increased over the last century due to increased longevity of the world population. Alterations of serum Zn, Cu and Fe levels are associated with the pathogenesis of AD/AMD diseases. Parallel studies between AD and AMD have led to a potential link being made between the two conditions. Understanding the common mechanisms may provide new insights into AD and AMD pathogenesis and treatment. In this study, it was indicated that Cu and Fe concentration appear to be higher than Zn in both AD and AMD in accordance with earlier

reported studies for the meta-analysis which was discussed in the introduction section.[85,196,15,72,17] Furthermore, serum Fe levels in AMD patients were slightly higher than in the AD study participants, whereas serum Zn and Cu were not significantly different between AD and AMD patients. It was not possible to obtain a set of control samples, thus our AMD and AD patients were compared with published data for healthy controls (aged 60+).[208,263] The results show a decrease in Zn and Fe serum level in AD and AMD patients compared to healthy controls[264,263] whereas serum Cu level appears notably increased in AD and AMD patients compared to healthy controls.[265,263] It seems that a decreased level of serum Zn, and increased serum Cu & Fe contribute in these diseases. The comparisons between controls and patients will be more reliable if they were of similar age groups and gender. Therefore, the next stage of this research will include phenotypic details such as, gender, age, nutrition and lifestyles of the anonymised participants. Such information would be derived from follow on clinical collaborations as part of the study, and would allow for comprehensive information and reliable comparisons. Additionally, for trace metal status, it is important to monitor any alteration in other factors during disease such as inflammation, cholesterol metabolism, oxidative stress, and homocysteine homeostasis. Therefore, combining several biomarkers and applying proteomic and metabolomic profiles are effective approaches for the development of serum-based diagnostic tests for age-related diseases such as AD/AMD.

Although measuring serum Zn is the most commonly accepted biomarker of Zn status, there is still controversy about measuring serum levels as a realistic way of studying the pathogenic pathway of diseases, as serum Zn concentrations are under tight homeostatic control and may not reflect changes in Zn intake and status. However, circulating Zn levels remains the most widely used method to determine Zn status, despite the known limitations. In addition, monitoring metal ions concentration in blood/serum is regarded as essential and needed on a regular basis in order to diagnose and prevent diseases linked with their deficiency and toxicity.

Bioimaging techniques are necessary for elucidating the role of metals in neurodegenerative diseases. Advancements in methodology are essential for greater understanding into the localization and distribution of metal ions at the cellular and tissue level, and their role in

disease development and progression. Zinc appears to play a crucial role in many cellular metabolic pathways and is found in high concentrations within the retina/choroid complexes. It is well known that Zn homeostasis changes during aging, thus contributing to several specific retinal disorders. Several imaging techniques have been used to study some trace elements in ocular tissues including GF-AAS, NAA, ICP-MS/ICP-OES,[267,186,42,343] , SXRF[186], μSXRF[288], PIXE[320,344], XFM [276,289]. The applications of bio imaging by using LA-ICP-MS reported in the literature are wide-ranging, and spatially resolved trace elemental data have been obtained from various biological specimens. However, there have been few reported studies of the distribution of Zn in the retina using LA-ICP-MS. In 2014 Konz *et al.* performed quantitative imaging of cryosectioned human eye lenses, revealing a homogeneous distribution of Zn in the lens.[170] A subsequent study by this group in 2018 imaged the retina and RPE cells, showing a preferential accumulation of Zn within the RPE compared to the retina and sclera using LA-ICP-MS.[302]

Detection of the small sized features present in the eye is challenging and complicated. This study reports for the first time the application of LA-ICP-MS for mapping relative concentrations of Zn across the retinal tissue of rats given either a conventional or a Zn-supplemented diet. The dose of Zn was based upon the approximate supplementation levels equivalent to those given to human AMD patients in the Age-Related Eye Disease Study (AREDS 1) to examine how this treatment affects the condition. A novel data processing method was used to evaluate the differences in Zn content in retina and RPE, taking the relative ratio of RPE/retina peak areas instead of the absolute signals. This procedure minimised human error from visually interpreting the small differences in the data. By fitting Gaussian peaks to all individual laser line scans in this study, the data were effectively smoothed to help calculate the peak area ratio. An alternative view is that the data should not be smoothed as the individual spikes within each peak may represent biological features. Although the resolution used here is comparable with the highest resolution LA-ICP-MS retinal imaging reported by others[302], spot sizes below 25 µm are required to determine whether the spikes correspond to biological features or noise and to distinguish between the different layers of the retina.

It was concluded that the relative Zn peak area in the RPE/retina did not vary significantly between the control and Zn fed rat, however, the distribution of the Zn was concentrated in a much narrower band across the RPE of the supplemented rat. The increased Zn level in the rat supplemented with Zn and Cu indicate that Cu has an influence on Zn levels. Multi-element analysis (Zn and Cu in this case) is required to enable an understanding of the role of Cu and Zn together. Further research in this area with more sensitive LA-ICP-MS instrumentation may enhance the work and give more specific assignments and further explanations.

Instrument design plays a fundamental role in improving elemental bio-imaging. In recent years a number of groups have introduced modifications to increase the speed of the analysis, through design of fast-washout LA instrumentation and implementation of faster data acquisition [294,323,324,337,338] (Loughborough University have produced a design now marketed by ESI). These innovations with possible modifications are expected to reach out to a wider market; currently few sites in the world have them. By increasing image acquisition speed and resolution without loss of sensitivity, the analysis time would be reduced significantly with larger numbers of samples analysed in a shorter time. The implementation of these increasingly faster and more efficient laser systems, with potential to reach ~1 µm resolution, will enable detailed imaging at higher sensitivity.

The arrival of the latest generation laser ablation platforms is expected to facilitate imaging of small features in ocular tissue with higher speed, sensitivity and spatial resolution than was possible during this PhD project. A good example of the future work is illustrated in Figure 6.1 which shows a recently acquired image, which was produced by ablation of a retinal section at Loughborough University by Dr Amy Managh using ESI's prototype 'NWR Image' Platform. The small section of stained rat retina tissue was ablated with a 1µm spot size, which enables individual cells in the outer nuclear layer to be clearly distinguished. This has huge implications for future work in retinal imaging.

Due to the massive amount of data generated (>4000 data points per one line scanned), there is a need for increased automation to speed up the data processing. The new software (LA-ICP-MS ImageTool v0.33, Reid-IT Limited, Loughborough UK)[334] created by Peter Reid in collaboration with Amy Managh is promising for fast imaging and data processing in future

work. The present study was carried out on aged and long-term Zn supplemented rats and the data presented here is a small-scale depiction to evaluate the method. A more detailed study, involving a greater number of replicate animals, and incorporating newer developments in imaging technology as outlined above, will be required to fully assess the biological significance of the results presented here.
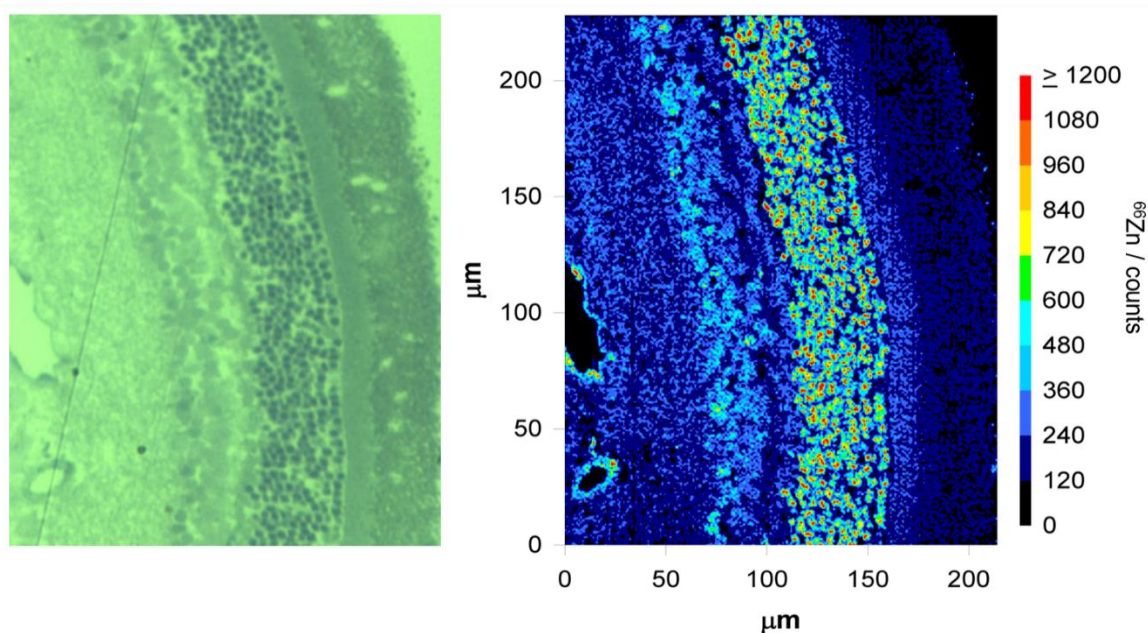


**Figure 6.1** Recently acquired example of high resolution imaging of a section of retina tissue (control sample) obtained from Dr Imre Lengyel, UCL Institute of Ophthalmology. Left panel: Microscopic image of rat retina tissue. Right panel: corresponding LA-ICP-MS image of 250×220µm section showing the distribution of $Zn^{66}$ (cps) which was sampled using a 1 micron laser spot size at Loughborough University using ESI's prototype 'NWR Image' Platform. Picture courtesy of Dr Amy Managh, Loughborough University.

An active research area in the LA-ICP-MS field is the investigation of calibration strategies, where it is important to avoid matrix effects, aerosol transport effects, plasma fluctuation, laser sample interaction, solid deposition, and mass discrimination. Quantification strategies for liquid samples are much more straightforward than those for solid samples,  due to the difficulty of obtaining matrix-matched standards for solids. Although external calibration is the most commonly recognised approach for quantitative elemental bio imaging by LA-ICP-MS, the limited availability of CRMs for a wide variety of matrices makes the normal routine analytical procedure of producing validated quantitative data a significant challenge. Hence,

most of the applications still depend on in-house prepared matrix-matched standards for quantitative analysis. Most of the calibrations using matrix-matched standards for biological tissue analysis are based on the use of homogenised tissue spiked with the elements of interest (such as using spiked homogenised human eye lenses as standards)[170], or powders of CRMs pressed into pellets.[167] Spiked gelatin standards were used in quantifying Zn in human retina and RPE.[302] Different strategies for elemental quantification in biological tissues using LA-ICP-MS reported in the literature include internal standardization, external calibration, standard addition, isotope dilution, matrix matched standards, film coating and ink jet printing. [176,284,345,346,347,292]

The retina is part of the central nervous system, and if Zn in the retina is bound in the same way as Zn in the brain, then it is likely that the total histochemically active (free) Zn is only around 10% of the total. Excess levels of "free" or loosely bound metal ions may cause toxic effects. The histochemical approaches have limitations in mapping Zn all over the retina as they can determine only loosely bound Zn. As the level of Zn is high in the retina, a large number of Zn ions are tightly bound to proteins and other molecules to ensure normal retinal function. Therefore, it is useful to combine elemental bio-imaging with molecular imaging techniques to provide complementary information to study the relationship between Zn and protein in human eye sections. For instance, the combination of LA-ICP-MS and matrix-assisted desorption/ionisation (MALDI) MS has broad potential to map the distribution of specific analytes bound with protein or molecules within biological systems. This technique could be applied to the retinal tissues or any biological tissue to enhance the growing field of spatially-resolved proteomics and thus get broad information and detect relationships between proteins associated with disease and specific trace elements. Grey et.al reported[348] experiments using MALDI-MS to identify the distribution of integral membrane proteins in human and bovine lens and retinal tissue. Also, Zn is mainly associated with low molecular mass proteins (e.g. MTs), hence quantitative speciation of Zn and other essential trace elements employing HPLC-ICP-MS to study their protein binding profile is highly important to gain a comprehensive understanding of the essential impact of metals and metal-binding proteins in the retina and RPE (or eye). The combination of LA-ICP-MS with LC-MS/MS and MALDI-MS is crucial to build protein-specific maps of tissue sections. Another bioimaging technique which showed a high potential for the analysis of metalloproteins in

ocular tissue sections is LA-ICP-MS using metal-tagged immunoprobes. This recent analytical technique can provide elemental and molecular information necessary to understand the roles of proteins in retinal sections.[349] Identifying and quantifying total (tightly and loosely bound) Zn in the different layers of the retina is crucial for future studies to achieve a better understanding of the functional importance of endogenous trace elements, possible toxic effects and their participation in retinal diseases.

Several aspects of the homeostasis of Zn and Cu in the retina are only partly understood and more research is required to elucidate these issues. More comprehensive information is essential to understand how Zn and Cu are carried on by the retina from blood; the turnover, interaction between RPE cells and photoreceptors together with their direct and/or indirect exchanges. Moreover, the influence of these metals on the pathogenesis of diseases including AMD needs additional study as modulating levels may provide a feasible therapeutic strategy.

Recommendations for strategies to bring enhancements in sensitivity, reliability of results, speed of experiments and data collection are listed as follows:[338,350,284,266,324]

- Sector-field ICP-MS, as used in this work, delivered adequate sensitivity for the applications described, but suffers from an inability to measure multiple isotopes in rapid succession (i.e. within the timeframe of a single LA peak). Quadrupole mass analysers are the most common choice in current ICP-MS instruments, due to their low cost and rapid scan capability. The best choice for simultaneous multi-elemental analysis could be TOF mass spectrometers. However, these two mass spectrometers provide 10-50 fold less sensitivity than sector-field instruments. Therefore, the best type of mass spectrometer for biological samples is still unclear and no commercial ICP-MS instrument available has all the desired attributes for highly sensitive multi-element analysis and bio-imaging.

- The LA cell design and the transfer tube affect the dispersion of the sample aerosol, sample transport efficiency and signal profile. Minimizing ablation cell volume and transfer tube length result in a low dispersion and thus allows fast and sensitive line scanning, fast wash-out time and reduced peak width.

- The use of ultra-short pulse lasers reduces target heating, minimizes volatility and fractionation, and improves accuracy and precision. Femtosecond lasers have the potential to further advance image resolution, making new research areas possible.

- 2D LA-ICP-MS imaging technique has led to a relatively new generation of 3D LA-ICP-MS imaging using acquisition of sequential layers of the target and developing this imaging approach would be extremely beneficial in biological/analytical research in the future.

- Improving sample stage automation and consistency of laser stage positioning would allow controlled scanning over a large area.

- Single cell imaging by LA-ICP-MS can provide appropriate information about metals' uptake and mobility, metabolic routes, metallodrugs and NPs' behaviour and release. Single cell analysis is valued in pharmaceutical research and development of new drugs. However, spatial resolution of LA-ICP-MS still needs improvement to facilitate imaging at the single-cell and cell organelles scale range.

- Software development is needed to manage the large and complex data sets produced by new laser systems, in particular when applied to clinical diagnosis. Software automation would be useful in a commercial instrument, to complement the increased analysis speed.

- The most significant aspect is waiting for these research findings to be commercialised because for bio-medical applications systems have to be robust, automated and easy to use.

Overall, the determination of key elements in biological samples such as serum, tissues and cells shows great potential. The biomedical research community seems to be moving towards looking at individual cells, and individual cell processes, so measuring elements within the cell or within specific biological structures, such as measuring Zn in RPE cells as mentioned earlier, is a promising direction for future research.

# 7 References

1    O. Selenius, B. Alloway, J. Centano, R. Finkelman, R. Fuge, U. Lindh, P. Smedley, Essentials of Medical Geology, Elsevier Academic Press, Tokyo, 2005.

2    N. Jakubowski, R. Lobinski and L. Moens, *J. Anal. At. Spectrom.*, 2004, **19**, 1–4.

3    C. E. Outten and T. V. O'Halloran, *Science*, 2001, **292**, 2488–2492.

4    W. Mertz, *Science*, 1981, **213**, 1332–1338.

5    B. R. Roberts, T. M. Ryan, A. I. Bush, C. L. Masters and J. A. Duce, *J. Neurochem.*, 2012, **120**, 149–166.

6    E. J. McAllum and D. I. Finkelstein, *J Mol Neurosci*, 2016, **60**, 279–288.

7    Y. Zhang, J. F. Clark, G. Pyne-Geithman and J. Caruso, *Metallomics*, 2010, **2**, 628–637.

8    S. A. Becherer and A. White, *J. Emerg. Nurs.*, 2010, **36**, 130–133.

9    M. Schaefer and J. D. Gitlin, *Am J Physiol*, 1999, **276**, G311–G314.

10    N. Lakdawala and J. M. Grant-Kels, *Clin. Dermatol.*, 2015, **33**, 414–419.

11    Z. Ullah, M. I. Ullah, S. Hussain, H. Kaul and K. P. Lone, *Biol. Trace Elem. Res.*, 2017, **175**, 10–16.

12    R. T. Ribeiro, D. Dos Santos-Neto, P. Braga-Neto and O. G. P. Barsottini, *Clin. Neurol. Neurosurg.*, 2013, **115**, 1536–1538.

13    M. A. Avelino, E. F. Fusão, J. L. Pedroso, J. H. Arita, R. T. Ribeiro, R. S. Pinho, K. Tuschl, O. G. P. Barsottini and M. R. Masruha, *J. Neurol. Sci.*, 2014, **341**, 150–152.

14    K. Gellein, PhD Thesis, Department of Chemistry, Norwegian University of Science and Technology, 2008.

15    L. Baum, I. H. S. Chan, S. K. K. Cheung, W. B. Goggins, V. Mok, L. Lam, V. Leung, E. Hui, C. Ng, J. Woo, H. F. K. Chiu, B. C. Y. Zee, W. Cheng, M. H. Chan, S. Szeto, V. Lui, J. Tsoh, A. I. Bush, C. W. K. Lam and T. Kwok, *Biometals*, 2010, **23**, 173–179.

16    N. Tabet, D. Mantle, Z. Walker and M. Orrell, *Int Psychogeriatr*, 2001, **13**, 265–275.

17    G. J. Brewer, S. H. Kanzer, E. A. Zimmerman, E. S. Molho, D. F. Celmins, S. M. Heckman and R. Dick, *Am. J. Alzheimers. Dis. Other Demen.*, 2010, **25**, 572–575.

18    M. Loef, N. V. Stillfried and H. Walach, *Nutr. Neurosci.*, 2012, **15**, 2–12.

19    World Health Organization, Environmental Health Criteria 221: Zinc, World Health Organization, Geneva, 2001.

20    R. Agarwal, S. Kushwaha, C. Tripathi, N. Singh and N. Chhillar, *Indian J. Clin. Biochem.*, 2008, **23**, 369–374.

21    V. Solfrizzi, F. Panza, V. Frisardi, D. Seripa, G. Logroscino, B. Imbimbo and A. Pilotto, *Expert Rev. Neurother.*, 2011, **11**, 677–708.

22    M. Loef and H. Walach, *Br. J. Nutr.*, 2012, **107**, 7–19.

23    R. Squitti, M. Siotto and R. Polimanti, *Neurobiol. Aging*, 2014, **35**, 40–50.

24    S. Gardener, Y. Gu, S. R. Rainey-Smith, J. B. Keogh, P. M. Clifton, S. L. Mathieson, K. Taddei, A. Mondal, V. K. Ward, N. Scarmeas, M. Barnes, K. A. Ellis, R. Head, C. L. Masters, D. Ames, S. L. Macaulay, C. C. Rowe, C. Szoeke and R. N. Martins, *Transl. Psychiatry*, 2012, **2**, 1–7.

25    G. Li, PhD Thesis, Department of Chemistry, Missouri-Columbia University, 2012.

26    K. Grungeriff, *J. Trace Elem. Exp. Med.*, 2002, **15**, 67–78.

27    C. F. Mills, Zinc in Human Biology, Springer-Verlag Berlin Heidelberg, New York, 1989.

28    J. E. Cummings and J. P. Kovacic, *J. Vet. Emerg. Crit. Care*, 2009, **19**, 215–240.

29    K. B. Handing, I. G. Shabalin, O. Kassaar, S. Khazaipoul, C. A. Blindauer, A. J. Stewart, M. Chruszcz and W. Minor, *Chem. Sci.*, 2016, **7**, 6635–6648.

30    T. Kambe, T. Fukada and S. Toyokuni, *Arch. Biochem. Biophys.*, 2016, **611**, 1–2.

31    G. Nowak, M. Siwek, D. Dudek, A. Ziêba and A. Pilc, *Polish J. Pharmacol. Pol. J. Pharmacol*, 2003, **55**, 1143–1147.

32    H. Tapiero and K. D. Tew, *Biomed. Pharmacother.*, 2003, **57**, 399–411.

33    M. Maciążek-Jurczyk, A. Szkudlarek, M. Chudzik, J. Pożycka and A. Sułkowska, *Spectrochim. Acta Part A Mol. Biomol. Spectrosc.*, 2018, **188**, 675–683.

34    A. Takeda, *BioMetals*, 2001, **14**, 343–351.

35    C. Corona, A. Pensalfini, V. Frazzini and S. L. Sensi, *Cell Death Dis.*, 2011, **2**, 176–186.

36    Y. Zheng, X. Xu, Z. Xu, J. Wang, H. Cai, Metallic Biomaterials: New Directions and Technologies, Wiley, Weinheim, Germany, 2017.

37    L. Castro and B. A. Freeman, *Nutrition*, 2001, **17**, 161–165.

38    P. A. Lachance, Z. Nakat and W. S. Jeong, *Nutrition*, 2001, **17**, 835–838.

39    O. Müller and M. Krawinkel, *Can. Med. Assoc. J.*, 2005, **173**, 279–86.

40    N. Barzegar Beforoei, PhD Thesis, Department of of Ocular Biology and Therapeutics,Institute of Ophthalmology,University College London, 2013.

41    D. Galaris and A. Evangelou, *Crit. Rev. Oncol. Hematol.*, 2002, **42**, 93–103.

42    N. K. Wills, V. M. Sadagopa Ramanujam, N. Kalariya, J. R. Lewis and F. J. G. M. Van Kuijk, *Exp. Eye Res.*, 2008, **87**, 80–88.

43    G. S. Devi, M. H. Prasad, I. Saraswathi, D. Raghu, D. N. Rao and P. P. Reddy, *Clin. Chim. Acta*, 2000, **293**, 53–62.

44     M. Bost, S. Houdart, M. Oberli, E. Kalonji, J. F. Huneau and I. Margaritis, *J. Trace Elem. Med. Biol.*, 2016, **35**, 107–115.

45     C. J. Gubler, M. E. Lahey, G. E. Cartwright and M. M. Wintrobe, *J. Clin. Invest.*, 1953, **32**, 405–414.

46     Z. L. Harris and J. D. Gitlin, *Am. J. Clin. Nutr.*, 1996, **63**, 836–841.

47     L. M. Gaetke and C. K. Chow, *Toxicology*, 2003, **189**, 147–163.

48     E. E. Battin, M. T. Zimmerman, R. R. Ramoutar, C. E. Quarles and J. L. Brumaghim, *Metallomics*, 2011, **3**, 503–512.

49     J. R. Turnlund, W. R. Keyes, G. L. Peiffer and K. C. Scott, *Am. J. Clin. Nutr.*, 1998, **67**, 1219–1225.

50     R. Barrera, *Nutr. Clin. Pract.*, 2003, **18**, 529–532.

51     W. Maret and H. H. Sandstead, *J. Trace Elem. Med. Biol.*, 2006, **20**, 3–18.

52     B. M. Todorich and J. R. Connor, *Ann. N.Y. Acad. Sci.*, 2004, **1012**, 171–178.

53     Z. Yang, K. G. Dewey, B. Lönnerdal, O. Hernell, C. Chaparro, S. Adu-Afarwuah, E. D. McLean, R. J. Cohen, M. Domellöf, L. H. Allen and K. H. Brown, *Am. J. Clin. Nutr.*, 2008, **87**, 1892–1898.

54     H. Xu, H. Jiang and J. Xie, *Front. Mol. Neurosci.*, 2017, **10**, 1–10.

55     J. Bornhorst, A. P. Kipp, H. Haase, S. Meyer and T. Schwerdtle, *TrAC - Trends Anal. Chem.*, 2017, **IN PRESS**, 1–8.

56     V. Günther, U. Lindert and W. Schaffner, *Biochim. Biophys. Acta - Mol. Cell Res.*, 2012, **1823**, 1416–1425.

57     A. C. Illing, A. Shawki, C. L. Cunningham and B. Mackenzie, *J. Biol. Chem.*, 2012, **287**, 30485–30496.

58     J. Osredkar and S. Natasa, *J. Clin. Toxicol.*, 2011, **3**, 1–18.

59      D. Roy, G. J. Steyer, M. Gargesha, M. E. Stone and L. Wilson, 2009, **292**, 342–351.

60      R. Giacconi, L. Costarelli, F. Piacenza, A. Basso, L. Rink, E. Mariani, T. Fulop, G. Dedoussis, G. Herbein, M. Provinciali, J. Jajte, I. Lengyel, E. Mocchegiani and M. Malavolta, *Eur. J. Nutr.*, 2017, **56**, 2457–2466.

61      R. Lobinski, J. S. Becker, H. Haraguchi and B. Sarkar, *Pure Appl. Chem.*, 2010, **82**, 493–504.

62      D. W. Koppenaal and G. M. Hieftje, *J. Anal. At. Spectrom.*, 2007, **22**, 111.

63      Z. Qin, J. A. Caruso, B. Lai, A. Matusch and J. S. Becker, *Metallomics*, 2011, **3**, 28–37.

64      W. Shi and M. R. Chance, *Curr. Opin. Chem. Biol.*, 2011, **15**, 144–148.

65      R. Ge and H. Sun, *Sci. China Ser. B Chem.*, 2009, **52**, 2055–2070.

66      C. Andreini, I. Bertini and A. Rosato, *Acc. Chem. Res.*, 2009, **42**, 1471–1479.

67      J. Szpunar, *Anal. Bioanal. Chem.*, 2004, **378**, 54–56.

68      M. Malavolta, F. Piacenza, L. Costarelli, R. Giacconi, E. Muti, C. Cipriano, S. Tesei, S. Spezia and E. Mocchegiani, *J. Anal. At. Spectrom.*, 2007, **22**, 1193–1198.

69      M. Vašák, *J. Trace Elem. Med. Biol.*, 2005, **19**, 13–17.

70      R. González-Domínguez, T. García-Barrera and J. L. Gómez-Ariza, *BioMetals*, 2014, **27**, 539–549.

71      D. M. Templeton, F. Ariese, R. Cornelis, L. Danielsson, H. Muntau, H. P. Van Leeuwen and R. LobinsK, *Pure Appl. Chem.*, 2000, **72**, 1453–1470.

72      A. Rembach, D. J. Hare, J. D. Doecke, S. C. Burnham, I. Volitakis, C. J. Fowler, R. A. Cherny, C. McLean, R. Grimm, R. Martins, D. Ames, C. L. Masters, A. I. Bush and B. R. Roberts, *Metallomics*, 2014, **6**, 1216–1219.

73      I. Beheshti, H. Demirel and H. Matsuda, *Comput. Biol. Med.*, 2017, **83**, 109–119.

74     N. Braidy, A. Poljak, C. Marjo, H. Rutlidge, A. Rich, T. Jayasena, N. C. Inestrosa and P. Sachdev, *Front. Aging Neurosci.*, 2014, **6**, 1–14.

75     I. O. Korolev, *Med. Student Res. J.*, 2014, **4**, 24–33.

76     I. Shcherbatykh and D. O. Carpenter, *J. Alzheimer's Dis.*, 2007, **11**, 191–205.

77     K. Kaarniranta, A. Salminen, A. Haapasalo, H. Soininen and M. Hiltunen, *J. Alzheimer's Dis.*, 2011, **24**, 615–631.

78     M. A. Lovell, J. D. Robertson, W. J. Teesdale, J. L. Campbell and W. R. Markesbery, *J. Neurol. Sci.*, 1998, **158**, 47–52.

79     S. Ayton, P. Lei and A. I. Bush, *Free Radic. Biol. Med.*, 2013, **62**, 76–89.

80     C. L. Lee and T. M. Pan, *Appl. Microbiol. Biotechnol.*, 2011, **91**, 461–469.

81     M. Azhdarzadeh, M. Noroozian, H. Aghaverdi, S. M. Akbari, L. Baum and M. Mahmoudi, *Sci. Rep.*, 2013, **3**, 2782–2787.

82     R. González-Domínguez, T. García-Barrera and J. L. Gómez-Ariza, *Metallomics*, 2014, **6**, 292–300.

83     J. Dong, J. D. Robertson, W. R. Markesbery and M. A. Lovell, *J Alzheimers Dis.*, 2009, **15**, 443–450.

84     Medical illustration courtesy of Alzheimer's Disease Research, a BrightFocus Foundation program. www.brightfocus.org/alzheimers.

85     B. Sedighi, M. Shafa and M. Shariati, *Neurol. Asia*, 2006, **11**, 107–109.

86     R. Anand, K. D. Gill and A. A. Mahdi, *Neuropharmacology*, 2014, **76**, 27–50.

87     C. Smorgon, E. Mari, A. R. Atti, E. D. Nora, P. F. Zamboni, F. Calzoni, A. Passaro and R. Fellin, *Arch. Gerontol. Geriatr. Suppl.*, 2004, **38**, 393–402.

88     E. Mocchegiani, C. Bertoni-Freddari, F. Marcellini and M. Malavolta, *Prog. Neurobiol.*, 2005, **75**, 367–390.

89    R. Stewart, *J Neurol Neurosurg Psychiatry*, 1998, **65**, 143–147.

90    S. Ayton, P. Lei and A. I. Bush, *Neurotherapeutics*, 2015, **12**, 109–120.

91    D. Hare, S. Ayton, A. Bush and P. Lei, *Front. Aging Neurosci.*, 2013, **5**, 1–19.

92    J. A. Duce and A. I. Bush, *Prog. Neurobiol.*, 2010, **92**, 1–18.

93    M. Azuma, K. Chung, A. Fujii and T. R. Shearer, *J. Ocul. Pharmacol. Ther.*, 2010, **26**, 367–371.

94    I. Lengyel and T. Peto, *Expert Rev. Ophthalmol.*, 2008, **3**, 1–4.

95    R. V. Leeuwen, S. Boekhoorn, J. R. Vingerling, J. C. M. Witteman, C. C. W. Klaver, A. Hofman and P. T. V. M. De Jong, *J. Am. Med. Assoc.*, 2005, **294**, 3101–3107.

96    E. Cho, M. J. Stampfer, J. M. Seddon, S. Hung, D. Spiegelman, E. B. Rimm, W. C. Willett and S. E. Hankinson, *Ann. Epidemiol.*, 2001, **11**, 328–336.

97    P. S. Prasad, S. D. Schwartz and J. Hubschman, *Maturitas*, 2010, **66**, 46–50.

98    U. Chakravarthy, J. Evans and P. J. Rosenfeld, *BMJ*, 2010, **340**, 526–530.

99    H. R. Coleman, C. Chan, F. L. Ferris and E. Y. Chew, *Lancet*, 2008, **372**, 1835–1845.

100   R. F. Mullins, S. R. Russell, D. H. Anderson and G. S. Hageman, *FASEB J.*, 2000, **14**, 835–846.

101   I. Lengyel, T. Peto, A. Bird and F. Vankuijk, *Exp. Eye Res.*, 2008, **86**, 862–863.

102   J. Ambati, J. P. Atkinson and B. D. Gelfand, *Nat Rev Immunol*, 2013, **13**, 438–451.

103   E. Stefánsson, A. Geirsdóttir and H. Sigurdsson, *Prog. Retin. Eye Res.*, 2011, **30**, 72–80.

104   E. W. Chong, T. Y. Wong, A. J. Kreis, J. A. Simpson and R. H. Guymer, *BMJ*, 2007, **335**, 755–762.

105   J. R. Evans, A. E. Fletcher and R. P. L. Wormald, *Br. J. Ophthalmol.*, 2005, **89**, 550–553.

106   H. Coleman and E. Chew, 2007, **18**, 220–223.

107   F. G. Holz and R. F. Spaide, Medical Retina, Springer Berlin Heidelberg, NewYork, 2007.

108   J. Evans, *BMJ*, 2007, **335**, 729–734.

109   I. Lengyel, J. M. Flinn, T. Peto, D. H. Linkous, K. Cano, A. C. Bird, A. Lanzirotti, C. J. Frederickson and F. J. G. M. Van Kuijk, *Exp. Eye Res.*, 2007, **84**, 772–780.

110   J. R. Evans, *Prog. Retin. Eye Res.*, 2001, **20**, 227–253.

111   P. Mitchell, J. J. Wang, S. Foran and W. Smith, *Ophthalmology*, 2002, **109**, 1092–1097.

112   B. N. Mukesh, P. N. Dimitrov, S. Leikin, J. J. Wang, P. Mitchell, C. A. McCarty and H. R. Taylor, *Ophthalmology*, 2004, **111**, 1176–1182.

113   R. Klein, B. E. Klein, S. C. Jensen, J. A. Mares-Perlman, K. J. Cruickshanks and M. Palta, *Ophthalmology*, 1999, **106**, 1056–1065.

114   P. L. Penfold, M. C. Madigan, M. C. Gillies and J. M. Provis, *Prog. Retin. Eye Res.*, 2001, **20**, 385–414.

115   L. A. Donoso, T. Vrabec and H. Kuivaniemi, *Surv. Ophthalmol.*, 2010, **55**, 227–246.

116   R. Klein, C. Zeiss, E. Chew and J. Tsai, *Science*, 2005, **308**, 385–389.

117   R. Nan, J. Gor, I. Lengyel and S. J. Perkins, *J. Mol. Biol.*, 2008, **384**, 1341–52.

118   J. Haines, M. Hauser, S. Schmidt, W. Scott, L. Olson, P. Gallins, K. Spencer, S. Kwan, M. Noureddine, J. Gilbert, N. Schnetz-Boutaud, A. Agarwal, E. Postel and M. Pericak-Vance, *Science*, 2005, **308**, 419–421.

119   R. Nan, I. Farabella, F. F. Schumacher, A. Miller, J. Gor, A. C. R. Martin, D. T.

Jones, I. Lengyel and S. J. Perkins, *J. Mol. Biol.*, 2011, **408**, 714–735.

120    D. Bok, *Proc. Natl. Acad. Sci.*, 2005, **102**, 7053–7054.

121    R. Nan, G. Ward, L. Gavigan, A. Miller, J. Gor, I. Lengyel and S. J. Perkins, *Mol. Immunol.*, 2010, **47**, 2263.

122    R. Nan, J. Gor, I. Lengyel and S. Perkins, *Mol. Immunol.*, 2008, **45**, 4126–4127.

123    S. P. Kelly, J. Thornton, G. Lyratzopoulos, R. Edwards and P. Mitchell, *BMJ*, 2004, **328**, 537–538.

124    C. Delcourt, J. Diaz, A. Sanchez and L. Papoz, *Arch. Ophthalmol.*, 1998, **116**, 1031–1035.

125    P. P. Connell, P. A.Keane, E. C.O'Neill, R. Altaie, E. Loane, KumariNeelam, A. John M.Nolan and S. Beatty, *J. Ophthalmol.*, 2009, **2009**, 1–39.

126    W. Smith, P. Mitchell and S. R. Leeder, *Arch. Ophthalmol.*, 1996, **114**, 1518–1523.

127    J. S. L. Tan, P. Mitchell, A. Kifley, V. Flood, W. Smith and J. J. Wang, *Arch. Ophthalmol.*, 2007, **125**, 1089–1095.

128    W. G. Christen, R. J. Glynn, J. E. Manson, U. A. Ajani and J. E. Buring, *J. Am. Med. Assoc.*, 1996, **276**, 1147–1151.

129    J. M. Seddon, W. C. Willett, F. E. Speizer and S. E. Hankinson, *J. Am. Med. Assoc.*, 1996, **276**, 1141–1146.

130    J. Thornton, R. Edwards, P. Mitchell, R. A. Harrison, I. Buchan and S. P. Kelly, *Eye*, 2005, **19**, 935–44.

131    E. J. Joohnson, *Curr Opin Clin Nutr Metab Care*, 2010, **13**, 28–33.

132    S. Tomany, K. Cruickshanks, R. Klein, B. Klein and M. Knudtson, *Arch Ophthalmol.*, 2004, **122**, 750–757.

133    E. Cho, S. Hung, W. Willett, D. Spiegelman, E. Rimm, J. Seddon, G. Colditz and S.

Hankinson, *Am. J. Clin. Nutr.*, 2001, **73**, 209–218.

134    A. S. Prasad, *J. Am. Coll. Nutr.*, 2009, **28**, 257–265.

135    J. Mares-Perlman, W. Brady, R. Klein, B. Klein, P. Bowen, M. Stacewicz-Sapuntzakis and M. Palta, *Arch Ophthalmol.*, 1995, **113**, 1518–1523.

136    E. J. Johnson and E. J. Schaefer, *Am. J. Clin. Nutr.*, 2006, **83**, 1494S–1498S.

137    B. Chua, V. Flood, E. Rochtchina, J. J. Wang, W. Smith and P. Mitchell, *Arch. Ophthalmol.*, 2006, **124**, 981–986.

138    W. Christen, D. Schaumberg, R. Glynn and J. Buring, *Arch Ophthalmol*, 2011, **129**, 921–929.

139    L. Hyman, A. P. Schachat, Q. He and M. C. Leske, *Arch Ophthalmol.*, 2000, **118**, 351–358.

140    R. E. Hogg, J. V. Woodside, S. E. C. M. Gilchrist, R. Graydon, A. E. Fletcher, W. Chan, A. Knox, B. Cartmill and U. Chakravarthy, *Ophthalmology*, 2008, **115**, 1046–1052.

141    S. C. Tomany, J. J. Wang, R. V. Leeuwen, R. Klein, P. Mitchell, J. R. Vingerling, B. E. K. Klein, W. Smith and P. T. V. M. De Jong, *Ophthalmology*, 2004, **111**, 1280–1287.

142    J. R. Vingerling, I. Dielemans, M. L. Bots, A. Hofman, D. E. Grobbee and P. T. V. M. De Jong, *Am J Epidemiol*, 1995, **142**, 404–409.

143    T. E. Clemons, N. Kurinij and R. D. Sperduto, *Arch. Ophthalmol.*, 2004, **122**, 716–26.

144    A. E. Fletcher, G. C. Bentham, M. Agnew, I. S. Young, C. Augood, U. Chakravarthy, P. T. V. M. De Jong, M. Rahu, J. Seland, G. Soubrane, L. Tomazzoli, F. Topouzis, J. R. Vingerling and J. Vioque, *Arch. Ophthalmol.*, 2008, **126**, 1396–403.

145    Age-Related Eye Disease Study Research Group, *Arch Ophthalmol*, 2001, **119**, 1417–1436.

146    S. Hughes and S. Samman, *J. Am. Coll. Nutr.*, 2006, **25**, 285–291.

147    N. M. Lowe, K. Fekete and Tama´s Decsi, *Am. J. Clin. Nutr.*, 2009, **89**, 2040–2051.

148    L. M. Jampol and F. L. Ferris, *J. Am. Med. Assoc.*, 2001, **286**, 2466–2468.

149    M. E. Hartnett, N. Tinkham, L. Paynter, P. Geisen, G. Koch and K. L. Cohen, 2010, **148**, 895–901.

150    W. Shi and M. R. Chance, *Cell. Mol. life Sci.*, 2008, **65**, 3040–3048.

151    N. Jakubowski, L. Moens and F. Vanhaecke, *Spectrochim. Acta Part B At. Spectrosc.*, 1998, **53**, 1739–1763.

152    R. Thomas, Practical Guide to ICP-MS, Marcel Dekker, New York, 2004.

153    E. Hoffmann and V. Stroobant, Mass Spectrometry: Principles and Applications, John Wiley & Sons, Chichester, England, 2007.

154    S. F. Durrant, *J. Anal. At. Spectrom.*, 1999, **14**, 1385–1403.

155    M. Montes-Bayón, K. DeNicola and J. A. Caruso, *J. Chromatogr. A*, 2003, **1000**, 457–76.

156    G. Alvarez-Llamas, M. R. F. laCampa and A. Sanz-Medel, *Trends Anal. Chem.*, 2005, **24**, 28–36.

157    J. S. Becker and N. Jakubowski, *Chem. Soc. Rev.*, 2009, **38**, 1969–83.

158    J. A. Horner, S. A. Lehn and G. M. Hieftje, *Spectrochim. Acta - Part B At. Spectrosc.*, 2002, **57**, 1025–1042.

159    C. Rappel and D. Schaumloeffel, *J. Anal. At. Spectrom.*, 2010, **25**, 1963–1968.

160    S. J. Hill, Inductively Coupled Plasma Spectrometry and its Applications, Blackwell Publishing, Oxford, 2007.

161   Element 2 Operator manual – Rev 2, Thermo Finnigan, 2001.

162   Thermo-Finnigan, Element 2XR Hardware Manual, Revision A-119 1410, 2005.

163   A. L. Gray, *Analyst*, 1985, **110**, 551–556.

164   M. Gastel, J. S. Becker, G. Küppers and H. J. Dietze, *Spectrochim. Acta B*, 1997, **52**, 2051–2059.

165   M. C. Santos, M. Wagner, B. Wu, J. Scheider, J. Oehlmann, S. Cadore and J. S. Becker, *Talanta*, 2009, **80**, 428–433.

166   C. Giesen, L. Waentig, T. Mairinger, D. Drescher, J. Kneipp, P. H. Roos, U. Panne and N. Jakubowski, *J. Anal. At. Spectrom.*, 2011, **26**, 2160–2165.

167   G. S. Pessôa, C. A. L. Júnior, K. C. Madrid and M. A. Z. Arruda, *Talanta*, 2017, **167**, 317–324.

168   F. Vanhaecke, M. Resano, J. Koch, K. McIntosh and D. Gunther, *J. Anal. At. Spectrom.*, 2010, **25**, 1259–1267.

169   B. Jackson, S. Harper, L. Smith and J. Flinn, *Anal. Bioanal. Chem.*, 2006, **384**, 951–957.

170   I. Konz, B. Fernández, M. L. Fernández, R. Pereiro, H. González-Iglesias, M. Coca-Prados and A. Sanz-Medel, *Anal. Bioanal. Chem.*, 2014, **406**, 2343–2348.

171   C. Austin, D. Hare, A. L. Rozelle, W. H. Robinson, R. Grimm and P. Doble, *Metallomics*, 2009, **1**, 142–147.

172   D. Hare, F. Burger, C. Austin, F. Fryer, R. Grimm, B. Reedy, R. A. Scolyer, J. F. Thompson and P. Doble, *Analyst*, 2009, **134**, 450–453.

173   A. Kindness, C. N. Sekaran and J. Feldmann, *Clin Chem*, 2003, **49**, 1916–1923.

174   A. J. Managh, PhD Thesis, Department of Chemistry, Loughborough University, 2014.

175     D. Günther, S. E. Jackson and H. P. Longerich, *Spectrochim. acta, Part B At. Spectrosc.*, 1999, **54**, 381–409.

176     D. Pozebon, G. L. Scheffler, V. L. Dressler and M. A. G. Nunes, *J. Anal. At. Spectrom.*, 2014, **29**, 2204–2228.

177     J. S. Becker, *Int. J. Mass Spectrom.*, 2010, **289**, 65–75.

178     R. E. Russo, X. Mao, H. Liu, J. Gonzalez and S. S. Mao, *Talanta*, 2002, **57**, 425–51.

179     P. K. Diwakar, S. S. Harilal, N. L. LaHaye, A. Hassanein and P. Kulkarni, *J. Anal. At. Spectrom.*, 2013, **28**, 1420–1429.

180     I. Horn and D. Günther, *Appl. Surf. Sci.*, 2003, **207**, 144–157.

181     J. L. Luque-Garcia and T. A. Neubert, *J. Chromatogr. A*, 2007, **1153**, 259–276.

182     H. Vanhoe, R. Dams and J. Versieck, *J. Anal. At. Spectrom.*, 1994, **9**, 23–31.

183     J. M. Harrington, D. J. Young, A. S. Essader, S. J. Sumner and K. E. Levine, *Biol. Trace Elem. Res.*, 2014, **160**, 132–142.

184     Y. Lu, M. Kippler, F. Harari, M. Grandér, B. Palm, H. Nordqvist and M. Vahter, *Clin. Biochem.*, 2015, **48**, 140–147.

185     C. S. Muniz, J. M. Marchante-Gayon, J. I. G. Alonso and A. Sanz-Medel, *J. Anal. At. Spectrom*, 1999, **14**, 193–198.

186     M. Ugarte, N. N. Osborne, L. A. Brown and P. N. Bishop, *Surv. Ophthalmol.*, 2013, **58**, 585–609.

187     S. García-Castiñeiras, *Exp. Eye Res.*, 2010, **90**, 664–678.

188     J. L. Dunaief, *Investig. Ophthalmol. Vis. Sci.*, 2006, **47**, 4660–4664.

189     J. C. Erie, J. A. Good, J. A. Butz and J. S. Pulido, *Am. J. Ophthalmol.*, 2009, **147**, 276–282.

190     O. Al Gwairi, L. Thach, W. Zheng, N. Osman and P. J. Little, *J. Ophthalmol.*, 2016,

**2016**, 1–7.

191    P. Hahn, G. S. Ying, J. Beard and J. L. Dunaief, *Neuroreport*, 2006, **17**, 1803–1806.

192    H. Haase and L. Rink, *Immun. Ageing*, 2009, **6**, 1–17.

193    M. Malavolta, F. Piacenza, A. Basso, R. Giacconi, L. Costarelli and E. Mocchegiani, *Mech. Ageing Dev.*, 2015, **151**, 93–100.

194    H. Kozlowski, A. Janicka-Klos, J. Brasun, E. Gaggelli, D. Valensin and G. Valensin, *Coord. Chem. Rev.*, 2009, **253**, 2665–2685.

195    K. Zabłocka-Słowińska, S. Płaczkowska, A. Prescha, K. Pawełczyk, I. Porębska, M. Kosacka, L. Pawlik-Sobecka and H. Grajeta, *J. Trace Elem. Med. Biol.*, 2018, **45**, 78–84.

196    H. Vural, H. Demirin, Y. Kara, I. Eren and N. Delibas, *J. Trace Elem. Med. Biol.*, 2010, **24**, 169–173.

197    H. Kozlowski, A. Janicka-Klos, J. Brasun, E. Gaggelli, D. Valensin and G. Valensin, *Coord. Chem. Rev.*, 2009, **253**, 2665–2685.

198    A. I. Bush, W. H. Pettingell, G. Multhaup, M. D. Paradis, J. P. Vonsattel, J. F. Gusella, K. Beyreuther, C. L. Masters and R. E. Tanzi, *Science*, 1994, **265**, 1464–1467.

199    D. Religa, D. Strozyk, R. Cherny, I. Volitakis, V. Haroutunian, B. Winblad, J. Naslund and A. Bush, *Neurology*, 2006, **67**, 69–75.

200    A. Alimonti, G. Ristori, F. Giubilei, M. A. Stazi, A. Pino, A. Visconti, S. Brescianini, M. S. Monti, G. Forte, P. Stanzione, B. Bocca, G. Bomboi, C. D'Ippolito, V. Annibali, M. Salvetti and G. Sancesario, *Neurotoxicology*, 2007, **28**, 450–456.

201    L. L. Rulon, J. D. Robertson, M. A. Lovell, M. A. Deibel, W. D. Ehmann and W. R. Markesber, *Biol Trace Elem Res*, 2000, **75**, 79–85.

202   M. Ventriglia, G. J. Brewer, I. Simonelli, S. Mariani, M. Siotto, S. Bucossi and R. Squitti, *J. Alzheimer's Dis.*, 2015, **46**, 75–87.

203   L. Gerhardsson, T. Lundh, L. Minthon and E. Londos, *Dement Geriatr Cogn Disord*, 2008, **25**, 508–515.

204   C. Gonzalez, T. Martin, J. Cacho, M. T. Brenas, T. Arroyo, B. Garcia-Berrocal, J. A. Navajo and J. M. Gonzalez-Buitrago, *Eur. J. Clin. Invest.*, 1999, **29**, 637–642.

205   R. Ozcankaya and N. Delibas, *Croat Med J*, 2002, **43**, 28–32.

206   F. Björkstén, A. Aromaa, P. Knekt and L. Malinen, *Acta Med Scand*, 1978, **204**, 67–74.

207   I. M. Rea, *Nutr. Res.*, 1989, **9**, 121–125.

208   Z. Wang, L. Tan, H. Wang, J. Ma, J. Liu, M. Tan, J. Sun, X. Zhu, T. Jiang and J. Yu, *J. Alzheimer's Dis.*, 2015, **47**, 565–581.

209   P. E. Johnson, D. B. Milne and G. I. Lykken, *Am. J. Clin. Nutr.*, 1992, **56**, 917–925.

210   M. Ventriglia, S. Bucossi, V. Panetta and R. Squitti, *J. Alzheimers. Dis.*, 2012, **30**, 981–984.

211   S. Bucossi, M. Ventriglia, V. Panetta, C. Salustri, P. Pasqualetti, S. Mariani, M. Siotto, P. M. Rossini and R. Squitti, *J. Alzheimer's Dis.*, 2011, **24**, 175–185.

212   H. Haraguchi, *J. Anal. At. Spectrom.*, 2004, **19**, 5–14.

213   J. Begerow, M. Turfeld and L. Dunemann, *J. Anal. At. Spectrom.*, 2000, **15**, 347–352.

214   J. Szpunar, J. Bettmer, M. Robert, H. Chassaigne, K. Cammann, R. Lobinski and O. F. X. Donard, *Talanta*, 1997, **44**, 1389–1396.

215   M. He, L. Huang, B. Zhao, B. Chen and B. Hu, *Anal. Chim. Acta*, 2017, **973**, 1–24.

216   H. Vanhoe, C. Vandecasteele, J. Versieck and R. Dams, *Anal. Chem.*, 1989, **61**,

1851–1857.

217    R. Forrer, K. Gautschi and H. Lutz, *Biol. Trace Elem. Res.*, 2001, **80**, 77–93.

218    J. P. Goullé, L. Mahieu, J. Castermant, N. Neveu, L. Bonneau, G. Lainé, D. Bouige and C. Lacroix, *Forensic Sci. Int.*, 2005, **153**, 39–44.

219    G. Li, J. D. Brockman, S. Lin, C. C. Abnet, L. A. Schell and J. D. Robertson, *Am. J. Anal. Chem.*, 2012, **3**, 646–650.

220    X. Liu, J. Piao, Z. Huang, S. Zhang, W. Li, Y. Tian and X. Yang, *J. Anal. Methods Chem.*, 2014, **2014**, 1–6.

221    I. D. Bravo, R. S. Castro, N. L. Riquelme, C. T. Diaz and D. A. Goyenaga, *J. Trace Elem. Med. Biol.*, 2007, **21**, 14–17.

222    J. Goullé, E. Saussereau, L. Mahieu and M. Guerbet, *Bioanalysis*, 2014, **6**, 2245–2259.

223    C. S. Muñiz, J. L. Fernández-Martin, J. M. Marchante-Gayón, J. I. G. Alonso, J. B. Cannata-Andía and A. Sanz-Medel, *Biol. Trace Elem. Res.*, 2001, **82**, 259–272.

224    P. Heitland and H. D. Köster, *J. Trace Elem. Med. Biol.*, 2006, **20**, 253–262.

225    X. Yu, B. Chen, M. He, H. Wang and B. Hu, *Talanta*, 2018, **179**, 279–284.

226    A. I. Barros, F. C. Pinheiro, C. D. B. Amaral, R. Lorençatto and J. A. Nóbrega, *Talanta*, 2018, **178**, 805–810.

227    E. Barany, I. A. Bergdahl, A. Schutz, S. Skerfving and A. Oskarsson, *J. Anal. At. Spectrom.*, 1997, **12**, 1005–1009.

228    M. Krachler and K. J. Irgolic, *J. Trace Elem. Med. Biol.*, 1999, **13**, 157–169.

229    A. Zayed, T. Shoeib, S. E. Taylor, G. D. D. Jones, A. L. Thomas, J. P. Wood, H. J. Reid and B. L. Sharp, *Int. J. Mass Spectrom.*, 2011, **307**, 70–78.

230    A. Zayed, PhD Thesis, Department of Chemistry, Loughborough University, 2012.

231     M. Maekawa, T. Taniguchi, H. Higashi, H. Sugimura, K. Sugano and T. Kanno, *Clin. Chem.*, 2004, **50**, 1480–1481.

232     J. A. Nóbrega, M. C. Santos, R. A. De Sousa, S. Cadore, R. M. Barnes and M. Tatro, *Spectrochim. Acta Part B*, 2006, **61**, 465–495.

233     K. S. Subramanian, *Spectrochim. Acta - Part B*, 1996, **51**, 291–319.

234     K. Caldwell, Laboratory Procedure Manual, Serum Multi-Element ICP-DRC-MS, 2012.

235     R. Forrer, K. Gautschi, A. Stroh and H. Lutz, *J. trace Elem. Med. Biol.*, 1999, **12**, 240–247.

236     H. J. Finley-Jones, J. L. Molloy and J. A. Holcombe, *J. Anal. At. Spectrom.*, 2008, **23**, 1214–1222.

237     J. J. Thompson and R. S. Houk, *Appl. Spectrosc.*, 1987, **41**, 801–806.

238     F. Vanhaecke, H. Vnhoe and R. Dams, *Talanta*, 1992, **39**, 737–742.

239     J. C. Miller and J. N. Miller, Statistic and Chemometrics for Analytical Chemistry, Pearson Education Limited, London, sixth., 2005., http://www.tandfonline.com/doi/abs/10.1198/tech.2004.s248.

240     Z. M. Memon, E. Yilmaz, A. M. Shah, U. Sahin, T. G. Kazi, B. R. Devrajani and M. Soylak, *Environ. Sci. Pollut. Res.*, 2017, **24**, 26513–26520.

241     T. Konz, E. Migliavacca, L. Dayon, G. Bowman, A. Oikonomidi, J. Popp and S. Rezzi, *J. Proteome Res.*, 2017, **16**, 2080–2090.

242     B. Bocca, G. Forte, F. Petrucci, O. Senofonte, N. Violante and A. Alimonti, *Ann. Ist. Super. Sanita*, 2005, **41**, 165–170.

243     F. M. Burnet, *Lancet.*, 1981, **1**, 186–188.

244     A. Haines, S. Iliffe, P. Morgan, T. Dormandy and B. Wood, *Clin Chim Acta*, 1991, **198**, 261– 266.

245    C. Jeandel, M. Nicolas, F. Dubois, F. Nabet-Belleville, F. Penin and G. Cuny, *Gerontology*, 1989, **35**, 275–282.

246    A. Ghasemi and S. Zahediasl, *Int. J. Endocrinol. Metab.*, 2012, **10**, 486–489.

247    P. Proitsi, M. K. Lupton, F. Dudbridge, M. Tsolaki, G. Hamilton, M. Daniilidou, M. Pritchard, K. Lord, B. M. Martin, J. Johnson, D. Craig, S. Todd, B. McGuinness, P. Hollingworth, D. Harold, I. Kloszewska, H. Soininen, P. Mecocci, B. Velas, M. Gill, B. Lawlor, D. C. Rubinsztein, C. Brayne, P. A. Passmore, J. Williams, S. Lovestone and J. F. Powell, *Neurobiol. Aging*, 2012, **33**, 1843.e9-17.

248    E. Cerman, M. Eraslan and O. Cekic, *Turkish J. Med. Sci.*, 2015, **45**, 1004–1009.

249    K. Ohno-Matsui, *Prog. Retin. Eye Res.*, 2011, **30**, 217–238.

250    C. Paquet, M. Boissonnot, F. Roger, P. Dighiero, R. Gil and J. Hugon, *Neurosci. Lett.*, 2007, **420**, 97–99.

251    J. M. Isas, V. Luibl, L. V. Johnson, R. Kayed, R. Wetzel, C. G. Glabe, R. Langen and J. Chen, *Investig. Ophthalmol. Vis. Sci.*, 2010, **51**, 1304–1310.

252    D. H. Anderson, K. C. Talaga, A. J. Rivest, E. Barron, G. S. Hageman and L. V. Johnson, *Exp. Eye Res.*, 2004, **78**, 243–256.

253    B. H. Anderton, *Philos. Trans. R. Soc. London.*, 1997, **352**, 1781–92.

254    H. Remsch, C. Spraul, G. Lang and G. Lang, *Graefes Arch Clin Exp Ophthalmol*, 2000, **238**, 960–964.

255    A. Roher, J. Debbins, M. Malek-Ahmadi, K. Chen, J. Pipe, S. Maze, C. Belden, C. Maarouf, P. Thiyyagura, H. Mo, J. M. Hunter, T. A. Kokjohn, D. G. Walker, J. C. Kruchowsky, M. Belohlavek, M. N. Sabbagh and T.G. Beach, *Vasc Heal. Risk Manag*, 2012, **8**, 599–611.

256    C. C. Klaver, A. Ott, A. Hofman, J. J. Assink, M. M. Breteler and P. T. De Jong, *Am. J. Epidemiol.*, 1999, **150**, 963–968.

257 T. E. Clemons, M. W. Rankin and W. L. McBee, *Arch. Ophthalmol.*, 2006, **124**, 537–543.

258 M. Zetterberg, S. Landgren, M. E. Andersson, M. S. Palmér, D. R. Gustafson, I. Skoog, L. Minthon, D. S. Thelle, A. Wallin, N. Bogdanovic, N. Andreasen, K. Blennow and H. Zetterberg, *Am. J. Med. Genet. Part B Neuropsychiatr. Genet.*, 2008, **147**, 720–726.

259 J. H. Kam, E. Lenassi and G. Jeffery, *PLoS One*, 2010, **5**, 1–12.

260 J. Ding, L. Johnson, R. Herrmann, S. Farsiu, S. Smith, M. Groelle, B. Mace, P. Sullivan, J. Jamison, U. Kelly, O. Harrabi, S. Bollini, J. Dilley, D. Kobayashi, B. Kuang, W. Li, J. Pons, J. Lin and C. Rickman, *PNAS*, 2011, **108**, 279–287.

261 L. V. Johnson, W. P. Leitner, M. K. Staples and D. H. Anderson, *Exp. Eye Res.*, 2001, **73**, 887–896.

262 T. D. L. Keenan, R. Goldacre and M. J. Goldacre, *J. Am. Med. Assoc*, 2014, **132**, 63–68.

263 D.-D. Li, W. Zhang, Z.-Y. Wang and P. Zhao, *Front. Aging Neurosci.*, 2017, **9**, 1–13.

264 H. Zhao, J. Lin, X. Wang, X. Cheng, J. Wang, B. Hu, Y. Zhang, X. Zhang and J. Zhu, *PLoS One*, 2013, **8**, 1–10.

265 A. Rembach, J. D. Doecke, B. R. Roberts, A. D. Watt, N. G. Faux, I. Volitakis, K. K. Pertile, R. L. Rumble, B. O. Trounson, C. J. Fowler, W. Wilson, K. A. Ellis, R. N. Martins, C. C. Rowe, V. L. Villemagne, D. Ames, C. L. Masters and A. I. Bush, *J. Alzheimer's Dis.*, 2013, **34**, 171–182.

266 A. J. Managh, S. L. Edwards, A. Bushell, K. J. Wood, E. K. Geissler, J. A. Hutchinson, R. W. Hutchinson, H. J. Reid and B. L. Sharp, *Anal. Chem.*, 2013, **85**, 10627–10634.

267 B. H. Grahn, P. G. Paterson, K. T. Gottschall-Pass and Z. Zhang, *J. Am. Coll. Nutr.*,

2001, **20**, 106–118.

268  M. A. Galin, H. D. Nano and T. Hall, *Investig. Ophthalmol. Vis. Sci.*, 1962, **1**, 142–148.

269  R. R. Caspi, *J. Clin. Invest.*, 2010, **120**, 3073–3083.

270  S. Cahyadi, PhD Thesis, Department of ocular biology and therapeutics, institute of Ophthalmology, University College London, 2012.

271  M. Ugarte and N. N. Osborne, *Prog. Neurobiol.*, 2001, **64**, 219–249.

272  H. J. Hyun, J. H. Sohn, D. W. Ha, Y. H. Ahn, J. Y. Koh and Y. H. Yoon, *Invest. Ophthalmol. Vis. Sci.*, 2001, **42**, 460–465.

273  M. W. Duncan, A. M. Marini, R. Watters, I. J. Kopin and S. P. Markey, *J. Neurosci.*, 1992, **12**, 1523–1537.

274  G. J. Lees, A. Lehmann, M. Sandberg and A. Hamberger, *Neurosci. Lett.*, 1990, **120**, 155–158.

275  D. J. Tate, M. V. Miceli and D. A. Newsome, *Free Radic. Biol. Med.*, 1999, **26**, 704–713.

276  A. Grubman, P. Guennel, K. A. Vessey, M. W. M. Jones, S. A. James, M. D. De Jonge, A. R. White and E. L. Fletcher, *Metallomics*, 2016, **8**, 1110–1121.

277  B. Knauer, P. Majka, K. J. Watkins, A. W. Taylor, D. Malamanova, B. Paul, H. Yu, A. I. Bush, D. J. Hare and D. Reser, *Metallomics*, 2017, **9**, 411–423.

278  M. W. Bourassa and L. M. Miller, *Metallomics*, 2012, **4**, 721–738.

279  F. M. Nadal-Nicolás, M. Vidal-Sanz and M. Agudo-Barriuso, *Neurobiol. Aging*, 2018, **61**, 146–168.

280  D. J. Tate, D. A. Newsome and P. D. Oliver, *Investig. Ophthalmol. Vis. Sci.*, 1993, **34**, 2348–2351.

281 C. T. Chasapis, C. A. Spiliopoulou, A. C. Loutsidou and M. E. Stefanidou, *Arch. Toxicol.*, 2012, **86**, 521–534.

282 D. A. Newsome, M. V. Miceli, D. J. Tate Jr., N. W. Alcock and P. D. Oliver, *J. Trace Elem. Exp. Med.*, 1996, **8**, 193–199.

283 C. Y. Cheung, M. K. Ikram, C. Chen and T. Y. Wong, *Prog. Retin. Eye Res.*, 2017, **57**, 89–107.

284 D. Pozebon, G. L. Scheffler and V. L. Dressler, *J. Anal. At. Spectrom.*, 2017, **32**, 890–919.

285 S. Novak, D. Drobne, J. Valant and P. Pelicon, *J. Nanomater.*, 2012, **2012**, 1–8.

286 J. Soto-Alvaredo, E. Blanco, J. Bettmer, D. Hevia, R. M. Sainz, C. López Cháves, C. Sánchez, J. Llopis, A. Sanz-Medel and M. Montes-Bayón, *Metallomics*, 2014, **6**, 1702–1708.

287 C. Carlier, B. Laforce, S. J. M. Van Malderen, F. Gremonprez, R. Tucoulou, J. Villanova, O. De Wever, L. Vincze, F. Vanhaecke and W. Ceelen, *J. Pharm. Biomed. Anal.*, 2016, **131**, 256–262.

288 J. M. Flinn, P. Kakalec, R. Tappero, B. Jones and I. Lengyel, *Metallomics*, 2014, **6**, 1223–8.

289 M. Ugarte, K. Geraki and G. Jeffery, *Metallomics*, 2016, **8**, 1071–1080.

290 S. Moncayo, F. Trichard, B. Busser, M. Sabatier-Vincent, F. Pelascini, N. Pinel, I. Templier, J. Charles, L. Sancey and V. Motto-Ros, *Spectrochim. Acta - Part B At. Spectrosc.*, 2017, **133**, 40–44.

291 R. W. Hutchinson, A. G. Cox, C. W. McLeod, P. S. Marshall, A. Harper, E. L. Dawson and D. R. Howlett, *Anal. Biochem.*, 2005, **346**, 225–233.

292 L. Feng, J. Wang, H. Li, X. Luo and J. Li, *Anal. Chim. Acta*, 2017, **984**, 66–75.

293 A. Sajnóg, A. Hanć, R. Koczorowski and D. Barałkiewicz, *Talanta*, 2017, **175**, 370–

381.

294     H. A. O. Wang, D. Grolimund, C. Giesen, C. N. Borca, J. R. H. Shaw-Stewart, B. Bodenmiller and D. Günther, *Anal. Chem.*, 2013, **85**, 10107–10116.

295     J. Feldmann, A. Kindness and P. Ek, *J. Anal. At. Spectrom.*, 2002, **17**, 813–818.

296     J. S. Becker, A. Matusch and B. Wu, *Anal. Chim. Acta*, 2014, **835**, 1–18.

297     D. Hare, B. Reedy, R. Grimm, S. Wilkins, I. Volitakis, J. L. George, R. a Cherny, A. I. Bush, D. I. Finkelstein and P. Doble, *Metallomics*, 2009, **1**, 53.

298     R. González de Vega, M. L. Fernández-Sánchez, J. Pisonero, N. Eiró, F. J. Vizoso and A. Sanz-Medel, *J. Anal. At. Spectrom.*, 2017, **32**, 671–677.

299     A. Hanc, A. Olszewska and D. Baralkiewicz, *Microchem. J.*, 2013, **110**, 61–69.

300     A. Sussulini, E. Wiener, T. Marnitz, B. Wu, B. Müller, B. Hamm and J. Sabine Becker, *Contrast Media Mol. Imaging*, 2013, **8**, 204–209.

301     A. Hanć, I. Komorowicz, M. Iskra, W. Majewski and D. Barałkiewicz, *Anal. Bioanal. Chem.*, 2011, **399**, 3221–3231.

302     S. Rodríguez-Menéndez, B. Fernández, M. García, L. Álvarez, M. Luisa Fernández, A. Sanz-Medel, M. Coca-Prados, R. Pereiro and H. González-Iglesias, *Talanta*, 2018, **178**, 222–230.

303     A. M. Race and J. Bunch, *Anal. Bioanal. Chem.*, 2015, **407**, 2047–2054.

304     M. S. A. Horstwood, G. L. Foster, R. R. Parrish, S. R. Noble and G. M. Nowell, *R. Soc. Chem.*, 2003, **18**, 837–846.

305     D. C. Lozano and M. D. Twa, *Investig. Ophthalmol. Vis. Sci.*, 2012, **53**, 8378–8385.

306     M. Ilia and G. Jeffery, *J. Comp. Neurol.*, 2000, **420**, 437–444.

307     H. El-Sayyad, A. M. Abou-El-Naga, S. A. Khalifa, E. A. El-Shahari and H. A. Jala, *J. Drug Metab. Toxicol.*, 2016, **7**, 1–7.

308 C. Sergeant, Y. Llabador, G. Devès, M. H. Vesvres, M. Simonoff, M. Yefimova, Y. Courtois and J. C. Jeanny, *Nucl. Instruments Methods Phys. Res. B*, 2001, **181**, 533–538.

309 Y. M. Shang, G. S. Wang, D. Sliney, C. H. Yang and L. L. Lee, *Environ. Health Perspect.*, 2014, **122**, 269–276.

310 T. M. Mayhew and D. Astle, *J. Neurocytol.*, 1997, **26**, 53–61.

311 S. J. Fliesler and L. Bretillon, *J. Lipid Res.*, 2010, **51**, 3399–3413.

312 A. R. Kay, *BMC Physiol.*, 2004, **4**, 1–9.

313 D. Autrique, A. Bogaerts, H. Lindner, C. C. Garcia and K. Niemax, *Spectrochim. Acta - Part B*, 2008, **63**, 257–270.

314 G. Craig, PhD Thesis, Department of Chemistry, Loughborough University, 2015.

315 J. M. Flinn, P. Kakalec, R. Tappero, B. Jones and I. Lengyel, *Metallomics*, 2014, **6**, 1223–1228.

316 R. F. Spaide and C. A. Curcio, *Retina*, 2011, **30**, 1441–1454.

317 J. C. Booij, D. C. Baas, J. Beisekeeva, T. G. M. F. Gorgels and A. A. B. Bergen, *Prog. Retin. Eye Res.*, 2010, **29**, 1–18.

318 S. D. Vogt, C. A. Curcio, L. Wang, C. M. Li, G. McGwin, N. E. Medeiros, N. J. Philp, J. A. Kimble and R. W. Read, *Exp. Eye Res.*, 2011, **93**, 413–423.

319 R. J. Ulshafer, C. B. Allen and M. L. Rubin, *Arch. Ophthalmol.*, 1990, **108**, 113–117.

320 M. Ugarte, G. W. Grime and N. N. Osborne, *Metallomics*, 2014, **6**, 274–278.

321 Moreland K. (2009) Diverging Color Maps for Scientific Visualization. In: Bebis G. et al. (eds) Advances in Visual Computing. ISVC 2009. Lecture Notes in Computer Science, vol 5876. Springer, Berlin, Heidelberg.

322 C. Hardin and L. Maffi, Color Categories in Thought and Language, Cambridge University Press, Cambridge,1997.

323 A. J. Managh, D. N. Douglas, K. Makella Cowen, H. J. Reid and B. L. Sharp, *J. Anal. At. Spectrom.*, 2016, **31**, 1688–1692.

324 D. N. Douglas, A. J. Managh, H. J. Reid and B. L. Sharp, *Anal. Chem.*, 2015, **87**, 11285–11294.

325 A. Kesler, V. Vakhapova, A. D. Korczyn, E. Naftaliev and M. Neudorfer, *Clin. Neurol. Neurosurg.*, 2011, **113**, 523–526.

326 B. Alamouti and J. Funk, *Br. J. Ophthalmol.*, 2003, **87**, 899–901.

327 F. Ko, P. J. Foster, N. G. Strouthidis, Y. Shweikh, Q. Yang, C. A. Reisman, Z. A. Muthy, U. Chakravarthy, A. J. Lotery, P. A. Keane, A. Tufail, C. M. Grossi and P. J. Patel, *Ophthalmology*, 2017, **124**, 105–117.

328 J. C. Mwanza, M. K. Durbin, D. L. Budenz, F. E. Sayyad, R. T. Chang, A. Neelakantan, D. G. Godfrey, R. Carter and A. S. Crandall, *Ophthalmology*, 2012, **119**, 1151–1158.

329 C. A. Curcio, J. D. Messinger, K. R. Sloan, A. Mitra, G. McGwin and R. F. Spaide, *Investig. Ophthalmol. Vis. Sci.*, 2011, **52**, 3943–3954.

330 J. Y. Won, S. E. Kim and Y.-H. Park, *Medicine*, 2016, **95**, 1–6.

331 A. M. Bagci, M. Shahidi, R. Ansari, M. Blair, N. Paul and R. Zelkha, 2009, **146**, 679–687.

332 J. S. Brown, D. I. Flitcroft, G. S. Ying, E. L. Francis, G. F. Schmid, G. E. Quinn and R. A. Stone, *Investig. Ophthalmol. Vis. Sci.*, 2009, **50**, 5–12.

333 R. E. Norman, J. G. Flanagan, S. M. K. Rausch, I. A. Sigal, I. Tertinegg, A. Eilaghi, S. Portnoy, J. G. Sled and C. R. Ethier, *Exp. Eye Res.*, 2010, **90**, 277–284.

334 P. Reid and A.J. Managh, LA-ICP-MS Image Tool, DOI: 10.5281/zenodo.1117206.

335    S. Chaychi, A. Polosa and P. Lachapelle, *PLoS One*, 2015, **10**, 1–16.

336    M. E. Pennesi, M. Neuringer and R. J. Courtney, *Mol. Aspects Med.*, 2012, **33**, 487–509.

337    S. J. M. Van Malderen, J. T. Van Elteren and F. Vanhaecke, *J. Anal. At. Spectrom.*, 2014, **30**, 119–125.

338    S. J. M. Van Malderen, A. J. Managh, B. L. Sharp and F. Vanhaecke, *J. Anal. At. Spectrom.*, 2016, **31**, 423–439.

339    R. Simó, M. Villarroel, L. Corraliza, C. Hernández and M. Garcia-Ramírez, *J. Biomed. Biotechnol.*, 2010, **2010**, 1–15.

340    L. Rink, Zinc in Human Health, IOS Press, Netherlands, 2011.

341    Calbiochem and Merck, ProteoExtract® Subcellular Proteome Extraction Kit manual, 2007.

342    B. Cai, Y. Wang, X. H. Zhao and Z. S. Gong, *Anal. Lett.*, 2017, **50**, 554–566.

343    N. K. Wills, N. Kalariya, V. M. Sadagopa Ramanujam, J. R. Lewis, S. Haji Abdollahi, A. Husain and F. J. G. M. van Kuijk, *Exp. Eye Res.*, 2009, **89**, 79–87.

344    M. Ugarte, G. W. Grime, G. Lord, K. Geraki, J. F. Collingwood, M. E. Finnegan, H. Farnfield, M. Merchant, M. J. Bailey, N. I. Ward, P. J. Foster, P. N. Bishop and N. N. Osborne, *Metallomics*, 2012, **4**, 1245.

345    D. Hare, C. Austin and P. Doble, *Analyst*, 2012, **137**, 1527.

346    N. Miliszkiewicz, S. Walas and A. Tobiasz, *J. Anal. At. Spectrom.*, 2015, **30**, 327–338.

347    K. Jurowski, B. Buszewski and W. Piekoszewski, *Talanta*, 2015, **131**, 273–285.

348    A. C. Grey, P. Chaurand, R. M. Caprioli and K. L. Schey, *Proteome*, 2010, **8**, 3278–3283.

349   M. Cruz-Alonso, B. Fernandez, L. Álvarez, H. González-Iglesias, H. Traub, N. Jakubowski and R. Pereiro, *Microchim. Acta*, 2018, **185**, 1–9.

350   P. J. Sylvester and S. E. Jackson, *Elements*, 2016, **12**, 307–310.

# 8 Appendices

## Appendix 1 – Ethics applications and approvals

**Protocol version 1.1. 22/04/2009**
Unravelling the molecular steps involved in the Ageing of the retina
Moorfields & Whittington Research Ethics Committee
Royal Free Hospital
Pond Street
London
NW3 2QG

Tel: 020 7794 0552
Dr Imre Lengyel
UCL Institute of Ophthalmology
11-43 Bath Street
EC1V 9EL

01 May 2009

Dear Dr Lengyel

| | |
|---|---|
| Study title: | Unravelling the molecular steps involved in the aging of the retina |
| **REC reference:** | **08/H0721/12** |
| Amendment number: | 1 |
| Amendment date: | 22 April 2009 |

The above amendment to investigate the effect of AMD associated conditions on cellular function and protein and RNA expression of cells isolated and/or cultured from donor samples was reviewed at the meeting of the Sub-Committee of the REC held on 01 May 2009

Ethical opinion
The members of the Committee present gave a favourable ethical opinion of the amendment on the basis described in the notice of amendment form and supporting documentation.

---

Lengyel Protocol V3 171109 ammended
Protocol version 3 17 November 2009
The molecular role of zinc and complement factor H in age-related macular degeneration
Chief Investigator: Tunde Peto
Principal Investigator: Imre Lengyel

Co-investigators: Stephen Perkins, Shomi Bhattacharya, Barry Sharp

Bromley Local Research Ethics Committee
Bromley PCT, Bassetts House,
Broadwater Gardens
Farnborough
Kent
BR6 7UA

Telephone: 01689 880592
Facsimile: 01689 855662
12 May 2008


Dr Tunde Peto
Associate Specialist
Moorfields Eye Hospital
162 City Road
London
EC1V 2PD

Dear Dr Peto

| Full title of study: | The molecular role of zinc and complement Factor H in causing deposits that lead to age-related macular degeneration in the eye |
|---|---|
| **REC reference number:** | **08/H0805/6** |

17th November 2009

Ms Carol Jones
REC Chair
Bromley Local Research Ethics Committee
Bromley PCT, Bassetts House,
Broadwater Gardens
Farnborough
Kent BR6 7UA

Dear Ms Jones

Full title of study: The molecular role of zinc and complement Factor H in causing deposits that lead to age-related macular degeneration in the eye
**REC reference:        08/H0805/6**

# Moorfields Eye Hospital NHS
NHS Foundation Trust

17th November 2009

Ms Carol Jones
REC Chair
Bromley Local Research Ethics Committee
Bromley PCT, Bassetts House,
Broadwater Gardens
Farnborough
Kent BR6 7UA

Dear Ms Jones

**Full title of study:**   **The molecular role of zinc and complement Factor H in causing deposits that lead to age-related macular degeneration in the eye**
**REC reference:**      **08/H0805/6**

## NOTICE OF MINOR AMENDMENT

I would like to notify the Ethics Committee of additional laboratory measurements we will be undertaking on the blood samples already obtained for the purposes of this study. These measurements would help us obtain a better understanding of the mechanisms leading to age-related macular degeneration and may facilitate the interpretation of our work on complement factor H and age-related macular degeneration.

The amendments are as follows:
- We will be measuring zinc levels in different compartments in 5 ml of blood.
- We will determine the speciation of zinc.
- We will measure expression levels of zinc transporter proteins and biomarkers, especially inflammatory biomarkers for AMD.

An updated version of our protocol (Version 3 dated 17th November 2009) with the changes highlighted is attached.   The patient information sheet does not need to be amended and we therefore feel that these amendments can be notified to the Committee as "Minor".

Yours sincerely

**Dr Tunde Peto**
**_Associate Specialist in Ophthalmology_**

**NRES Committee London - Harrow**

Level 7 Maternity, Room 019
Northwick Park Hospital
Watford Road
Harrow
HA1 3UJ

Tel: 020 8869 3928
Fax: 020 8869 5222

12 January 2012

Dr Craig W Ritchie
Honorary Consultant Psychiatrist, Senior Clinical Research Fellow
West London Cognitive Disorders Treatment & Research Unit
Brentford Lodge
Boston Manor Road
Brentford, London
TW8 8DS

Dear Dr Ritchie

| | |
|---|---|
| **Study title:** | **The association between Age-related Macular Degeneration and Alzheimer's disease** |
| **REC reference:** | **09/H0710/10** |
| **Amendment number:** | **5.1** |
| **Amendment date:** | **30 November 2011** |

The above amendment was reviewed by the sub-committee in correspondence on 11 January 2012.

**Ethical opinion**

The members of the Committee taking part in the review gave a favourable ethical opinion of the amendment on the basis described in the notice of amendment form and supporting documentation.

**Approved documents**

The documents reviewed and approved at the meeting were:

| Document | Version | Date |
|---|---|---|
| Participant Consent Form: Carer | 5.2 | 11 January 2012 |
| Participant Consent Form: Patient | 5.2 | 11 January 2012 |
| Participant Information Sheet | 5.2 | 11 January 2012 |
| Protocol | 5.2 | 11 January 2012 |

A Research Ethics Committee established by the Health Research Authority

180

| Carer Declaration Form | 5.2 | 11 January 2012 |
|---|---|---|
| Notice of Substantial Amendment (non-CTIMPs) | 5.1 | 30 November 2011 |
| Covering Letter | | 06 December 2011 |

Please note *the declaration form will also require the clause (point 3) which has been added to the consent form about agreeing to the research data being accessible to regulatory authorities*

**Membership of the Committee**

The members of the Committee who took part in the review are listed on the attached sheet.

**R&D approval**

All investigators and research collaborators in the NHS should notify the R&D office for the relevant NHS care organisation of this amendment and check whether it affects R&D approval of the research.

**Statement of compliance**

The Committee is constituted in accordance with the Governance Arrangements for Research Ethics Committees and complies fully with the Standard Operating Procedures for Research Ethics Committees in the UK.

| 09/H0710/10: | **Please quote this number on all correspondence** |
|---|---|

Yours sincerely

PP *Alison okane*
**Dr Jan Downer**
**Chair**

E-mail: alison.okane@nwlh.nhs.uk

Enclosures:    *List of names and professions of members who took part in the review*

Copy to:        *N/A. R&D contact not specified in database.*
                *Ms Maria Tsappis, West London Mental Health Trust*

**NRES Committee London - Harrow**

**Attendance at Sub-Committee of the REC meeting 11 January 2012**

| | |
|---|---|
| **Dr. J. Downer (Chair)** | **Consultant Anaesthetist** |
| **Ms. V. Bernstein** | **Lay Member** |

# Appendix 2 – Supplementary figures data for chapter 2

**Table 8.1** Figures of merit (regression equations, correlation coefficient ($R^2$), and limit of detection and quantification) of serum Zn, Cu and Fe in all experiments

| Zn$^{66}$ | Linear equation | $R^2$ | LOD | LOQ |
|---|---|---|---|---|
| EXP 1 | y= 13802x + 6611.2 | 0.9972 | 0.20 | 0.65 |
| EXP 2 | y = 14503x + 1103.5 | 0.9997 | 0.39 | 1.30 |
| EXP 3 | y = 14092x - 593.16 | 0.9988 | 0.57 | 1.91 |
| EXP 4 | y = 5565.6x + 4939.5 | 0.9972 | 0.83 | 2.75 |

| Cu$^{65}$ | Linear equation | $R^2$ | LOD | LOQ |
|---|---|---|---|---|
| EXP 1 | y = 52106x + 6270.6 | 0.9998 | 0.29 | 0.96 |
| EXP 2 | y = 60096x - 1990.8 | 0.9999 | 0.08 | 0.28 |
| EXP 3 | y = 55074x - 13127 | 0.9984 | 0.66 | 2.20 |
| EXP 4 | y = 50795x + 8279.3 | 0.9977 | 0.63 | 2.09 |

| Fe$^{57}$ | Linear equation | $R^2$ | LOD | LOQ |
|---|---|---|---|---|
| EXP 1 | y = 4647.2x + 3655.9 | 0.9971 | 0.29 | 0.96 |
| EXP 2 | y = 5758.6x + 5167 | 0.9998 | 0.27 | 0.90 |
| EXP 3 | y = 5004.4x + 2795.7 | 0.9993 | 0.18 | 0.59 |
| EXP 4 | y = 4316.8x + 4664.8 | 0.9958 | 0.93 | 3.11 |

**Table 8.2** Kolmogorov–Smirnov method of Zn in AD patients*

| X (Zn-AD) | Z | Cumulative frequency | Step cumulative distribution | Normal cumulative distribution | Difference |
|---|---|---|---|---|---|
| 0.58 | -1.58 | 1 | 0.02 | 0.06 | -0.034 |
| 0.59 | -1.46 | 2 | 0.05 | 0.07 | -0.026 |
| 0.61 | -1.34 | 3 | 0.07 | 0.09 | -0.021 |
| 0.61 | -1.33 | 4 | 0.09 | 0.09 | 0.002 |
| 0.61 | -1.30 | 5 | 0.12 | 0.10 | 0.019 |
| 0.62 | -1.23 | 6 | 0.14 | 0.11 | 0.030 |
| 0.64 | -1.06 | 7 | 0.16 | 0.14 | 0.019 |
| 0.66 | -0.92 | 8 | 0.19 | 0.18 | 0.007 |
| 0.66 | -0.89 | 9 | 0.21 | 0.19 | 0.022 |
| 0.68 | -0.74 | 10 | 0.23 | 0.23 | 0.004 |
| 0.68 | -0.74 | 11 | 0.26 | 0.23 | 0.027 |
| 0.69 | -0.70 | 12 | 0.28 | 0.24 | 0.036 |
| 0.69 | -0.69 | 13 | 0.30 | 0.24 | 0.058 |
| 0.69 | -0.69 | 14 | 0.33 | 0.25 | 0.080 |
| 0.70 | -0.61 | 15 | 0.35 | 0.27 | 0.078 |
| 0.71 | -0.53 | 16 | 0.37 | 0.30 | 0.072 |
| 0.72 | -0.45 | 17 | 0.40 | 0.33 | 0.068 |
| 0.73 | -0.35 | 18 | 0.42 | 0.36 | 0.056 |
| 0.74 | -0.30 | 19 | 0.44 | 0.38 | 0.058 |
| 0.74 | -0.27 | 20 | 0.47 | 0.39 | 0.071 |
| 0.75 | -0.20 | 21 | 0.49 | 0.42 | 0.066 |
| 0.76 | -0.16 | 22 | 0.51 | 0.44 | 0.074 |
| 0.77 | -0.04 | 23 | 0.53 | 0.48 | 0.052 |
| 0.78 | 0.04 | 24 | 0.56 | 0.52 | 0.041 |
| 0.79 | 0.08 | 25 | 0.58 | 0.53 | 0.049 |
| 0.79 | 0.11 | 26 | 0.60 | 0.54 | 0.062 |
| 0.80 | 0.20 | 27 | 0.63 | 0.58 | 0.047 |
| 0.80 | 0.21 | 28 | 0.65 | 0.58 | 0.068 |
| 0.81 | 0.30 | 29 | 0.67 | 0.62 | 0.055 |
| 0.83 | 0.40 | 30 | 0.70 | 0.66 | 0.042 |
| 0.83 | 0.44 | 31 | 0.72 | 0.67 | 0.049 |
| 0.84 | 0.48 | 32 | 0.74 | 0.68 | 0.062 |
| 0.86 | 0.65 | 33 | 0.77 | 0.74 | 0.025 |
| 0.90 | 0.96 | 34 | 0.79 | 0.83 | -0.041 |
| 0.92 | 1.19 | 35 | 0.81 | 0.88 | -0.069 |
| 0.93 | 1.20 | 36 | 0.84 | 0.88 | -0.048 |
| 0.93 | 1.25 | 37 | 0.86 | 0.89 | -0.033 |
| 0.93 | 1.25 | 38 | 0.88 | 0.89 | -0.011 |
| 0.95 | 1.37 | 39 | 0.91 | 0.92 | -0.008 |
| 0.98 | 1.65 | 40 | 0.93 | 0.95 | -0.021 |
| 0.99 | 1.69 | 41 | 0.95 | 0.95 | -0.001 |
| 0.99 | 1.70 | 42 | 0.98 | 0.96 | 0.021 |
| 1.07 | 2.38 | 43 | 1.00 | 0.99 | 0.009 |

*For n=43 and P= 0.05, the critical value is 0.192, Since 0.080 <0.192 we can accept the null hypothesis that the data come from a normal population with mean 0.78 and standard deviation 0.125

**Table 8.3** Kolmogorov–Smirnov method of Cu in AD patients*

| X (Cu-AD) | Z | Cumulative frequency | Step cumulative distribution | Normal cumulative distribution | Difference |
|---|---|---|---|---|---|
| 0.77 | -1.74 | 1 | 0.02 | 0.04 | -0.017 |
| 0.79 | -1.66 | 2 | 0.05 | 0.05 | -0.002 |
| 0.81 | -1.57 | 3 | 0.07 | 0.06 | 0.012 |
| 0.85 | -1.42 | 4 | 0.09 | 0.08 | 0.015 |
| 0.87 | -1.31 | 5 | 0.12 | 0.09 | 0.022 |
| 0.94 | -1.01 | 6 | 0.14 | 0.16 | -0.017 |
| 0.95 | -0.97 | 7 | 0.16 | 0.17 | -0.002 |
| 0.95 | -0.97 | 8 | 0.19 | 0.17 | 0.019 |
| 0.98 | -0.86 | 9 | 0.21 | 0.20 | 0.013 |
| 0.98 | -0.85 | 10 | 0.23 | 0.20 | 0.034 |
| 1.02 | -0.68 | 11 | 0.26 | 0.25 | 0.007 |
| 1.03 | -0.65 | 12 | 0.28 | 0.26 | 0.021 |
| 1.04 | -0.60 | 13 | 0.30 | 0.27 | 0.028 |
| 1.06 | -0.51 | 14 | 0.33 | 0.30 | 0.021 |
| 1.08 | -0.44 | 15 | 0.35 | 0.33 | 0.018 |
| 1.09 | -0.39 | 16 | 0.37 | 0.35 | 0.023 |
| 1.10 | -0.33 | 17 | 0.40 | 0.37 | 0.023 |
| 1.11 | -0.31 | 18 | 0.42 | 0.38 | 0.040 |
| 1.13 | -0.21 | 19 | 0.44 | 0.42 | 0.024 |
| 1.15 | -0.14 | 20 | 0.47 | 0.45 | 0.020 |
| 1.17 | -0.04 | 21 | 0.49 | 0.48 | 0.006 |
| 1.19 | 0.04 | 22 | 0.51 | 0.52 | -0.004 |
| 1.19 | 0.05 | 23 | 0.53 | 0.52 | 0.017 |
| 1.20 | 0.11 | 24 | 0.56 | 0.54 | 0.016 |
| 1.20 | 0.11 | 25 | 0.58 | 0.54 | 0.038 |
| 1.23 | 0.23 | 26 | 0.60 | 0.59 | 0.013 |
| 1.24 | 0.27 | 27 | 0.63 | 0.61 | 0.020 |
| 1.24 | 0.28 | 28 | 0.65 | 0.61 | 0.041 |
| 1.25 | 0.31 | 29 | 0.67 | 0.62 | 0.053 |
| 1.29 | 0.46 | 30 | 0.70 | 0.68 | 0.021 |
| 1.29 | 0.47 | 31 | 0.72 | 0.68 | 0.041 |
| 1.31 | 0.54 | 32 | 0.74 | 0.71 | 0.038 |
| 1.32 | 0.60 | 33 | 0.77 | 0.73 | 0.042 |
| 1.32 | 0.62 | 34 | 0.79 | 0.73 | 0.058 |
| 1.33 | 0.64 | 35 | 0.81 | 0.74 | 0.075 |
| 1.35 | 0.72 | 36 | 0.84 | 0.77 | 0.071 |
| 1.35 | 0.73 | 37 | 0.86 | 0.77 | 0.093 |
| 1.42 | 1.04 | 38 | 0.88 | 0.85 | 0.033 |
| 1.50 | 1.38 | 39 | 0.91 | 0.92 | -0.010 |
| 1.53 | 1.48 | 40 | 0.93 | 0.93 | -0.001 |
| 1.54 | 1.55 | 41 | 0.95 | 0.94 | 0.014 |
| 1.70 | 2.23 | 42 | 0.98 | 0.99 | -0.010 |
| 1.83 | 2.78 | 43 | 1.00 | 1.00 | 0.003 |

*For n=43 and P= 0.05, the critical value is 0.192, Since 0.093 <0.192 we can accept the null hypothesis that the data coming from a normal population with mean 1.18 and standard deviation 0.234

**Table 8.4** Kolmogorov–Smirnov method of Fe in AD patients*

| X (Fe-AD) | Z | Cumulative frequency | Step cumulative distribution | Normal cumulative distribution | Difference |
|---|---|---|---|---|---|
| 0.51 | -1.38 | 1 | 0.02 | 0.08 | -0.060 |
| 0.52 | -1.36 | 2 | 0.05 | 0.09 | -0.040 |
| 0.53 | -1.35 | 3 | 0.07 | 0.09 | -0.018 |
| 0.56 | -1.27 | 4 | 0.09 | 0.10 | -0.008 |
| 0.56 | -1.27 | 5 | 0.12 | 0.10 | 0.014 |
| 0.66 | -1.05 | 6 | 0.14 | 0.15 | -0.007 |
| 0.69 | -0.98 | 7 | 0.16 | 0.16 | -0.001 |
| 0.76 | -0.81 | 8 | 0.19 | 0.21 | -0.023 |
| 0.77 | -0.80 | 9 | 0.21 | 0.21 | -0.003 |
| 0.80 | -0.72 | 10 | 0.23 | 0.24 | -0.003 |
| 0.81 | -0.71 | 11 | 0.26 | 0.24 | 0.018 |
| 0.81 | -0.70 | 12 | 0.28 | 0.24 | 0.038 |
| 0.86 | -0.60 | 13 | 0.30 | 0.28 | 0.027 |
| 0.88 | -0.54 | 14 | 0.33 | 0.29 | 0.032 |
| 0.89 | -0.51 | 15 | 0.35 | 0.30 | 0.045 |
| 0.92 | -0.45 | 16 | 0.37 | 0.33 | 0.045 |
| 0.95 | -0.39 | 17 | 0.40 | 0.35 | 0.046 |
| 0.95 | -0.38 | 18 | 0.42 | 0.35 | 0.066 |
| 0.96 | -0.37 | 19 | 0.44 | 0.36 | 0.087 |
| 0.96 | -0.36 | 20 | 0.47 | 0.36 | 0.105 |
| 1.02 | -0.23 | 21 | 0.49 | 0.41 | 0.078 |
| 1.06 | -0.13 | 22 | 0.51 | 0.45 | 0.064 |
| 1.06 | -0.13 | 23 | 0.53 | 0.45 | 0.086 |
| 1.09 | -0.07 | 24 | 0.56 | 0.47 | 0.088 |
| 1.16 | 0.09 | 25 | 0.58 | 0.54 | 0.045 |
| 1.19 | 0.15 | 26 | 0.60 | 0.56 | 0.045 |
| 1.22 | 0.23 | 27 | 0.63 | 0.59 | 0.039 |
| 1.23 | 0.25 | 28 | 0.65 | 0.60 | 0.054 |
| 1.24 | 0.27 | 29 | 0.67 | 0.61 | 0.066 |
| 1.24 | 0.28 | 30 | 0.70 | 0.61 | 0.086 |
| 1.29 | 0.39 | 31 | 0.72 | 0.65 | 0.067 |
| 1.35 | 0.53 | 32 | 0.74 | 0.70 | 0.041 |
| 1.40 | 0.63 | 33 | 0.77 | 0.73 | 0.033 |
| 1.41 | 0.66 | 34 | 0.79 | 0.74 | 0.046 |
| 1.43 | 0.71 | 35 | 0.81 | 0.76 | 0.054 |
| 1.66 | 1.23 | 36 | 0.84 | 0.89 | -0.053 |
| 1.70 | 1.32 | 37 | 0.86 | 0.91 | -0.046 |
| 1.76 | 1.45 | 38 | 0.88 | 0.93 | -0.043 |
| 1.87 | 1.71 | 39 | 0.91 | 0.96 | -0.049 |
| 1.95 | 1.90 | 40 | 0.93 | 0.97 | -0.041 |
| 2.05 | 2.12 | 41 | 0.95 | 0.98 | -0.030 |
| 2.29 | 2.66 | 42 | 0.98 | 1.00 | -0.019 |

*For n=42 and P= 0.05, the critical value is 0.192, Since 0.105 <0.192 we can accept the null hypothesis that the data coming from a normal population with mean 1.12 and standard deviation 0.44

**Table 8.5** Kolmogorov–Smirnov method of Zn in AMD patients*

| X (Zn-AMD) | Z | Cumulative frequency | Step cumulative distribution | Normal cumulative distribution | Difference |
|---|---|---|---|---|---|
| 0.52 | -1.32 | 1 | 0.02 | 0.09 | -0.069 |
| 0.56 | -1.16 | 2 | 0.05 | 0.12 | -0.077 |
| 0.57 | -1.08 | 3 | 0.07 | 0.14 | -0.070 |
| 0.57 | -1.06 | 4 | 0.09 | 0.14 | -0.050 |
| 0.59 | -0.97 | 5 | 0.12 | 0.17 | -0.050 |
| 0.62 | -0.87 | 6 | 0.14 | 0.19 | -0.052 |
| 0.62 | -0.85 | 7 | 0.16 | 0.20 | -0.035 |
| 0.63 | -0.79 | 8 | 0.19 | 0.22 | -0.029 |
| 0.65 | -0.72 | 9 | 0.21 | 0.24 | -0.027 |
| 0.65 | -0.70 | 10 | 0.23 | 0.24 | -0.009 |
| 0.66 | -0.67 | 11 | 0.26 | 0.25 | 0.004 |
| 0.66 | -0.67 | 12 | 0.28 | 0.25 | 0.027 |
| 0.68 | -0.57 | 13 | 0.30 | 0.28 | 0.017 |
| 0.69 | -0.53 | 14 | 0.33 | 0.30 | 0.026 |
| 0.70 | -0.49 | 15 | 0.35 | 0.31 | 0.036 |
| 0.71 | -0.43 | 16 | 0.37 | 0.33 | 0.039 |
| 0.71 | -0.43 | 17 | 0.40 | 0.33 | 0.061 |
| 0.72 | -0.39 | 18 | 0.42 | 0.35 | 0.071 |
| 0.73 | -0.35 | 19 | 0.44 | 0.36 | 0.077 |
| 0.74 | -0.29 | 20 | 0.47 | 0.39 | 0.078 |
| 0.75 | -0.24 | 21 | 0.49 | 0.40 | 0.083 |
| 0.77 | -0.15 | 22 | 0.51 | 0.44 | 0.071 |
| 0.78 | -0.08 | 23 | 0.53 | 0.47 | 0.066 |
| 0.84 | 0.19 | 24 | 0.56 | 0.58 | -0.017 |
| 0.85 | 0.24 | 25 | 0.58 | 0.59 | -0.012 |
| 0.85 | 0.26 | 26 | 0.60 | 0.60 | 0.002 |
| 0.86 | 0.30 | 27 | 0.63 | 0.62 | 0.012 |
| 0.86 | 0.30 | 28 | 0.65 | 0.62 | 0.032 |
| 0.87 | 0.31 | 29 | 0.67 | 0.62 | 0.052 |
| 0.88 | 0.40 | 30 | 0.70 | 0.66 | 0.042 |
| 0.95 | 0.71 | 31 | 0.72 | 0.76 | -0.041 |
| 0.98 | 0.87 | 32 | 0.74 | 0.81 | -0.063 |
| 1.02 | 1.04 | 33 | 0.77 | 0.85 | -0.083 |
| 1.04 | 1.12 | 34 | 0.79 | 0.87 | -0.078 |
| 1.19 | 1.86 | 35 | 0.81 | 0.97 | -0.154 |
| 1.26 | 2.19 | 36 | 0.84 | 0.99 | -0.148 |
| 1.32 | 2.49 | 37 | 0.86 | 0.99 | -0.133 |
| 1.33 | 2.53 | 38 | 0.88 | 0.99 | -0.111 |

*For n=38 and P= 0.05, the critical value is 0.192, Since 0.154 <0.192 we can accept the null hypothesis that the data  coming from a normal population with mean 0.80 and standard deviation 0.211

**Table 8.6** Kolmogorov–Smirnov method of Cu in AMD patients*

| X (Cu-AMD) | Z | Cumulative frequency | Step cumulative distribution | Normal cumulative distribution | Difference |
|---|---|---|---|---|---|
| 0.77 | -1.53 | 1 | 0.02 | 0.06 | -0.039 |
| 0.83 | -1.30 | 2 | 0.05 | 0.10 | -0.051 |
| 0.85 | -1.22 | 3 | 0.07 | 0.11 | -0.041 |
| 0.87 | -1.12 | 4 | 0.09 | 0.13 | -0.038 |
| 0.91 | -0.96 | 5 | 0.12 | 0.17 | -0.051 |
| 0.92 | -0.91 | 6 | 0.14 | 0.18 | -0.041 |
| 0.93 | -0.88 | 7 | 0.16 | 0.19 | -0.028 |
| 0.95 | -0.78 | 8 | 0.19 | 0.22 | -0.032 |
| 0.98 | -0.68 | 9 | 0.21 | 0.25 | -0.038 |
| 0.98 | -0.66 | 10 | 0.23 | 0.25 | -0.021 |
| 0.98 | -0.65 | 11 | 0.26 | 0.26 | -0.001 |
| 0.99 | -0.61 | 12 | 0.28 | 0.27 | 0.010 |
| 1.01 | -0.56 | 13 | 0.30 | 0.29 | 0.015 |
| 1.01 | -0.55 | 14 | 0.33 | 0.29 | 0.033 |
| 1.02 | -0.51 | 15 | 0.35 | 0.30 | 0.044 |
| 1.03 | -0.47 | 16 | 0.37 | 0.32 | 0.052 |
| 1.04 | -0.41 | 17 | 0.40 | 0.34 | 0.053 |
| 1.07 | -0.29 | 18 | 0.42 | 0.39 | 0.033 |
| 1.07 | -0.28 | 19 | 0.44 | 0.39 | 0.052 |
| 1.09 | -0.22 | 20 | 0.47 | 0.41 | 0.052 |
| 1.14 | -0.02 | 21 | 0.49 | 0.49 | -0.004 |
| 1.15 | 0.02 | 22 | 0.51 | 0.51 | 0.004 |
| 1.15 | 0.05 | 23 | 0.53 | 0.52 | 0.015 |
| 1.16 | 0.07 | 24 | 0.56 | 0.53 | 0.031 |
| 1.16 | 0.07 | 25 | 0.58 | 0.53 | 0.054 |
| 1.20 | 0.26 | 26 | 0.60 | 0.60 | 0.001 |
| 1.21 | 0.29 | 27 | 0.63 | 0.61 | 0.015 |
| 1.22 | 0.32 | 28 | 0.65 | 0.63 | 0.024 |
| 1.31 | 0.69 | 29 | 0.67 | 0.75 | -0.080 |
| 1.33 | 0.77 | 30 | 0.70 | 0.78 | -0.080 |
| 1.34 | 0.83 | 31 | 0.72 | 0.80 | -0.077 |
| 1.37 | 0.95 | 32 | 0.74 | 0.83 | -0.084 |
| 1.41 | 1.10 | 33 | 0.77 | 0.87 | -0.098 |
| 1.42 | 1.15 | 34 | 0.79 | 0.87 | -0.084 |
| 1.48 | 1.41 | 35 | 0.81 | 0.92 | -0.107 |
| 1.49 | 1.46 | 36 | 0.84 | 0.93 | -0.090 |
| 1.61 | 1.95 | 37 | 0.86 | 0.97 | -0.114 |
| 1.92 | 3.25 | 38 | 0.88 | 1.00 | -0.116 |

* For n=38 and P= 0.05, the critical value is 0.192, Since 0.116<0.192 we can accept the null hypothesis that the data  coming from a normal population with mean 1.14 and standard deviation 0.240

**Table 8.7** Kolmogorov–Smirnov method of Fe in AMD patients

| X (Fe-AMD) | Z | Cumulative frequency | Step cumulative distribution | Normal cumulative distribution | Difference |
|---|---|---|---|---|---|
| 0.51 | -1.84 | 1 | 0.02 | 0.03 | -0.010 |
| 0.63 | -1.57 | 2 | 0.05 | 0.06 | -0.012 |
| 0.68 | -1.45 | 3 | 0.07 | 0.07 | -0.004 |
| 0.74 | -1.30 | 4 | 0.09 | 0.10 | -0.003 |
| 0.84 | -1.10 | 5 | 0.12 | 0.14 | -0.020 |
| 0.87 | -1.03 | 6 | 0.14 | 0.15 | -0.012 |
| 0.96 | -0.82 | 7 | 0.16 | 0.21 | -0.044 |
| 0.99 | -0.76 | 8 | 0.19 | 0.22 | -0.039 |
| 1.03 | -0.67 | 9 | 0.21 | 0.25 | -0.042 |
| 1.06 | -0.59 | 10 | 0.23 | 0.28 | -0.044 |
| 1.08 | -0.56 | 11 | 0.26 | 0.29 | -0.032 |
| 1.11 | -0.50 | 12 | 0.28 | 0.31 | -0.030 |
| 1.13 | -0.44 | 13 | 0.30 | 0.33 | -0.029 |
| 1.18 | -0.32 | 14 | 0.33 | 0.37 | -0.047 |
| 1.24 | -0.20 | 15 | 0.35 | 0.42 | -0.070 |
| 1.25 | -0.17 | 16 | 0.37 | 0.43 | -0.058 |
| 1.26 | -0.16 | 17 | 0.40 | 0.44 | -0.041 |
| 1.26 | -0.14 | 18 | 0.42 | 0.44 | -0.025 |
| 1.29 | -0.09 | 19 | 0.44 | 0.46 | -0.021 |
| 1.30 | -0.07 | 20 | 0.47 | 0.47 | -0.008 |
| 1.31 | -0.04 | 21 | 0.49 | 0.49 | 0.003 |
| 1.32 | -0.02 | 22 | 0.51 | 0.49 | 0.021 |
| 1.52 | 0.44 | 23 | 0.53 | 0.67 | -0.134 |
| 1.59 | 0.59 | 24 | 0.56 | 0.72 | -0.163 |
| 1.60 | 0.62 | 25 | 0.58 | 0.73 | -0.150 |
| 1.63 | 0.67 | 26 | 0.60 | 0.75 | -0.144 |
| 1.64 | 0.69 | 27 | 0.63 | 0.76 | -0.128 |
| 1.68 | 0.78 | 28 | 0.65 | 0.78 | -0.132 |
| 1.68 | 0.79 | 29 | 0.67 | 0.79 | -0.111 |
| 1.72 | 0.87 | 30 | 0.70 | 0.81 | -0.111 |
| 1.83 | 1.12 | 31 | 0.72 | 0.87 | -0.148 |
| 1.88 | 1.25 | 32 | 0.74 | 0.89 | -0.149 |
| 2.06 | 1.65 | 33 | 0.77 | 0.95 | -0.183 |
| 2.20 | 1.95 | 34 | 0.79 | 0.97 | -0.184 |
| 2.41 | 2.42 | 35 | 0.81 | 0.99 | -0.178 |

*For n=35 and P= 0.05, the critical value is 0.192, Since 0.184 <0.192 we can accept the null hypothesis that the data coming from a normal population with mean 1.33 and standard deviation 0.447
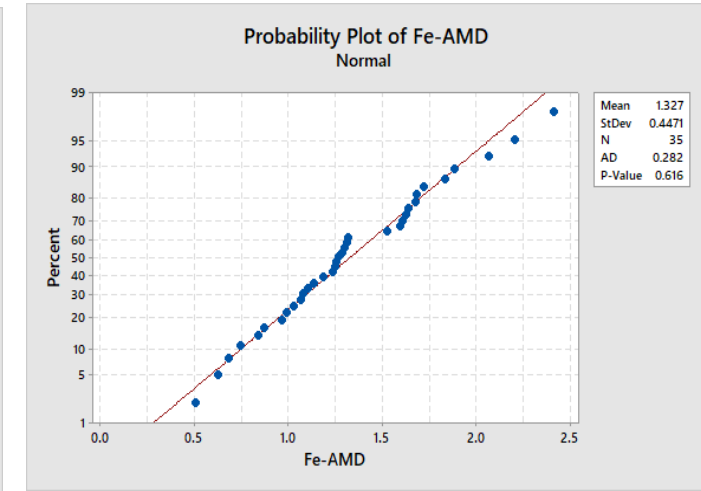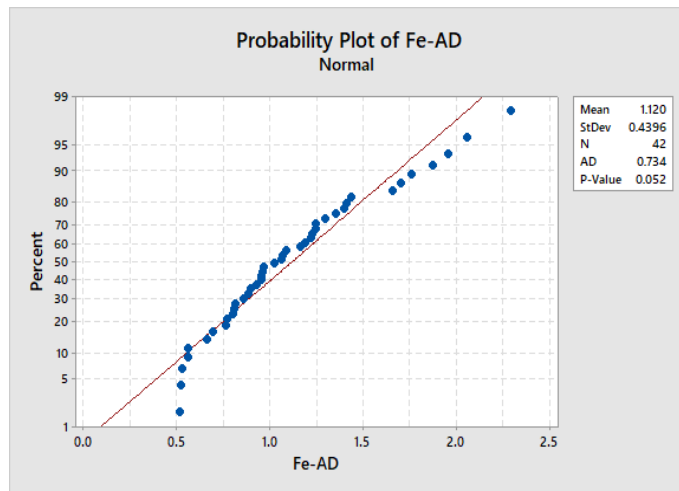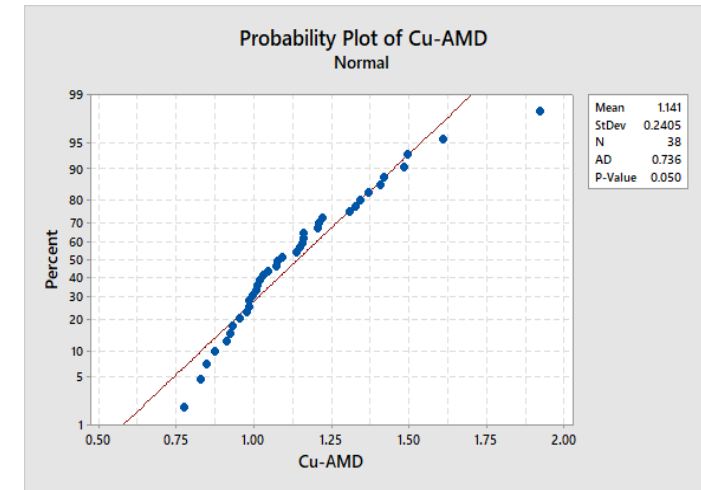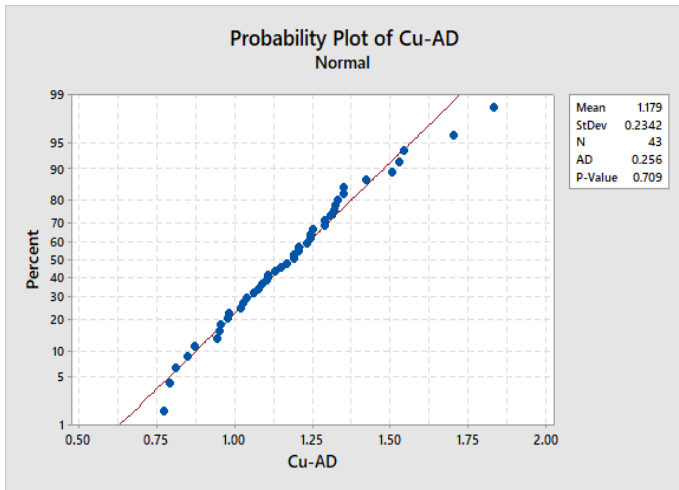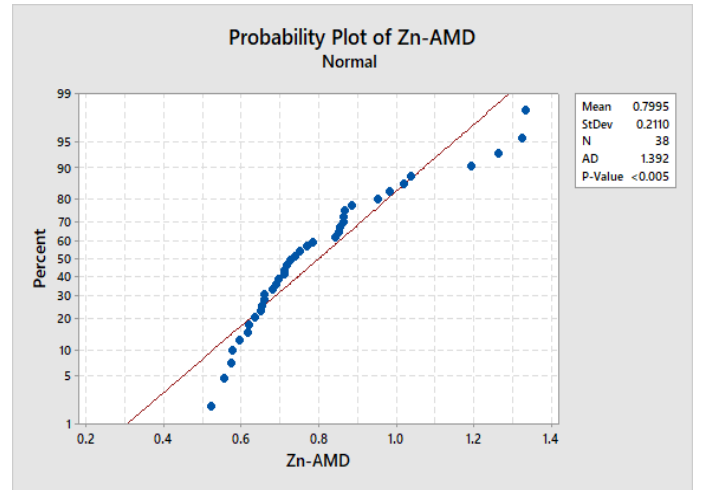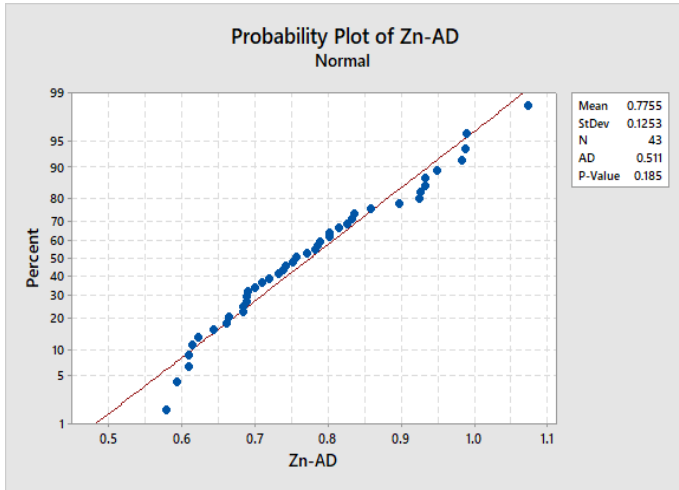
**Figure 8.1** Normal probability plot for the Zn, Cu and Fe levels for both AD and AMD patients obtained using Minitab software.
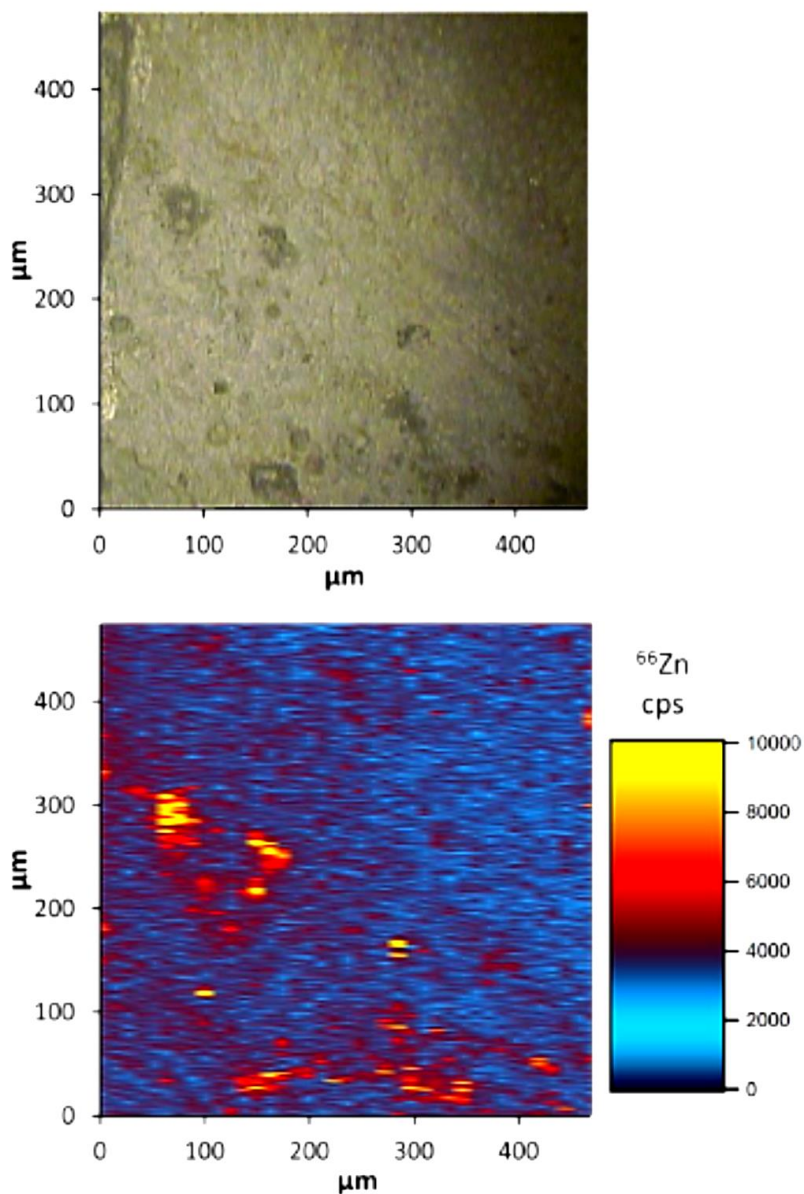
**Figure 8.2** Top: microscopic images of a 475 x 468 µm section of RPE tissue (D2), obtained using the built-in microscope on the UP-213 laser ablation system. Bottom: LA-ICP-MS image of the same section, showing the distribution of Zn. The colour scale depicts the signal intensity in counts per second (cps).

**Figure 8.3** Top: Microscopic image of a 4.5×2.33 mm section of rat retina tissue, (obtained from Dr Imre Lengyel, UCL Institute of Ophthalmology). Bottom: corresponding LA-ICP-MS image showing the distribution of Zn in control slide (5.3). The colour scale depicts the signal intensity in counts per second (cps). Complete laser parameters are given in Table 3.6.

**Figure 8.4** Top: Microscopic image of a 5.00× 1.78 mm section of rat retina tissue, (obtained from Dr Imre Lengyel, UCL Institute of Ophthalmology). Bottom: corresponding LA-ICP-MS image showing the distribution of Zn in control slide (3.1). The colour scale depicts the signal intensity in counts per second (cps). Complete laser parameters are given in Table 3.6.

**Figure 8.5** Top: Microscopic image of a 5.00×2.19 mm section of rat retina tissue, (obtained from Dr Imre Lengyel, UCL Institute of Ophthalmology). Bottom: corresponding LA-ICP-MS image showing the distribution of Zn. The rat was on Zn diet (slide 10.2). The colour scale depicts the signal intensity in counts per second (cps). Complete laser parameters are given in Table 3.6.
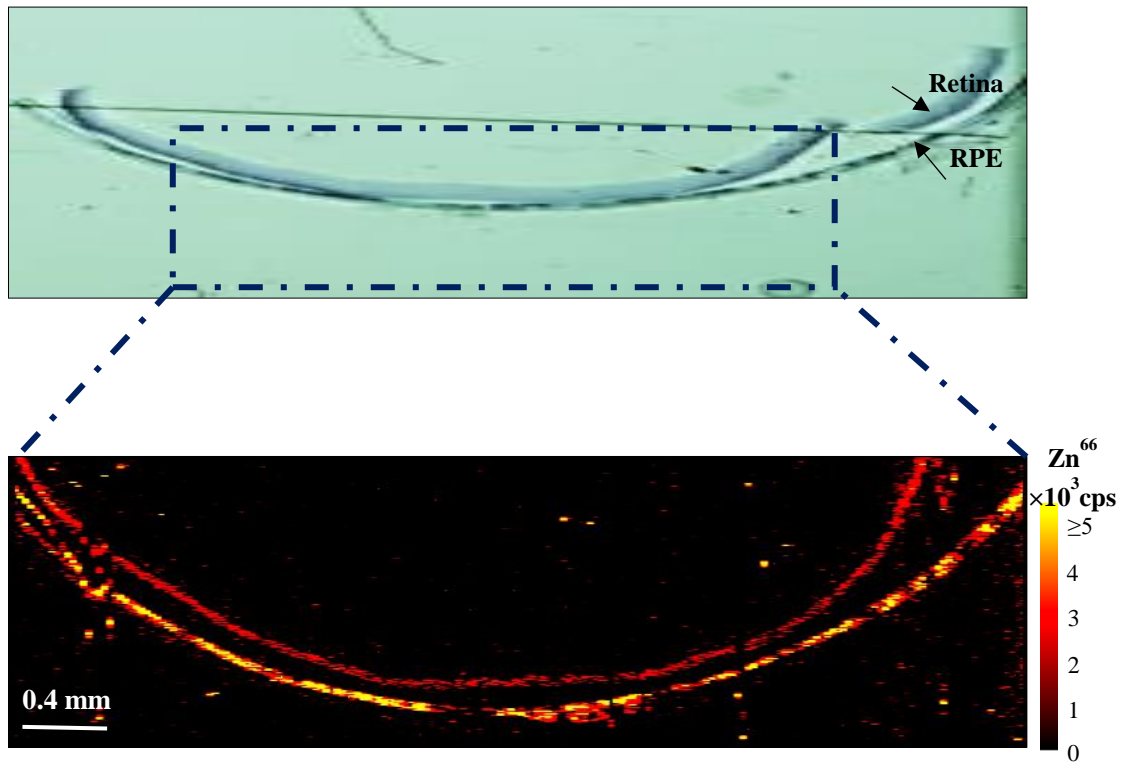
**Figure 8.6** Top: Microscopic image of a 4.8×1.37 mm section of rat retina tissue, (obtained from Dr Imre Lengyel, UCL Institute of Ophthalmology). Bottom: corresponding LA-ICP-MS image showing the distribution of Zn. The rat was on Zn diet (slide 6.1). The colour scale depicts the signal intensity in counts per second (cps). Complete laser parameters are given in Table 3.6.
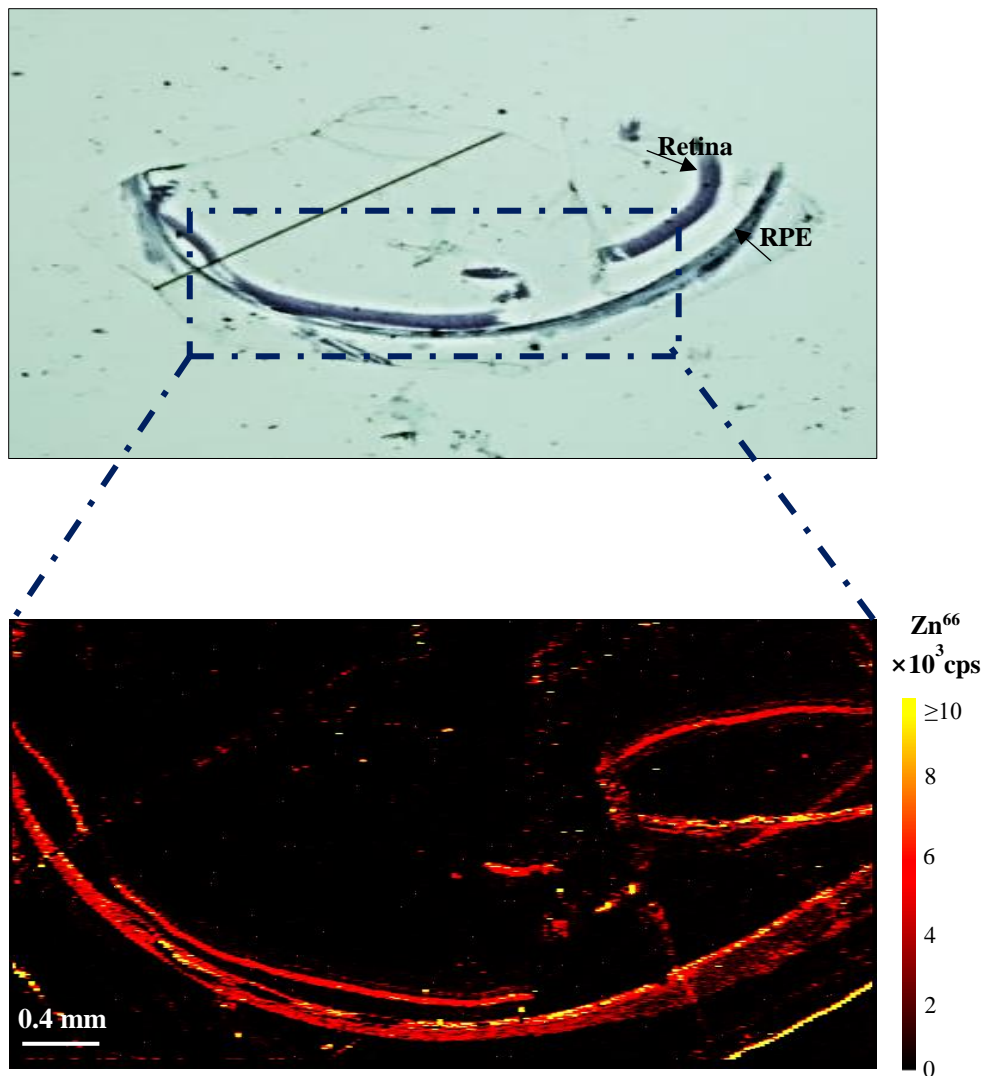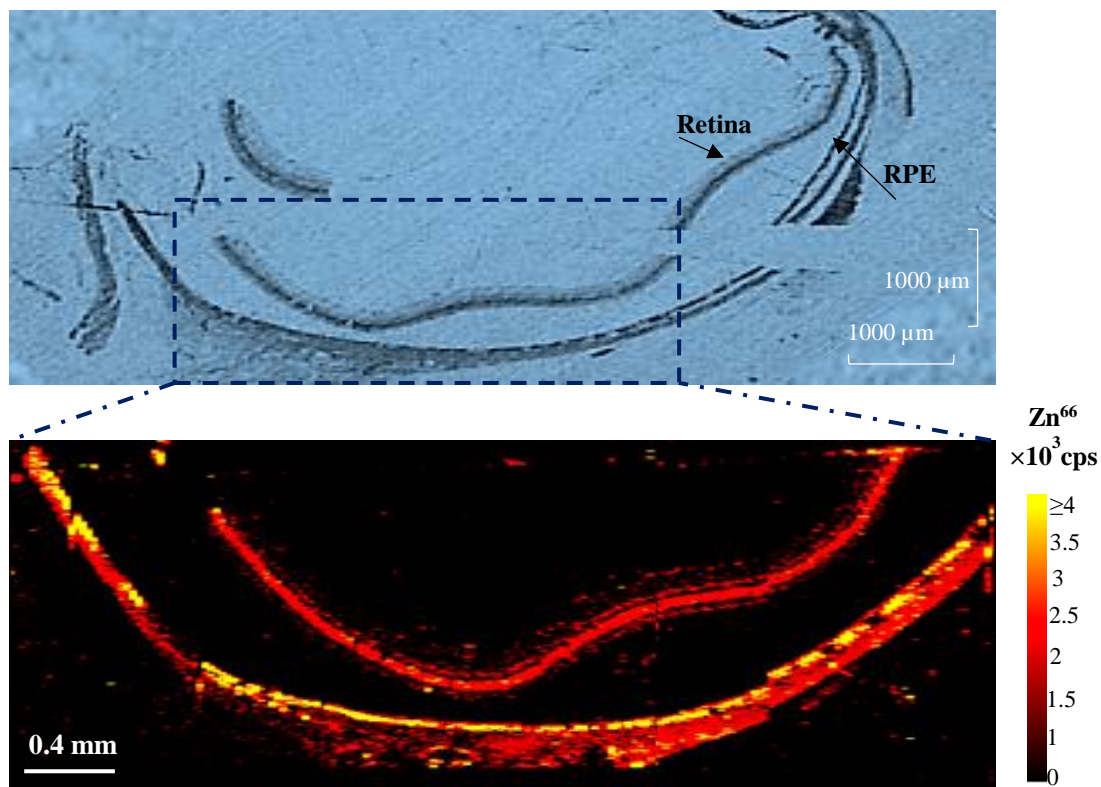
**Figure 8.7** Top: Microscopic image of a 4.5 ×1.55 mm section of rat retina tissue, (obtained from Dr Imre Lengyel, UCL Institute of Ophthalmology). Bottom: corresponding LA-ICP-MS image showing the distribution of Zn. The rat was on Zn& Cu diet (slide 15.1). The colour scale depicts the signal intensity in counts per second (cps). Complete laser parameters are given in Table 3.6.
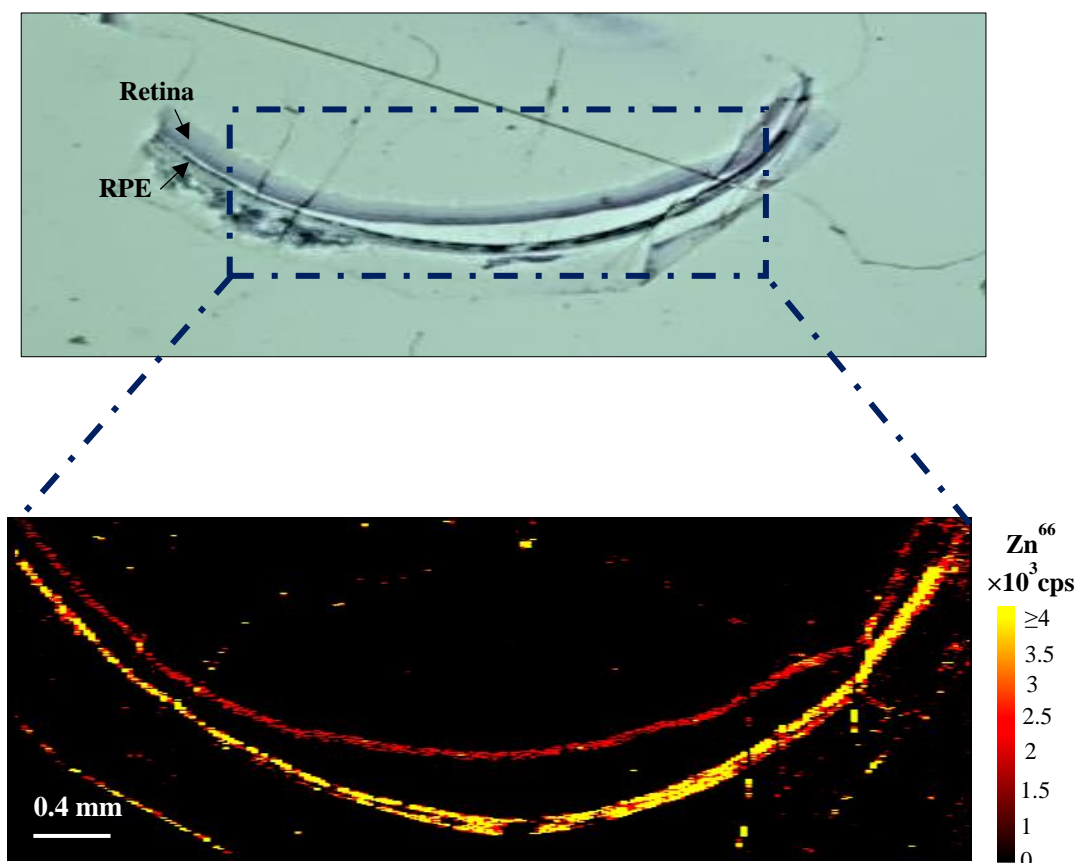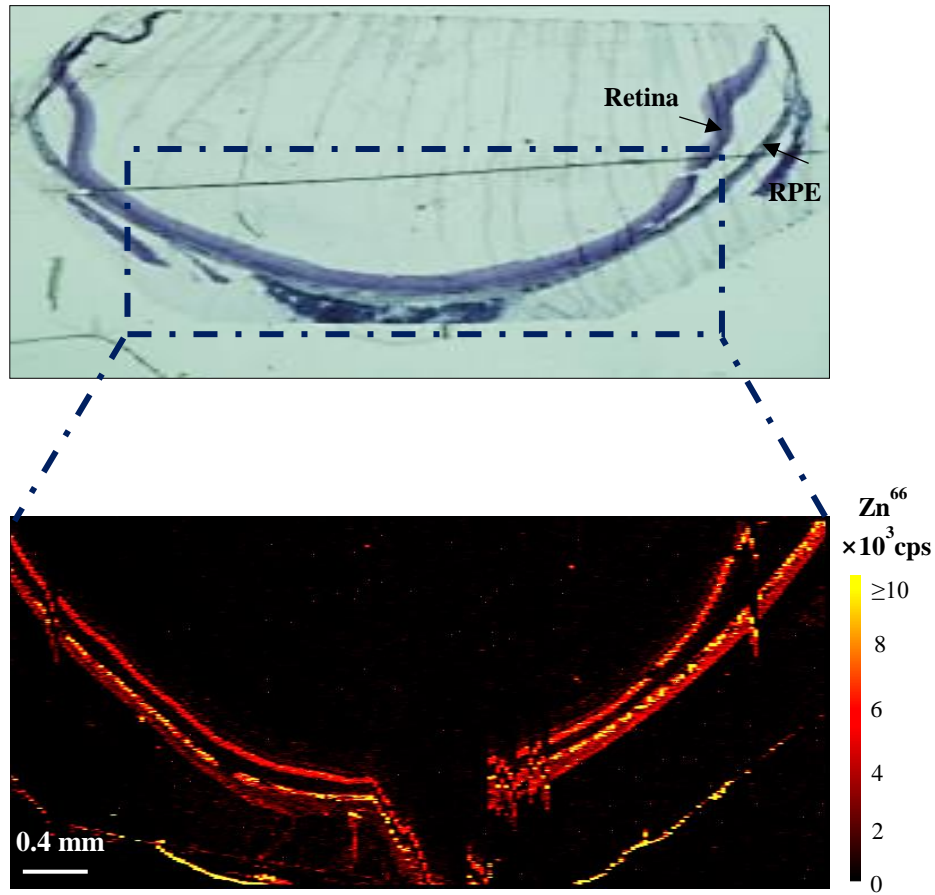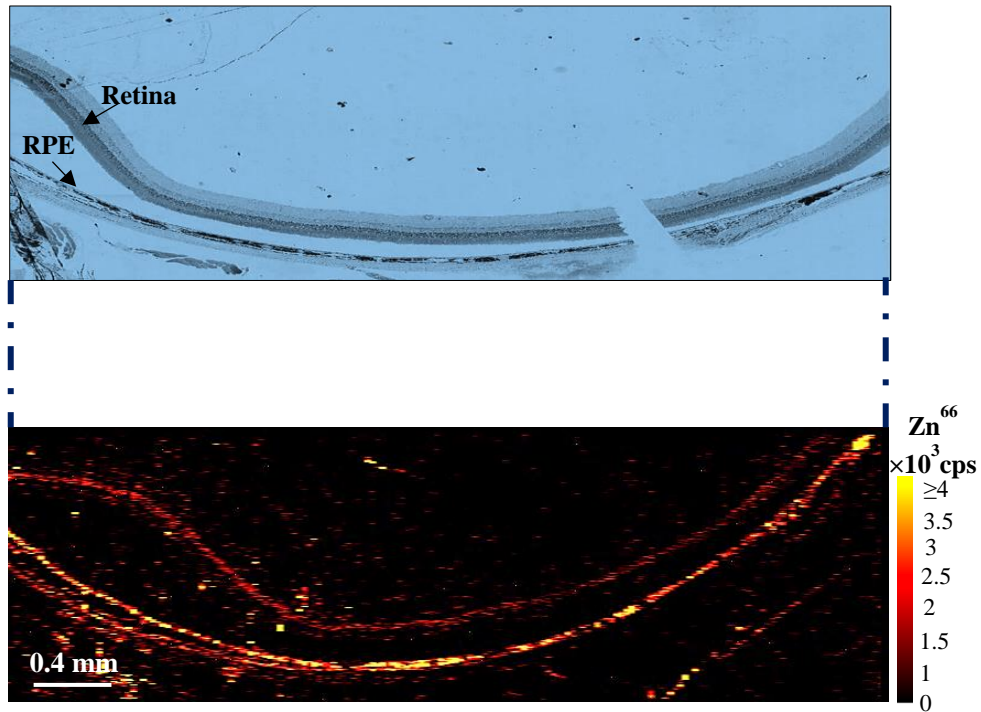
**Figure 8.8** Top: Microscopic image of a 4.53×1.41 mm section of rat retina tissue, (obtained from Dr Imre Lengyel, UCL Institute of Ophthalmology). Bottom: corresponding LA-ICP-MS image showing the distribution of Zn. The rat was on Zn& Cu diet (slide 12.1). The colour scale depicts the signal intensity in counts per second (cps). Complete laser parameters are given in Table 3.6.

# Appendix 4 –Presentations, conferences and training records

## Conferences and Presentations

The work contained in this thesis has been presented in poster format. This includes presentations /attending at scientific conferences as well as departmental meetings.

**Annual meeting/conference**: The 3rd ZINC-UK meeting, UCL Institute of Ophthalmology, London — 28/02/2011

**Annual meeting/conference**: The 4th ZINC-UK meeting, University of Central Lancashire — 18/07/2011

**Department Research Network Meeting** — 25/04/2012
**Poster** titled: A Metallomics Study of Zn Biology in Relation to Age Related Macular Degeneration, **Loughborough University**

**Research School of Health and Life Sciences Student Conference** — 28/05/2012
**Poster** titled: A Metallomics Study of Zn Biology in Relation to Age Related Macular Degeneration, **Loughborough University**

**The 6th Saudi International Conference - SIC 2012** — 11/10/2012
**Poster** titled: A Metallomics Study of Zn Biology in Relation to — 14/10/2012
Age Related Macular Degeneration, **Brunel University**

**University Research Network Meeting** — 21/05/2014
**Poster** titled: Bioimaging of Zinc in retina tissue by Laser Ablation Inductively Coupled Plasma Mass Spectrometry, **Loughborough, UK**

**European Winter Conference on Plasma Spectrochemistry** — 22- 26/02/15
**Poster** titled: Bioimaging of Zinc in retina tissue by Laser Ablation Inductively Coupled Plasma Mass Spectrometry, **University of Münster, Germany**

# Training

A list of the Loughborough University lectures, staff development and safety courses, workshops and seminars attended during the course of the PhD is provided below:

| | |
|---|---|
| **Inaugural lecture:** From Laboratory to Clinic-Analytical Chemistry in Action, Professor Barry Sharp | 08/02/2012 |
| **RSC lecture:** Mass spectrometry simplified: ambient ionization and miniature mass spectrometers, Professor R. Graham Cooks | 23/02/2012 |
| **Departmental lecture**: Atomic and Molecular Spectroscopy lectures (CMP052) | 26/10/2010 28/10/2010 |
| **Departmental lecture**: Mass Spectrometry and Associated Techniques lectures (CMP051) | 16/11/2010 23/11/2010 30/11/2010 |
| **Workshop**: Thermo Scientific Gas and Liquid Phase Chromatography Workshops, University of Reading | 13-14/07/2011 |
| **Workshop**: 10th East Midlands Proteomics Workshop, Loughborough University | 02/11/2011 |
| **Training**: ICP-MS, including Fixing problems-Mass calibration-Mantenance (David Douglas, Claire Camp). | 17/12/2010 02/03/2011 03/03/2011 31/03/2011 15/06/2011 |
| **Training**: Gel electrophoresis/GE-ICP-MS ( Razi Haider) | 22/11/2010 10/12/2010 16-19/08/2011 |
| **Training**: LabVIEW training day: National instruments Ltd | 01/03/2011 |
| **Training**: LTQ (Dr. Tamer Shoeib, Aref Zayed, Sarah Taylor). | 24/03/2013 26/07/2012 01/06/2011 |
| **Training**: Basic LC-MS  (Aref Zayed) | 01/06/2011 |
| **Training**: Nano LC (Thermo scientific) | 31/02/2014 |

**Training**: LA-ICP-MS (Amy Managh)                              05/12/2013
                                                                  23/01/2014
**Training**: Igor Iolite programme (visualisation and processing of mass    17/01/2014
spectrometric data), by Amy Managh

**Training**: D-plot Programme (Grant Craig)

**Training**: Lab Demonstration CMB010                            17/05/2012

**Training:** Cell Culture Training                               17/03/2014
Sport science/Chemical bioengineering, John Pugh                  20/03/2014
                                                                  31/03/2014
                                                                  03/04/2014
                                                                  07/04/2014
                                                                  10/04/2014


**Safety seminar**: Good laboratory practice, Professor Paul Thomas    22/02/2012
                                                                  13/11/2013
**Safety seminar**: Flammable materials, Anish Patel
                                                                  14/03/2012
**Safety seminar**: Fire extinguisher training, Rod Harrison
                                                                  16/04/2012
**Safety seminar**: Liquefied gases, Cryogenics, Claire Camp
                                                                  18/04/2012
**Safety seminar**: Corrosive materials, Paul O'Hara
                                                                  23/05/2012
**Safety seminar**: Pressurised gasses, Shuo Kang
                                                                  06/06/2012
**Safety seminar**: Electrical Hazards, Iain Kirkpatrick
                                                                  05/07/2012
**Safety seminar**: High pressure/high temperature operation, Tom Smith
                                                                  26/09/2012
**Safety seminar**: Radioactive materials and ionizing radiation,
Monica Felipe-Sotelo                                              25/10/2012
**Safety seminar**: Vacuum Systems, Neil Devenport/Caitlyn Da Costa
                                                                  22/11/2012
**Safety seminar**: Waste disposal, Nolwenn Derrien
                                                                  16/01/2013
**Research Seminar**: Inorganic
                                                                  24/10/2010
**Research Seminar**: Physical & Analytical
                                                                  06/01/2011

**Research Seminar**: Analytical, Ridiochem, Inorganic            23/02/2011

**Research Seminar**: Better Instrumentation and Measurements through Spectrochemical Research, by Prof. Gary Hieftje — 29/03/2011

**Research Seminar** with Prof. Derek Tocher (UCL), Dr. Claire Eyers (University of Manchester). — 07/12/2011

**Research Seminar** with Prof. Keith Oldham (Trent University, Canada) — 28/03/2012

**Research seminar:** From the electronics of molecules to molecular electronics, Professor Paul Low. — 30/05/2012

**Research Seminar:** Surface Mobility, Structure Modulation and Host-Guest Effects in Supramolecules — 07/06/2012

**Research Seminar**: Introduction to statistics for researchers — 24/07/2012

**Research Seminar**: with Dr Malachy McCann from NUI Maynooth, 'Syphilis, MRSA and Cancer – Cures Containing Metal Ions — 17/10/2012

**Research Seminar**: with Prof. Patrick Guiry (UCD), — 24/10/2012

**Graduate school course**: Postgraduate Research Students Induction — 02/11/2010

**Graduate school course**: Database in Focus - Web of Science — 24/11/2010

**Graduate school course**: Finding Resources for your Literature Review and Beyond — 18/01/2011

**Graduate school course**: RefWorks — 10/02/2011

**Graduate school course**: Qualitative Analysis - an Introduction to Collecting and Analysing — 25/02/2011

**Graduate school course**:
Excel 2007 Intermediate - Pivot Tables and Pivot Charts — 25/05/2011

**Graduate school course**: **Teaching Skills**
Preparing to teach and promoting learning/ Supervising practical activities (3 parts) — 28/03/2011 / 04/04/2011 / 26/05/2011

**Graduate school course**: Getting Noticed - The Databases that Help you Choose Where to publish — 9/06 2011

**Graduate school course**: Blood Borne Viruses and other Pathogens — 12/01/2012

**Graduate school course**:                                                 13/02/2012
Excel 2010 - An Introduction course-part 1         14/03/2012
Excel 2010 - An Introduction course- part 2       21/03/2012
Excel 2010 - An Introduction course- part 3

**Graduate school course**:                                                 21/11/2012
Writing your Thesis with Word 2010A            28/11/2012
Writing your Thesis with Word 2010B

**Webinar**: Identifying and Quantifying the Uncertainty Associated with   27/10/2011
Instrumental Analysis.

**Webinar**: Rapid Quantitative Analysis of Immunosuppressant Drugs in   15/11/2011
Blood and Plasma by LC-MS/MS in Clinical Research.

**Meeting** with Dr. Imre Lengyel UCL Institute of Ophthalmology,   17/11/2011
London                                                            18/12/2013
                                                            12/02/2014

**Meeting**: Project meeting with sport science, Professor Mark Lewis   28/06/2012

**Meeting**: Skype sessions with Dr. Imre Lengyel UCL Institute of   06/03/2014
Ophthalmology,                                          07&26/02/2014

## 1- Determination of Zn, Cu and Fe in Patients' Serum using Micro-Sampling ICP-MS and Sample Dilution.

*Tharwat N. Abduljabbar[a,b] , Helen J. Reid[a], Neda Barzegar-Befroeid[c], Tunde Petod[e], Imre Lengyel[c,d] and Barry L. Sharp[a]\**

**To be submitted to Talanta.**

## Abstract

A high-throughput, sensitive and rapid method was developed for the determination of Zn, Cu and Fe in small volumes (30 µL) of human serum using inductively coupled plasma mass spectrometry (ICP-MS). The sample preparation procedure employed simple dilution of the serum samples by 100-fold with 1.0 % butanol, 0.5 % v/v ammonia, 0.02 % v/v Triton X-100 and 0.01 % v/v $HNO_3$. The reliability of the method was evaluated using serum UTAK certified reference material, and the results matched well with the certified values. The method was applied to determine Zn, Cu and Fe in 81 human serum samples from Alzheimer disease (AD) and age related macular degeneration (AMD) patients. No significant difference was found in Zn and Cu levels between AD and AMD patients, whereas the content of Fe in AMD patients was slightly higher than in AD patients. The results showed a decrease in serum Zn and a notable increase in serum Cu in both AD and AMD patients compared to healthy controls, but Fe serum levels in AMD patients were not significantly different from the controls.

*Keywords: AD; AMD; ICP-MS; Serum analysis; Trace elements.*

## 2- Bio-imaging of Zinc in Retina Tissue by Laser Ablation Inductively Coupled Plasma Mass Spectrometry

*Tharwat N. Abduljabbar[a,b], Amy Managh[a], Helen J. Reid[a], Imre Lengyel[c], Barry L. Sharp[a]\**

## Abstract

Elemental bio-imaging using laser ablation inductively coupled plasma-mass spectrometry (LA-ICP-MS) was employed to image Zn in twelve rat retina sections. The rats were given either a conventional, a Zn or Zn/Cu-supplemented diet to study the correlation between diet and specific retinal disorders. LA line scans were run approximately orthogonal to the retina which showed that that the Zn was largely concentrated in the retinal pigmented epithelium (RPE) and the retina. It was found that the distribution of Zn across these features was well modelled by a Gaussian distribution and this was used to evaluate differences in the relative uptake of Zn across the ocular features. The difference between the three differentially fed rat groups was not statistically significant for the relatively small group of twelve rats investigated here. However, The distribution of Zn in the RPE was found to be significantly narrowed in the rats receiving both Cu and Zn supplementation. Thus elemental imaging, as demonstrated here, is shown to be a powerful means of studying the uptake of Zn in the eye.

*Keywords: AMD; LA- ICP-MS, bioimaging, Retina, Zinc*